A Bottom-Up Approach to Building an Artificial Cell by Self-Assembly

A thesis submitted to the National University of Ireland in fulfilment of the requirements for the degree of

Doctor of Philosophy

By

Urszula Magdalena Migas, B.Sc.

Department of Chemistry
Maynooth University

March 2016

Research Supervisor: Dr. Jennifer McManus
Head of Department: Dr. John Stephens

Dedicated to my parents, Ewa and Jerzy
and Elso, Darek, Ewelina, Sergiusz and Sławek.
Thank you for all of your support along the way.

Declaration

I hereby certify that this thesis has not been submitted before, in whole or in part, to this or any university for any degree and is, except where otherwise stated, the original work of the author.

Signed:_____

Date:_____

Maynooth University

Acknowledgements

First and foremost, I would like to sincerely thank my supervisor and thesis advisor, Dr. Jennifer McManus, for her help, support and guidance. I have learned so much throughout my academic pursuit under your leadership. Without your advice and patience this PhD project would not have been as enjoyable an endeavour and as learned an experience as it has proven to be.

I would like to thank to my co-supervisor, Prof. Marc Devocelle, for giving me the chance to work in such a fascinating area of research and for his help and support during my time at the Royal College of Surgeons in Ireland (RCSI). Thanks are also due to Aoife O'Connor and Lukasz Frankiewicz for their help with the experiments and endless patience.

I would also like to thank all those who have helped me accomplish this research. Both Prof. John Lowry and Dr. John Stephens for affording me the opportunity to carry out my research in the Department of Chemistry. A special thank you to BioAT for providing necessary financial framework to Prof. Christine Loscher, Prof. Paul Moynagh, Joan Kelly, Jane Wall and everybody involved in the BioAT programme. Thank you to Mr. Brenton Cavanagh from the RSCI for his assistance with TEM images and to Dr. Illona Dix from the Biology Department at Maynooth University (MU) for her help with the confocal imaging. Finally to all the BioAT postgrads, especially Adam, Helen, Ashling, Ronan, Siobhan and Zita, for their help with cell culture and the company at various courses.

My sincere thanks to all other members of the Chemistry Department for their support and assistance, to the administration staff: Niamh, Carol and Donna and the technicians and lab co-ordinators for their advice and help with all of the little things that helped create this much bigger thing; your presence throughout my time at MU has been crucial and much appreciated. To Noel Williams, for his invaluable help with all of the computer-related disasters. Thank you for always being there to answer any questions and providing help when needed.

A big thank you to all the members of the research group, past and present. Thank you for being there for me, when…well, you know when. Ruth, thank you so much for making me feel so welcome in the lab, for our little chats out front, and my Irish Accent. To Susan, for your delicacies from India and a supply of strange phrases. To Alice, for your eccentric life wisdom, and eventful, memorable dinners; and to Michelle, for the Legendary Lemon Lime Cheesecake and the motivation (not only in the form of a letter) but most of all, thank you guys for your enlightening explanations of the various rules of grammar (I still don't get it). And last but not least, to Mark, for all the phrases and quotes, not only from Frozen.

To all of the postdocs and postgrads in the Chemistry Department, past and present (I'm not using names because I'll forget about someone) for your help and support over the past four-and-a-half years, for all the good times, your pleasurable company during lunch and tea, for sharing jokes (especially the Halloween and Cheese-related ones), delicious cakes, and late nights out…

To my friends, Sarah, Jenny, Charlotte, Patrick, Wayne, Ronan and Barry. Thanks so much for everything (food, drinks, movies, chats and shoulders to cry/sleep on). If it wasn't for you guys, I would have been a Doctor long ago…I got there eventually!

Dziękuję moim rodzicom, Ewie i Jerzemu, dzięki którym miałam możliwość kształcić się i zdobywać cenną wiedzę, którzy stale mnie mobilizowali i wspierali. Dziękuję rodzeństwu Darkowi, Ewelinie, Sergiuszowi, Sławomirowi, bratanicy Darii i całej rodzinie za słowa otuchy i motywację. Bez waszej pomocy i wsparcia nie udałoby mi się przebrnąć przez te wszystkie lata.

Finally, I would like to thank to my love, Elso, for always being there for me. For your help, support and encouragement; and most of all for your patience and understanding, especially when everything seemed as if it was spinning out of control. You were there for me, and it meant the world. We made it!

Abstract

Synthetic biology is a rapidly growing field in which recent advances now allow the formation of minimal or artificial cells composed of a minimum number of components, capable of performing specific functions. New developments contributing to the complexity of artificial cells or making their design more cell-like increases the number of possible applications. To-date many processes and chemical reactions have been studied in these cells; many more remain to be explored. However, more sophisticated approaches to artificial cell design and preparation will be required to do this. The results presented here provide insights into how artificial cell development can contribute to our understanding of the self-assembly of biomolecules.

The formation of lipid based vesicles is an inherent element of artificial cell development, which requires reliable techniques to prepare vesicles of cell size. The most widely applied methods have been evaluated here based on the size, quality and abundance of vesicles formed as well as the ease of encapsulating biological solutes. The effect of various lipid compositions, particularly cholesterol, has also been analysed. This comparison provides reliable information for tailoring the selection of experimental approach when building a model cell.

Functionalisation of the artificial cell surface and its interior is required for many applications. For surface modification, there is growing interest in using glycolipids to fulfil a molecular recognition role. A synthetic glycolipid has been incorporated into the phospholipid membrane of giant unilamellar vesicles at biologically relevant concentrations. The synthetic glycolipid shows concentration-dependent phase behaviour in binary mixtures with DOPC and in ternary mixtures with DOPC and cholesterol. At low concentrations, the glycolipid is fully dispersed in the GUV membrane. At concentrations above 10%, the formation of lipid tubules was observed, consistent with the formation of a columnar lipid phase. Lipid tubules are observed in aqueous and oil solvents, suggesting that both hexagonal and inverted hexagonal lipid arrangements can be formed.

The self- assembly of proteins in cells is required for normal biological function and unintended self-assembly also can occur following a change in environmental conditions, in some cases leading to disease. To understand these processes more fully, experiments

performed in controlled, but closer to physiological conditions are required. Artificial cells provide an idea platform to do this. Bovine Serum Albumin (BSA) was encapsulated in phospholipid based giant unilamellar vesicles of cell size. The formation of aggregates within the GUV was analysed using a fluorescent dye (Thioflavin T) and various modes of microscopy. While protein aggregation was observed inside the vesicles, harsh environmental conditions were required to induce this aggregation (e.g.heat, low pH).

An approach to investigate protein condensation upon *in-situ* expression in physiologically relevant conditions was also explored. In this case, a protein that aggregates at physiological temperature and pH (the P23T mutant of human gamma D crystallin) was expressed *in-situ* inside a GUV using a cell-free expression system. The formation of P23T specific aggregates was observed after incubation for several hours at 37°C. These aggregates have a fractal dimension lower than those normally observed for amorphous protein aggregate. Furthermore, we have demonstrated that the self-assembly of P23T can also be induced following transfection in mammalian cells, providing deeper insights into the mechanism by which the genetic cataract associated with this mutation occurs.

List of Abbreviations

%T – percentage transmission
A – absorbance
APS – ammonium persulphate
Bodipy FL C_5 ceramide –N-(4,4-difluoro-5,7-dimethyl-4-bora-3a,4a-diaza-s-indacene-3-pentanoyl) sphingosine
Bodipy TR ceramide – N-((4-(4,4-difluoro-5- (2-thienyl)-4-bora-3a, 4a-diaza-s-indacene-3-yl) phenoxy) acetyl sphingosine
BSA – bovine serum albumin
BSM – 18:0 brain sphingomyelin
c – speed of light
[*c*] – concentration
CCD – charged coupled device
cDICE – continuous droplet interface crossing encapsulation
cDMEM – complete Dulbecco's Modified Eagle Medium
CF – correction factor
sfDMEM – serum-free Dulbecco's Modified Eagle Medium
DAD – diode array detector
D_B – fractal dimension
DMF – dimethylformamide
DMSO – dimethyl sulfoxide
DOPC – 1,2-dioleoyl-sn-glycero-3-phosphocholine
DPPC – 1,2-dipalmitoyl-sn-glycero-3-phosphocholine
DTT – dithiothreitol
E – energy
EDTA – ethylenediaminetetraacetic acid
Egg-PC – 1, 2-Diacyl-sn-glycero-3-phosphocholine
EmGFP – emerald GFP
FITC – fluorescein isothiocyanate
FRAP – fluorescence recovery after photobleaching
g – gravitational force
GFP – green fluorescent protein
GUV – giant unilamellar vesicle
h – Planck's constant
HAS – Human serum albumin
HCl – hydrochloric acid
HEK – human embryonic kidney cells
HPLC – high performance liquid chromatography
HGD – human γD crystallin
I_0 – intensity of light
IMAC – immobilized metal ion affinity chromatography
IPTG – Isopropyl β-D-1-thiogalactopyranoside
k – rate constant
LB broth – lysogeny broth
Liss Rhod PE (18:1) – 1, 2-dioleoyl-sn-glycero-3-phosphoethanolamine-N -(lissamine rhodamine B sulfonyl) (ammonium salt)
MLV – multilamellar vesicle
MWCO – molecular weight cut off
MWM – molecular weight marker
n – refractive index
NA – numerical aperture
NaCl – sodium chloride
NBD-PC (14:0-12:0) – 1-Myristoyl-2-[12-[(7-nitro-2-1,3-benzoxadiazol-4-yl)aminododecanoyl]-sn-Glycero-3-Phosphocholine
OD – optical density
OVV – Oligovesicular vesicle
PAGE – polyacrylamide gel electrophoresis
PBS – phosphate-buffered saline
PCR – polymerase chain reaction
PEG-DOPE – 1,2-dioleoyl-sn-glycero-3-phospho-ethanolamine-N-[methoxy (polyethylene glycol) - 2000] (ammonium salt)
Q – quantum yield
rpm – rotation per minute
S_0 – ground state
S_1 – lowest excited state
SDS – sodium dodecyl sulphate
SE-HPLC – size exclusion HPLC
SPM – scanning probe microscopy
TEM – transmission electron microscopy
TEMED – tetramethylethylenediamine
ThT – thioflavin T
T_m – melt transmission temperature
t – time
t_R – retention time
TIRF – total internal reflectance fluorescence microscopy
Tyr – Tyrosine
UV/Vis – ultraviolet/visible
ε – extinction coefficient
λ – lambda (wavelength)
ρ – packing parameter
τ – fluorescence lifetime
ν – frequency

Table of Contents

Chapter 1

Introduction

1.1 Synthetic biology

Synthetic biology emerged as a field of research over a decade ago.[1,2] It combines scientific and engineering approaches to study and manipulate cellular processes. The origin of synthetic biology can be traced back to 1961 and a study of the *lac* operon in *E.coli*, postulating the existence of a mechanism regulating the cell's response to the environment.[3] Technological and scientific advancements, such as the discovery of transcriptional regulation, the PCR technique, automated DNA sequencing and modelling have significantly enhanced the ways in which biological systems can be manipulated.[2] Of great interest to synthetic biology is how to assemble cells from individual molecular components in a bottom up manner. There are three different paths to do just that; the protocell, the minimal cell and the artificial cell.[4]

Protocell preparation involves the development of scenarios explaining the origin of life in prebiotic conditions. The cells are assembled from prebiotic molecules, containing either a small amount or none of the genetic information, in the form of peptides or RNA.[5–7]

The minimal (or synthetic) cell method involves integrating DNA information and a simple metabolism into lipid compartments in order to prepare entities capable of self-reproduction based on a minimal genome.[4,8,9]

The artificial (or model) cell methodology, which is employed in this thesis, entails assembling cell-sized compartments equipped to perform biological functions by integrating natural and synthetic molecules to construct hybrid systems with new characteristics and functions.[10–12] These types of compartments are not only used to model biological processes but also as microreactors.[13] These synthetic cell assemblies may be prepared using either a top down approach, where synthetic DNA can be used to control viable bacterial cells[14] or a bottom up approach where synthetic or semi-synthetic components are used to reconstruct biological processes.[15–17]

Another area of synthetic biology research is the creation of gene regulatory circuits, which carry out functions in a similar way to electrical circuits, to program cells to perform specific tasks.[18,19] Various cell processes and functions have been developed using gene circuits, such as togglling between two stable expression states in response to external signals,[20] ordered, periodic oscillation of repressor protein expression,[21] cell phenotype switches,[22] cell-cell communication[23] or the creation of permanent memory.[24,25] One of the successes of gene circuit research was the heterologous

production of precursors to artemisinin (an antimalarial drug),[26] which resulted in 2013 in large scale production of the drug in yeast.[27] Another important development was the emergence of the clustered, regularly interspaced, short palindromic repeat (CRISPR) technology, which is a new approach for generating RNA-guided nucleases, such as Cas9, which can be targeted to almost any sequence.[2,28,29] Genome editing using CRISPR technology has been used to modify endogenous genes in a variety cell types and in organisms and to regulate endogenous gene expression or label specific genomic loci in living cells.[30–32]

Other applications of the synthetic biology approach include information storage,[33] incorporation of unnatural nucleotides[34,35] and amino acids,[36–38] reduced amino acid libraries[39] or engineered proteins[40–42] and others.[43–45]

1.2 The artificial cell

The artificial (or model) cell is a simplified system mimicking properties of biological cells, various components of cells or processes.[46,47] The simplest model cells are vesicles formed by lipid self-assembly into bilayers in aqueous solution. The lipid bilayer may be composed of natural lipids, identical to those present in cell membranes or may contain other components, such as polymers,[48] synthetic glycolipids,[49] transmembrane proteins[50] or pore forming proteins.[51]

Vesicles composed of a variety of lipids have been used to study membrane related processes such as budding,[52,53] fusion,[54] fission[55] and various aspects of membrane dynamics,[56–58] membrane composition and phase behaviour.[59,60]

While sometimes challenging, a variety of molecules have been encapsulated inside minimal cells, including small molecules,[61] nanoparticles,[62] biological molecules[63] and protein mixtures or cells.[64,65]

Protein synthesis inside vesicles is an important aspect of artificial cell research. Initially cell extracts form *E. coli*[66] or wheat germ[67] were used. However, quick energy depletion and protein degradation by enzymes present in those extracts were a major disadvantage. Development of a purified cell-free system provided a new tool for synthetic biology and model cell research in particular.[68–70] The PURE system contains purified proteins, ribosomes, t-RNAs, recombinant T7 RNA polymerase and low molecular weight components necessary for the transcription and translation processes. Additionally, all of the components of the PURE system bear His-tag, which allows for

quick purification of the synthesized protein if necessary. The PURE system has several advantages over earlier expression systems, such as lower levels of proteases, nucleases and phosphatases, greater reproducibility and flexibility.[71] The PURE system can also be modified to mimic the macromolecular crowding of the cell.[72] It allows for the simultaneous expression of multiple polypeptides in a single reaction as shown for the heterotrimeric core of cytochrome c oxidase.[73] Recently published analysis of the gene expression dynamics provide valuable insights into the fine tuning of the expression process.[74] To date, various cell-free protein expression systems have been developed.[75–79] Numerous proteins have been expressed inside lipid vesicles using cell-free expression systems, such as functional membrane proteins[80–84] and various water soluble proteins.[51,85–87]

Due to advancements in methods for solution encapsulation and cell-free expression systems, various biological processes have been recreated in model cells, such as enzymatic reactions,[88,89] synthesis of nucleic acids[90,91] or lipids,[92] actin polymerization[93] or self-reproduction[94] and more recently self-proliferation.[95,96]

Assembly processes, inevitable in biological cells may also be recreated in synthetic cells. Actin polymerization and the assembly of an actin cortex upon encapsulation of its building blocks within liposomes has been studied extensively providing insights into cell mechanics.[97,98] Xenopus egg extract have been used to recreate the process of assembly of cortical actin networks.[99,100] The understanding of the cell division processes and more specifically the formation of the mitotic spindle have been advanced by studying the embryos or the egg extracts of a variety of microorganisms.[101,102] One of the first self-assembly processes observed within lipid bilayers was the *in-situ* expression of α-hemolysin followed by the formation of a membrane pore via assembly of α-hemolysin heptamer following expression.[51] The possibility of pore formation also provided insights into extending the expression process of the cell-free system enclosed inside liposomes by means of providing a feeding solution on the exterior of the vesicle.

In recent years there has been growing interest in using vesicles as microreactors for the analysis of biochemical reactions[103–105] or as a drug delivery vehicles.[106–110]

Advances in synthetic biology and model cell research, some of which has been mention here, provides valuable insights into various biological processes such as ribosome synthesis,[111,112] cell adhesion,[106] mechanics,[65,113] reproduction[94] and proliferation.[95,96]

1.3 Self-assembly of biological molecules

Self-assembly is a spontaneous process tending towards equilibrium, in which individual components, that do not change their character upon integration, assemble in a specific way to form a well-defined structure uniquely determined by the size, number of components, geometry, and strength of interactions among the components.[114] Self-assembly is driven by non-covalent interactions which are generally weaker than covalent bonds thus are reversible.[115] Self-assembly is an essential process in biological systems and virtually all biomolecules undergo self-assembly, which determines their structure and influences their function.[116–118] Various biological structures formed by a self-assembly process include the formation of the cell membrane, cytoskeleton, viral capsid or protein complexes involved in transcription and translation of genetic information.[119–121] Self-assembly has also been explored in the context of non-biological applications such as nanotechnology and supramolecular or materials chemistry.[115,122,123]

1.3.1 Forces governing the assembly of biomolecules

The self-assembly of biomolecules occurs as a result of non-covalent interactions between the assembling components. The stable and specific arrangement of components is a result of multiple non-covalent interactions. Non-covalent interactions are weaker than the covalent bonds (bond strengths on the order of 1-5 kcal/mol), therefore are reversible at physiological temperature and take place over longer distances, ca. 2 to 10 Å.[124,125] Due to the nature of non-covalent interactions, the self-assembled structures usually remain in thermodynamic equilibrium and have the capability to rearrange.[115]

Non-covalent interactions can be formed within a molecule (intra-) as in protein folding or between different molecules (inter-).[126] The main types of non-covalent interactions include: hydrogen bonds, van der Waals interactions, hydrophobic interactions and electrostatic interactions.

1.3.1.1 Hydrogen bonding

The hydrogen bonding is an attractive interaction between a hydrogen atom covalently bonded to an electronegative donor atom of one molecule and an electronegative atom (acceptor) with at least one lone pair of electrons of the same or different molecule. The partial positive charge on the hydrogen atom, formed due to the polar character of the H-donor bond is the basis of its attraction to the lone pair of

electrons on the acceptor atom. In case of biological systems the electronegative atoms participating in hydrogen bonding are usually nitrogen and oxygen. The length of most hydrogen bonds is between 0.26 nm and 0.32 nm (0.27 nm in the water molecule) and has a strength of ~5 kcal/mol between water and 1 to 2 kcal/mol for biomolecules.[124] The strength of the hydrogen bond depends on the distance and the bond angle between donor and acceptor, with the strongest formed when the donor, the hydrogen, and the acceptor atom all lie in a straight line. Nonlinear hydrogen bonds are weaker but multiple nonlinear hydrogen bonds may act together.

Hydrogen bonding is particularly important in driving self-assembly due to its cooperative nature. The complex structure of biological molecules reveal the presence of multiple donor and acceptor sites within a single molecule. Hydrogen bonding, however weak in nature, is capable of stabilizing assembled structures.

1.3.1.2 Van der Waals interactions

Van der Waals are non-specific attractive interactions resulting from the momentary random fluctuations in the distribution of the electrons of an atom, which results in a transient electric dipole. When two atoms are close enough the transient dipole in one atom generates a transient dipole in the second atom, and the two dipoles are weakly attracted by each other. This type of interaction occurs in all types of molecules. The strength of the van der Waals interaction is approximately 1 kcal/mol and depends on the distance between the two atoms; the larger the distance the weaker the interaction.[124] The distance over which the Van de Waals interactions occurs is generally twice the distance of the covalent bond between the same atoms, e.g. for a C-H interaction it is roughly 0.2 nm.[127]

1.3.1.3 The hydrophobic effect

Hydrophobic interactions are relatively strong attractive interactions between non-polar groups, such as hydrocarbon chains of lipid molecules, separated by water. When non-polar groups are placed into water, their presence disrupts the hydrogen bonding network of the surrounding water molecules. This forces the rearrangement of water molecules around a hydrophobic surface, thus decreasing the number of possible orientations, which in turn decreases the entropy of the water. The assembly of hydrophobic groups occurs with the aim of decreasing the size of the hydrophobic surface in contact with water molecules (by excluding water from the hydrophobic region). The

increase in order of hydrocarbon groups is small compare to the increase in entropy related to the release of water molecules. The overall effect is the increase of entropy of the system.[117,128] Hydrophobic interactions are long range (up to 10 nm).[129]

1.3.1.4 Electrostatic interactions

The electrostatic potential has either attractive or repulsive character depending on the relative sign and magnitude of the interacting charges.[129]

A double layer is formed in the vicinity of the particle surface (e.g. biomolecules such as proteins) when exposed to a fluid (figure 1.1). The first layer, called the stern layer, consists of an increased concentration of strongly bound counter-ions. In the diffuse layer those counter-ions are less tightly bound. The slipping plane is located at the boundary between the diffuse layer and the bulk liquid, where the ions are uniformly distributed. The electrical potential at the slipping layer is referred to as zeta potential and it represents the magnitude of electrostatic interactions between the particles.

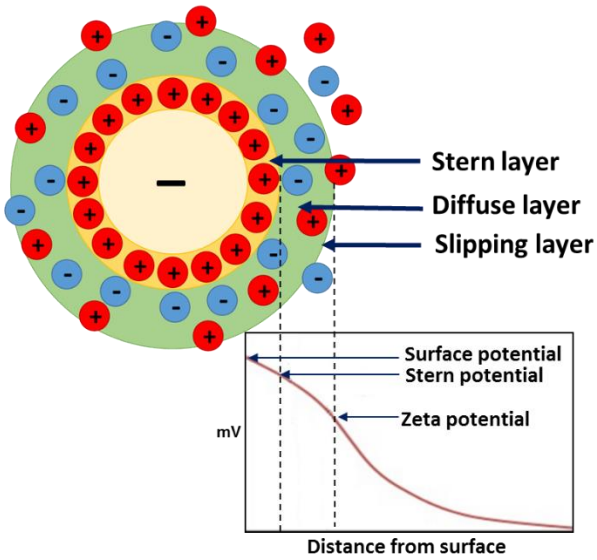

Figure 1.1 *Schematic representation of the electronic double layer and zeta potential.*

The interaction potential between two proteins can be described using DVLO theory (Derjaguin, Landau, Verwey and Overbeek). This theory combines the effects of the electrostatic repulsion and the van der Waals attraction. The electrostatic repulsion increases exponentially as the distance between particles decreases and the van der Waals' attraction increases as an inverse power of separation. The net attraction between proteins can be characterised by negative interaction potential (figure 1.2a) and repulsive interactions by positive potential (figure 1.2b).

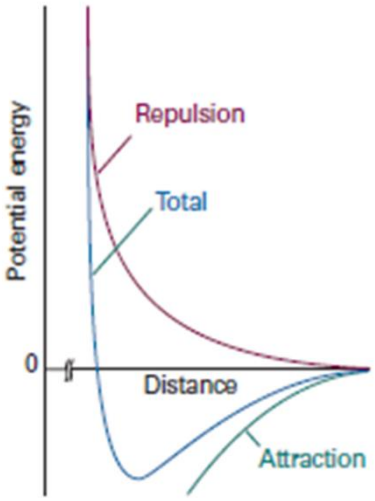

Figure 1.2 *Schematic representation of an interaction potential between protein molecules.*[130]

1.4 Lipid structure and self-assembly

1.4.1 Characteristics of lipids

Lipid molecules are composed of hydrocarbon chains and a hydrophilic head group and in a similar way to other amphiphilic molecules, self-assemble in aqueous environments forming a variety of structures, such as micelles, vesicles or flat bilayers as shown in figure 1.3.

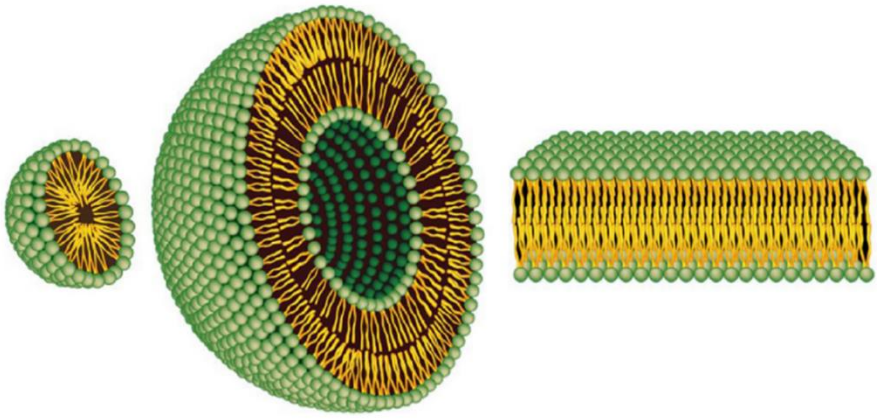

Figure 1.3 *Cross-section view of lipid organization in a micelle (left), vesicle (middle) and lipid bilayer (right), formed by lipids in aqueous solutions.*[131]

The assembly of lipid molecules in aqueous environments occurs due to the hydrophobic effect.[132] Hydrocarbon chains are water-insoluble and their assembly occurs in order to minimise the size of the hydrophobic surface in contact with water molecules. The overall effect is to increase the entropy of the system and it is the driving

force for the lipid assembly process.[117,128] Other non-covalent interactions playing a role in lipid self-assembly include hydrogen bonding, van der Waals and ionic interactions.[125]

Lipid molecules assemble into a variety of structures, depending on the nature of both the head group and hydrocarbon chains.[133] The shape and size of structures formed upon assembly may be predicted based on the Israelachvili–Mitchell–Ninham packing parameter ρ, expressed by equation 3.1,[134,135]

$$\rho = \frac{v}{a_0 \, l_c} \qquad 1.1$$

where v is the volume of the hydrocarbon chain, a_o is the optimal headgroup area and l_c is the critical chain length. Cone-like shaped lipids (figure 1.4a), usually with one hydrocarbon chain and relatively large head group form mainly micelles. Lipid molecules with cylindrical shapes (figure 1.4b), with packing parameter between 0.5 and 1, assemble into bilayers, and inverted lipid structures (figure 1.4c) are usually formed by lipids with small head groups and bulky hydrocarbon chains.[136]

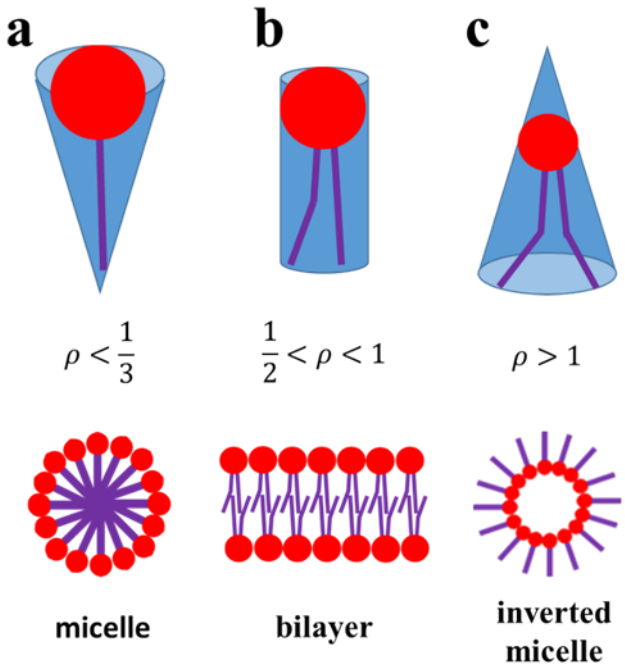

Figure 1.4 *Schematic representation of various shapes of lipid molecules; (a) cone, (b) cylindrical and (c) inverted cone, and main types of self-assembled lipid structures formed by those types of lipids.*

1.4.2 Lipid phases

Geometric arrangements of lipid molecules include lamellar, hexagonal or cubic mesophases; with normal or inverse topography (figure 1.5) as well as nanotubes and toroidal structures.[117] The self-assembly process is driven by non-covalent interactions with the hydrophobic effect as the largest contribution. The type of self-assembled structure formed depends on variety of factors, including the nature of the lipid molecules, especially the head group, the interfacial curvature, temperature and the water content within the medium in which the assembly process occurs.[136,137]

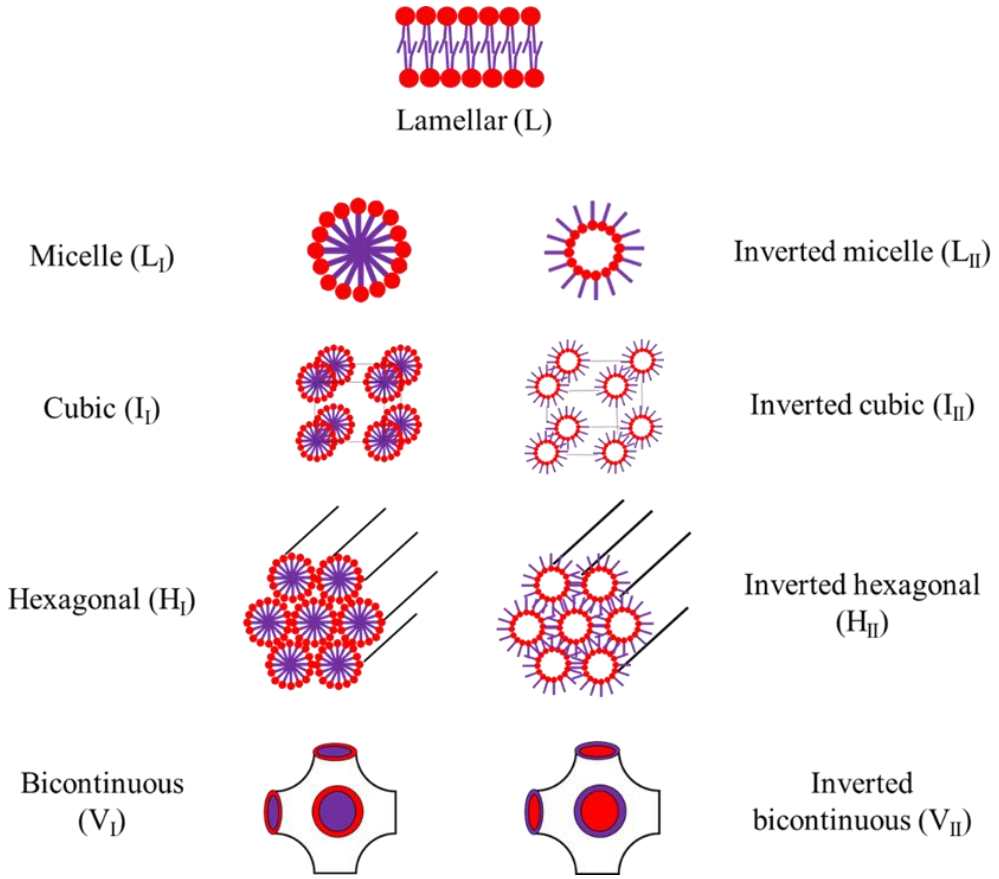

Figure 1.5 *Schematic representation of self-assembled structures formed by amphiphilic molecules.*

A lamellar phase consists of two lipid layers with their hydrophilic head groups facing towards the water interface and the hydrophobic region facing each other, forming a lipid bilayer. This lipid arrangement is found in all biological and synthetic membranes. However, non-lamellar phases, including hexagonal and cubic phases are also observed within biological and synthetic systems.[137–139] Large numbers of non-lamellar lipids are present in biological membranes have been implicated in maintaining the structure and

therefore preserving the function of membrane proteins.[140] The transition between lamellar and non-lamellar phases may be induced by varying the composition or the temperature.[137]

Biological and synthetic membranes are vastly dynamic assemblies. The types of lipid movements that can occur within the bilayer include lateral diffusion (exchange places with neighbouring lipid), transverse diffusion (or flip-flop, movement from one leaflet to the other), axial rotation and intra-chain motion (known as kink formation).[141] The rate at which a specific type of movement occurs depends on the nature and composition of the bilayer. Proteins within membranes can diffuse laterally, but not between the leaflets.

Lipid bilayers of both natural and synthetic membranes exist in different physical states (figure 1.6), which are categorised by the lateral organisation and mobility within the membrane. The character of the bilayer may be altered by adjusting temperature, pH, ionic strength or modifying the lipid composition of the bilayer or the addition of cholesterol.[141]

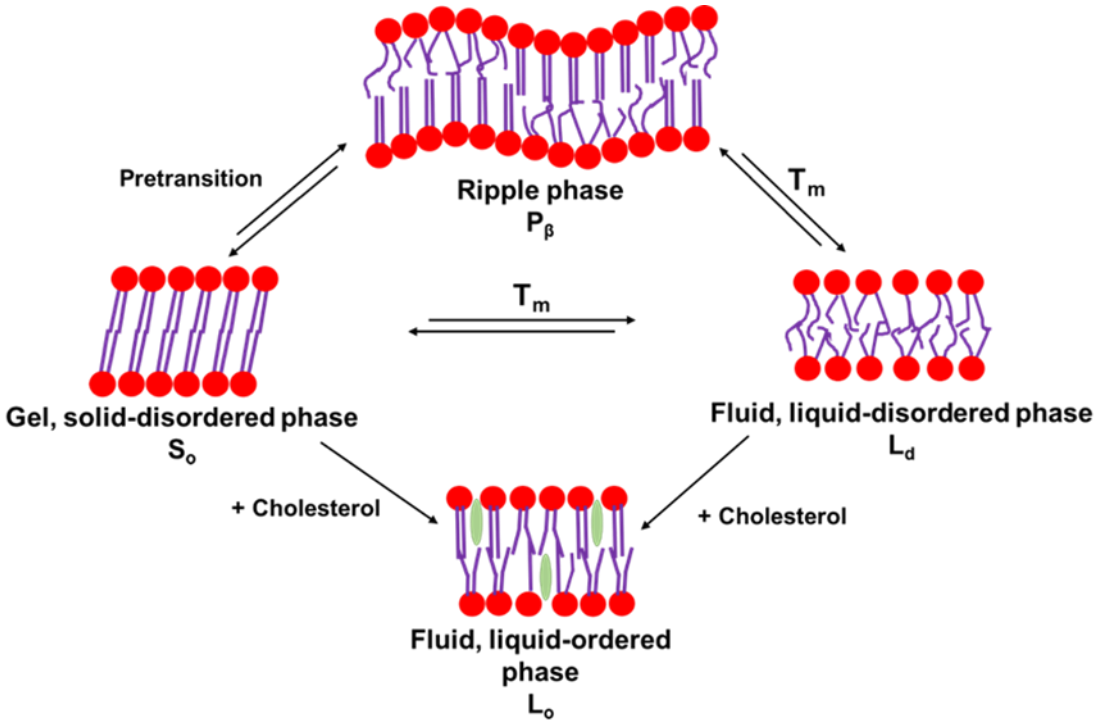

Figure 1.6 *Schematic representation of physical states adopted by lipid bilayers in aqueous solution.*

The solid-ordered phase (also known as gel phase) is characterized by low mobility and a compact arrangement of lipid molecules due to a *trans*-configuration of the hydrocarbon chains, which may be tilted ($L_{\beta'}$) or (L_β) with regard to the bilayer surface

depending on water content (the lower the water content, the smaller the angle of the tilt).[142,143] Among the fluid phases, liquid-disordered (L_d) and liquid-ordered (L_o) phases may be distinguished.[141] The L_d phase is characterized by trans-gauche configuration resulting in shortening of the acyl chains and high degree of lateral and rotational movement of the lipid molecules. The transition between the S_o and L_d occurs at a temperature known as a phase transition (or melting) temperature (T_m), which depends on the length of the hydrocarbon chain, the structure of the headgroup and the degree of unsaturation and is specific for a given lipid type.[141] The lipid-ordered phase, also known as the liquid crystalline phase, is formed in the presence of cholesterol and is characterised by lateral and rotational diffusion that are similar to those of the L_o phase, but with a conformational order similar to the solid-ordered phase.[144–146] The ripple phase P_β exists prior to the main chain melting and is characterized by periodic one-dimensional undulations on the surface of the lipid bilayer as a result of a periodic array of ordered and disordered domains.[147]

The lipid phases, liquid-disordered, liquid-ordered and solid-ordered phase can coexist in the same bilayer. The coexistence of lipid phases has been observed in lipid bilayers composed of various lipid mixtures, usually containing cholesterol.[146,148–150] Various types of lipid molecules preferentially partition into either liquid-ordered or liquid-disordered phase, depending on their structure.

Phospholipids favour the liquid-disordered lipid phase due to the structure of their hydrocarbon chains, the presence of *cis* double bonds which induces a kink and prevents very compact assemblies. Glyco- and sphingolipids on the other hand preferentially partition into the liquid-ordered phases within bilayers due to the characteristics of both the headgroup and the acyl chains.[151,152] Their ordered assembly is stabilized by the hydrogen bonding and van der Waals forces between these groups.[153]

1.4.3 Phase separation in biological membranes

Various studies suggest that preferential partitioning of lipids and the formation of liquid-ordered phases enriched in cholesterol and sphingolipid occurs also in biological membranes.[154,155] However, the presence of these heterogeneous domains, also called lipid rafts, within biological membranes is still under debate.[156] Lipid rafts are usually small, 10-200 nm in diameter[157,158] but may form larger structures by stabilizing protein-protein and protein-lipid interactions.[159,160] Lipid rafts play an important role in many

biological processes, such as the sorting and the transport of both membrane proteins and lipids during endocytosis and exocytosis, in cascade signalling as well as in other cellular processes such as apoptosis, membrane fusion, cell adhesion and migration.[155,157,161,162] It has been also suggested that lipid rafts are the target sites for cellular entry of various pathogens due to the high concentration of cellular receptors[163] and platforms for the assembly of the β-amyloid protein, associated with Alzheimer's disease.[164]

Biological membranes are extremely complex structures, therefore various mimetics have been developed, such as lipid monolayers, supported lipid bilayers or lipid vesicles, to facilitate studies of the behaviour and properties of membranes.[141]

1.4.4 Giant unilamellar vesicles (GUVs)

Lipid vesicles, also called liposomes are cell-mimicking compartments consisting of lipid bilayers. Depending on the size, small (SUV, 20-200 nm), large (LUV, 200- 800 nm) and giant unilamellar vesicles (vary from 1-300 μm) can be distinguished. In biological cells lipid membranes provide a 4 nm thick barrier between the interior and the exterior of a cell.[165] They were first described in the 1950s.[166] Bilayers of GUVs may be formed, depending on the purpose, from a variety of lipid categories, including phospholipids, sphingolipids, glycolipids or sterols. Structural differences between various lipid classes are manifested by differences in their behaviour within a lipid bilayer. Vesicles may also be prepared using block copolymers with amphiphilic properties.[119]

1.4.4.1 Preparation of GUVs

The preparation of GUVs was first described in 1969 by a method now known as gentle hydration.[167] Since then a large number of methods are used to produce GUVs for many applications and these have been described in a several reviews.[165,168,169]

Electroformation (or electro-swelling) is a widely used method for GUV preparation. Liposome formation induced by a static (DC) field was first described in 1986[170] and then modified by application of an alternating (AC) electric field.[171] Electroformation may be performed by depositing a thin layer of lipid in organic solvent onto conductive indium tin oxide (ITO) coated glass, or a platinum wire and applying an external electric field. Spin-coating the lipid onto the slide creates lipid films with defined thickness which aids GUVs formation from lipid mixtures which do not easily form vesicles.[172]

GUVs may also be produced using hydration methods. There are several advantages of hydration methods over electroformation since large vesicle sizes are produced and the preparation conditions are mild.[173] Rapid hydration also produces cell-sized vesicles and requires very short preparation times.[174] A recently developed method involving lipid hydration on an agarose film[175] facilitates the formation of a high yield of cell-size GUVs in solution at high ionic strength and from lipid mixtures usually found to be problematic (for example asolectin). It has also been used to encapsulate biomolecules, while retaining their biological activity.[65]

An emulsion method (also termed inverted or w/o emulsion) was originally described by Pautot *et al*.[176] and involves the assembly of a bilayer on an aqueous droplet by lipid molecules dispersed in oil. The formation of cell-size vesicles, the possibility of forming asymmetric bilayers and high encapsulation efficiencies are among the many advantages of this method.[177,178] The emulsion transfer method has also been used to encapsulate a cell-free expression system. The continuous droplet interface crossing encapsulation (cDICE)[64] method was developed specifically for encapsulation and has been shown to lead to a high yield of cell-size vesicles. The cDICE method has been used to encapsulate a variety of solutions, including colloids, red blood cells, actin filaments[64] and parasites.[179]

Other methods used to produce GUVs include fusion of small vesicles,[180,181] lipid stabilized w/o/w double emulsion,[182] lipid –coated ice droplets,[183,184] lipid dissolved in a water-miscible solvent[185] or micellar lipid solution methods,[186] among others.

1.4.4.2 Applications for GUVs

Since their discovery, GUVs have been used to study biological processes such as budding,[52,53] fusion[54] and fission[55] or various aspects of membrane dynamics,[56,57] membrane composition and phase behaviour.[59,60] In recent years there has been growing interest in using vesicles as microcontainers for the analysis of biochemical reactions[105] and for the development of model cells.[16,187,188]

1.4.5 Lipid molecules used for liposomes preparation.

1.4.5.1 Phospholipids

Depending on the alcohol group, phospholipids are commonly divided into glycerophospholipids and sphingomyelins. Glycerophospholipids are the lipids most

commonly used for the preparation of liposomes. They are the main components of the eukaryotic cell membrane, fulfilling a mainly structural role. They are composed of a glycerol backbone and symmetric hydrocarbon chains typically from 16 to 18 carbons long (figure 1.7).[189] The two main classes of glycerophospholipids used for GUV preparation include phosphatidylcholine (PC) and phosphatidylethanolamine (PE).[190] Two phosphatidylcholines used in this thesis are 1, 2-dioleoyl-sn-glycero-3-phosphocholine (DOPC) and 1, 2-dipalmitoyl-sn-glycero-3-phosphocholine (DPPC). DPPC is the main component of pulmonary surfactant, where it lowers the surface tension. Phosphatidylcholines are the most abundant lipids; they account for more than 50% of lipid molecules in eukaryotic membranes. They are located mainly in the outer leaflet where they are part of the permeability barrier.[190] Phosphatidylcholines with unsaturated acyl hydrocarbon chains usually occur in liquid phase at room temperature. Due to a small head group they have nearly cylindrical shape and self-assemble into a planar bilayer and their inclusion into bilayers causes curvature stress.[191]

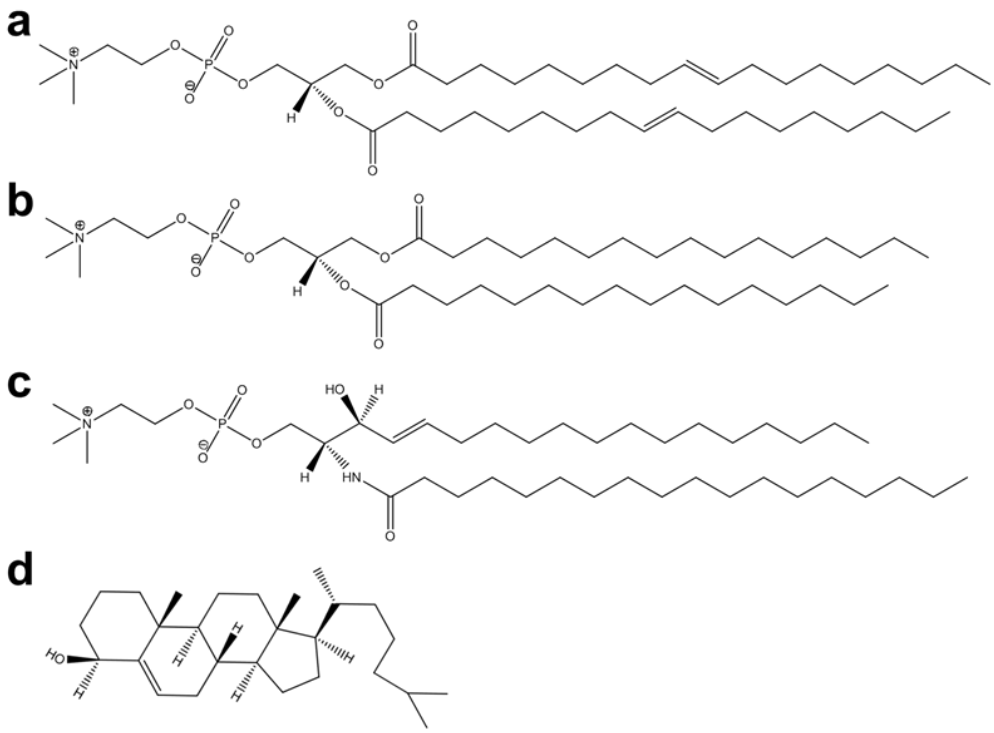

Figure 1.7 *Chemical structures of the phospholipids: DOPC (a), DPPC (b), brain sphingomyelin (c) and cholesterol (d).*

Sphingomyelins (SM) are abundant in cell membranes (2-15% of total lipid content), with higher concentrations found in nerve and red blood cells.[190] The chemical structure of brain sphingomyelin is shown in figure 1.7c. Sphingomyelins are composed

of a sphingosine backbone and asymmetric acyl chains in the tail. They exhibit more tight packing (gel phase) compared to PC due to a higher degree of saturation within the chains (on average 0.1-0.35 cis-double bonds in amide-linked acyl chains). The typical length of an acyl chain is usually more than 20 carbons. Sphingomyelins colocalize and strongly interact with cholesterol both in biological and synthetic membranes.

1.4.5.2 Cholesterol

Cholesterol is a non-polar molecule and in biological membranes is responsible for maintaining structural integrity and fluidity (figure 1.7d). Most of the molecule is embedded within the hydrophobic portion of the bilayer while the –OH group interacts with head groups of other lipids.[190] Cholesterol has been shown to interact preferentially with sphingomyelin than with other non-saturated glycerophospholipids, which dictates the properties of SM/cholesterol bilayers (including low permeability). The strong interaction between sphingomyelin and cholesterol results from the van der Waals interactions between cholesterol and saturated lipid acyl chain of the sphingomyelin.[192] This interaction leads to the formation of a liquid-ordered phase within the lipid bilayers of both natural and synthetic membranes. In biological cells this favoured mixing of sphingomyelin and cholesterol has been implicated in the formation of lipid rafts, dynamic and ordered microdomains serving as an attachment for variety of protein molecules and implicated in membrane signalling and trafficking processes.[154,155,193]

1.4.5.3 Glycolipids

Glycolipids are a class of lipids containing sugar-based headgroups. There are several classes of glycolipids, including glycoglycerolipids, glycophosphatidylinositols and glycosphingolipids.[194] Glycolipids, are major components of biological membranes, especially the outer leaflet. They are also abundant in intracellular membranes such as mitochondria, the Golgi apparatus, the nuclear membrane, lysosome, endosomes and the endoplasmic reticulum[195] or the apical side (facing inwards to the lumen) of polarized epithelial cells.[196]

Glycolipids are composed of a carbohydrate-based head group which is continuously exposed at the surface of a bilayer, maximising the surface available for interactions and hydrocarbon chains buried within the hydrophobic portion of the lipid bilayer (figure 1.8). Glycolipids, like other lipids are amphiphilic, therefore upon self-assembly (usually in mixtures with other lipids) can adopt a variety of structures,

including lamellar, hexagonal or cubic phases.[117] A variety of other structures, including helical ribbons have been observed in the presence of glycolipids.[197] The type of assemblies formed is dictated by the structure of both the head group and the hydrocarbon chain, expressed by a packing parameter.[136] Within the lipid bilayer of biological and synthetic membranes glycolipids can adopt both gel and fluid phases.[198] Transitions between these lamellar phases as for other lipids, is governed by the fluidity of the hydrocarbon chains (and strongly affected by temperature). For the majority of lipid types, the structure of the head group may shift the melt transition temperature in some cases, but generally it is as simple as determining the surface area per lipid molecule.

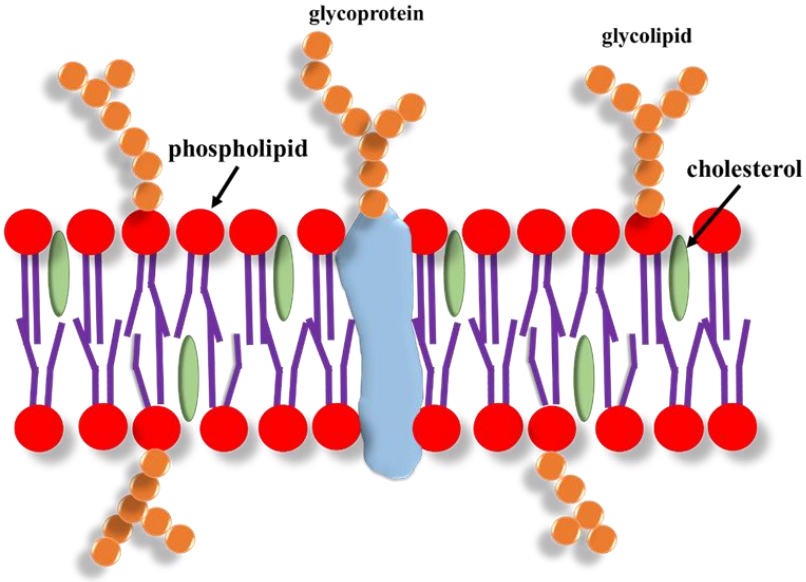

Figure 1.8 *Schematic representation of lipid bilayer composed of phospholipids, cholesterol, glycolipids and glycoproteins.*

However, this is not the case for glycolipid molecules where altering the structural features of the sugar-based head group such as the anomeric configuration of the glyosidic bond, isomeric configuration (D-galactose, D-galactose, D-mannose, etc.), charge or polarity also significantly alters the phase behaviour.[199–201] Hydration of the head group and the penetration of water into the interface have been shown to govern the type of non-lamellar phases adopted by glycolipids.[202] Due to these interesting properties and the biological relevance of these membrane components, the phase behaviour and phase morphology of glycolipids have been extensively studied using both experimental and molecular dynamics simulation approaches.[203–207]

Glycolipids contain a linkage area located between the head group and hydrocarbon chain capable of acting as both H-bond donor and acceptor. Hydrogen

bonding can also occur between the sugar head groups leading to the formation of clusters of molecules and therefore denser packing.[208] Interactions with other lipids, such as sphingolipids and cholesterol and a variety of membrane proteins leads to the formation of glycolipid-rich domains within phospholipid bilayers.[209] The types of microdomains containing glycolipids include glycosynapses (involved mainly in adhesion processes) or lipid rafts (with functions in signalling).[210–212] Glycolipids can also interact with complementary carbohydrates or proteins displayed on neighbouring cells which facilitates the specificity and direction of the interaction.[213]

1.4.5.4 Biological functions of glycolipids.

Glycolipids are involved in a variety of biological functions. For many of those functions, recognition and signal transduction occurs within glycolipid-containing microdomains and through their interactions with other signal modulators such as kinases, G-coupled proteins, GPI-anchored proteins, immunoreceptors, tetraspanins and growth factor receptors.[196,210,214]

The primary cellular functions involving carbohydrate-based signal processing includes cell adhesion, motility, differentiation,[215] growth,[216] proliferation and apoptosis.[217] Interactions between cell surface receptors and carbohydrates present on pathogens leads to recognition of infection and immune response. The most widely studied glycoconjugates are lipopolysaccharides (LPS), present on the surface of Gram-negative bacteria. Their interaction with toll-like receptors (TLRs) and other members of the signalling complex leads to activation of the innate immune system and initiation of inflammation.[218] Interactions between pathogens and host surface glycolipids are often a way to mediate entry into host cells.[209,219,220] Glycolipids have been shown to play a role in the maintenance of membrane integrity,[221,222] photosynthesis[223] or certain aspects of energy transduction within biological systems.[224]

1.4.5.5 Fluorescent lipid analogues

The properties, behaviour and various processes occurring within lipid membranes are often studied using different modes of fluorescent microscopy, such as wide field, confocal or superresolution microscopy.[225] In order to visualize these processes fluorescent lipid analogues are incorporated into lipid membranes. Commercially available fluorescent lipid analogues vary depending on the type of lipid used, the structure and therefore the spectral properties of the fluorescent label and its

location within the lipid molecule (head or chain). Their properties and cellular localization strongly depends on their structure.

Apart from visualization by fluorescence microscopy, fluorescent lipids are also used as a phase-specific labels in phase behaviour studies, sensors of the cellular environment or trackers in cellular transport studies.[226]

1.5 Protein structure and assembly

Proteins are polymeric chains composed of amino acids and are synthesized on ribosomes. They have a primary structure, which refers to the linear sequence of amino acids, determined by genetic information and these are held together by peptide bonds (figure 1.9).

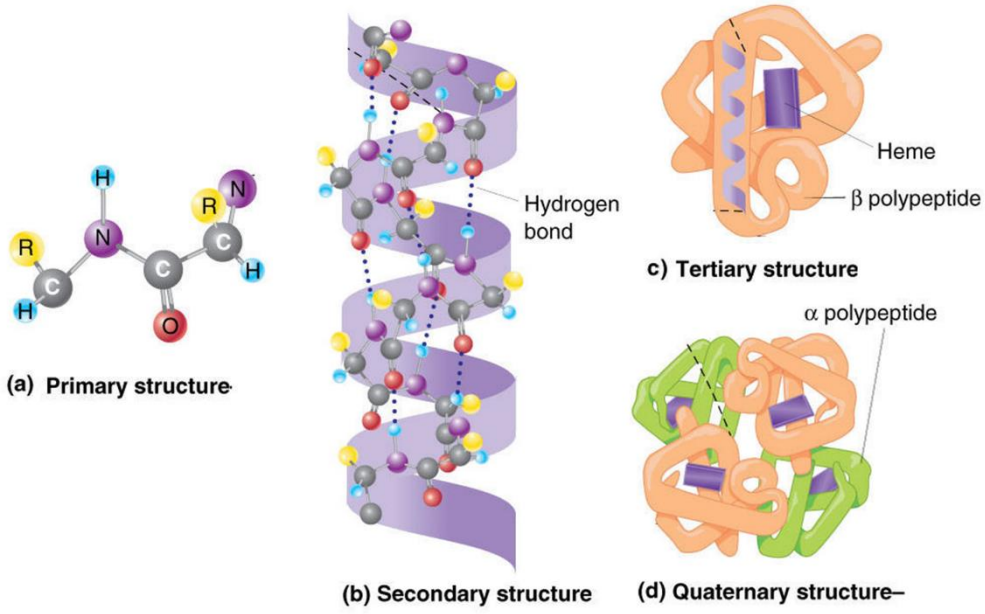

Figure 1.9 *Levels of protein structure.*[227]

The polypeptide chains contain regions of localized organization with specific spatial arrangements, referred to as the secondary structure, stabilized by hydrogen bonding, such as in an α helix (right hand spiral conformation with 3.6 amino acids per turn), β sheet (fully extended alignments of short β strands) or a turn (U-shaped 4 residues long, with a H-bond between the end residues). Regions of polypeptide chains without stabilizing interactions assume a random-coil arrangement.[124]

The protein tertiary structure refers to the three-dimensional protein structure driven by hydrophobic interactions between the nonpolar side chains, stabilized by hydrogen bonding, salt bridges and, in some proteins, by disulphide bonds. These stabilizing forces fold the α helices, β strands, turns, and random coils in a compact

internal scaffold. The quaternary structure of a protein describes the number and relative positions of the subunits in a multimeric protein and is stabilized by the same types of non-covalent interactions and disulphide bonds as the tertiary structure.[227]

1.5.1 Intramolecular self-assembly

Folding a protein into its three-dimensional structure occurs by an intramolecular self-assembly process and is driven by the requirement to lower the free energy. Folding protein may assume various partially folded conformations before reaching the native folded state. Random sampling of possible conformations would require timescales beyond a biological lifetime.[228] The idea of a protein folding pathway was introduced to explain details of protein folding. Another way to present the protein folding is a statistical energy landscape representing possible partially folded states with a corresponding free energy.[229] For protein folding via a two-state transition mechanism in which only the denatured and native states are populated, the energy landscape is relatively smooth, lacking deep valleys and high barriers. However folding scenarios for most proteins involves rough, rugged landscapes representing multiple transient non-native species.

Protein folding has been extensively studied providing insights into the structural diversity of non-native states, folding pathways or the folding efficiency.[230–234] However much remains unknown as the folding pathways of large proteins, membrane proteins or modified proteins have not yet been studied in great detail.[235–237]

1.5.2 Intermolecular self-assembly

Proteins are often found to form oligomers composed of two or more subunits held together by various non-covalent interactions, such as hydrogen bonding, salt bridges or disulphide bonds. The quaternary protein structure is closely linked with its function and interactions with other proteins.[238,239] The four types of proteins based on their structure include fibrous, globular, integral membrane proteins, and disordered proteins. Regardless of the structure type, proteins can self-assemble into larger structures generally termed macromolecular assemblies.[124]

Fibrous proteins assemble into rod or wire-like protein filaments usually via a coiled coil arrangement. Collagen is an example of a fibrous protein. It is a major protein of the extracellular matrix, forming 30-100 nm thick fibrils.[240] Collagen is a structural protein, providing strength to tissues. The collagen triple helix has a super-coiled, right-

handed structure composed of three parallel α-chains, each with a polyproline II helical conformation.[241]

Membrane proteins are either embedded into lipid bilayers (transmembrane protein) or are bound to their surface by electrostatic interactions with anionic lipids. Transmembrane proteins are usually composed of three domains: two water-soluble portions (cytosolic and exoplasmic) and one spanning the membrane, rich in hydrophobic amino acids.[124] Membrane proteins often self-assemble into multidomain complexes, such as ion channels, transporters or receptors.[242,243] One of the most commonly studied transmembrane complexes is the potassium channel. Its transmembrane domain is composed of four identical subunits forming an ion pore at the centre. The pore may be open or closed by conformational change within the channel in response to different signals requiring sensor domain transmitting information to the pore domain. Potassium channels contain a selectivity filter formed by a highly conserved sequence of five residues.[235,243]

Globular proteins are spherical, water soluble molecules found in cytosol and body fluids. They form a variety of self-assembled complexes performing specific functions within the cellular environment. In the case of viruses, the capsid formed by protein assembly is a shell in which its genome is encapsulated.[244] Viruses, such as the tobacco mosaic virus or small plant viruses self-assemble spontaneously from a solution containing capsid proteins and single-stranded RNA.[245,246] Other self-assembled structures formed within the cellular environment include the nuclear pore complex, receptor/signalling complexes, proteasome, DNA polymerase III holoenzyme, RNA polymerase II holoenzyme or nucleosome.[247–253]

1.5.3 Non-native protein assembly

Occasionally, proteins which normally do not form assemblies do so due to changes to solution conditions or conformational change within their structure. Structures formed as a result of non-native protein assembly, also referred to as aggregation, can adopt various conformations (folded up to fully unfolded) and different sizes (from small monomer up to hundreds of micrometres).[254,255] Aggregates can be associated by either covalent bond or non-covalent interactions.

Understanding how and why proteins aggregate is extremely important in various branches of food and in the biopharmaceutical industry.[256] The effects of protein

aggregates present in biopharmaceutical formulations include decreased efficacy and stability or in some cases immunogenic response in patients.[257] Formation of protein aggregates has also been linked to several diseases such as Alzheimer's or Parkinson's disease and therefore better understanding of the aggregation process may lead to development of new strategies resulting in its prevention.[258,259]

Protein solutions are a colloidal fluid (with radius of gyration ca. 1-2 nm) and therefore their stability can be considered in terms of both, the structural stability of the protein molecule and the solution stability.[260–262] The structural stability refers to the preservation of the native (folded) protein conformation. The solution stability discusses the ability of the protein molecules to exist as monomers in solution. Structural and colloidal stability are closely related since the aggregate formation often involves the presence of unfolded or partially folded protein species.[261]

Techniques routinely employed in aggregation studies include chromatography, electrophoresis, mass spectrometry and UV-Vis spectroscopy, circular dichroism spectroscopy, various modes of microscopy and many more.[254,263]

1.5.3.1 Morphology of protein aggregates

Based on morphology, aggregates can be divide into two types: amorphous or fibrillar.[263] Fibrillar aggregates have an average width of 10-20 nm, and are formed by the constituting proteins aligning perpendicular to the fibrillar axis,[264] resulting in a cross-β-sheet structure, identified by an X-ray diffraction signature known as the cross-β pattern.[265] They can be detected using various methods, most commonly by transmission electron microscopy (TEM), optical birefringence and increased fluorescence upon association of dyes such as Congo red and Thioflavin T(ThT).[266] Insoluble amyloid fibrils are formed from soluble proteins, usually by a nucleation driven mechanism.[264] It has been shown that lipid membranes play a role in fibril formation.[267] The mechanism of fibril formation has not yet been proven, however some studies suggests that the initial step involves binding of the protein to the lipid bilayer driven by the electrostatic attraction. Bound proteins are thought to undergo a structural transformation to the β-sheet followed by the oligomerization of membrane bound proteins.[267] Lipid membranes and lipid rafts have also been shown to be the target for the toxic species.[164,267] Several studies have suggested that the oligomeric species formed in the earlier stage of amyloid aggregation are the main cytotoxic species.[268]

Amyloid fibrils have been linked to pathological changes observed in many neurodegenerative diseases. Parkinson's disease is associated with the formation of intracellular fibrillar deposits of aggregated α-synuclein, known as Lewy bodies, in the dopaminergic neurons of the *substantia nigra* of the midbrain and other monoaminergic neurons in the brain stem.[269] Moreover, mutations associated with the early-onset forms of Parkinsonism give rise to neuronal degeneration in the absence of the accumulation of Lewy bodies.[270] Other neurodegenerative disorders associated with formation of protein fibrils include Alzheimer's disease, Huntington's disease and type II diabetes.[271–274] Protein fibrils are also involved in physiological processes. Examples of such protein include a Pmel17 which is a structural template for the formation of melanine polymers or the secretory granules of the endocrine system.[275]

The term amorphous aggregate is used to describe a heterogeneous population of particulates formed in protein solutions, which do not exhibit a long range order. Studying amorphous aggregates has proven difficult due to their heterogeneity and light scattering properties, leading to notions that they lack distinguishable structure.[263]

Certain amorphous aggregates associate with Congo red and ThT, dyes known to bind to the β-sheet structures found in fibrillar aggregates. This suggests that at least some amorphous aggregates undergo structural rearrangement increasing its β-sheet content as observed for insulin in the presence of sulfate anion.[276] However ThT was also shown to bind to hydrophobic pockets of globular proteins, such as human serum albumin[277] or acetylcholinesterase.[278] ThT binding in this case is mediated by the presence of aromatic residues and involves extensive π-stacking with Tyr and Trp residues.

Formation of amorphous aggregates commonly occurs during protein processing,[279] in food (production of dairy products and wine) and in the biopharmaceutical industry.[256,280] The effects of protein aggregates present in biopharmaceutical formulations include decreased efficacy and stability or in some cases immunogenic response in patients.[257] Amorphous aggregates have also been linked to the formation of cataract, the opacity of the eye lens as a result of protein condensation. In congenital forms of cataract the formation of protein condensed phases such as crystals[281] or aggregates[282] is caused by a single amino acid substitution (due to single point mutation) in the sequence of the crystallin proteins. In age related types of cataract, a change in the solution behaviour of the crystallin proteins found in the eye lens occurs as a result of environmental changes, such as oxidative or osmotic stress.[283,284]

1.5.3.2 Factors influencing the aggregation process

Protein solutions are generally thermodynamically unstable and therefore predisposed to aggregation. However aggregation is also strongly influenced by various factors, depending on both the nature of the protein as well as the solution conditions.

Single point mutations have been shown to be a cause aggregation of crystallin proteins without any significant changes within their structure.[282,285,286] The substitution of certain amino acids results in the formation of attractive patches on the surface of crystallin proteins (mainly gamma D crystallin), causing an increase in net protein-protein attractive interactions which in turn leads to the formation of aggregates and crystals of the crystallin proteins.[287,288] Aggregation can be induced by chemical modification of individual amino acids, such as deamidation and oxidation of methionine or cysteine.[255] One particular example of such a modification is the fluorescent labelling of proteins, routinely performed on studies involving fluorescence microscopy. It has been shown that the use of even small fractions of labelled protein may increase the net protein-protein attractive interactions.[289]

Protein aggregation is also strongly influenced by the solution conditions. Altering the pH of the solution changes the overall charge of the protein and higher charge of the protein results in stronger electrostatic repulsion between molecules.[290] The addition of salts at high concentrations may cause screening of charges and therefore a reduction in the electrostatic repulsions. The presence of various co-solutes has been shown to stabilize the native protein conformation.[291,292] Aggregation of various proteins can also be influenced by the presence of lipid bilayers, mainly in case of fibrillar proteins.[293,294]

1.5.3.3 Mechanisms of protein aggregation

The aggregation of proteins depends on the solution conditions as well as the thermodynamic stability of the folded protein. Aggregates may form via several pathways, often occurring simultaneously within a protein solution, resulting in a formation of aggregates with various characteristics.[295] There are five main mechanisms of protein aggregation.

1. Reversible association of the native monomer

This mechanism involves monomer assembly into small oligomers due to self-complementarity of protein monomers in their native state.[295] This process may be

reversible if the aggregates are formed by non-covalent interaction, or irreversible if formation of covalent bonds (such as disulphide linkages) is involved.

2. Aggregation of a conformationally - altered monomer

This mechanism occurs when a protein undergoes a conformational change or partial unfolding (transition state) and is generally irreversible.[295] Studies suggests that it is the most dominant mechanism of aggregation, easily promoted by heat or shear stress and implicated in many diseases, involving aggregation of prions or alpha-synuclein.[296]

3. Aggregates formed from a chemically-modified product

This mechanism involves chemical degradation, such as oxidation, deamidation or proteolysis of the native monomer. The chemically modified monomers can induce the aggregation of native monomers by altering their structural properties. Aggregates formed via this mechanism can be composed of chemically modified monomers, but can also include native monomers.[295]

4. Nucleation-controlled aggregation

This mechanism involves two stages; nucleation and growth. Nucleation is the rate limiting step and involves the assembly of monomers to form a critical sized nucleus. Once formed nucleus acts as a seed for further growth of the aggregates.[263,295]

5. Surface induced aggregation

This mechanism involves an adsorption to surfaces during protein handling and storage. It is initiated by binding (usually reversible) of the native monomer to surfaces, which induces a conformational change in the monomer structure.[295] Aggregation propagates either on the surface or in the bulk, if the altered monomer is released into the solution. Surface induced aggregation is similar to nucleation-controlled aggregation, with the surface acting as a nucleus.

1.5.4 Characteristics of proteins used in this research

1.5.4.1 Green fluorescent protein (GFP)

Green fluorescent protein was first isolated, together with aequorin, from the *Aequorea victoria* jellyfish (figure 1.10a) by Shimomura et al.[297] Soon after the excitation/emission spectrum of GFP was published,[298] followed by its crystal structure[299] and the identification of the structure of the chromophore.[300] However, it was not until the cloning[301] and expression of GFP in other organisms,[302,303] showing that all of information necessary for synthesis of functional protein was contained within

its sequence, that the potential of fluorescent proteins has been realized.[304] GFP and other fluorescent proteins are used for a large number of applications including detection of gene expression, monitoring localization and fate of fusion proteins, fluorescent tag addition to various cell organelles or detection of various conditions such as Ca^{2+} level or membrane potential.[304]

The structure of wild-type GFP is referred to as a β-can (figure 1.10b). It is composed of an 11-stranded β-barrel with an α-helix running inside the barrel along the axis of the cylinder and other short helical fragments at the ends of the cylinder.[305] The chromophore, p-hydroxybenzylideneimidazolinone is formed from residues Ser65-Tyr66-Gly67 and is buried in the centre of the cylinder (figure 1.10 c). A large number of polar amino acids, including Gln69, Arg96, His148, Thr203, Ser205, and Glu222 and structured water molecules are buried adjacent to the chromophore.[304]

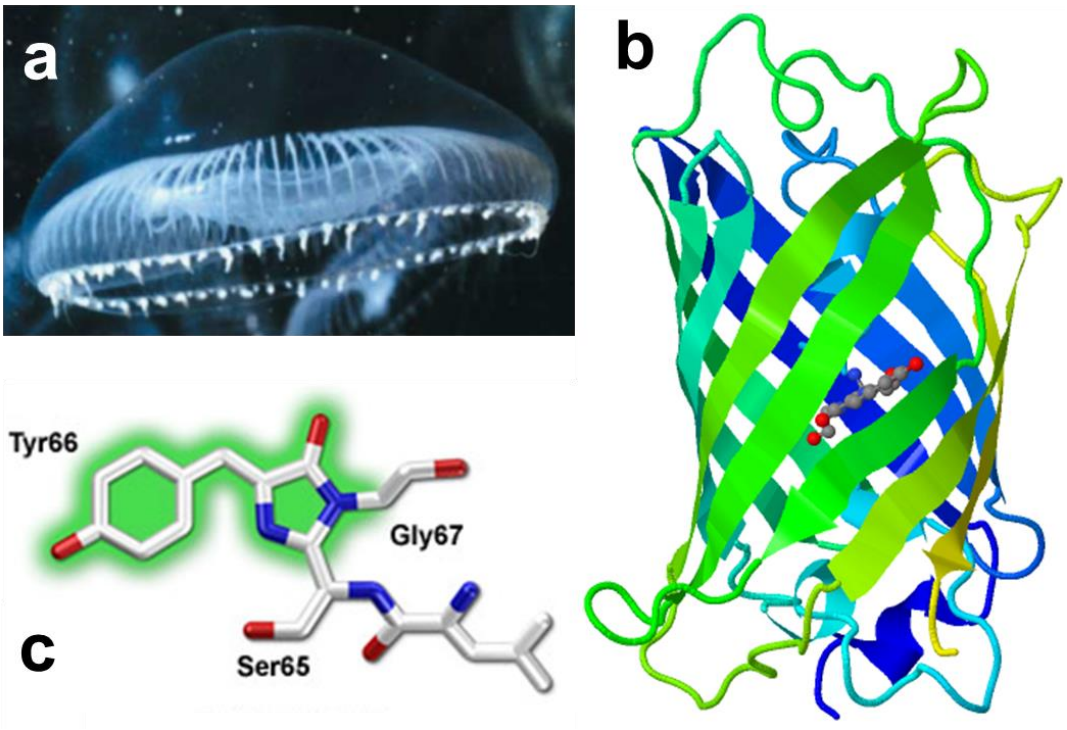

Figure 1.10 *Aequorea victoria jellyfish (a) from which the wild-type GFP was initially purified,*[306] *(b) crystal structure of wild-type GFP with the 11 β-sheets forming a β can structure (Protein Date Bank Id code 1WMA) and the structure of the chromophore of (c).*[307]

Wild-type GFP has a major excitation peak at 395 nm and a minor peak at 475 nm. Excitation at 395 nm results in emission peaking at 508 nm, while excitation at 475 nm gives an emission maximum at 503 nm.[308] The dependence of the emission spectrum on the wavelength of the exciting light is a result of the presence of two distinct species, both protonated and deprotonated which are not equilibrated within the lifetime of the

excited state.[304] Folding of wild-type GFP is efficient at or below room temperature, but it is greatly reduced at higher temperatures.

A large number of GFP variants have been developed by introducing various mutations, altering components of the chromophore or altering properties of the protein, such as improved folding at 37°C or reduced aggregation at high concentrations. GFP variants are usually classified based on the nature of the chromophore, into seven classes, which have a distinct set of excitation and emission wavelengths.[304]

Emerald GFP belongs to a class 2 grouping variants with phenolate anions forming the chromophore. Replacement of serine at position 65 with threonine causes ionisation of the chromophore, resulting in increased maturation,[309] suppression of the 395 nm excitation peak (natural phenol) and the enhancement and shift of the 470-475 nm peak to 489-490 nm.[310] Other mutations, such as F64L, S72A, N149K, M153T and I167T (figure 1.11), improve folding at higher temperatures, resulting in greater brightness.

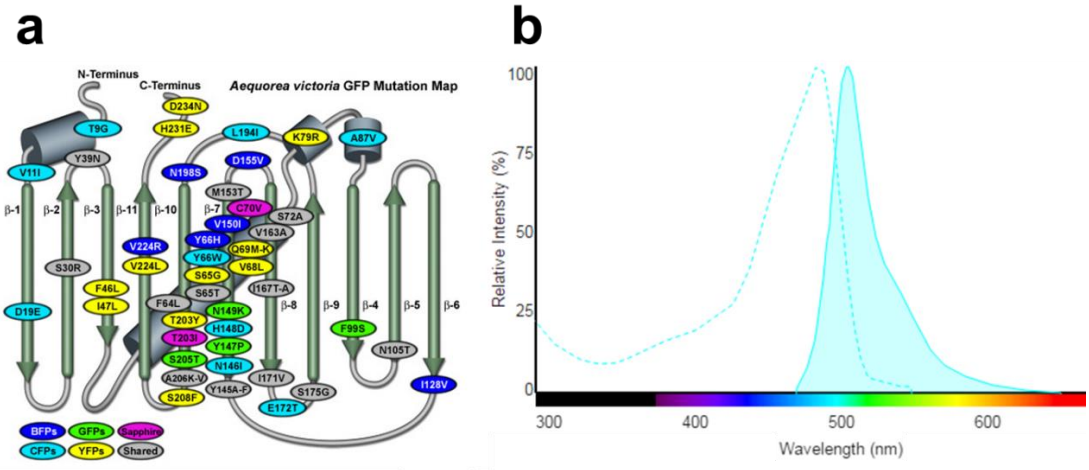

Figure 1.11 *GFP mutation map listing common mutations overlapped with a topological layout of the peptide structure (a). The β-sheets are represented as green cylinders (arrow pointing towards the C-terminus) and α-helices are shown as gray cylinders. Mutations are color-coded to represent the variants of fluorescent protein to which they apply (bottom left corner); folding, shared and monomerizing mutations are shown in gray. Emission/excitation spectrum of the emerald GFP protein (b), one of the green variants of GFP.*

EmGFP has quantum yield of 0.68, molar extinction coefficient of 57 $mM^{-1}cm^{-1}$ and relative fluorescence of 100%, making it one of the brightest variants of GFP in its class.[311] Measuring photostability of this protein has been difficult due to an initial photobleaching component. Recent results of photostability measurements reported as time required to photobleach from 1,000 to 500 photons per second per molecule in live cells under widefield arc-lamp illumination, was found to be 101 s for EmGFP.[312] In

comparison, that value for the superfolded EmGFP was found to be 157 s. Other recent publications do not report photostability issues in a number of applications, including cell-free protein synthesis[313] or fluorescence imaging.[314]

1.5.4.2 Bovine serum albumin (BSA)

Bovine serum albumin is also known as "Fraction V" which refers to the Cohn method of purification of blood plasma and its use as a treatment for severe blood lost.[315] Serum albumin is a globular protein produced in the liver and has a half-life of up to 19 days. It is the most abundant protein in the blood and is responsible for maintaining the colloidal osmotic pressure in blood vessels.[316] Other functions of serum albumin include transport and the distribution of a variety of molecules including metabolites, hormones or drugs, buffering pH or preventing degradation of folic acid.[317] Albumins have several binding sites facilitating binding of various molecules.

BSA has a structure similar to human serum albumin with 76% sequence homology.[318] The primary structure of BSA, containing 583 amino acids leads to the synthesis of a multi-domain monomer of BSA[319] with molecular weight of 66 kDa. The sequence of albumins has a unique arrangement of disulphide double loops. Nine such loops are found in the BSA structure, forming three homologus domains: I, II, and III, shown in figure1.12. These are further divided into subdomains; A consisting of six helices and B with four helices.[317] Some interesting characteristics of BSA's amino acid sequence include a high percentage of cysteine and charged residues as well as lack of sites for enzymatic glycosylation. The secondary structure of BSA consists of α-helices (55%), β-sheets (16%) and disordered structure (29%) and its tertiary structure is stabilized by 17 disulphide bridges.

Most structural investigations of albumin have been based on human serum albumin with more than 50 crystal structures of HAS available in the Protein Data Bank. Recent studies of the BSA structure reveal differences in the structure of serum albumin from various mammals.[316,319]

BSA is widely used in research, mainly as a nutrient in cell culture, as a reagent in a variety of assays, such as ELISA, immunoblotting, immunohistochemistry or as a molecular weight standard.[319] BSA is also commonly used as a model protein drug.[320,321]

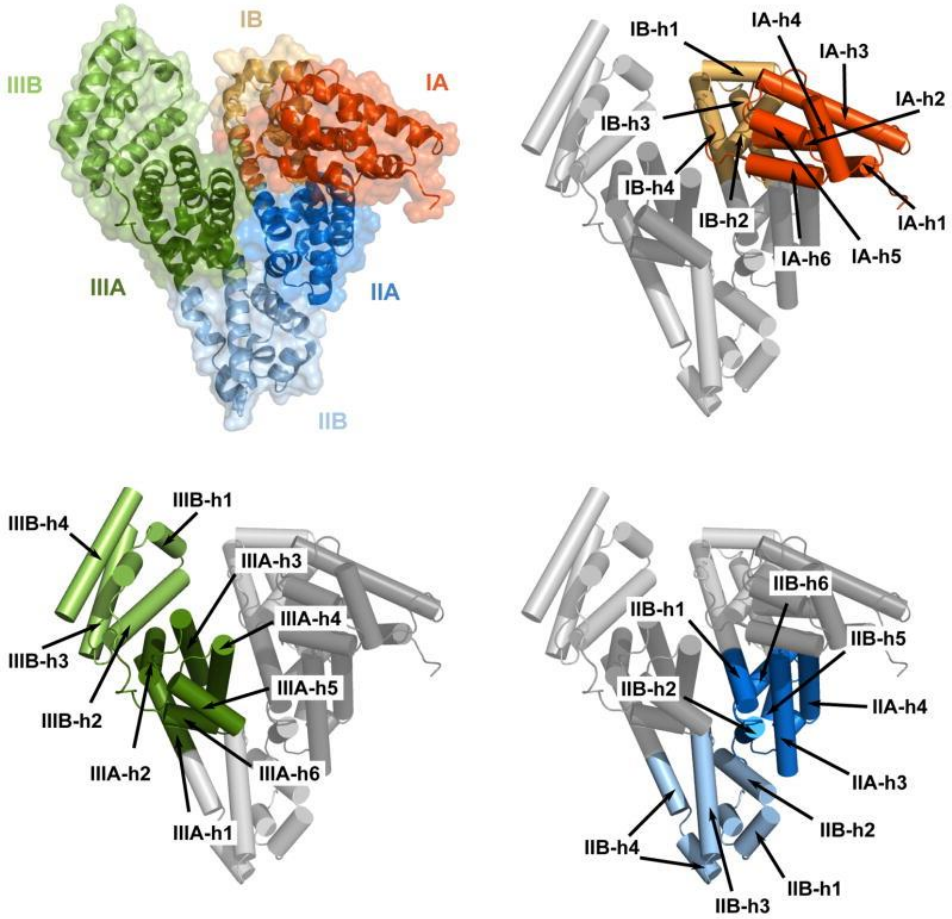

Figure 1.12 *Structure of bovine serum albumin; domains and elements of secondary structure,*[316] *Protein Data Bank Id code 3V03.*

1.5.4.3 Human γD-crystallin (HGD) and the Pro23 to Thr (P23T) single mutant

The α-, β- and γ-crystallins are the most abundant proteins of fibre cells in the eye lens of vertebrates.[322] The concentration of crystallin proteins within the eye lens exceeds 400 mg/ml,[323] which results in a high refractive index, up to 1.418 in the centre of lens,[324] which is required for correct light focusing on the retina. Crystallins are mainly structural proteins, however α-crystallin also functions as a molecular chaperone preventing aberrant protein interactions.[325]

The γ-crystallins are small, compact, globular proteins. They exhibit short range attractive interactions, unlike the α- and β-crystallins, which were shown to display mainly repulsive interactions in solution.[326] Due to this difference in behaviour γ-crystallins are responsible for reducing the osmotic pressure in the fibre cells and maintaining the transparency of the eye lens.[322,327] The γ-crystallins are soluble at very

high concentrations but their attractive interactions result in increased susceptibility to phase separation.

Human γD-crystallin (HGD) is one of the most abundantly expressed γ-crystallin in the lens.[328] It is composed of 174 residues with two polypeptide domains forming a monomer shown in figure 1.13.[329] Several single point mutants of γD-crystallin resulting in protein condensation (causing increased light scattering) have been implicated in congenital cataract.[281,282] Age-related cataract is the formation of aggregates as a result of environmental stress or post-translational protein modifications.[330]

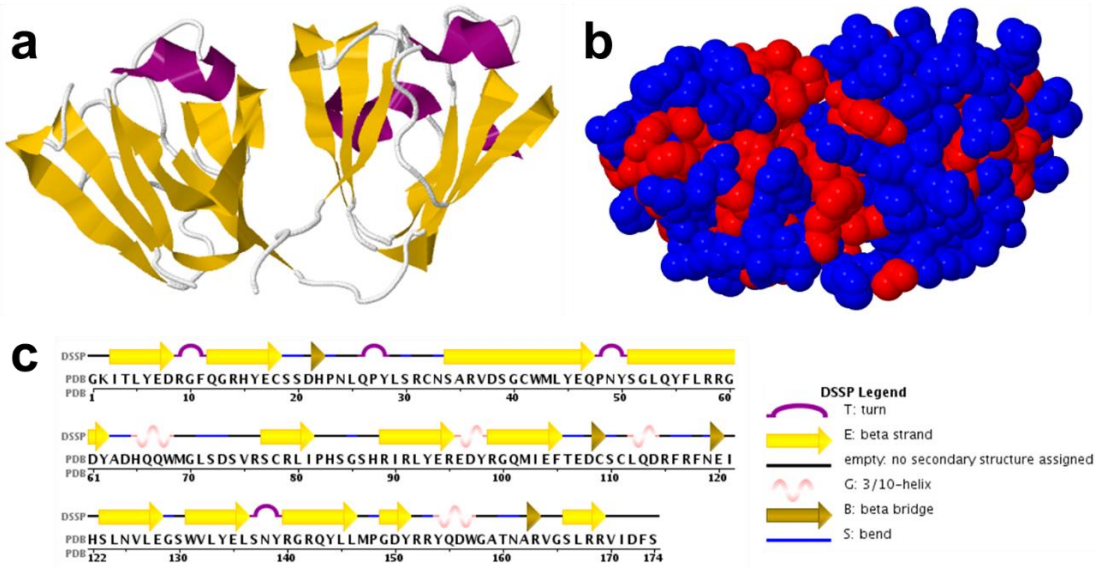

Figure 1.13 *Crystal structure of human γD-crystallin, cartoon representation of the secondary structure (a), the space fill representation illustrating hydrohobicity (b) and the amino acid sequence (c). Protein Data Bank Id code 1hk0.*

One of the single point mutations of the human γD-crystallin is the Pro23 to Thr (P23T) substitution. This mutation results in significant decrease in solubility (2 mg/ml at room temperature) compared to wild-type HGD[282] without major conformational changes in the protein structure.[331] Additionally, the solubility of P23T decreases with increases in temperature.[282] It has been proposed that lower solubility of the P23T mutant is caused by increased hydrophobicity due to the presence of "sticky patches" on the protein surface and decreased flexibility of the backbone.[285,286,332] Other substitutions at the 23 position such as P23V and P23S were also shown to invert the temperature dependence of the solubility line but result in a less drastic decrease in solubility.[282,287]

1.6 Thesis motivation

The motivation for this work was to further our understanding of self-assembly of biomolecules and its role and applications in model cell development. To-date, the self-assembly of lipids and glycolipids have been extensively studied, however many aspects of their phase behaviour remain unclear. In particular the phase behaviour of synthetic glycolipids is of interest since these types of molecules can be used as a mimics for molecular recognition studies.

The self-assembly of proteins is not only a feature of natural biological function but can also be associated with a pathological state in protein condensation diseases (such as Parkinson's disease, Alzheimer's disease or cataract disease) or reduced quality of biopharmaceutical protein products. Protein aggregation has traditionally been studied in a bulk, but this approach is not always optimal since it is not the best representation of the cellular environment. Studies of assembly in model cells offers a cell-like environment, but without the complexity of biological cells. The model cell can therefore be designed to contain only the required components, making both observation of the assembly (potentially without the use of fluorescent labels) and the interpretation of data less problematic. Additionally, model cells are much more resistant to a range of environmental conditions, which are unsuitable for live cell imaging, such as broad pH range or increased temperature and as such they can be used as a microreactors, to study processes in cell-like volumes but beyond only physiological conditions.

Chapter 2

Experimental techniques and data analysis

2.1 Buffer and regents preparation

2.1.1 Buffers

For the preparation of buffers, analytical grade salts and Milli-Q water (ultra-pure) were used. The pH of the buffer solutions was adjusted using appropriate concentrated acid or base solutions. Buffer solutions were filtered through 0.45 μm, 47 mm nylon membranes (Merck Millipore, Ireland) and degassed using a vacuum pump (Merck Millipore, Ireland) if necessary. Buffers for preparation of protein solutions were supplemented with 0.02% of sodium azide (Fisher, UK).

2.1.1.1 Sodium phosphate

Sodium phosphate buffers at pH 7.4 at various molarities were prepared by dissolving disodium phosphate (Na_2HPO_4, 268.07 g/mol; Fisher, UK) and monosodium phosphate (NaH_2PO_4, 156.01 g/mol; Fisher, UK) (quantities listed in table 2.1) in 1 L of Milli-Q water. If necessary pH was adjusted using appropriate concentrated acid or base solution.

Table 2.1 *Quantities of the components of sodium phosphate buffer with varying molarity.*

	5 mM	**20 mM**	**50 mM**
Na_2HPO_4	1.037 g	4.149 g	10.37 g
NaH_2PO_4	0.176	0.705 g	1.76 g

2.1.1.2 Tris-HCl

0.5 M Tris-HCl at pH 6.8 was prepared by dissolving 6.06 g of Tris base (121.1 g/mol; Merc, Germany) in 100 ml of Milli-Q water and adjusting pH with concentrated HCl.
1 M Tris-HCl at pH 8.8 was prepared by dissolving 30.3 g of Tris base (121.1 g/mol; Calbiochem, USA) in 250 ml of Milli-Q water and adjusting pH with concentrated HCl.

2.1.1.3 Glycine-HCl

50 mM glycine-HCl at pH 3 was prepared by dissolving 3.752 g of glycine (75.07 g/mol, Calbiochem, USA) in 1 L of Milli-Q water) and adjusting pH with concentrated HCl.

2.1.1.4 Sodium acetate

50 mM sodium acetate at pH 4 was prepared by dissolving 244.96 mg of sodium acetate (136 g/mol; Fisher, UK) in 200 ml of Milli-Q water and adjusting pH with acetic acid.

2.1.1.5 Sodium borate

50 mM sodium borate, pH 8.5 was prepared using 1.55 g of boric acid (61.8 g/mol; Sigma, USA) in 500 ml of Milli-Q water and adjusting pH with concentrated NaOH.

2.1.1.6 Loading buffer – 20 mM sodium phosphate 0.5 M sodium chloride 30 mM imidazole 0.02% sodium azide

Loading buffer for protein purification, pH 7.4, was prepared using 4.149 g of disodium phosphate, 0.705 g of monosodium phosphate, 29.22 g of sodium chloride (58.44 g/mol; Fisher, UK), 2.042 g of imidazole (68.08 g/mol; Sigma, Ireland) and 0.2 g of sodium azide (65 g/mol) in 1 L of Milli-Q water.

2.1.1.7 Elution buffer – 20 mM sodium phosphate 0.5 M sodium chloride 1 M imidazole 0.02% sodium azide

Elution buffer for protein purification, pH 7.4, was prepared by dissolving 4.149 g of disodium phosphate, 0.705 g of monosodium phosphate, 29.22 g of sodium chloride, 68.08 g of imidazole and 0.2 g of sodium azide in 1 L of Milli-Q water.

2.1.2 Reagents

2.1.2.1 Sucrose

A 2 M sucrose solution was prepared by dissolving 17.114 g of sucrose (342.29 g/mol; VWR, Belgium) in Milli-Q water and made up to 25 ml.

2.1.2.2 Thioflavin T (ThT)

4 mM thioflavin T stock solution was prepared by dissolving 12.75 mg of ThT (318.86 g/mol; Sigma, USA) in Milli-Q water and made up to 10 ml. The solution was filtered through 0.22 μm syringe driven filters (Millipore, Durapore) and stored at 4°C for up to a week.

2.1.2.3 Fluorescein isothiocyanate (FITC)

A 5 mM FITC stock solution was prepared using 9.73 mg of FITC (389.38 g/mol; Fisher, USA) in 5 ml of Milli-Q water. FITC solutions were stored at -20°C for up to a month. A 10mg/ml FITC for BSA labelling was prepared using 10 mg of FITC in 1 ml of DMF.

2.1.2.4 Sodium chloride (NaCl)

A 2 M sodium chloride solution was prepared by dissolving 11.68 g of sodium chloride in Milli-Q and made up to 100 ml.

2.1.3 Reagents for the *E. coli* culture

Where indicated, reagents for the *E.coli* cell culture were autoclaved at 121°C and 0.212 MPa pressure for 20 minutes in a SX-500E TOMY autoclave (Seiko, Japan).

2.1.3.1 Ampicillin stock solution

A 50 mg/ml ampicillin solution was prepared using 1 g of ampicillin (Fisher, China) in 20 ml of Milli-Q water. The solution was filtered through a 0.22 μm filter and stored at -20°C.

2.1.3.2 LB agar for agar plates

37 g of LB agar (Fisher, Ireland) was dissolved in 1 L of Milli-Q water and autoclaved. Upon cooling (ca. 50°C) a stock solution of ampicillin was added to a final concentration of 100 μg/ml. The solution was poured into 10 cm petri dishes, allowed to set and stored at 4°C for up to a week.

2.1.3.3 LB broth

25 g of LB broth (Fisher, Ireland) was dissolved in 1 L of Milli-Q water and autoclaved. Upon cooling (ca. 37°C) a stock solution of ampicillin was added to a final concentration of 100 μg/ml and the broth was inoculated from a single *E. coli* colony selected from an LB agar plate.

2.1.3.4 IPTG stock solution

1 M IPTG solution was prepared using 4.76 g of Isopropyl β-D-1-thiogalactopyranoside (238 g/mol; Fisher, Ireland) in 20 ml of Milli-Q water. Aliquots were stored at -20°C.

2.1.3.5 Cell lysis buffer

Lysis buffer was prepared by dissolving 0.0788 g (50 mM) of Tris-HCl, 0.01461 g (25 mM) of NaCl and 0.0074 g (2 mM) of ethylenediaminetetraacetic acid (EDTA; Fisher, USA) in 10 ml of Milli-Q water.

2.1.4 Reagents for the mammalian cell culture

The solutions listed below were prepared using sterile reagents and solvents. All of the steps were performed in the laminar air flow cabinet using aseptic technique. Cell culture media were stored at 4°C and stock solutions at -20°C.

2.1.4.1 Complete cell culture media (cDMEM)

450 ml of DMEM (4.5 g/l glucose, 4 mM L-glutamine, no sodium pyruvate; HyClone, USA) was supplemented with 50 ml of bovine calf serum (BCS) or fetal bovine serum (FBS) (heat inactivated at 54°C for 45 min; Sigma, USA) and 2.5 ml of penicillin (10000 units/ml) - streptomycin (10 mg/ml) stock solution (Sigma, USA) and stored at 4°C.

2.1.4.2 Serum free cell culture media (sfDMEM)

50 ml of DMEM was supplemented with 250 µl of Pen-Strep stock solution.

2.1.4.3 Poly-D-lysine stock solution

A 100 mg/ml stock solution was prepared using 5 mg poly-D-lysine (70-150 kDa; Sigma, USA) in 50 ml of Milli-Q water. The solution was filter sterilized (0.22µm) and stored at 4°C.

2.1.4.4 Phosphate-buffered saline (PBS buffer)

To prepare 1X PBS, 10 ml of 10X (Sigma, USA) solution was added to 90 ml of Milli-Q water. Alternatively a PBS tablet (Oxoid, UK) was dissolved in 100 ml of Milli-Q water. The solution was filter sterilized (through 0.22 µm filters). Aliquots were stored at -20°C.

2.1.4.5 Blasticidin stock solution

A 0.2 mg/ml blasticidin stock solution was prepared by dissolving 2 mg of Blasticidin S HCl (Fisher, Ireland) in 10 ml of Milli-Q water. The solution was filter sterilized (through 0.22 µm syringe driven filters). Aliquots were stored at -20°C.

2.1.4.6 L-glutamine stock solution

A 200 mM L-glutamine stock solution was prepared by dissolving 2.923 g of L-glutamine (146.15 g/ml; Fisher, Brazil) in 100 ml of Milli-Q water. The solution was filter sterilized (0.22 µm filters). Aliquots stored at -20°C.

2.1.4.7 Trypsin-EDTA solution

To prepare a 1X trypsin-EDTA solution, 300 µl of 10X trypsin-EDTA (Sigma, Ireland) was added to 2.7 ml of sterile PBS buffer.

2.2 Protein solutions

2.2.1 Bovine serum albumin (BSA) stock solution

BSA (Sigma, USA, Lot SLBL2871V) was used without further purification. A fresh protein solution was prepared each time by dissolving BSA in 20 mM sodium phosphate buffer pH 7.4, incubated for 1 hour at room temperature and then washed of co-precipitated salts by repeated ultrafiltration using Amicon Ultra 10 kDa (Millipore, Ireland) centrifugal devices at 3500 g. BSA concentrations were determined by UV/Vis absorbance using the extinction coefficient 0.66 ml mg^{-1} cm^{-1}.

2.2.1.1 BSA labelling

FITC is widely used to fluorescently tag a variety of proteins. The isothiocyanate group, which in the isomer I is located on the C-4 of the benzene ring reacts preferentially with surface exposed primary amines and the terminal amino group. Here BSA solution was fluorescently labelled with the isomer I of FITC (Pierce Biotechnology, USA).

Procedure: FITC was dissolved in DMF at 10 mg/ml. The BSA was hydrated for 1 hour in the conjugation buffer (50 mM borate buffer at pH 8.5) at final concentration of 2-2.5 mg/ml. The FITC solution was added at a 20-fold molar excess to the BSA and incubated at room temperature in the dark. The excess of unbound FITC was removed using fluorescent dye removal columns (Pierce Biotechnology, Rockford) followed by multiple washes using Amicon Ultra 10 kDa centrifugal filter units, until no FITC was detected within the filtrate.

Calculations: The concentration of labelled BSA was calculated as follows:

$$protein\ conc.(M) = \frac{A_{280} - (A_{\max} \times CF)}{\varepsilon} \times dilution\ \ factor \qquad 2.1$$

where: A_{max} is the absorbance of the dye solution at the wavelength maximum (λ_{max} for FITC is 494 nm), CF is the correction factor adjusting for the amount of FITC absorbance at 280 nm (CF for FITC is 0.3) and ε is the molar extinction coefficient of BSA, 43,824 $M^{-1}cm^{-1}$. To calculate the degree of labelling following equation was used:

$$degree\ of\ labelling = \frac{A\ of\ \ labelled\ \ BSA}{\varepsilon' \times BSA\ conc.\ (M)} \times dilution\ \ \ factor \qquad 2.2$$

where ε' is the molar extinction coefficient of FITC, 68,000 $M^{-1}cm^{-1}$.

2.2.2 Emerald green fluorescent protein (EmGFP) stock solution

EmGFP was expressed in *E. coli* and purified via affinity chromatography (see section 2.7 and 2.9). Upon purification the elution buffer was exchanged with 20 mM sodium phosphate, pH 7.4 and the solution was stored in the dark (to prevent photobleaching) at 4°C. Buffer exchange was performed using a stirred ultrafiltration unit and Ultracel 10 kDa membranes (Millipore, Ireland). For small volumes and to increase concentration, Amicon Ultra 10 kDa were used, with centrifugation at 3500 g. EmGFP concentrations were determined by UV/Vis absorbance using the extinction coefficient 0.918 ml mg^{-1} cm^{-1}.

2.3 Microscopy

2.3.1 Introduction

Microscopy is a technique which produces magnified images of objects or features not visible to the human eye. The first optical microscope, composed of a single lens, was invented by Robert Hook in the 1660s. Over the next few centuries the design of the microscope was altered by new approaches and discoveries, such as optimisation of the single lens design by Anton von Leeuwenhoek or the introduction of Kohler illumination.[333] Modern microscopes are equipped with interchangeable components incorporating multiple modes of microscopy in one instrument. Components of microscopes may be arranged as inverted or an upright designs. Inverted microscopes are becoming more popular, especially in biological sciences due to the possibility of direct observation of cells directly in culture flasks.

There are three main branches of microscopy which include optical, electron and scanning probe microscopy. Optical microscopy uses light and multiple component optical systems. There are several optical microscopy techniques based on the type of sample illumination. Electron microscopy uses a beam of accelerated electrons as a source of sample illumination. Scanning probe microscopy (SPM) uses a physical probe to scan the specimen and offers resolution of the order of fraction of a nm.[334]

2.3.2 Light microscopy techniques

2.3.2.1 Components of light microscope and bright field analysis

Light is electromagnetic radiation with properties of both particles (energy defining wavelength and vibrational frequency) and waves (electric and magnetic field, oscillating as sinusoidal waves in perpendicular planes). These properties can be related using the following equation:

$$E = \frac{hc}{\lambda} = h\nu \qquad 2.3$$

where E is the energy (ergs), , h is Plank's constant, c is the speed of light (3×10^8 m/s), λ is the wavelength (μm) and ν is the frequency (cycles/s).

The electromagnetic spectrum is shown in figure 2.1. The resolution limit of the human eye, electron and light microscopy is indicated above the scale. The visible light, used in light microscopy is a small portion of the spectrum.

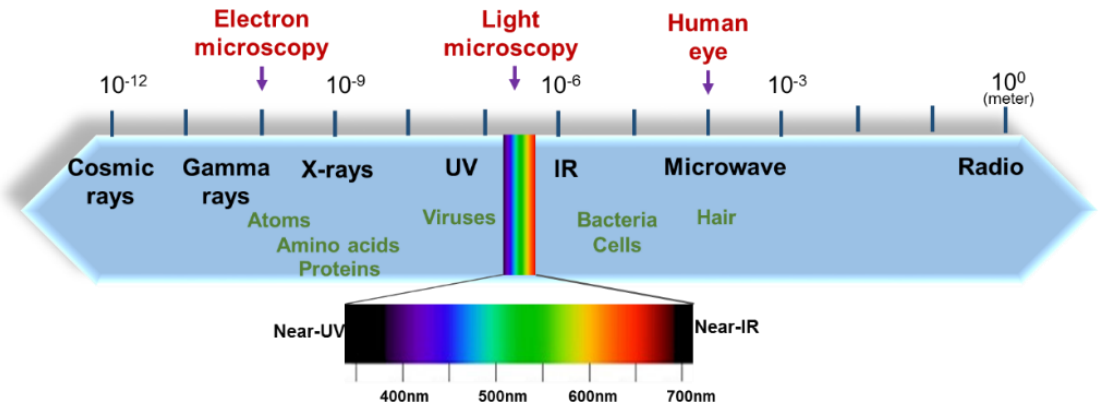

Figure 2.1 *The electromagnetic spectrum with different classes of electromagnetic radiation in the range of wavelengths between picometer up to a meter.*

A typical microscope setup is illustrated in figure 2.2. Objectives are designed to image specimens either with air (refractive index, n=1) between the objective and the cover glass (n=1.5) or with other media, most commonly oil (n=1.51), water (n=1.33) or glycerol (n=1.47). Using an immersion medium reduces the difference in refractive index (the ratio of speed of light in vacuum and in the medium), therefore preventing the refraction of light at the lower surface of the lens and allowing higher working numerical apertures to be achieved.[335]

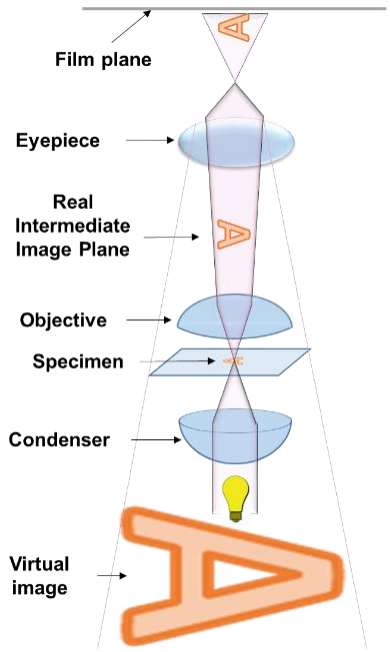

Figure 2.2 *Image formation in modern light microscope.*

The resolution of a microscope is the shortest distance between two points of a specimen that can be viewed as separate entities. The limit of resolution of a microscope is restricted by the wavelength of light but also depends on the numerical aperture of the objectives, substage condenser and proper alignment of the optical components. A simple equation to calculate the limit of resolution when the $NA_{cond} \geq NA_{object}$ is shown below

$$R = 0.61\lambda / NA \qquad 2.4$$

where, R is the resolution (µm), λ is the wavelength of light (µm) and NA is the numerical aperture of the objective. If the $NA_{cond} < NA_{object}$ then the resolution is expressed as:

$$R = \frac{1.22\lambda}{condenser\ NA + objective\ NA} \qquad 2.5$$

The resolving power of a microscope increases when light with shorter wavelengths is used. Therefore the best resolution is achieved when using near-ultraviolet, followed by blue, green and then red light.

Final magnification of an image is a result of both the magnification of the objective and the eyepiece.[333,336] The optimal magnification required to resolve a details present within the image is set between 500 and 1000 times of the NA. Use of higher magnification will enlarge the object but will not add further detail resulting in blurred or indistinct images.

Protocol: Bright field images were acquired using an Olympus BX61 microscope (Japan), equipped with various lenses (between 10x and 100x; Olympus, Japan). Images

were viewed and recorded using CellF software and processed using ImageJ.[337–339] Figures were prepared using FigureJ plugin for ImageJ.[340]

2.3.2.2 Phase contrast microscopy

Phase contrast microscopy was developed in the 1930's by Frits Zernike. His discovery revolutionised biology and medicine (Nobel Prize in 1953). This technique facilitates high-contrast imaging of transparent, unstained specimens, which do not absorb much light, such as living cells. Such objects, known as phase objects induce a phase shift of light passing through them due to diffraction and scattering, however either the human eye or a digital camera cannot detect differences in the phase of light. The optics of the phase contrast microscope transform the differences in phase of light to amplitude differences within the image.[333]

In phase contrast microscopy the light passing through an object is divided into two components (direct and diffracted waves) shown in figure 2.3 by an annulus ring positioned at the front focal plane of the condenser.[336]

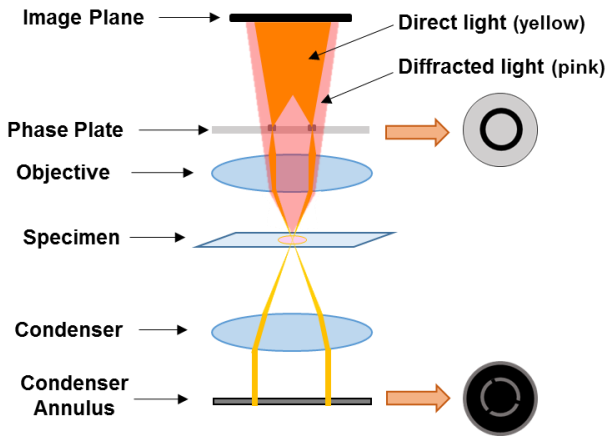

Figure 2.3 *Path of light and the location of optical components in phase contrast microscopy.*

The direct (or surrounding) bright light do not interact with the specimen. The scattered diffracted wave is relatively faint and retarded compared to the direct wave. Light passing through the specimen forms a ring of light at the rear focal plane of the objective. Light rays diffracted after interaction with the specimen are distributed over the objective's focal plane. A phase difference of the two components (increasing the contrast) is achieved by placing a phase plate at the rear focal plane of the objective. The design of the phase plate is such that the surrounding light travels through the thinner part (so shorter distance) of the plate and therefore travels faster compared to the diffracted light. The plate is also coated with an absorbing film, reducing the amplitude of passing

light. Both of the waves are focused at the intermediate image plane, where the phase differs by λ/2 which results in a destructive interference pattern.[341] In the positive (or dark) phase contrast image dark specimen is observed on the light background.

The main limitation of phase contrast microscopy is the presence of optical artefacts in the form of halos around outlines of specimens. The presence of halos affects the detection of boundaries within the specimen.[333]

Protocol: Phase contrast images were acquired using an Olympus BX61 microscope (Japan), equipped with a phase rings and UPlanFLN lenses of various magnifications. Images were recorded using CellF software and processed using ImageJ. Figures were prepared using FigureJ plugin for ImageJ.

2.3.2.3 Polarized light microscopy

Polarization microscopy is used to study several properties, such as molecular order, thickness and the refractive index of a variety of specimens. Diverse biological specimens studied using polarized light include lipid bilayers,[342,343] microtubules and actin filaments,[344] chloroplast,[345] collagen[346] and cell walls.[347] Polarization microscopy is also commonly used in geology, chemistry, optical crystallography and material sciences.[348]

In a beam of linearly polarized light, electric field vectors of all waves vibrate in planes parallel to each other. The orientation of the plane in which vibrations occur is described by the angle of the tilt.[336] Polarized light can be obtained using a polarizer such as a Polaroid sheet, which is a film of parallel arrays of polyiodide crystals. Such a filter has a transmission axis, which allows light through, vibrating parallel to that axis and blocking other rays. Two polarizers (the second one is usually called the analyser) with their transmission axis parallel to each other will transmit polarized light (figure 2.4). As the relative orientation of the transmission axis changes from parallel to perpendicular, the amount of transmitted light decreases. In the case of crossed polarizers (arranged at 90°) linear light from the polarizer is blocked by the analyzer resulting in final transmission of light close to 0.[336]

Birefringent materials, such as quartz are optically anisotropic and cause splitting of a ray of light into two rays (linearly polarized and with electric field vectors vibrating in perpendicular planes) travelling through it by separate paths; the ordinary (following the laws of refraction) and extraordinary ray.[336] This is known as double refraction and is caused by the geometrical arrangement of the crystal and the differences of its refractive

index with the respect of the direction. Birefringent materials contain a unique optical axis (called uniaxial) and if the beam of light is perpendicular to that axis the resulting rays exit at the same location but are shifted in phase due to different path lengths.[348] The perpendicular orientation of the two vectors and the phase shift give rise to elliptically polarized light. This is how most biological samples are viewed using polarized light microscopy.[336]

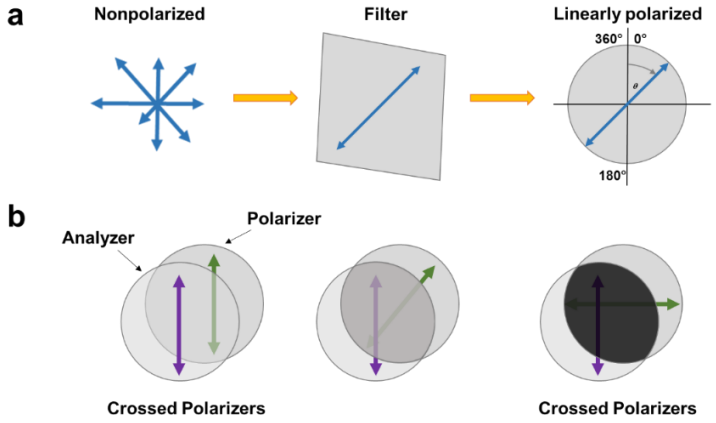

Figure 2.4 *Polarization of light obtained with a polarizing filter (a). The light transmission through the analyzer and polarizer depends on the orientation of their transmission axis (b).*

The speed of light in a given medium is influenced by the interaction of light with electric fields present in that medium. This property is known as the dielectric constant (ε) and is related to the refractive index (*n*) of the medium ($\varepsilon = n^2$). Polarized light microscopy of biological samples is possible due to the polarizability (distortion from the normal distribution of the electron cloud upon the interaction with light[130] of biological molecules. The more polarizable the molecule the more extensive its interaction with light resulting in lower velocity of passing light.[336] Biological polymers, such as cellophane, composed of cellulose are polarizable in the direction parallel to the polymeric chain. In this direction the refractive index is the highest, resulting in the slowest light transmission. Therefore the polarizability of larger structures, such as cellulose fibers strongly depends on their orientation and so the orientation of their optical axis in respect to the direction of polarized light.

Any compound microscope may be converted into a polarizing microscope by addition of the polarizer and analyzer into the light path. Birefringent specimens observed using both the polarizer and the analyzer produce images of light and dark contrast depending on the shape and molecular orientation of ordered structures.

Protocol: Polarized light images were acquired using an Olympus BX61 microscope, equipped with polarizer (rotatable) and (stationary) analyser and various magnification

lenses. Images were recorded using CellF and processed using ImageJ. Figures were prepared using FigureJ plugin for ImageJ.

2.3.2.4 Fluorescence microscopy

Fluorescence microscopy is a technique used to study properties of a variety of organic and inorganic molecules. Fluorescence is a property of atoms or molecules with the ability to absorb light of a specific wavelength followed by emission of light of a longer wavelength (therefore lower energy). Fluorescence microscopy is especially popular in material sciences and biology due to the difficulties in obtaining sufficient contrast when using other types of microscopy.[349]

Absorption of a photon of light of specific wavelength by a fluorescent molecule happens on a timescale of femtoseconds and results in the excitation of the molecule from the ground state to its excited state as shown in figure 2.5. The excited states may be formed as a result of physical (absorption), mechanical or chemical processes.[350]

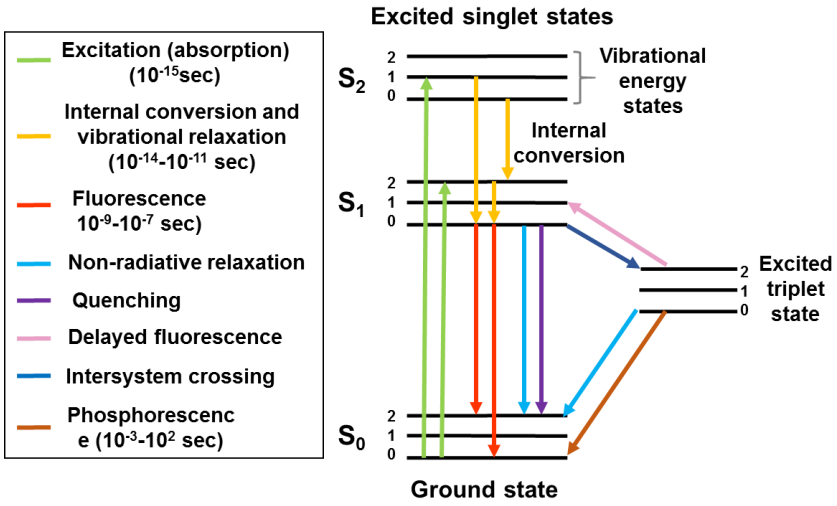

Figure 2.5 *Example of a Jabłoński diagram.*[350]

Excitation is followed by relaxation to the lowest excited state (S_1) in a process referred to as internal conversion, most widely known as Franck-Condon principle. It results in a loss of energy due to a collisions of the excited fluorophore with solvent molecules.[351] Relaxation from the lowest excited state to the ground state is accompanied by emission of photons of lower energy and is referred to as fluorescence.[352] If the relaxation to the ground state involves intersystem crossing to a triplet state, the light emission occurs in a process known as phosphorescence.[353] Delayed fluorescence can also be observed as a result of transitions occurring from the excited triplet state through

the lowest excited (singlet state) and back to the ground state.[351] These transitions are graphically presented in the form of a Jabłoński diagram (figure 2.5).

2.3.2.5 Fluorescent molecules

Molecules capable of producing fluorescence are known as fluorophores (or chromophores). They can be divided into two main groups.[354] Intrinsic fluorophores are naturally fluorescing molecules, such as aromatic amino acids (phenylalanine, tryptophan and tyrosine), enzyme cofactors (NADH), and fluorescent proteins (GFP). Extrinsic fluorophores (fluorescent dyes) are fluorescent molecules added to the sample (or chemically bonded to it) in order to provide the fluorescence or change the characteristics of an intrinsic fluorescence.[352,355] Fluorophores absorb and emit light over a characteristic spectrum of wavelengths, known as absorption/emission spectra (figure 2.6). The shape of the peaks depends on solvent conditions, such as pH, O_2 concentration, the nature of the solvent, etc. and whether the given fluorophore is free in solution or bound to another molecule.[336] The difference in wavelength between the absorption and emission maxima is known as the Stokes shift. Fluorescent molecules having a large Stokes shift are particularly useful in microscopy since it is easier to separate their emission and absorption using appropriate filters.[352]

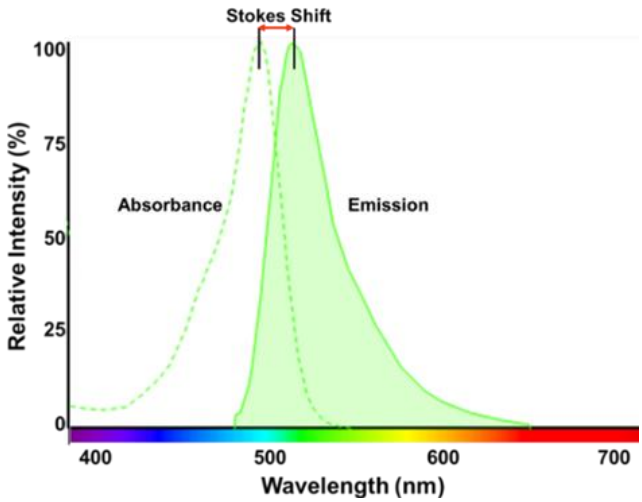

Figure 2.6 *Absorption and emission spectrum of FITC (Fluorescence SpectraViewer, Fisher).*

The molar extinction coefficient of a fluorophore is a measure of its ability to absorb light under specific conditions. It is reported at specific wavelengths and is used to convert units of absorbance to the molar concentration.[350] The quantum yield (Q) represents the efficiency of a given fluorophore to emit fluorescence and is calculated as

a ratio of emitted photons relative to the number of absorbed photons.[354] Fluorescence is proportional to the absorbed light multiplied by the quantum yield:

$$F = I_0 \varepsilon [c] x Q \qquad 2.6$$

where I_0 is the intensity of light illuminating the solution, ε is the molar extinction coefficient (at the absorption λ_{max}), $[c]$ is the concentration of the fluorophore and x is the pathlength of the beam of light passing through the solution.[351] If values of I_0, ε, x and Q are known, the concentration c can be determined as a function of F.

Another important characteristic of fluorescent molecules is the fluorescence lifetime which is a measure of time during which the fluorophore remains in excited state before the relaxation process take place.[354] In a uniform population of molecules excited with a brief pulse of light, the decay of fluorescence intensity as a function of time can be described by following exponential function:

$$I(t) = I_0 e^{(-t/\tau)} \qquad 2.7$$

where $I(t)$ is the intensity measured at time t, I_0 is the initial intensity and τ is the fluorescence lifetime, the time during which the fluorescence decays to $1/e$ of I_0.

As shown by Herman (1998)[351] the contribution of processes, such as quenching, phosphorescence and internal conversion, competing with the fluorescence (and therefore reducing its intensity) for access to the electrons in the excited state can be combined into a single variable named the non-radiative rate constant (k_{nr}). The quantum yield can be expressed as:

$$Q = \frac{photons\ emitted}{photons\ absorbed} = \frac{k_f}{k_f + k_{nr}} = \frac{\tau_F}{\tau_o} \qquad 2.8$$

where k_f is the rate constant for the fluorescence decay, τ_o is the intrinsic fluorescence (the lifetime of the excited state in the absence of non-radiative processes, it is an inverse of the rate constant of fluorescence decay) and τ_F is the measured lifetime which includes a contribution from the intrinsic lifetime and non-radiative processes.

Fluorescence microscopes commonly use epi-illumination systems (figure 2.7) where the light from the source is reflected by a dichromatic beam splitting mirror onto the back aperture of the objective which acts as a condenser.[351] A beam splitter reflects light with shorter wavelengths and transmits light of longer wavelengths. Fluorescence emitted by the specimen is collected by the objective and passed onto the detector (photomultiplier tube or a camera). Since fluorescence emitted by specimens is usually

quite weak the objectives used need to have a high numerical aperture (and preferably oil immersion) in order to collect as much of the light emitted in all directions.

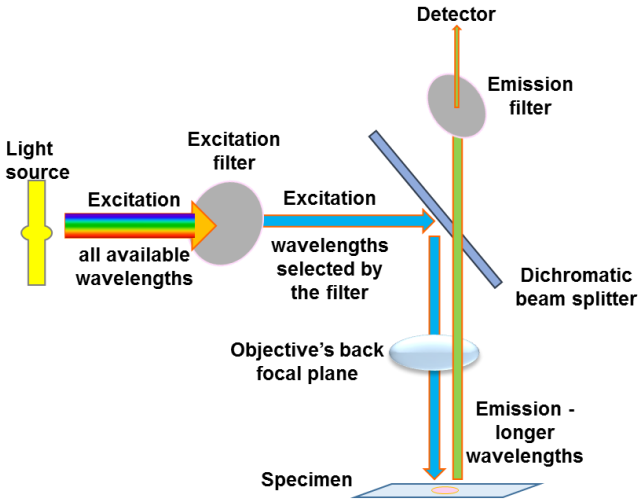

Figure 2.7 *Path of light and the location of optical components in fluorescence microscopy.*

The most commonly used light sources used in fluorescence microscopy include xenon arc and mercury vapour lamps. They emit light of various wavelengths, the wavelengths required for excitation of the specimen are selected using an excitation filters. Undesirable wavelengths which did pass through the filter (usually only a small percentage) are transmitted by the beam splitter. The emission filter also allows for selected wavelengths to be passed onto the detector, preventing the detection of scattered, not-filtered excitation light. The excitation and emission filters consist of glass disks coated with either a refractive or interference coating. Depending on the coating, various ranges (long and short or narrow pass filters) of wavelengths may be passed through while others are blocked. Combinations of short and long pass filters are used when very specific wavelengths are required.

The epi-fluorescence set-up is one of many fluorescence techniques available. The choice of the type of fluorescence microscopy depends on the nature of the dyes and the specimen and the type of information to be obtained. A variety of advanced microscopic techniques utilising fluorescent emission have been developed, such as superresolution, fluorescence recovery after photobleaching (FRAP), total internal reflectance fluorescence microscopy (TIRF) and many more.[350,356]

Protocol: Fluorescence microscopy images were acquired using an Olympus BX61 microscope with either UPlanSApo or UPlanFLN PH3 lenses. Fluorophores were excited using a mercury vapour lamp and either FITC (excitation 470 nm – 495 nm, emission 510

nm – 550 nm) or CY5 (excitation 620 nm – 660 nm, emission, long pass from 665 nm) filters. Images were viewed and recorded using CellF software and processed using ImageJ. Figures were prepared using FigureJ plugin.

2.3.2.6 Confocal microscopy

Confocal microscopes have several advantages over traditional fluorescence microscopy, such as control over depth of field, significant background reduction and removal of out of focus fluorescence (through spatial filtering), which is very useful when imaging thick specimens.[357] Most of the optical elements of the confocal and widefield fluorescence microscopy perform identical functions. The most commonly used light source is a laser system. For confocal microscopy, emitted light passes through a pinhole aperture located in a conjugated plane with a scanning point on the specimen.[358] A second pinhole aperture is located in front of the detector. Laser light is reflected by the dichromatic mirror onto the specimen in a defined focal plane. Fluorescence emitted by the specimen is focused as a confocal point at the pinhole aperture below the detector.

Some of the differences between confocal and widefield microscopy include the detection system (confocal consists of a photomultiplier tube) or use of pinhole aperture acting as a spatial filter (not used in widefield microscopy).[357] Another significant difference is the specimen illumination, which in traditional fluorescence microscopy has a shape of wide cone which results in high background emission from object located beyond and above the focal plane. In confocal microscopy the specimen is illuminated by a point of illumination. This significantly reduces the photobleaching and the out-of-focus emission, resulting in high-contrast images.

Protocol: Images were acquired using an Olympus FluoView1000 laser scanning confocal microscope (Tokyo, Japan), using 458 and 633 nm lasers as a source of excitation. Images were analysed using FluoView (Olympus) and ImageJ. Figures were prepared using FigureJ plugin for ImageJ

2.3.3 Transmission electron microscopy (TEM)

Transmission electron microscopy (TEM) is a microscopic technique where images are obtained using an electron beam. TEM is widely used to study the structure, morphology and chemical properties of variety of samples, including biological material, metals or minerals. Development of the first TEM designed by Knoll and Ruska in 1931 was driven by the limit of resolution encountered by light microscopy.

The source of the electron beam in a TEM instrument is usually a tungsten filament, connected to voltage source, which releases electrons upon introduction of a sufficiently high current.[359] A gas pressure of around 10^{-4} Pa is used to prevent generation of an electrical arc and to reduce the collisions of electrons with gas atoms. A small electron beam (between 5 and 0.1 nm in diameter) is necessary to achieve a good image quality.[341,360] The wavelength of an electron depends on its velocity; the higher the velocity the smaller the resulting wavelength. The wavelength of an electron is also related to its energy and in TEM, λ may be as little as 0.004 nm for a 100 keV electron microscope.[361] Shifts in the beam of the electron path are introduced with the aid of an electrostatic field.[360] Magnification in TEM is achieved by varying the ratio of the distances between the specimen and the objective lens. Apertures are used to control the intensity of the electron beam and to remove scattered electrons.[362]

Thin specimens for TEM analysis are usually deposited onto a copper grid, which then is placed onto the sample holder and introduced into the path of the beam of electrons.[363] The interaction of the electron beam with the specimen occurs simultaneously with its passage through it. If necessary, the specimen may be stained with a variety of reagents, such as uranyl acetate to aid imaging. TEM yields black and white images, where the darker areas represent more dense parts of the specimen.

Protocol: TEM analysis was performed at the Royal College of Surgeons in Ireland. TEM images were acquired using Hitachi H-7650 Transmission Electron Microscope with a side mount 2k AMT camera. Specimen was mounted onto pioloform mesh copper grids, blotted and air dried for several minutes. TEM was operated at 100 kV. Images were taken at 7 k or 10 k magnifications. Figures were prepared using FigureJ plugin.

2.4 Preparation of giant unilamellar vesicles (GUVs)

2.4.1 Lipid stocks

The synthetic glycolipid used in these experiments was obtained as a white powder, stored at -20°C and used without further purification. All of the lipids purchased from commercial sources were used without further purification. Stocks were prepared in chloroform or a 9:1 chloroform/methanol solution and the aliquots were stored under argon at -20°C or -80°C in case of fluorescent dyes.

Lipids used for vesicle preparation are listed in the table 2.2.

Table 2.2 *Lipids used for vesicles preparation.*

DOPC	1,2-dioleoyl-sn-glycero-3-phosphocholine	Avanti Polar Lipids (Alabama, USA)
DPPC	1,2-dipalmitoyl-sn-glycero-3-phosphocholine	Avanti Polar Lipids (Alabama, USA)
PEG-DOPE	1,2-dioleoyl-sn-glycero-3-phospho-ethanolamine-N-[methoxy (polyethylene glycol) - 2000] (ammonium salt)	Avanti Polar Lipids (Alabama, USA)
BSM	18:0 Brain sphingomyelin	Avanti Polar Lipids (Alabama, USA)
Cholesterol	(3β)-cholest-5-en-3-ol	Calbiochem (Germany)
Egg-PC	1, 2-Diacyl-sn-glycero-3-phosphocholine	Sigma (USA)
Liss Rhod PE (18:1)	1, 2-dioleoyl-sn-glycero-3-phosphoethanolamine-N -(lissamine rhodamine B sulfonyl) (ammonium salt)	Avanti Polar Lipids (Alabama, USA)
NBD-PC (14:0-12:0)	1-Myristoyl-2-[12-[(7-nitro-2-1,3-benzoxadiazol-4-yl)aminododecanoyl]-sn-Glycero-3-Phosphocholine	Avanti Polar Lipids (Alabama, USA)
Bodipy FL C_5 ceramide	N-(4,4-difluoro-5,7-dimethyl-4-bora-3a,4a-diaza-s-indacene-3-pentanoyl) sphingosine	Invitrogen (California, USA)
cholesteryl bodipy FL C_{12}	cholesteryl 4,4-difluoro-5,7-dimethyl-4-bora-3a,4a-diaza-s-indacene-3-dodecanoate	Invitrogen (California, USA)
Bodipy TR ceramide	N-((4-(4,4-difluoro-5- (2-thienyl)-4-bora-3a, 4a-diaza-s-indacene-3-yl) phenoxy) acetyl sphingosine	Invitrogen (California, USA)

Lipid mixtures were prepared by addition of appropriate amounts of the stock solution of each component, based on weight or molar ratios. When necessary, solutions were diluted using chloroform or 9:1 chloroform: methanol mixtures. All of the lipid solutions were handled using a 100 µl Hamilton gas tight glass syringe and glass bottles.

2.4.2 Electroformation

An electroformation cell was built in-house on a microscope slide using a protocol based on Okamura *et. al.*[364] Three sets of incisions, 2 mm apart, were made on the bottom of a perfusion chamber (Grace Bio-labs, USA) to accommodate two platinum wires (Fisher, Ireland) and a narrow glass capillary, 50-100 µm in diameter (figure 2.8). The

glass capillary was coated with a thin layer of a 0.1 M lipid solution in chloroform, and allowed to dry for several minutes. A perfusion chamber was placed onto the adhesive surface of an imaging spacer (Secure-Seal, Grace Bio-labs, USA) which was in turn placed onto a microscope slide and allowed to adhere for several minutes. The chamber then was filled with Milli-Q water ensuring no air bubbles were formed around the Pt wires or the glass capillary. The platinum wires were connected to a function generator (built in-house) operating at 10 Hz and 2 V using crocodile clips.

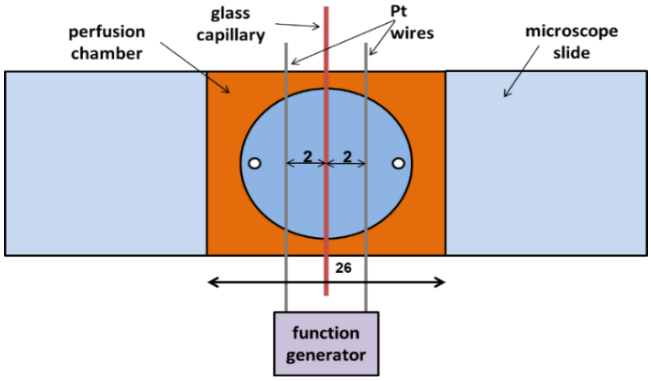

Figure 2.8 *Experimental setup for electroformation on a standard glass microscope slide.*

Electroformation was carried out typically for two hours. For visualization and measurement, the assembly was disconnected from the function generator and placed directly under the microscope. During electroformation evaporating Milli-Q water can be replace through the opening in the cover of the perfusion chamber if necessary.

2.4.3 Gentle hydration

A previously described method was used.[173] 20 µl of lipid of the required composition, dissolved in chloroform (0.1 M) was placed in a pear-shaped flask. 180 µl of chloroform was added. Excess chloroform was removed by evaporation, forming a thin layer of lipid on the inner surface of the flask. The flask was then placed under vacuum for 24 hours to remove any remaining chloroform. Nitrogen gas was passed through MilliQ water at 50ºC and then onto the dried lipid film for 40 minutes. Enough sucrose solution (0.1 M) was added (gently to avoid disturbing the film) to the flask up to cover the lipid film. The flask was the sealed and placed in an oven at 50ºC for 24 hours. The contents of the flask were gently swirled once to ensure homogeneity but further movement was limited to minimise shearing of GUVs before observation.

2.4.4 Rapid hydration

A previously published protocol[174] was modified slightly as follows; 20 µl of lipid of the required composition, dissolved in chloroform (0.1 M) was placed in a pear-shaped flask. A mixture of 150µl of ethanol and 900 µl of chloroform were added. Milli-Q water (7 ml) was added to the flask along the inside wall and the organic phase was removed using a rotary evaporator at temperature ca. 40ºC.

2.4.5 Lipid film hydration on an agarose film

A protocol published by Horger *et al*.[175] and modified by Tsai *et al*.[65] was used. Agarose was dissolved in Milli-Q water (1% w/w), and boiled for up to 2 minutes. 300µl of agarose was spin-coated onto a glass microscope slide at a speed of 1380-1500 rpm for 30 sec (SCK-100 Spin Coater, Instras Scientific). The slide was then dried for 30 minutes at 37ºC. A lipid mixture containing DOPC and PEG-DOPE at the appropriate ratio was dissolved at a concentration of 3.75 mg/ml in 95:5 (v/v) chloroform/methanol and deposited onto the agarose film by spin-coating (150 µl for 5 minutes at 1380-1500 rpm). The slide was placed under vacuum for 1 hour. An imaging chamber was placed on top of the microscope slide. 200 µl of 50 mM sodium phosphate buffer or Milli-Q water was injected into the chamber and incubated for 1 hour. For encapsulation experiments, 30 µl of 0.25 mM FITC in 20 mM sodium phosphate or 25 µl of cell-free expression medium was placed on top of the lipid film and incubated for 1 h (at 4°C in case of cell-free solution). To aid visualisation vesicles were diluted by adding a further 300 µl of the sodium phosphate.

2.4.6 Inverted (or w/o) emulsion method

A protocol based on the method originally described by Pautot *et al*.,[176] and modified by Noireaux and Libchaber[51] was used. A lipid mixture of the desired lipid composition was dissolved in mineral oil (Sigma, Ireland) at a concentration of 5 mg/ml. The mixture was then heated and sonicated at 50ºC for 1 hour and incubated overnight at room temperature. 200 µl of the clear supernatant and 1-1.5 µl of PBS buffer were vortexed for a few seconds to form a water-in-oil emulsion. After leaving the emulsion to rest for a few minutes, 50 µl of the emulsion was placed on top of PBS buffer (950 µl) and centrifuged at 2000 rpm for 1 hour to form GUVs.

A modified version of the above protocol was also used, mainly for the encapsulation experiments.[365] Egg-PC solution at 10 mg/ml in 9:1 chloroform: methanol was prepared. The solution was placed in a glass bottle and the solvent was evaporated under a stream of nitrogen. A bottle containing the lipid film was place under vacuum overnight to remove traces of solvent. Mineral oil was added to a final concentration of 0.5 mM (ca. 0.38 mg/ml). The solution was incubated at room temperature for 1 hour and then sonicated for 1 hour at a temperature below 40°C.

For the encapsulation experiments two solutions were prepared:

1. the inner solution containing molecules to be encapsulated, such as FITC, BSA, EmGFP in 20 mM sodium phosphate, pH 7.4 or cell-free expression medium.
2. the outer solution composed of sodium phosphate or small molecular weight component of the cell-free expression medium supplemented with sucrose at a concentration matching the osmolarity of the inner solution.

30 µl of the inner solution was added to 300 µl of a lipid in oil solution and vortexed gently or pipetted up and down to form an emulsion, which was then equilibrated for a few minutes. 250 µl of the emulsion was placed on top of the outer solution and centrifuged at 18000 g, 4°C, for 30 minutes. The GUV suspension was removed from the bottom of the tube by gentle aspiration.

2.4.7 Continuous droplet interface crossing encapsulation (cDICE)

A previously published cDICE method protocol was used.[64] A 0.5 mM egg-PC solution in mineral oil was prepared as described for the emulsion method. The formation chamber was made of two 35 mm petri dishes lids (one with an opening of 1 cm) glued together. The chamber was filled with 3 ml of the outer solution (sodium phosphate buffer supplemented with sucrose at concentration matching the osmolarity of the internal protein solution), 3.5 ml of lipid in oil solution and 1 ml of decane (Sigma, USA) as shown in figure 2.9.

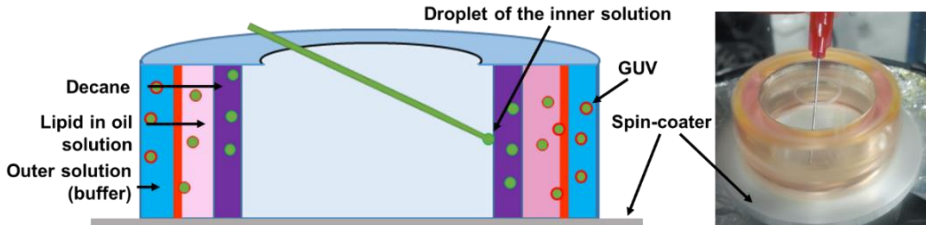

Figure 2.9 *Side and top view of the set-up used for GUV preparation by the cDICE method.*

The chamber was then fixed on a spin coater. A needle of gauge 30 to 34 (Radionics, Ireland), connected to a syringe containing the internal solution, was introduced through the opening. Larger size needles were selected if concentrated protein solutions were used to avoid clogging of the needle tip. The chamber was rotated at 1400 rpm separating the different liquid phases into layers. The internal solution was injected from the needle at 2-30 μl/min for 5 to 20 min. After the formation was completed the spin coater was gradually stopped and the aqueous layer containing vesicles was withdrawn through the opening of the chamber.

2.5 Size distribution analysis

Images of vesicles prepared using various conditions were recorded using CellF software. The diameter of 200 randomly selected, spherical and free in solution vesicles was measured (unless stated otherwise). Multilamellar, oligovesicular or liposomes with visible membrane deformations were not included in the size distribution analysis.

For each composition and for each method used, experiments were conducted in triplicate/quadruplicate (unless stated otherwise); meaning that for each size distribution, 600-800 GUVs have been measured, unless indicated otherwise. The vesicle diameters were averaged across the 3-4 repeat experiments and the distribution was normalized.

2.6 Incorporation of glycolipid into a lipid bilayer

The synthetic glycolipid used here was synthesised using L-aspartic acid building blocks.[366] The glycolipid was dissolved in chloroform or a chloroform: methanol mixture, depending on the method used for preparation. The glycolipid was incorporated into the bilayer with other lipids, DOPC, cholesterol, PEG-DOPE and fluorescent lipid dyes. Various mixtures of lipids in chloroform or chloroform/methanol at concentrations required by each method were prepared. The amount of each component was calculated as a weight or mole fraction.

The GUVs and the lipid tubules were imaged using phase contrast, polarized light and fluorescent microscopy. The fluorescent dyes added to lipid mixtures included the bodipy FL C_5 ceramide, bodipy TR ceramide, cholesteryl bodipy FL C_{12} and (14:0-12:0) NBD-PC. These dyes were used at concentrations between 0.1 to 1 mol percent of the total lipid composition.

2.7 EmGFP expression in *E. coli*

2.7.1 Transformation and growth of DH5α Competent cells for plasmid propagation

The pRSET-EmGFP Bacterial Expression Vector (Invitrogen, Ireland) was propagated in Library efficiency DH5α Competent cells (Invitrogen, Ireland). Cells were transformed using the protocol recommended by the manufacturer, consisting of a heat-shock procedure. Cultures were grown in LB broth containing 100 μg/ml ampicillin, at 37°C with vigorous shaking (300 rpm) in an Innova 42 incubator shaker (New Brunswick Scientific Co., INC). Plasmid DNA was isolated and purified with a Qiagen plasmid purification midi kit (Qiagen GmbH, Germany) using a method recommended by the manufacturer. The concentration of plasmid DNA was obtained using a SpectraMax M2e microplate reader (Molecular Devices, USA) by measuring UV absorbance at 260 nm, and using the relationship that A_{260} equal to 1 corresponds to 50 μg/ml of dsDNA. The purity of DNA was determined from the A_{260}/A_{280} ratio of diluted DNA solution. The nucleotide sequence of the emerald GFP was confirmed by sequencing with the T7 promoter primer using an automated capillary DNA sequencer (MRCPPU, University of Dundee, Scotland).

2.7.2 Transformation and growth in BL 21-Gold (DE3) Competent cells for protein overexpression

EmGFP protein was expressed in BL 21-Gold (DE3) Competent cells (Stratagene, USA). Cells were transformed with the EmGFP plasmid using the protocol recommended by the manufacturer and were cultured in 1.2 L of LB broth containing 100 μg/ml ampicillin at 37°C and shaken at 225 rpm. Expression was induced after 3-4 hours of growth (OD_{600} between 0.8 and 1) by addition of isopropyl β-D-1-thio-galactopyranoside (IPTG) to a final concentration of 0.83 mM. The culture was grown for a further 5 hours. Cells were harvested by centrifugation at 6000 rpm for 8 minutes. Cell pellets were stored at -80°C before protein extraction.

2.7.2.1 Preparation of bacterial cell stock

Bacterial cell stocks for long term storage were prepared by aliquoting 2 ml of the BL 21-Gold (DE3) Competent cells (in Log phase growth) into sterile cryogenic vials (Nalgene, Ireland). Stocks were stored at -80°C.

2.7.3 Site directed mutagenesis and molecular cloning

Site directed mutagenesis is a method for creating specific changes at a specific site in the DNA sequence. The mutation may be a substitution, deletion or insertion of one or more bases. This method requires synthesis of two short DNA oligomers (forward and reverse sequence), complementary to the DNA and containing the desired mutation. A PCR reaction using high fidelity DNA polymerase leads to production of copies containing the mutated sequence. The PCR product is transformed into *E. coli*.

The Human γD crystallin (HGD) bacterial expression vector coding for the eye lens γD-crystallin was used to prepare HGD P23T plasmid DNA coding for its single mutant (proline to threonine substitution at the 23 position). Oligonucleotides with following sequence were used for the P23T mutation[282];

Forward primer: 5′-GCA GCA GCG ACC ACA CCA ACC TGC AGC CC-3′

Reverse primer: 5′-GGG CTG CAG GTT GGT GTG GTC GCT GCT GC-3′.

Oligonucleotides were synthesized by Life Technologies (Dublin, Ireland). Mutagenesis was performed with QuikChange II site-directed mutagenesis kit (Stratagene, USA) using procedure recommended by the manufacturer. The PCR reaction was assembled as follows:

5 µl of 10X PCR reaction buffer
1.01 µl (50 ng) of ds DNA template
0.39 µl (125 ng) of forward primer
0.37 µl (125 ng) of revers primer
1 µl of dNTP mix
1 µl of PfuUltraHF DNA polymerase
Milli-Q to final volume of 50 µl

The PCR reaction mixture was assembled in a thin-walled PCR tube, gently vortexed and briefly centrifuged before being subjected to the following heating cycles:

Pre-heat led step	105°C	2 min
1 cycle	95°C	30 sec
16 cycles	95°C	30 sec
	65°C	1 min
	68°C	9 min

Following the removal of methylated DNA, containing the unchanged sequence, plasmid was transformed into *E.coli* (section 2.7.1). The plasmid was amplified, purified and sequenced as described in section 2.9.1.

2.8 Protein expression in cell-free medium.

Cell-free protein synthesis was carried out using PURExpress (New England Biolabs, USA), the *E. coli* based, purified *in-vitro* transcription and translation system.

As per manufacturer instruction the components of the kit (solutions A and B) were combined on ice using RNAse free pipette tips. The reaction mixture was supplemented with 20 units of RNase Inhibitor (New England Biolabs, USA) and 350 ng of plasmid DNA. The total volume was adjusted to 25 µl with Milli-Q water. Protein expression in solution was carried out at 37°C. The concentration of expressed protein was quantified using a SDS-PAGE protein quantification technique and ImageJ (described in section 2.9).

Protein expression in cell-free medium was also performed inside GUVs. In order to do so, 25 µl of the cell-free expression was encapsulated inside GUVs using the inverted emulsion method. The outer solution was composed of the low molecular components of the cell-free expression kit (solution A) supplemented with 50 mM sucrose.

2.9 Protein extraction, purification and characterization

2.9.1 Protein extraction

Cell pellets containing *E. coli* overexpressing EmGFP were thawed at 30°C in a water bath. The pH of the cell suspension was adjusted to 7. The cell pellet was resuspended (by vortexing) in lysis buffer (10 ml) and complete protease inhibitor cocktail tablet (25 MU, Roche) was added. The cell suspension was incubated at room temperature for 2 hours before the addition of 160 µl of a 50 mg/ml lysozyme solution. The solution was vortexed and incubated at room temperature for a further 30 minutes. The cell suspension was subjected to four freeze (liquid nitrogen) – thaw (30°C water bath) cycles. After the last cycle, 2 ml of 1 mg/ml DNAse and 1 ml of 1 M $MgSO_4$ (premixed) was added and solution was incubated at room temperature for 30 minutes. The pH was adjusted to 7 and the solution was centrifuged at 10 000g overnight or until cell debris was fully removed. The supernatant was stored at 4°C for chromatographic purification and the cell pellet was analysed by SDS-PAGE and if necessary stored at -80°C for further extraction.

2.9.2 Immobilized metal ion affinity chromatography (IMAC)

Affinity chromatography is an analytical purification method used for biochemical mixtures. It exploits a specific interaction between the stationary phase and the analyte.[367] In immobilized metal ion affinity chromatography (IMAC) the stationary phase contain metal ions (nickel, cobalt, iron or others) which have a high affinity for a specific tag (His-tag or sites of phosphorylation) introduced to the molecule structure via recombinant DNA technology.[368] Elution of the analyte is usually induced by change of pH or introduction of competing molecules (imidazole).

IMAC set up: Immobilized metal ion affinity chromatography was carried out using AKTAprime plus (GE Healthcare BioSciences, Sweden) and the PrimeView 5.0 software (GE Healthcare, Sweden) was used to control the instrument. Absorbance spectra at 280 nm were obtained using the optical unit. A glass column (XK 16) was packed with ca. 10 ml of Ni Sepharose™ High Performance (GE Healthcare, Sweden) using the protocol provided by the manufacturer.

Purification procedure: IMAC was used for purification of EmGFP present in the *E. coli* cell lysate. Prior to each purification, the system was rinsed with 200 ml of Milli-Q water and 100 ml of the loading buffer. Once the column was connected the flow rate was set to 2 ml/min (or less) with a maximum pressure of 0.3 MPa (3 bar). The column was rinsed with 3 column volumes of Milli-Q (to remove ethanol used for storage) and 10 column volumes of the loading buffer. Before loading onto the column, the cell lysate containing the crude protein (after centrifugation step) was filtered through 0.22 μm Millex-Gv Millipore low protein binding (PVDF) membrane filter units (Millipore, Ireland). The pH, sodium chloride and imidazole concentration in the cell lysate was matched to that of the loading buffer. The cell lysate was introduced onto the column via one of the solvent lines. In order to remove any unbound proteins the column was rinsed with 100 ml of the loading buffer. The EmGFP was removed from the column by gradient elution using imidazole at concentrations from 30 mM to 500 mM. After each purification the column was rinsed with 5 column volumes of Milli-Q water to remove the imidazole. For long term storage, the column was filled with a 20% ethanol solution.

2.9.3 High Performance Liquid Chromatography (HPLC)

HPLC is an analytical technique used to separate or quantify components of a mixture based on their distribution in two immiscible phases. Size-exclusion HPLC

separates molecules based on their size. In this method, the liquid mobile phase moves, together with the analyte, through the pores of the stationary phase. Larger molecules are eluted first, smaller molecules interact more with the matrix of the packing material and therefore have a longer retention time.[369] HPLC analysis was performed in order to assess the purity of EmGFP after affinity chromatography separation.

HPLC set up: Size exclusion HPLC was carried out using a Shimadzu SPD HPLC system. Shimadzu LC solution software was used to control the instrument. Absorbance spectra were obtained using a diode array detector (DAD) at 190 – 800 nm. A Superdex 200 10/300 column (GE Healthcare, Sweden) composed of crosslinked agarose and dextran, with a molecular weight range 10-600 kDa was used.

Procedure: Prior to use the HPLC lines were purged and rinsed with the correct buffer to remove any air bubbles. The column was then rinsed until a stable baseline was attained. A sample analysis was performed using 100 mM sodium phosphate buffer (pH 7) as the mobile phase and a flow rate of 0.5 ml/min. Samples were prepared in glass vial with rubber seal and introduced onto the column via autosampler set to a 20 µl injection volume.

Sample preparation: An EmGFP solution (from liquid chromatography purification) at 2 mg/ml in 100 mM sodium phosphate buffer, pH 7 was prepared, filtered through the 0.22 µm syringe filter (Millipore, Ireland) and placed into a glass vial.

Calibration of the column: A mixture of five proteins (listed in figure 2.10) with various molecular weights were dissolved at 2 mg/ml in 100 mM sodium phosphate buffer and filtered through 0.22 µm syringe driven filters into a glass vial. Proteins were run individually to assign a retention time and as a mixture to establish a column calibration curve.

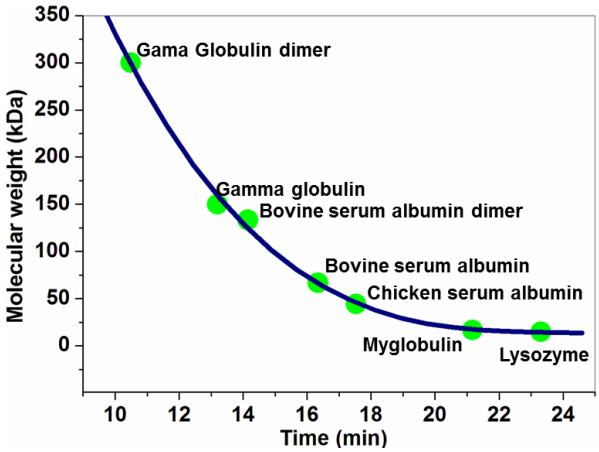

t_R	Protein (molecular weight)
10.49	Gama Globulin dimer (300 kDa)
13.20	Gamma globulin (150 kDa)
14.15	Bovine serum albumin dimer (133.4 kDa)
16.34	Bovine serum albumin (66.7 kDa)
17.53	Chicken serum albumin (44.2 kDa)
21.17	Myglobulin (21.06 kDa)
23.31	Lysozyme (14.7 kDa)

Figure 2.10 *Calibration of Superdex 200 10/300 HPLC column.*

2.9.4 SDS-PAGE analysis

SDS-PAGE is a type of electrophoresis in which the separation, detection or purification of molecules is based on their molecular weight.[370] In this method an anionic detergent (sodium dodecyl sulphate or SDS) binds to the protein giving it an overall negative charge (driving their migration in electric field towards the anode) and causing protein unfolding by breakage of hydrogen bonds. Whenever breakage of disulphide bonds is desired, a reducing agent, such as 2-mercaptoethanol may be used.

SDS-PAGE analysis was performed in order to check if the desired protein is present in cell lysate or the pellet (after purification), to assess the purity of the protein solution or to quantify a specific protein in the mixture.

Gel preparation: Gel plates were assembled in the mini-protean tetra cell (Bio-Rad, Ireland) as per the manufacturer's manual. The following solutions were prepared:

Resolving gel (12.5%) solution:	Stacking gel (4%) solution:
3.15 ml of Milli-Q water	3.05 ml of Milli-Q water
2.5 ml of 1 M Tris-HCl pH 8.8	0.65 ml of acrylamide bis
100 µl of 10% w/v SDS	1.25 ml of 0.5 M Tris-HCL pH 6.8
4.2 ml of acrylamide/Bis (30% stock)	50 µl of 10% w/v SDS

The components of the resolving gel were mixed and degassed, followed by the addition of 50 µl of freshly prepared 10% (w/v) ammonium persulfate (Riedel-de-Haën, Germany) and 5 µl of tetramethylethylenediamine (TEMED) (Thermo Scientific, USA). Next, the solution was poured between the glass plates and allowed to set for 30 minutes. A thin layer of tert-amyl alcohol was placed on top of the gel to remove air bubbles and prevent drying. Once the gel was set, the tert-amyl alcohol was rinsed off, and the stacking gel (4%) was prepared by mixing its components and degassing the solution for 30 min. 25 µl of 10% (w/v) ammonium persulfate and 5 µl of TEMED were added. The solution was poured on top of the resolving gel and allowed to set. Gels were stored (in cling film to prevent drying) at 4°C for up to a week before use.

Sample preparation: Samples for SDS-PAGE analysis were mixed with the sample buffer, heated at ca. 95°C for 5 minutes and briefly centrifuged before loading onto the gel. For reducing SDS-PAGE sample buffer was supplemented with β-mercaptoethanol in a 1: 20 ratio. Molecular weight markers (Bio-Rad) (figure 2.11) were diluted in reducing sample buffer (1:20), and 10 µl aliquots were stored at -20°C.

Before use markers were thawed, heated at 95°C and briefly centrifuged.

Sample buffer:
4 ml of Milli-Q
1 ml of 0.5 M TRIS-HCl pH 6.5
0.8 ml of glycerol
1.6 ml of 10% w/v SDS
0.5 mg of bromethyl blue (Sigma Aldrich, Germany)

Gels were run in a 4-gel electrophoresis tank (Bio-Rad) with the power source set to 200 mV. Tris-glycine buffer was used as the running buffer. In order to visualise protein bands, gels were stained in Coomassie brilliant blue R-250 (Biorad, Ireland) for a minimum of 2 hours. Gels were de-stained in a 1:3:6 acetic acid: methanol: Milli-Q (v/v/v) solution.

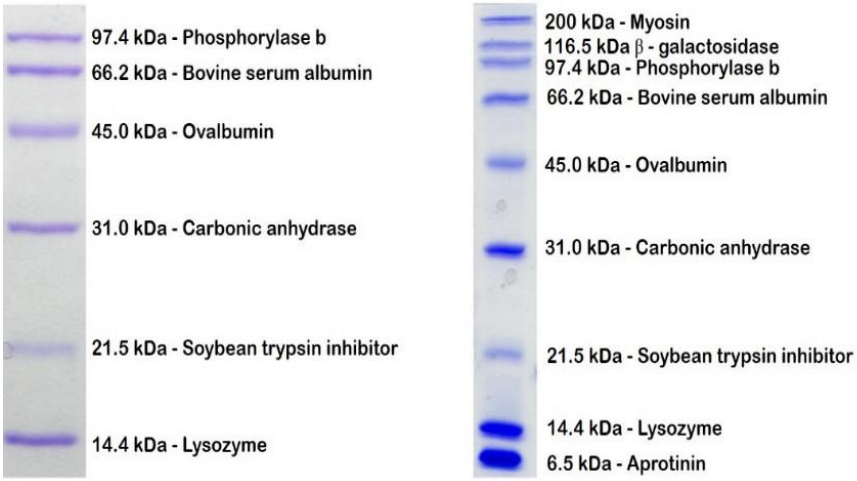

Figure 2.11 *Low range (left) and broad range (right) molecular weight markers (MWM).*

2.9.5 Protein quantification using SDS-PAGE

The Concentration of P23T protein, expressed in the cell-free mix was quantified based on the intensity of the band from the SDS-PAGE gel analysis. A calibration curve was prepared for each gel and used for protein quantification with either BSA or HGD protein as standards. A range of concentrations of the standard were used. The cell-free expression samples and the calibration standards were mixed with the reducing sample buffer, heated at 95°C and briefly centrifuged before 15 µl of each was loaded onto a gel.

The gel was run using the set-up and parameters described above and stained in Coomassie brilliant blue R-250 solution overnight. De-staining of the gel was performed in a 1:3:6 acetic acid: methanol: Milli-Q (v/v/v) solution.

Gel were scanned and digital images were saved in .tif or .png format. Densiometric analysis was performed using the ImageJ software.

2.10 Determination of protein concentration in GUVs

The amount of light absorbed by the fluorophore can be related to its concentration

$$F = kcQI_0 \qquad 2.10$$

where k is a constant, c is the concentration fluorophore, Q is the quantum yield and I_0 is the intensity of light illuminating the solution.[351] This equation relates values of F and c at low concentration of the fluorophore. At higher fluorophore concentrations the fluorescence intensity is independent of its concentration:

$$F = QI_0 \qquad 2.11$$

When using the fluorescent intensity measurement to calculate the concentration of the fluorophore the value of I_0 must be kept constant. The intensity of illuminating beam can be monitored using a fluorescent standard.

2.10.1 Monitoring mercury lamp intensity.

Measurement of the fluorescence intensity may be affected by various factors, with the intensity of the illuminating beam being one of them. MultiSpeck Multispectral fluorescence microscopy standards (Molecular Probes, USA) were used to monitor the day to day performance of the mercury lamp, mainly the fluctuation in the intensity of illuminating light.

MultiSpeck fluorescence standard is a suspension of microspheres, 4 µm in diameter emitting red, green and blue fluorescence when excited with the appropriate wavelength of light. 1 µl of the microsphere suspension was deposited onto a microscope slide and air dried. When fully dry, the mounting medium supplied with the kit was added and a coverslip was placed on top. Microspheres were imaged every time protein quantification or related calibration curve measurements were performed.

Monitoring of the intensity of illuminating light allows for the detection of variation in the instrument performance. The fluorescence intensity measurements performed on the days when such variations arise may therefore be either repeated or corrected.

2.10.2 Calibration curve preparation for protein quantification

A calibration curve for measuring the protein concentration in GUVs was obtained using glass capillaries (Hilgenberg, Germany) with internal diameters of 20, 30, 40, 50, 70, 80 and 100 µm. Capillaries were filled with EmGFP solution in 20 mM phosphate buffer at pH 7.4. Filling of the capillaries was performed by capillary action (which lead to an uneven distribution of the protein solution across the length) and by connecting the capillaries with a syringe via silicon tubing then filling it by immersing the free tip of capillary in the GFP solution and slowly withdrawing the protein solution until a droplet of liquid was observed on the opposite tip of the capillary (the one connected to the syringe). The following concentrations of EmGFP were used: 0.21, 0.348, 0.506, 0.84 and 1.08 mg/ml.

Each capillary filled with the EmGFP solution was observed and two images were recorded using fluorescence microscopy (figure 2.12a) with 10x and 20x magnification. Images with various exposure times were also recorded, but a 20 ms exposure time was used for constructing the calibration curves presented here. The calibration curve was constructed by: (1) measuring the fluorescence intensity in the centre of the capillary (mid-point in relation to its width) or (2) recording the fluorescent intensity profiles across the width of the capillary (perpendicular to its length). Graphs representing the calibration plots were prepared using Origin V6.1 software.

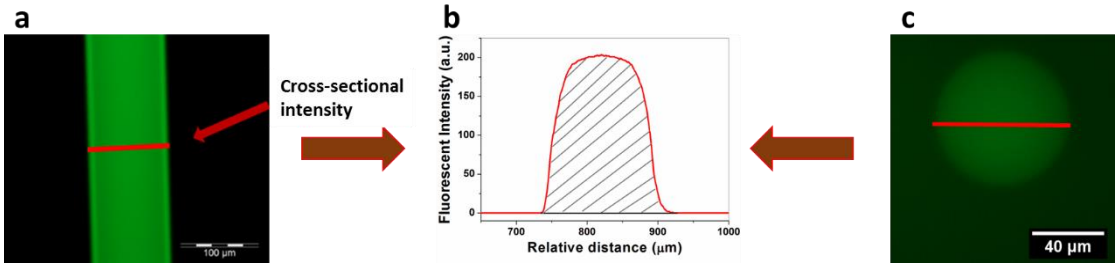

Figure 2.12 *Schematic representation of the measurement of cross-sectional intensity of GFP-filled capillary (a) or vesicle (c) and the resulting fluorescent intensity plot (b); used for either the preparation of calibration curve or direct measurement of protein concentration inside the vesicle.*

In both cases a total of six measurements (three for each image) were obtained for each capillary size and each protein concentration. A separate calibration curve was constructed for each capillary size by plotting the average fluorescence intensity, measured within the center of GUVs or obtained by measuring the area under the peak for each fluorescent intensity profile.

2.10.3 Conversion between various objectives and exposure times.

The calibration curve of protein (EmGFP) concentration as a function of the fluorescence intensity and diameter was recorded using 10x and 20x lenses. Since images of vesicles encapsulating EmGFP were recorded using either 60x or 100x, a scaling factor was determined using fluorescent microspheres as a standard. To do this, microspheres were imaged using objectives with magnification from 10x to 100x and their fluorescence intensity was measured as in section 2.7.2, table 2.3. The scaling factor was thereby determined as a difference of the fluorescence intensity within microspheres observed with 10x and any other objective. Fluorescence intensity of EmGFP encapsulated within a GUV may therefore be multiplied by the scaling factor corresponding to the objective used to record a given image. The obtained value corresponds to the EmGFP concentration which can be obtained from the calibration plot.

Table 2.3 *Conversion table listing fluorescence intensity measurements obtained using a fluorescent standard and a range of lenses. The scaling factor (for 10x calibration) allows conversion of intensity between higher magnification lenses used for imaging of GUVs and the 10 X lens used to obtain measurements for the calibration curve.*

Lens	**10x**	**20x**	**40x**	**60x***	**60x****	**60x****	**60x****	**100x**
Exposure time	10 ms	10 ms	10 ms	10 ms	10 ms	5 ms	2 ms	10 ms
Fluorescence intensity (au)	180.36	510.67	681.67	1225.3	1413.3	977.94	516.69	1315.6
Scaling factor (10x)	-	0.353	0.264	0.147	0.1276	0.184	0.349	0.137

* UPlanFLN objective ** UPlanSapo objective

2.10.4 Quantification of protein concentration within GUVs

Liposomes were prepared and protein solutions were encapsulated using one of the previously described methods. Upon formation, vesicles containing protein solutions were imaged using either 60x or 100x magnification. Fluorescence images were analysed using CellF and ImageJ software.

For vesicles containing EmGFP solutions, fluorescence intensity was measured either in the centre of the vesicle (point measurement) or across the vesicle's diameter and used to construct the intensity plot. The area under the curve and the scaling factor for a given lens were used to obtain the EmGFP concentration for a given GUV size.

Quantification of BSA encapsulated inside vesicles was performed indirectly, by measuring the concentration of EmGFP present in the GUV. EmGFP was added to a BSA solution at 0.5% of the total protein concentration. The EmGFP concentration was obtained using the procedure above. The BSA concentration was then inferred by calculating the concentration of EmGFP and its contribution to the total protein concentration.

Analysis of the effect of BSA on the fluorescence of EmGFP

The fluorescence measurements were conducted using SpectraMax M2e multi-platform reader. Solutions of EmGFP and EmGFP/BSA mixtures in 20 mM sodium phosphate buffer, pH 7.4 were prepared and placed in quartz cuvette. The sample was excited at 487 nm and emission spectra between 450 and 600 nm were recorded.

2.11 Aggregation of BSA in various solution conditions.

2.11.1 In bulk solution

Experiments to monitor BSA solution behaviour were performed in 96-well, clear bottom plates. A BSA stock solution at a concentration of 100 mg/ml was prepared in 5 mM sodium phosphate buffer, pH 7.4 and diluted to 10 mg/ml using an appropriate 50 mM buffer: glycine-HCl (pH 2.2 and 3), sodium acetate (pH 4) and sodium phosphate (pH 7.4). ThT (if used) was added to a final concentration of 200 µM and NaCl was added from a 2 molar stock to achieve final concentrations ranging from 0 - 100 mM. The total volume in each well was fixed at 150 µl. Plates were incubated either at room temperature or at 65°C and cooled to room temperature before analysis. Fluorescence intensity measurements were performed immediately after preparation and at set time points (every 12 hours for when incubated at room temperature and every 20 minutes when incubated at 65°C) using a SpectraMax M2e microplate reader. The excitation wavelength was set to 435 nm and the emission spectrum was recorded between 465 and 565 nm. Additionally absorbance at 450 nm and 600 nm was recorded and percentage transmittance (*%T*) was calculated using following equation:

$$\%T = 10^{(2-A)} \qquad 2.12$$

The measurements were performed in triplicate and the results reported as an average.

2.11.2 Protein inside vesicles

A 100 mg/ml BSA stock solution was prepared for the encapsulation experiments in 5 mM sodium phosphate buffer at pH 7.4.

The inner solution (to be encapsulated in GUVs) was composed of:

- a buffer at the correct pH: glycine-HCl (pH 2.2 and 3), sodium acetate (pH 4) or sodium phosphate (pH 7.4),
- BSA at concentrations of 10, 20 or 40 mg/ml,
- ThT at a concentration of 200 µM
- 50 mM NaCl was added to solutions where indicated.

The inner solution was prepared immediately before the encapsulation.

The outer solution (in which GUVs were suspended upon formation) was composed of:

- a buffer at the correct pH,
- sucrose at concentration (established experimentally) required to match the osmotic pressure of the BSA filled liposomes,
- ThT at a concentration of 200 µM
- 50 mM NaCl was added to solutions where indicated.

After formation the GUVs suspension was removed from under the oil layer, gently mixed and incubated at room temperature for approximately two hours. Next, the vesicle suspension was transferred into PCR tubes and incubated at either room temperature for up to 5 days or at 65°C for up to 100 minutes.

2.12 Mammalian cell culture

2.12.1 HEK 293T/17 cell line

HEK 293T/17 was purchased from LGC (UK). HEK 293 is an epithelial cell line derived from human embryonic kidney cells transfected with mechanically sheared adenovirus 5 DNA, which then was integrated into chromosome 19.[371,372] The 293T cell line was created by inserting the temperature sensitive gene for the SV40 T-antigen. Clone 17 was selected due to its high transfectability.

2.12.2 Initiation of cell culture

Vials containing frozen stocks of cells were defrosted at 37°C in a water bath for 2 minutes. From this point all of the operations were carried out in a biological safety

cabinet (SafeFast Classic, Faster S.r.l.) under strict aseptic conditions. The contents of the vial were transferred into a falcon tube containing 9 ml of the complete DMEM and centrifuged at 125 g for 7 minutes. The supernatant was removed and cell pellet was resuspended in 6.5 ml of cDMEM and transferred into a T25 flask (Corning). Cells were grown in Memmert INCO 153 incubator (Germany) at 37°C, 90% humidity and 5% CO_2.

2.12.3 Subculturing and maintenance of culture

The cultures were maintained by refreshing the cDMEM every 2-3 days as indicated by confluence or change in colour of the cDMEM caused by change an in pH due to the presence of metabolites. When the culture reached 90% confluence, cells were subcultured using the following procedure (volumes are given for T25 flasks). The medium was removed and the cells were rinsed with 1X PBS, followed by the addition of 1 ml of trypsin-EDTA (500 mg/L porcine trypsin, 200 mg/L EDTA.4Na) in PBS solution. The flask was incubated at 37°C until the cells detached (but for no longer than 10 minutes). 9 ml of cDMEM was added and the cells were harvested by gently aspirating the medium. The cell suspension was placed in a falcon tube and centrifuged at 125 x g for 10 minutes. The supernatant was discarded and the cells were resuspended in fresh medium. Cells were counted using a hemicytometer and seeded at an appropriate concentration, usually $2x10^5$ cells/ml.

2.12.4 Cryopreservation of cell stocks

Once confluent, cells were harvested using the protocol described above and resuspended in the cryopreservation medium composed of 95% of complete DMEM and 5% diethyl sulfoxide (DMSO) at 3 x 10^6 cells/ml. The cell suspension was aliquoted into cryopreservation vials. The vials were first placed at 4°C for 5 minutes, next in a -20°C freezer for 1 hour followed by -80°C for 1 hour and finally into a liquid nitrogen storage container for long term storage.

2.13 Protein expression in mammalian cells

2.13.1 Transfection

Transfection is a process by which a nucleic acids are introduced into a mammalian cell. There are several methods for transfection routinely used. Here, Lipofectamine 2000 (Invitrogen, USA) was used as the transfection reagent. It is a

cationic liposome formulation which forms complexes with DNA, via electrostatic interactions with the nucleic acid charge.[373]

A mammalian expression vector containing the sequence of a fusion protein EmGFP-HGD was designed and the vector was synthesized by GeneArt (Thermofisher, GeneArt division, Germany). The mammalian vector pc-DNA6.2_C-EmGFP-DEST vector was used and the HGD gene was inserted at the C-terminus. The EmGFP-P23T vector was obtained by performing site directed mutagenesis of the mammalian expression vector. Mutagenesis was performed with QuikChange II site-directed mutagenesis kit using a primers and protocol described in section 2.9.3. The correct nucleotide sequence was confirmed by sequencing (MRCPPU, University of Dundee, Scotland) (see section 2.9.1 for details).

The mammalian cells expressing EmGFP were obtained by transfection with the Vivid Colors™ pcDNA™ 6.2/EmGFP GW/TOPO mammalian expression vector (Invitrogene, USA).

Transfection was performed once cells seeded in 6-well plate reached 90% confluency. Prior to transfection, the medium was exchanged to DMEM without serum (sfDMEM). The DNA plasmid was diluted in sfDMEM (2.5 µg in total of 100 µl per well). Lipofectamine was diluted in sfDMEM (5 µl into 95 µl of DMEM per well) and incubated at room temperature for 5 minutes. Diluted Lipofectamine was added to the diluted DNA, mixed and incubated at room temperature for 20 minutes. Next the DNA-Lipofectamine complex solution was added to the cells and incubated at 37°C for 4 hours. Following that time the medium was exchanged for complete DMEM (containing serum). Transfected cells were visualized 4 days from the transfection date.

2.13.2 Generating stable cell lines

The fusion plasmids used here contain the Blasticidin resistance gene to allow for selection of stable cell lines. In order to do that the minimum concentration of the antibiotic required to kill untransfected cells must be determined.

Determining sensitivity of the HEK 293T/17 cells to Blasticidin: Cells were grown in 6-well plate. When confluency of around 25% was reached, the medium was replaced with fresh complete DMEM containing various Blasticidin concentrations ranging from 0 to 10 µg/ml. The growth of cells was monitored for 2 weeks.

A blasticidin concentration of 5 µg/ml was found to be the minimum concentration required to kill untransfected cells. Stable transfectants were selected using following protocol. The day after transfection (approximately 24 hours), cells were washed with PBS and fresh medium was added. On day 2, cells were split into fresh DMEM and seeded at 25% confluency. Cells were allowed to adhere for ~ 4 hours and the medium was replaced with the complete DMEM containing 5 µg/ml of blasticidin. The medium was replenished every 2-3 days for at least 2 weeks.

2.13.3 Microscopic imaging of live cells

In order to facilitate cell growth on glass coverslips, surface treatment with poly-D-lysine was performed. The coverslips were first cleaned and sterilised. Next, their surface was coated with 300 µl of 100 mg/ml poly-D-lysine (70-150 kDa) solution and incubated at 37°C. After 40 minutes, the coverslips were thoroughly rinsed with sterile Milli-Q water and allowed to dry for at least two hours. Coated glass slides were stored at 4°C.

Coated glass cover slides were placed in the wells of 6- or 12- well plates. Cells were seeded at $2x10^5$ cells/ml. Once the desired confluency was reached the medium was replaced with complete, phenol red-free DMEM and cells were incubated for 30 minutes. Prior to imaging the cover slide was placed on a glass slide and covered with second coverslip. An imaging spacer was placed between the two coverslips to prevent crushing the cells. The coverslip was sealed with melted agarose. Slides containing live cells, either with transient or stable transfectants, were imaged on a heated stage set to 37°C. Cells were observed using both phase contrast and fluorescence microscopy (section 2.3). Images were recorded using CellF software and processed using ImageJ.

2.14 Fractal dimension analysis

A Fractal, also known as expanding symmetry is a natural or mathematical phenomenon characterized by repeating patterns exhibited at every scale (figure 2.13). The word ‘fractal’ originates from the Latin *fractus*, which means “to break” but also “irregular” and was coined by Benoit Mandelbrot[374]

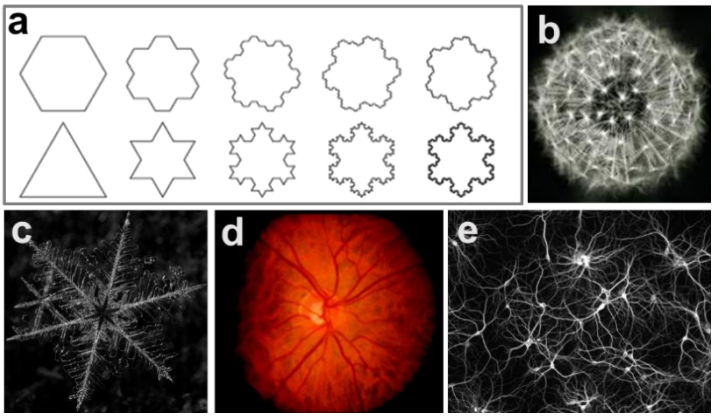

Figure 2.13 *Mathematical fractals (a): Gosper island and Koch snowflake and fractal patterns found in nature (b-e) (taken from mathworld.wolfram.com, fractalfoundation.org, sya.deviantart.com, cohabitaire.com and* [375]*).*

2.14.1 Introduction: theory behind fractal analysis

Fractals are self-similar, which means that the same pattern is observed regardless of scale or size. This can be realized using a lens to zoom in on the image, uncovering repeating shapes with no change or new detail.[374] Another characteristic of fractal structures is the fact that they follow non-linear scaling rules and their fractal dimension is greater than their topological dimension. For example if a 1-dimensional straight line is divided into three pieces each of them will be 1/3 of the original length resulting in fractal dimension of 1. This is not the case for a fractal object. For example if the Koch snowflake (also 1-dimensional) is divided into four pieces, each will have 1/3 of the original length (figure 2.14). Fractals cannot be measured using traditional approaches as the fractal curve is infinitely long.[376] It has been proposed that the boundary length of a fractal object can be expressed as a power law[377]:

$$L(r) = N \cdot r^{D_H} \qquad 2.13$$

where *L(r)* is the boundary length, *r* is the length of straight line fragments used to measure the boundary length, *N* is the number of such fragments and D_B is the Hausdorff dimension, which after rearrangement becomes:

$$D_H = \lim_{r \to 0} \frac{logN}{\log(\frac{1}{r})} \qquad 2.14$$

The Hausdorff dimension has a value between the topological dimension of the object and the topological dimension of the space which it occupies. A more complex boundary of a fractal object correlates to a higher value of the Hausdorff dimension.

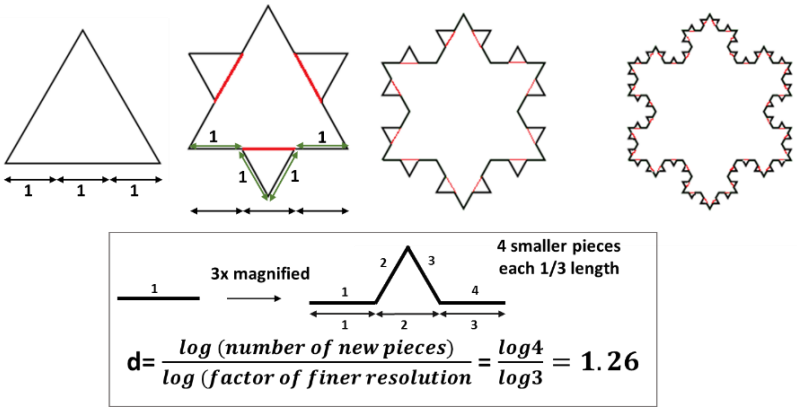

Figure 2.14 *Fractal dimension of the Koch curve.*[376]

Fractal analysis is used to quantify and analyze similarities between patterns otherwise hard to describe. Approximate fractals can be found in nature (figure 2.13) and include snowflakes,[378] coastlines or earthquake locations[379] and river networks. Fractal dimensions have also been frequently used to analyse biological and biomedical images including retinal vasculature,[380] tumours,[381,382] cellular morphology,[383,384] bacterial growth patterns[385] or protein aggregates.[386,387] Fractal dimension analysis of biological samples is used to represent complexity of the shape of an object and to compare morphological features.[388]

There are a large number of fractal dimensions, (some used only in pure mathematics) as well as several methods of measuring a fractal dimension. The methods most popular for analysing biological images include: box counting, perimeter-stepping[389] or pixel dilation.[390] The fractals found in nature exhibit random fluctuations in their self-similar patterns, which results in statistical self-similarity expressed by a divider fractal dimension[391] or box-counting dimension.[377] Various types of software offering fractal dimension calculations are available such as Benoit,[392] BCF,[393] Fractal Analysis v02[394] and the FracLac plugin for ImageJ.[395]

2.14.2 Box-counting method

ImageJ free software was used to prepare the digital images and the FracLac plugin for ImageJ, developed by A. Karperien was used for the fractal dimension calculation. The method outline was taken from the FracLac manual.[395]

Image preparation

In order to be analysed, digital microscopy images must be converted to binary images. This can be done using a threshold function, which divides pixels of an image

converting ones below a set value to black and above that set value to white, therefore assigning the background and foreground pixels. Binary images can further be converted to one-pixel wide outlines or skeletonized drawings (with lines of unchanging diameter).

Box-counting method

Box-counting is a method of data gathering for fractal dimension measurements. It involves a series of grids (boxes) of decreasing size laid over a digital image. Data collection involves counting how many boxes of each grid contains foreground pixels. Changing the grid calibre (the size of the box) results in changes in the number of pixels (or so called "mass") in each box. The mean mass and the average number of foreground pixels per box at any given size may be used to calculate a mass dimension, lacunarity (inhomogeneity or texture) and multifractality.

Fractal dimension is a measure of how a detail changes with resolution and is based on the concept of a dimension arising from $N=R^D$ where N is the number of counted parts of a pattern and R is the relative scale. FracLac uses a bounding box, which is the smallest rectangle oriented box enclosing all of the foreground pixels within an image, to determine the relative size of the largest box within the grid calibre and the scale for a given box counting scan. The degree of complexity is given by:

$$D = \frac{logN_\varepsilon}{log\varepsilon} \qquad 2.15$$

where N is the number of new pieces and ε is the scale applied to an object and equal to box size/image size (so the size of boundary enclosing the foreground pixels). The fractal dimension is approximated as the slope of regression line from:

$$D_B = \lim_{\varepsilon \to 0} \frac{logN_\varepsilon}{log\varepsilon} \qquad 2.16$$

The slope of the regression line is given by:

$$m = \frac{n\sum SC - \sum S \sum C}{\sum S^2 - (\sum S)^2} \qquad 2.17$$

where S is the log of the scale or size (ε), C is the log of the count, which is the number of sampling elements (boxes) containing foreground pixels, and n is the number of sizes.

FracLac allows the user to choose the number of grid positions, meaning the orientations of the grid with respect to an image. The first four orientations assume the grid positioning in the corners of the bounding box. If more than four grid positions were selected, the locations of remaining orientations are selected based on predetermined

random numbers generating the coordinates within the biggest box in the series of a given grid calibres and with respect to the four corner locations. 12 grid positions were selected for the fractal dimension calculations used here. The use of more than 12 positions was found to significantly increase the time required for measurement without any gain in the accuracy of the result.

Since multiple grid locations were used, delivering multiple D_B values, the mean fractal dimension was calculated using equation 2.18.

$$\overline{D}_B = \sum_{G=1}^{Grids} D_{B(G)} \times Grids^{-1} \qquad 2.18$$

FracLac also allows for custom selection of other options, such as the box size or shape. The box size was set to optimum values based on the image size. The smallest size of a grid was not predetermined, the largest grid was set to 45% of the image size.

The results of fractal analysis, reported in table format were averaged over several digital images representing a set of experimental conditions. The standard deviation and the coefficient of variation were reported for each data set.

Chapter 3

Preparation of giant unilamellar vesicles by a range of techniques

3.1 Introduction

Lipid vesicles can be prepared from a variety of lipids using numerous methods of preparation. Both the lipid composition and method of preparation affect various properties of the lipid bilayer within these vesicles.

Since their discovery, lipid vesicles have been a work horse of cell membrane research, providing a better understanding of membrane properties and the processes occurring within. In recent years there has been growing interest in using vesicles as microcontainers for analysis of various biochemical reactions[105] or for development of model cells,[16,187,188] the latter being pursued in this work.

The number of methods available for liposome preparation is large and still growing, due to recent technological advancements, such as improvements in microfluidic techniques. The choice of the right experimental approach however still remains unclear, as various methods produce different types of vesicles, with various yields, depending on the type of lipids used. Therefore the choice of method is strongly influenced by the intended application. Since comparison with published data is not always possible, a reliable and fast approach for the comparison of results of various methods of preparation is presented here.

GUVs are commonly used to study the phase behaviour of model membranes.[60,146,149,396–398] The presence of coexisting liquid phases (liquid-ordered and liquid-disordered) was previously shown for variety of lipid mixtures such as ternary lipid mixtures containing DOPC, cholesterol and DPPC or sphingomyelin (SM). In fact, only small differences were observed between phase diagrams for mixtures containing DPPC and/or the sphingomyelin.[145,399] Similar lipid mixtures were used to observe phase behaviour within lipid bilayers prepared by gentle hydration method.

Giant unilamellar vesicles have been prepared by electroformation, lipid hydration methods (hydration on an agarose film, gentle and rapid hydration), water-in-oil emulsion and continuous droplet interface crossing encapsulation (cDICE). For each method investigated GUVs were assessed qualitatively (by appearance, lamellarity, presence of surface defects, tendency to cluster) and also by constructing size distribution profiles. For electroformation and hydration methods lipid composition and the aqueous solution in which formation was performed were varied in order to assess the influence of a given parameter on the characteristics of vesicles formed. The base lipid composition used for most of the experiments was an 80:20 DOPC/DPPC mixture, since this

composition produced consistent GUVs by a number of different methods. Cholesterol and sphingomyelin were added to the membranes to assess how their presence altered both the quality and size distribution of the GUVs formed. Egg PC was mainly used in the cDICE and emulsion method, since it has previously been shown to form large and abundant GUVs.

While there are a number of methods available to prepare GUVs, it is often difficult to predict if the GUVs formed will be suitable for the experiment that a particular application requires, especially where the desired membrane composition differs from the one described in the literature. The diameter of vesicles is of particular interest since depending on the method of analysis a particular range of sizes may be required. While smaller vesicles (1-2 μm) may be sufficient for many applications, it is often easier to see features, such as lipid phase separation or details of liposome's interior in substantially larger ones.[400]

Several of the most widely used methods for GUV production were analysed, mainly those that do not require specialized or expensive equipment. Typical size distribution data and qualitative analysis of vesicles formed was provided for each method using a variety of lipid compositions.

Additionally the applicability of the above methods for encapsulation of biomolecules was determined based. Above results provide information necessary for selecting the best method for specific application.

3.2 Results

3.2.1 Qualitative assessment of GUVs

Vesicles prepared by each of the methods listed above were observed by light microscopy. Their quality was assessed based on their appearance, the presence of surface defects, lamellarity and theformation of clusters or vesicles nests (number of small vesicles entrapped inside a larger one). Images of vesicles prepared by each of these methods are shown in figure 3.1. The quantities of each of the components are expressed in terms of molar ratios.

Formation of vesicles consisting of a single bilayer is important for analysing membrane dynamics or lipid phase behaviour. Lamellarity also affects the encapsulation of molecules inside liposomes.[401] In order to assess the lamellarity, vesicles were observed using widefield fluorescent and confocal microscopy. These techniques allow

observation of multiple lipid layers within onion-like vesicles or oligovesicular vesicles (OVV). Due to the resolution limit light microscopy may not always be sufficient to distinguish between single and multiple lipid layers remaining in close contact with each other. This type of assessment requires bending elasticity measurements[402] or fluorescence quenching assay.[403]

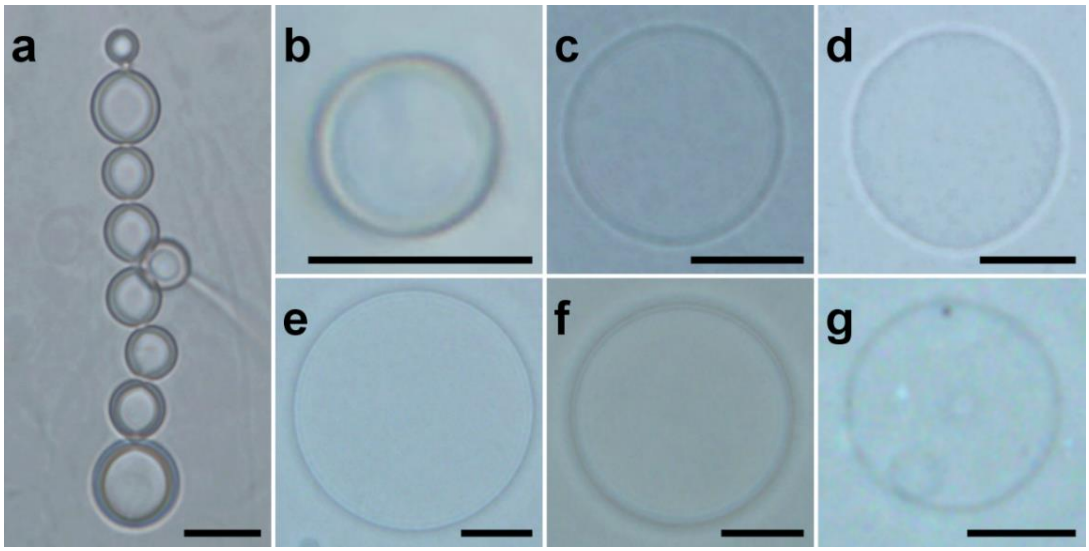

Figure 3.1 *Phase contrast microscopy images of GUVs prepared by each of the methods described; a) 56:14:30 DOPC/DPPC/Cholesterol by electroformation; b) 80:20 DOPC/DPPC by electroformation; c) 64:16:20 DOPC/DPPC/Cholesterol by gentle hydration; d) 80:20 DOPC/DPPC by rapid hydration; e) 95:5 DOPC/PEG-DOPE by lipid hydration on an agarose film; f) Egg-PC by cDICE method and g) Egg-PC by w/o emulsion method. Scale bar = 5 µm.*

Examples of unilamellar vesicles prepared by lipid hydration on an agarose film and composed of 80:20 DOPC/DPPC with 0.05% of fluorescent the dye, bodipy TR ceramide, imaged by both confocal and widefield fluorescent microscopy are presented in figure 3.2. The fluorescent intensity plots are constructed by measuring fluorescent intensity across the diameter of the vesicle. The maximum intensity on the fluorescent intensity plots corresponds to the location of the bilayer. Differences in the images and the intensity plots arise from the characteristics of each of the techniques. Confocal microscopy uses spatial filtering to eliminate background fluorescent and out of focus light observed due to the thickness (diameter) of the vesicle exceeding the thickness of focal plane. Since spatial filtering is not available in widefield fluorescent microscopy, fluorescence of the dye incorporated into the membrane is observed also inside the vesicle. This effect can be slightly reduced by a decrease in the exposure time or reducing the amount of dye incorporated into the membrane.

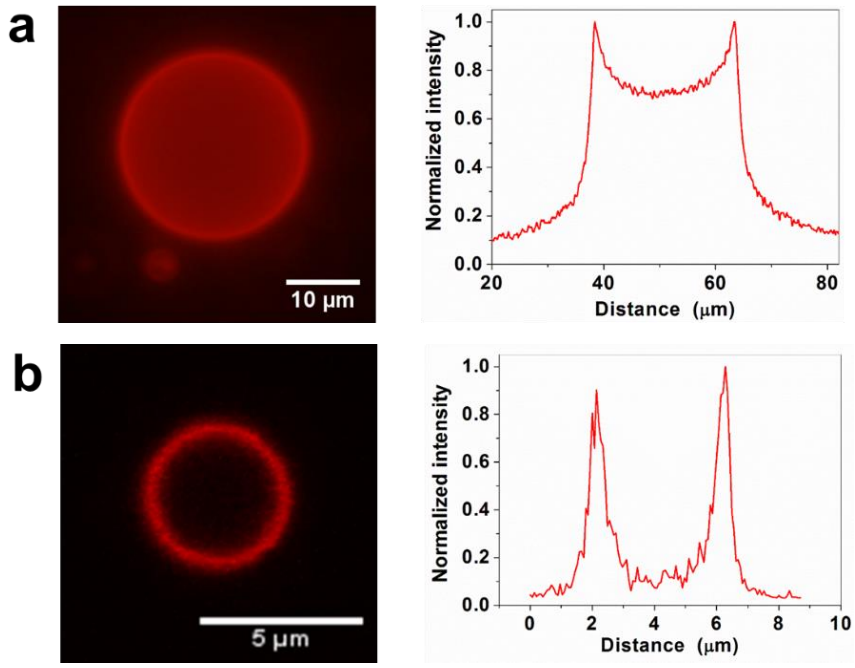

Figure 3.2 *Images and fluorescent intensity plots of unilamellar vesicles observed by widefield fluorescent (a) and confocal (b) microscopy.*

Most methods of vesicle preparation yield, in addition to unilamellar vesicles a number of multilamellar GUVs and nests of vesicles. The term multilamellar vesicles (MLV) is used to describe multiple vesicles of nearly the same size and in close contact with each other, which cannot be distinguished by optical microscopy (figure 3.3c) as opposed to nest of vesicles which refers to a larger GUV containing a smaller one with a diameter less than 20% smaller (figure 3.3b).[404] Oligovesicular vesicles (OVV), which are simply small vesicles inside larger ones are also commonly observed (figure 3.3a).[133] These can be easily identified by both phase contrast and widefield fluorescent microscopy, as shown in figure 3.3 (for vesicles formed by lipid hydration on an agarose film, composed of 80:20 DOPC/DPPC with 0.05% of bodipy TR ceramide). The number of lipid bilayers may be estimated by analysis of the fluorescent intensity plots obtained from high resolution images. A small percentage of multilamellar vesicles were observed in every method analyzed. Nests of vesicles were observed mainly within samples prepared by the lipid hydration on an agarose film method and the emulsion method.

In the protocols for vesicle preparation by both the emulsion and cDICE methods, the inclusion of mineral oil dispersed with lipid molecules is required. For that reason traces of oil may also be present in the bulk of the aqueous solvent or within the bilayer. Oil droplets can usually be distinguished simply by observation with light microscopy. Since a monolayer of lipids may be present on the surface of the droplets, the detection of oil droplets using fluorescent lipid dyes may not be appropriate. To improve upon this,

we introduced a hydrophobic dye, Sudan Red, to the mineral oil used for GUV preparation (figure 3.4a). As a second way to distinguish oil droplets from GUVs unambiguously, we included FITC in the aqueous solvent. Aqueous compartments will encapsulate FITC, while oil droplets will exclude it (figure 3.4b and c), providing an easy classification method.

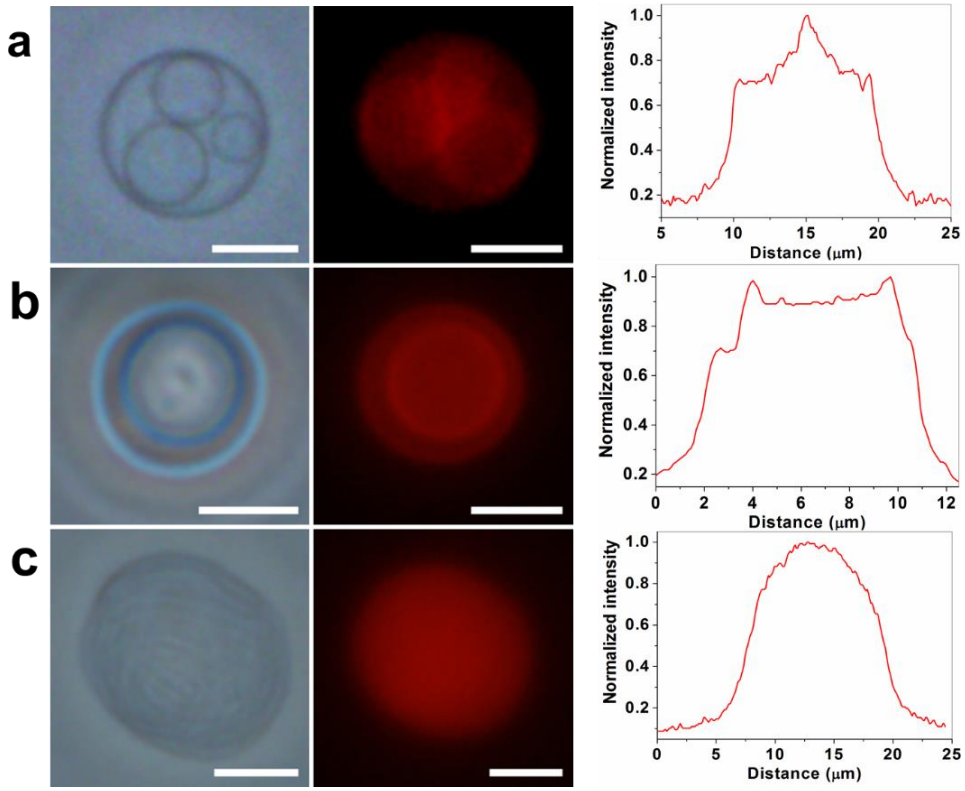

Figure 3.3 *Oligovesiclular vesicles (a), nest of unilamellar vesicles (b) and vesicle resembling onion-like structure (c) observed by phase contrast (left) and widefield fluorescent microscopy in the presence of 0.05% of bodipy TR ceramide dye (middle); fluorescent intensity plots (right). Scale bar = 5 μm.*

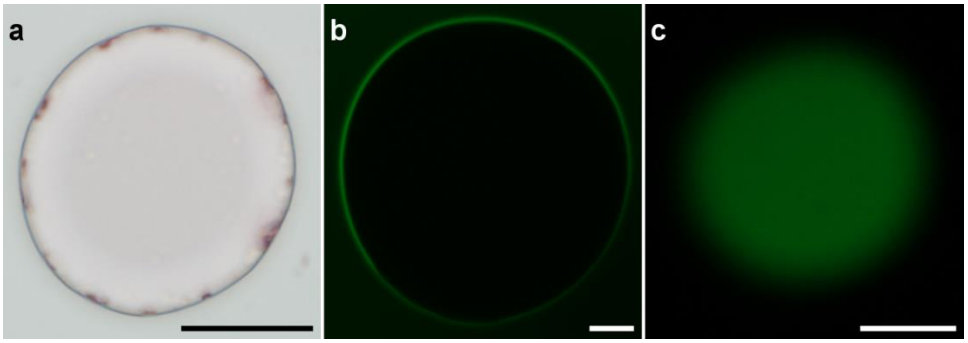

Figure 3.4 *Identification of GUVs and mineral oil droplets. Mineral oil droplets exclude FITC aqueous solution (b) but the Sudan red, a dye only soluble in non-aqueous solvents was found to localize in the mineral oil droplets, with several Sudan Red crystals observed at the oil/water interface (a). GUVs formed by the inverted emulsion method can also be identified by encapsulation of FITC solution inside aqueous interior of the vesicle (c). Scale bar = 20 μm.*

3.2.2 Quantitative assessment of GUVs

Size distributions for each method have been constructed by measuring the diameters of GUV after imaging using light microscopy. By selecting 300-800 spherical and unilamellar vesicles the sizes of vesicles produced by each method were determined. Only isolated vesicles were counted, and GUVs were randomly sampled across the full sample volume. Lower numbers (100-200) were considered for methods with a low yield of vesicles fulfilling above criteria. The vesicle diameters were averaged across the 3-4 repeat experiments and the size distribution plots were normalized. For all of the methods used here, large numbers of vesicles below 5 μm were observed and measured. However, for such small structures, determining the edges of the vesicles may produce some error.

A summary of GUV sizes obtained by each of the different methods is shown in table 3.1. Whilst for all of the size distributions shown all data is included, for reporting vesicles sizes in table 1, the proportion of vesicles above both 5μm and 10μm respectively are used to compare each of the methods, since larger vesicles are most desired and this allows the usefulness of each method in terms of producing optimal vesicles sizes to be compared.

3.2.3 Electroformation

Electroformation is a fast and highly reproducible method for the preparation of cell-sized GUVs. It is widely used, especially in membrane phase behaviour studies since it yields good quality unilamellar vesicles with bilayers free of organic solvents. An inexpensive setup, built on a microscope slide (developed previously in the lab) was used for these experiments (see experimental section). It facilitates GUVs formation from a dried lipid film deposited onto a glass surface by the application of an external electric field. The electroformation cell facilitates direct observation of the vesicles under an upright or inverted microscope. If desired, GUVs can be retrieved from the chamber through the opening at the top of the perfusion chamber.

Vesicles were produced for 80:20 DOPC/DPPC lipid mixtures and for DOPC/DPPC/cholesterol mixtures with increasing concentrations of cholesterol (from 10 to 30 mole percent). Size distributions for each membrane composition prepared are shown in figure 3.5.

Table 3.1 *Summary of GUVs sizes for different lipid compositions prepared by various methods.*

Method	Composition	Buffer	% GUVs above 5µm	% GUVs above 10µm	Largest GUV observed (µm)
Electroformation	80:20 DOPC/DPPC	Milli-Q H_2O	42	8	24
	72:18:10 DOPC/DPPC/Cholesterol	Milli-Q H_2O	47	6	23
	64:16:20 DOPC/DPPC/Cholesterol	Milli-Q H_2O	38	6	23
	56:14:30 DOPC/DPPC/Cholesterol	Milli-Q H_2O	24	3	20
	80:20 DOPC/BSM	Milli-Q H_2O	56	7	22
	50:25:25 DOPC/BSM/Cholesterol	Milli-Q H_2O	37	6	17
Gentle Hydration	80:20 DOPC/DPPC	Milli-Q H_2O	36	4	17
	64:16:20 DOPC/DPPC/Cholesterol	Milli-Q H_2O	82	33	78
	33:33:33 DOPC/DPPC/Cholesterol	Milli-Q H_2O	39	12	14
	33:33:33 DOPC/BSM/Cholesterol	Milli-Q H_2O	23	3	15
	47:23:30 DOPC/BSM/Cholesterol	Milli-Q H_2O	26	4	16
Rapid Hydration	80:20 DOPC/DPPC	Milli-Q H_2O	56	13	33
	64:16:20 DOPC/DPPC/Cholesterol	Milli-Q H_2O	14	3	30
Hydration on an agarose film	98.5:1.5 DOPC/PEG-DOPE	Milli-Q H_2O	60	27	68
	95:5 DOPC/PEG-DOPE	Milli-Q H_2O	52	18	30
	98.5:1.5 DOPC/PEG-DOPE	50mM Na_3PO_4	69	18	37
	95:5 DOPC/PEG-DOPE	50mM Na_3PO_4	63	21	46
Emulsion method	Egg-PC	20mM Na_3PO_4	60	25	28
cDICE	Egg-PC	20mM Na_3PO_4	73	55	60

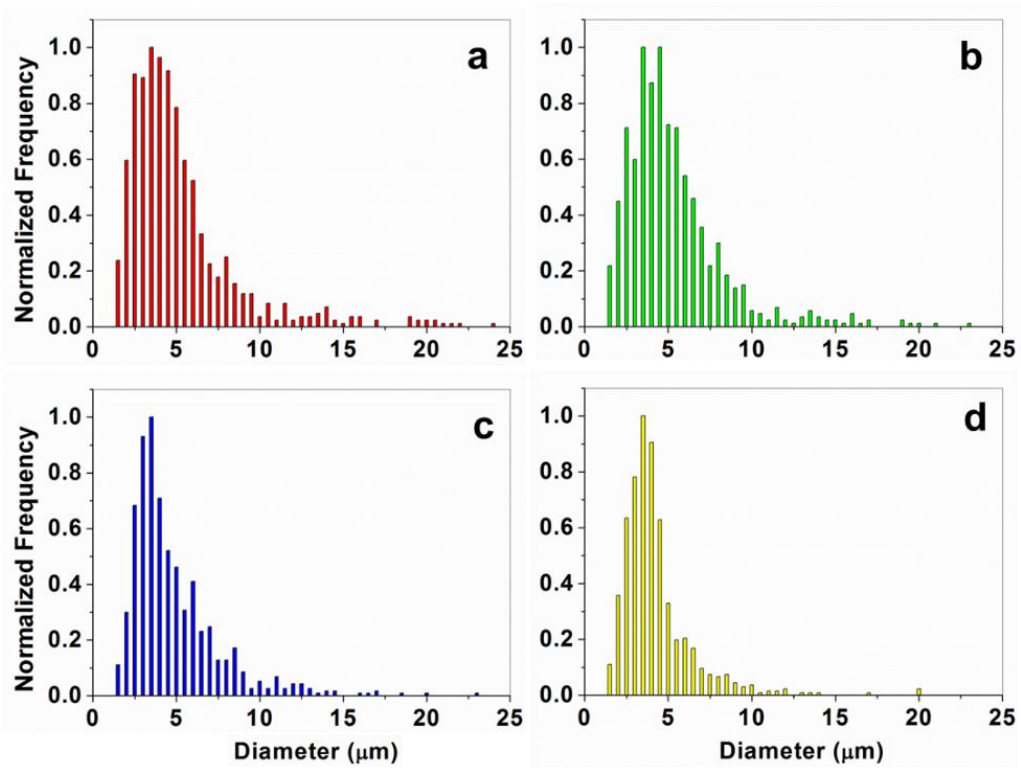

Figure 3.5 *Size distributions for GUVs prepared by electroformation; in the absence of cholesterol a) 80:20 DOPC/DPPC and with increasing cholesterol concentration b) 72:18:10 DOPC/DPPC/Cholesterol; c) 64:16:20 DOPC/DPPC/Cholesterol and d) 56:14:30 DOPC/DPPC/Cholesterol.*

GUVs obtained by this method were almost exclusively spherical, with rare membrane defects (figure 3.1b). Vesicle formation occurs by swelling of a thin lipid film deposited onto a glass capillary. Often GUVs remain attached to the surface of the glass capillary, which may be advantageous during microscopy observation.[405] This method rarely produces multilamellar vesicles (MLVs).[404] The absence of MLVs was confirmed by fluorescence microscopy. For the 20:80 DPPC/DOPC mixture, 42% of the GUVs formed were larger than 5 μm and a rather small percentage (8%) were larger than 10 μm (table 3.1). This was not altered significantly by the addition of 10% cholesterol. A cholesterol content above 20% decreases the average size of GUVs formed (figure 3.5c), narrows the size distribution and induces membrane irregularities (i.e. vesicles have various, also non-spherical shape and tend to stick to each other).[404,406] For lipid compositions containing 30% cholesterol, in addition to single GUVs, the formation of a network of connected GUVs was also observed (figure 3.1a), which is a feature consistent with lipid phase separation into lipid-ordered and lipid-disorder phases, corresponding to the formation of lipid rafts within biological membranes. Indeed studies of lipid phase behavior are often conducted with similar proportions of cholesterol.[145,146] At the highest

cholesterol content, only 24% of the GUVs are larger than 5 μm and a very small fraction (3%) are larger than 10 μm (table 3.1). Electroformation using the microscope slide setup up on the microscope slide yields vesicles with diameters ranging up to 24 μm for phospholipid only vesicles and up to 20 μm for vesicles containing 30% cholesterol.

GUVs were also formed by electroformation from lipid mixtures containing sphingomyelin (BSM) instead of DPPC. As mentioned before due to the shape of sphingomyelin, its molecules tend to pack more tightly and have previously been included, together with cholesterol, in lipid mixtures used for vesicles formation in order to observe lipid phase separation and lipid raft formation.[399] A high yield of spherical and unilamellar vesicles was observed. The size distributions for lipid mixtures composed of 80:20 DOPC/BSM and 50:25:25 DOPC/BSM/cholesterol are shown in figure 3.6. The size distributions are to some extent wider than for phospholipid-based liposomes. The addition of 25% of cholesterol to vesicles containing sphingomyelin has a similar, although a slightly smaller effect than for phospholipid vesicles, decreasing the number of vesicles above 5 μm from 56% to 37% for DOPC/BSM based GUVs (table 3.1).

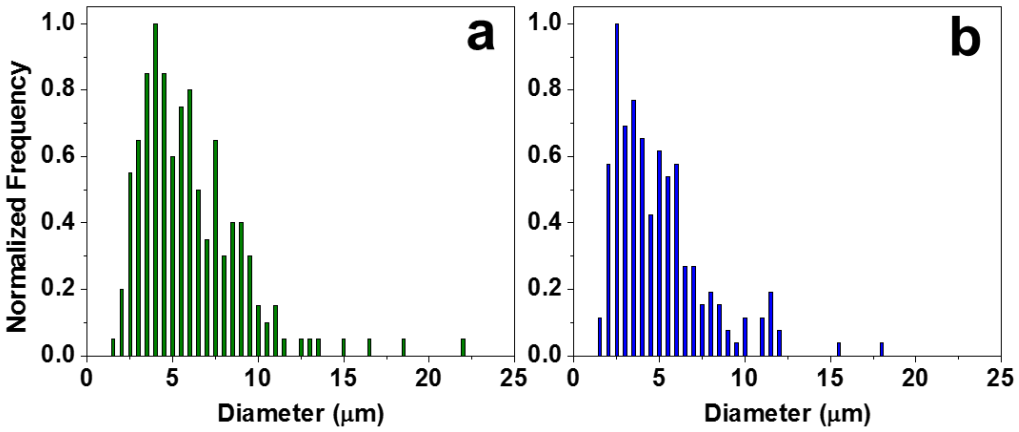

Figure 3.6 *Size distributions for GUVs prepared by electroformation; a) 80:20 DOPC/BSM; b) 50:25:25 DOPC/BSM/Cholesterol.*

3.2.4 Methods employing lipid film hydration

Three methods based on the principle of lipid film hydration as a step leading to GUVs formation have been selected; lipid hydration on an agarose film, gentle and rapid hydration. These methods facilitate vesicle preparation across a wide range of aqueous solutions and at physiological salt concentrations. They also allow charged or PEG-containing lipids to be efficiently incorporated into the membrane. Lipid hydration

methods facilitate entrapment of molecules inside liposomes, but the encapsulation efficiency differs significantly among those methods.

3.2.5 Gentle hydration

Vesicles prepared by the gentle hydration of a thin lipid film deposited onto a glass surface were mostly spherical with rare membrane defects (figure 3.1c). Isolated vesicles were used for the diameter measurements, but liposomes occurring in clusters were also observed. 36% of vesicles formed by this method at 80:20 DOPC/DPPC lipid composition were larger than 5 μm, with only 4% larger than 10 μm and sizes did not exceed 17 μm (figure 3.7a). Interestingly, the addition of cholesterol actually increased the mean diameter, the distribution of sizes and also the occurrence of larger GUVs. 64:16:20 DOPC/DPPC/Cholesterol yielded the largest vesicles, with 82% of vesicles larger than 5 μm and 33% larger than 10 μm. The largest vesicles observed were 78 μm in diameter (figure 3.7b).

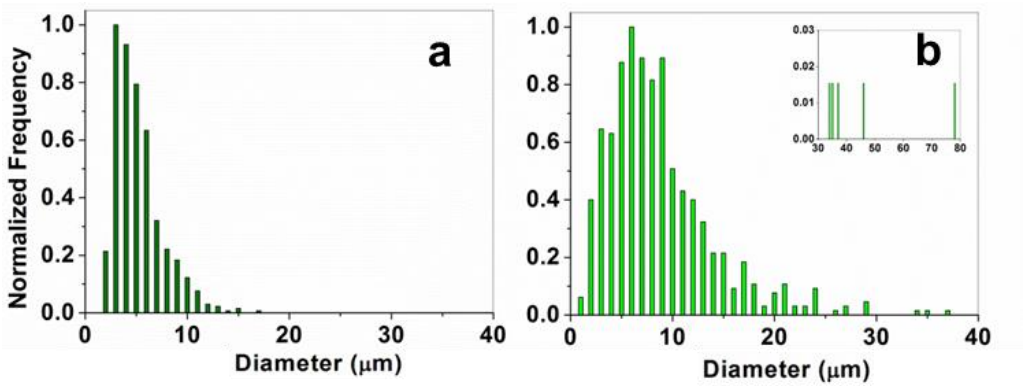

Figure 3.7 *Size distributions for GUVs prepared by gentle hydration; a) 80:20 DOPC/DPPC; b) 64:16:20 DOPC/DPPC/Cholesterol.*

Giant unilamellar vesicles are frequently used as a model to study the phase behavior of a variety of lipids. Gentle hydration is one of the methods used for the preparation of vesicles for studying lipid phase behavior.[407,408] A lipid composition of 1:1:1 DPPC/DOPC/cholesterol, previously shown to exhibit coexistence of liquid phases,[399] was used to form GUVs.

Similar to previous results, phase separation manifested by the presence of dark regions within fluorescent bilayer. Clusters and nests of vesicles were also observed (figure 3.8a). Besides spherical and isolated GUVs, with sizes up to 14 μm (12% of vesicles with size above 10 μm) a large number of clusters and small vesicles inside

bigger ones were observed. Due to a generally low yield, 100 vesicles were used for the size distribution analysis (figure 3.9a).

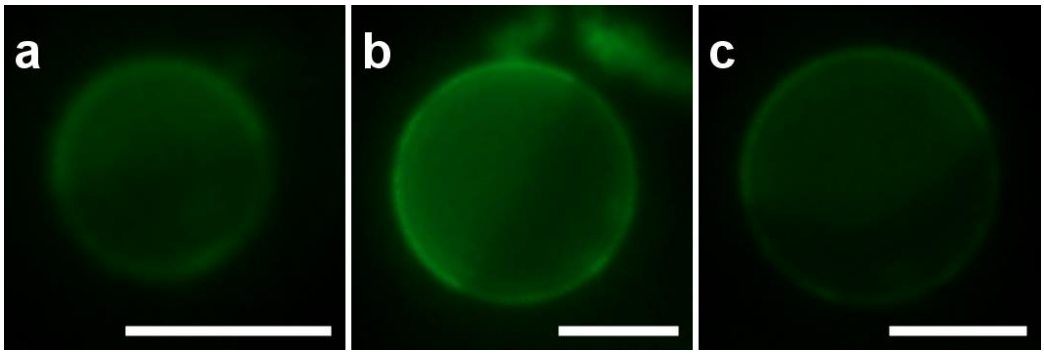

Figure 3.8 *Lipid phase separation in vesicles prepared by gentle hydration method and composed of (a) 33:33:33 DPPC/DOPC/cholesterol, (b) 23:47:30 BSM/DOPC/cholesterol and (c) 33:33:33 BSM/DOPC/cholesterol. Scale bar = 5 µm.*

Sphingomyelin is often used as a component of lipid mixtures for preparation of vesicles exhibiting lipid phase separation. Liposomes composed of 23:47:30, 33:33:33 and 53:27:20 BSM/DOPC/cholesterol were prepared. As shown in figure 3.8 (b and c) phase separation was observed within bilayers composed of 23:47:30 and 33:33:33 BSM/DOPC/cholesterol. Due to a high percentage of vesicle aggregates, GUVs within aggregates were also included in size measurements (where the edges of vesicles were clearly visible). Lipid bilayers containing 23 and 33% of sphingomyelin have narrow size distributions, similar to those with a high DPPC content (figure 3.9b), with the majority of vesicles below 5 µm (table 1.1).

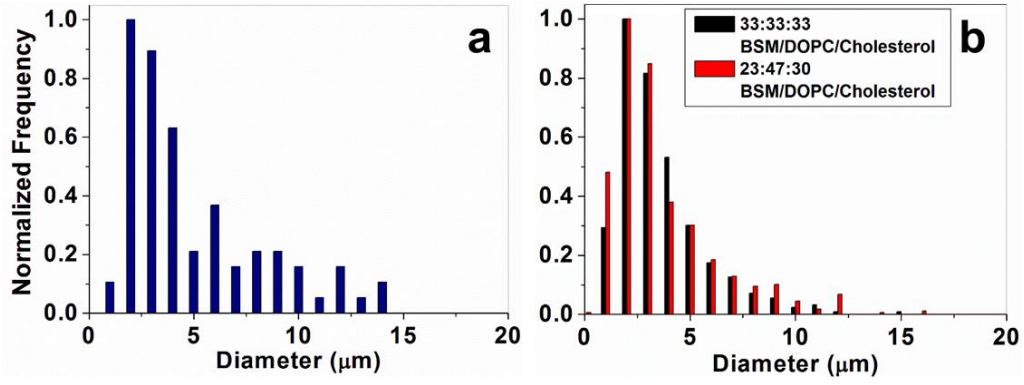

Figure 3.9 *Size distributions for GUVs prepared by gentle hydration; a) 33:33:33 DPPC/DOPC/cholesterol; b) 23:47:30, 33:33:33 (red) and 53:27:20 (black) BSM/DOPC/cholesterol.*

A lipid composition containing 53 mole percent sphingomyelin resulted in a very low vesicle yield, which didn't allow a size distribution analysis to be completed. Also

the majority of vesicles formed with high sphingomyelin content were multilamellar, star-shaped and arranged in clusters. Phase separation in bilayers containing 53% sphingomyelin could not be explicitly confirmed.

3.2.5.1 Rapid hydration

The rapid hydration method generates mostly spherical vesicles with no membrane defects (figure 3.1d) and diameters below 33 μm (table 3.1). While 56% of the vesicles formed in the phospholipid mixture 80:20 DOPC/DPPC were greater than 5 μm in size, this reduced significantly with the addition of cholesterol (figure 3.10a). The lipid composition 64:16:20 DOPC/DPPC/cholesterol lead to the formation of vesicles with diameters up to 30 μm and the narrowest size distribution of all the methods and lipid compositions used (figure 3.10b). Only 14% of vesicles were 5 μm in diameter or larger. A significant number of smaller vesicles with sizes in the region of 1μm were also observed at this composition.

Due to relatively narrow size distribution and the use of organic solvent during preparation, rapid hydration was found not to be suitable for the observation of phase separation or encapsulation.

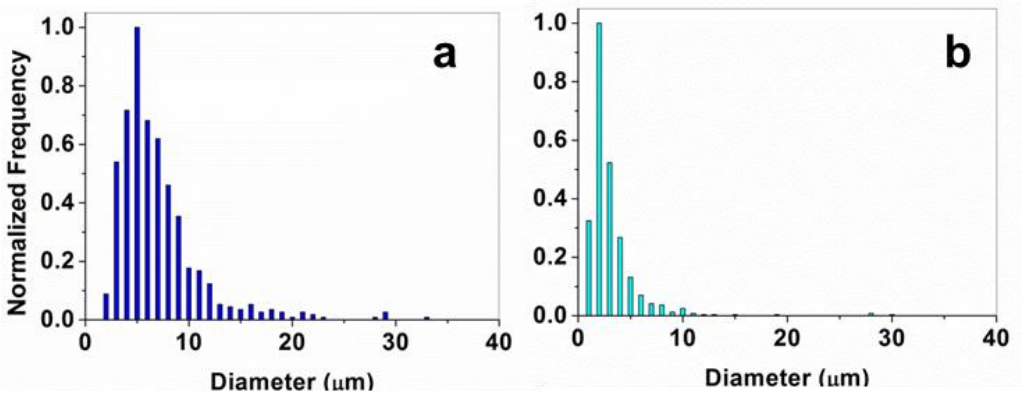

Figure 3.10 *Size distributions for GUVs prepared by rapid hydration; a) 80:20 DOPC/DPPC; b) 64:16:20 DOPC/DPPC/Cholesterol.*

3.2.5.2 Lipid hydration on an agarose film

A method involving lipid hydration on an agarose film[65,175] lead to a high yield of cell-size GUVs across a range of solution conditions, even at high ionic strength. The lipid mixture used for lipid film preparation contained 5% PEG-DOPE, which reduces liposome aggregation commonly occurring in solutions at high ionic strength. Here, that

composition was reproduced but the size distributions obtained were smaller on average than those reported previously.[65,175] Also it was observed that a number of GUVs prepared by this method contained a number of smaller vesicles inside larger ones. There are several reasons why this may have been the case. Water or low ionic strength buffer was used to hydrate the GUVs, whereas Tsai *et. al.* encapsulated actin in physiological buffer. Additionally, a basic spin coating device was used to produce an agarose film, which may not have been as precise as in the earlier work. GUVs were also measured after being washed off the agarose film, so any larger vesicles which were attached to the agarose film would not have been observed. Formation of GUVs with lower proportions of PEG-DOPE (1.5 mole %) compared to 5 mole % used previously showed no significant difference in the sizes of GUVs prepared (figure 3.11). Both compositions had the majority of GUVs above 5μm, with 18-27% of GUVs formed above 10μm in size, depending on the composition and ionic strength of the aqueous medium used to hydrate the lipid film (table 3.1).

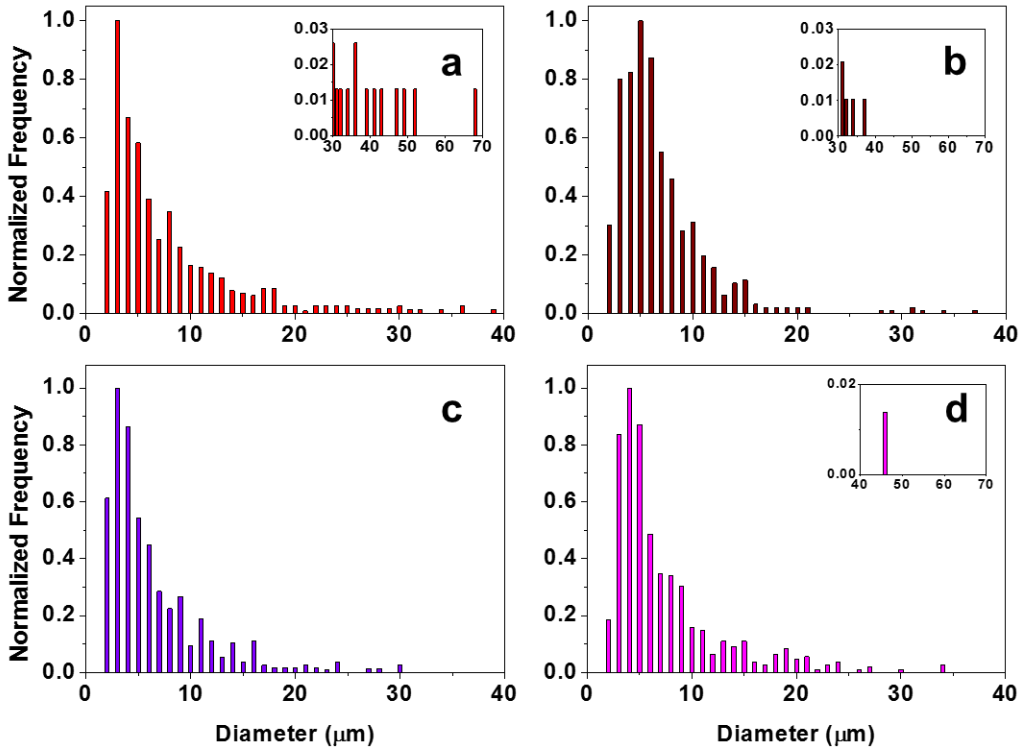

Figure 3.11 *Size distributions for GUVs prepared by lipid hydration on an agarose film; a) 98.5:1.5 DOPC/PEG-DOPE hydrated with MilliQ water; B) 98.5:1.5 DOPC/PEG-DOPE hydrated with 50mM sodium phosphate buffer; c) 95:5 DOPC/PEG-DOPE hydrated with MilliQ; d) 95:5 DOPC/PEG-DOPE hydrated with 50mM sodium phosphate buffer.*

3.2.6 Methods employing lipid-in-oil dispersion

In addition to creating a lipid film by hydration, GUVs may also be prepared from lipids dispersed in mineral oil. The two methods employing this strategy are selected here. The inverted w/o emulsion and the continuous droplet interface crossing encapsulation (cDICE) method have been used and assessed.

3.2.6.1 Inverted emulsion method

The inverted emulsion method was first described by Pautot *et. al.*[176] It involves the preparation of a water-in-oil emulsion, where the droplets, which constitute the inner solution of vesicles, are surrounded (and stabilized) by lipid molecules. Forcing the lipid coated droplets through an oil-water interface, using centrifugal force, into another (outer) aqueous solution, results in the formation of second monolayer (outer leaflet).

A very high yield of vesicles were formed by the inverted emulsion method using egg-PC lipid, which were mainly spherical and free in solution (figure 3.1g). However, a high percentage of vesicles were either multilamellar, arranged in clusters or entrapped one inside another vesicle (figure 3.3). As mentioned previously these structures can be identified using a fluorescent lipid dyes.

An emulsification process leads to the presence of mineral oil droplets within the bulk of solution. The presence of oil within the bilayer limits their use to study membrane phase behaviour. However the high yield and large sizes of GUVs makes this method desirable for encapsulation experiments. The emulsion method forms mostly cell-sized vesicles (figure 3.12a), with 60% of total liposomes with size above 5 µm and 25% above 10 µm (table 3.1).

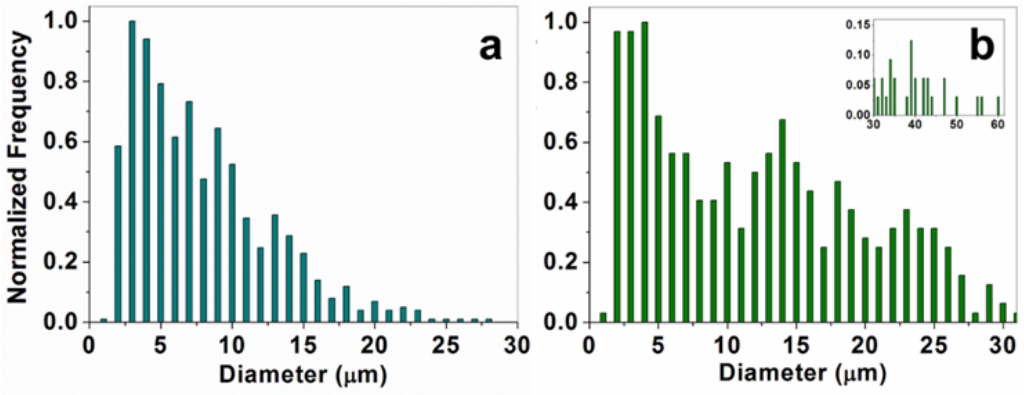

Figure 3.12 *Size distributions for GUVs prepared by inverted emulsion (a) and cDICE method (b).*

3.2.6.2 Continuous droplet interface crossing encapsulation (cDICE) method.

The continuous droplet interface crossing encapsulation (cDICE) method[64] involves the formation of vesicles by forcing aqueous droplets through a lipid-rich oil-water interface facilitated by centrifugal force. A good yield of spherical vesicles with no membrane defects was observed (figure 3.1f). A small percentage of small GUVs entrapped within bigger ones was also present. A wide size distribution (up to 60 μm) of vesicles prepared by the cDICE method was observed (figure 3.12b). 73% and 55% of the total number of GUVs formed had sizes above 5 and 10 μm respectively (table 3.1). A narrower size distribution and better control over the mean size could have been achieved using glass capillaries with a smaller diameter instead of 30 gauge needles with internal diameter of 80 μm. Similar to the inverted emulsion method, the presence of mineral oil droplets within vesicle suspensions was also observed.

3.2.7 Comparison of GUV preparation methods based on suitability for encapsulation.

All of the methods mentioned above can be used to encapsulate molecules inside vesicles, some more successfully than others. When selecting a suitable method of preparation, a number of factors, such as preparation time or use of organic solvents, must be taken into consideration. Vesicles prepared by electroformation or by gentle or rapid hydration are widely used in studies mimicking biological processes, such as membrane fusion or phase behaviour. These methods are less often selected for applications involving encapsulation due to lengthy preparation, use of electric fields or organic solvents. Also with these methods the composition of the interior and exterior solutions are identical during formation and additional steps (microdialysis or centrifugation) are required to change the outer solution.

From the methods analysed here, three were selected for encapsulation experiments (in later chapters); the lipid hydration on an agarose film, the inverted emulsion and cDICE methods (figure 3.13). The lipid hydration on an agarose film has been previously used for encapsulation of cytoskeletal protein networks.[65] It offers a good yield of vesicles and relatively good encapsulation efficiency. However since the ‘inner’ solution is simply placed on top of the lipid film, there is no control over how much of that solution is successfully encapsulated and how much of it is mixed with the

external solution. This leads to high background when encapsulating fluorescent molecules.

The continuous droplet interface crossing encapsulation method has been designed with encapsulation in mind.[64] It is fast and produces the largest vesicles among the methods analysed. The range of sizes produced by this method can be tuned by varying the experimental parameters (e.g. needle diameter and the centrifugal force). A large volume of the external and internal solution or requirements for few specific tools (e.g. needles or rotating motor) are the main disadvantages of this method.

The w/o emulsion method has been successfully used to encapsulate a variety of molecules, including proteins,[113] enzymes[177] or components of *E.coli* extract.[51] Small volumes of the inner and outer solution, high yields of cell-sized vesicles and a high encapsulation efficiency are among the most important advantages of this method. However, the possibility of oil residues within the bilayer may be undesirable.[113]

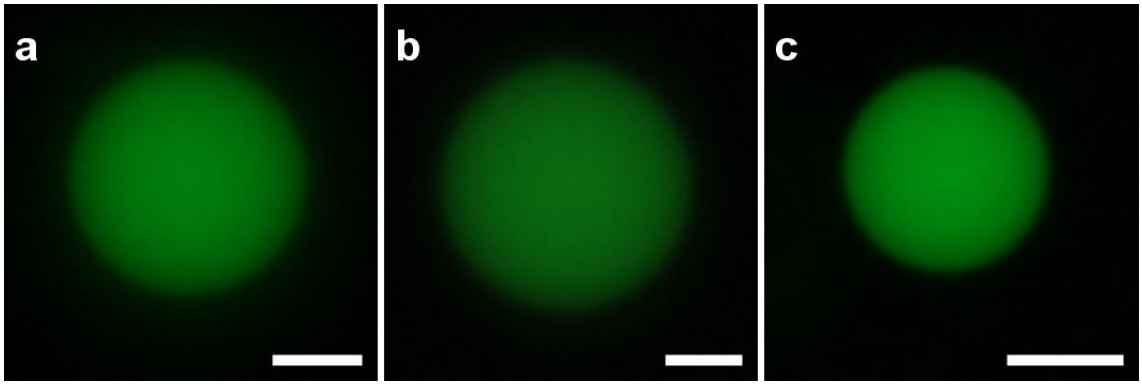

Figure 3.13 *EmGFP solution in 20 mM sodium phosphate buffer encapsulated inside phospholipid vesicles, prepared by hydration on an agarose (a), cDICE (b) and inverted emulsion (c) methods. Scale bar 5 µm.*

3.3 Conclusions

Giant unilamellar vesicles may be prepared by several different methods (electroformation, lipid film hydration or methods involving lipid dispersion). The methods described here are relatively easy, rarely require specialized equipment and exhibit a high degree of reproducibility. Each of the methods examined here produce unilamellar vesicles of biological cell size (or larger) which facilitates their observation by phase contrast microscopy and with addition of fluorescent dye, also by fluorescence microscopy. The proportion of vesicles of larger sizes formed depends on both the method

used to prepare them and as well as the lipid mixture used. For a fixed composition, substantially larger vesicles can be prepared by selecting an alternative method. Here, size distributions have been measured for a set of membrane compositions using several of the methods described. Comparison of the overall size distributions and the proportions of larger vesicles formed for each lipid composition and method may simplify the process of selecting a method optimal for a given application.

During the course of the project some undesirable forms of vesicles (or artifacts) have been observed. Approaches for their identification have been proposed, and include addition of fluorescent lipid dye for identification of MLVs and vesicle nests and oil-soluble dye for detection of oil droplets.

All of the methods described above may be used for encapsulation (of biomacromolecules, for example); however the success will depend strongly on the method chosen. Electroformation along with gentle and rapid hydration are generally not selected for encapsulation for several reasons,[165] mainly due to low efficiency. The applicability of a given method for encapsulation was determined based on the use and time required for preparation, reproducibility of the results and finally the level of encapsulation efficiency. Here, lipid hydration on an agarose film or the inverted emulsion and cDICE method were selected and used for this purpose, which will be discussed in following chapters.

The above results provide comparison of several methods of vesicle preparation based on the size and quality of vesicles, as well as the ability to efficiently encapsulate variety of molecules. This type of assessment provides information necessary for application tailored selection of method.

Chapter 4

Phase behaviour of a synthetic glycolipid in mixtures with phospholipids

4.1 Introduction

Glycolipids are a highly diverse class of lipids. In addition to naturally occurring molecules, a range of synthetic glycolipids have been developed.[203,204,409–411] This structural and functional variety is widely used in a range of academic and industrial applications.[412–415] Glycolipid biosurfactants have potential antimicrobial applications due to their ability to damage cell membranes or to prevent the formation of biofilms.[416] A variety of biological processes such as cellular uptake, molecular trafficking and certain aspects of immune response have been studied within natural and model membranes using fluorescent, photoactive, biotinylated and radio-labelled glycolipid-based probes discussed extensively in a recent review.[417]

Glycolipids (both natural and synthetic) may be incorporated into the lipid bilayers of giant unilamellar vesicles. These types of vesicles are used to study glycolipid phase behaviour and the properties of glycolipid-rich domains.[418–420] Studies involving the phase behaviour, shape transformation or fission of GUVs containing lipopolysaccharides (LPS) are of special interest since LPS are strongly involved in the inflammation process.[421,422] Glycolipid containing vesicles, due to the specificity of carbohydrate interactions are investigated as vehicles for targeted drug delivery.[423,424] The defined structure of the carbohydrate head group facilitates delivery onto selected organs or tissues, by specific interaction with an appropriate receptor (for the carbohydrate used). For example vesicles containing sialyated Lewis antigens, which bind to selectin receptors present on the surface of various cell types, such as endothelial cells, platelets and leukocytes can mimic biological antigens and therefore alter the immune response of targeted cells.[425–427] A variety of drugs may be encapsulated within glycolipid vesicles providing a way to induce an immune response,[428] alternative therapies for immunodeficiency,[429] inflammation[430] or cancer[431] to name just a few. Recently, liposomes incorporating glycolipids have also been used for targeted delivery of gene-based therapeutics.[432] Growing interest in the role of glycolipids in bacterial and viral infections and studies involving the interaction of pathogenic antigens with glycolipid vesicles may lead to new glycolipid-based therapeutic strategies or novel approaches to drug delivery and molecular recognition.[433,434]

The preparation of a model cell mimicking cell adhesion or signalling requires the presence of molecules involved in this processes within the lipid bilayer. The aim of this study was to incorporate a protected synthetic glycolipid, with a galactose-based

headgroup and two asymmetrical hydrocarbon tails, into phospholipid and phospholipid-cholesterol based liposomes at biologically relevant concentrations. The stability and the appearance of the glycolipid-containing vesicles were observed by phase contrast and fluorescence microscopy. The phase behaviour of the synthetic glycolipid was analysed using various modes of microscopy (phase contrast, polarized light and fluorescence) with the aid of various fluorescent dyes depending on its concentration in the lipid mixture.

The use of synthetic structures as glycolipid mimetics also removes the necessity of difficult and often time consuming purification of naturally occurring forms. The synthetic design of the glycolipid used here provides the opportunity for further modification of the functionality of the carbohydrate head group, greatly extending the number of ways in which the specificity of the interaction may be altered.

4.2 Results and discussion

4.2.1 Incorporation of glycolipid within bilayer.

Giant unilamellar vesicles were prepared using variety of methods, including electroformation, gentle and rapid hydration, the water-in-oil emulsion method and the hydration on an agarose film method, as described in section 2.4. Lipid mixtures used were composed of DOPC, cholesterol, a range of fluorescent lipid-based dyes and the synthetic glycolipid which structure is shown in figure 4.1. The synthesis of the glycolipid has been described previously.[366] Its structure consists of an acetylated (-OAc instead of -OH) galactose-based head group, flexible ethylene linker and two asymmetric hydrocarbon tails.

The aim of the initial experiments was to confirm the presence of the protected synthetic glycolipid within the lipid bilayer formed. A lipid film consisting of only the synthetic glycolipid (100%) does not swell after hydration and therefore does not produce vesicles. Vesicles were produced when glycolipid concentrations between 1-5 mol percent were added to binary lipid mixtures with DOPC or ternary lipid mixtures with DOPC and cholesterol. At concentration greater than 5 mol % of glycolipid, in addition to vesicles, tubular structures, discussed in section 4.3.3, were also observed.

Successful formation of vesicles in the presence of glycolipid was achieved using all of the methods attempted, such as the electroformation, lipid film hydration methods or the inverted emulsion method.

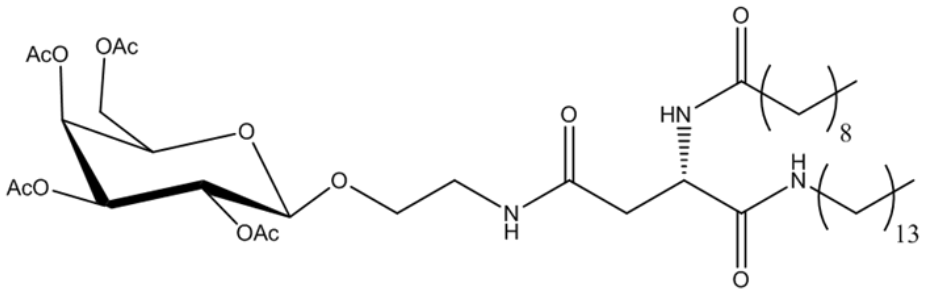

Figure 4.1 *Chemical structure of the synthetic glycolipid.*

4.2.1.1 Fluorescent dyes used in microscopic analysis of structures formed in the presence of the synthetic glycolipid

Direct observation of the glycolipid within bilayer was not possible, since there is no label attached directly to it. Lipid bilayer containing the synthetic glycolipid was observed by widefield fluorescent microscopy in the presence of fluorescent dyes, such as bodipy FL C_5 ceramide, bodipy TR ceramide or cholesteryl bodipy FL C_{12} (figure 4.2). The amount of dye used depends on its photo-stability, lifetime and the quantum yield. Additionally it was shown that for majority of fluorescent dyes the addition of dye below 2 mol % of total lipid content have negligible effect on mechanical properties of membrane.[435] Nonetheless, the presence of the fluorescent dye within the bilayer was not a conformation of the incorporation of the glycolipid. Instead to confirm the presence of the synthetic glycolipid within the lipid membrane the properties of vesicles formed in the presence of the glycolipid was compared to those formed in its absence.

4.2.1.2 Evidence of glycolipid incorporation into GUVs

During the preparation of the vesicles, care was taken to ensure that the synthetic glycolipid was fully dispersed within the solvent (chloroform or mineral oil) and within the resulting lipid film. Low total lipid concentrations (10 mM) and spin-coating instead of droplet deposition (where applicable) were used to ensure the formation of a thin and uniform lipid film which in turn promotes its full hydration and complete swelling. Following the completion of vesicle formation, no evidence of the presence of a lipid film still present on the surfaces was observed, which indicated that the glycolipid did swell at the same time as the other lipids present in the film. Also, no artefacts or free-floating material of any sort was present within the vesicle suspension. This strongly suggests that all of the glycolipid present within the lipid film was fully incorporated into the lipid bilayer.

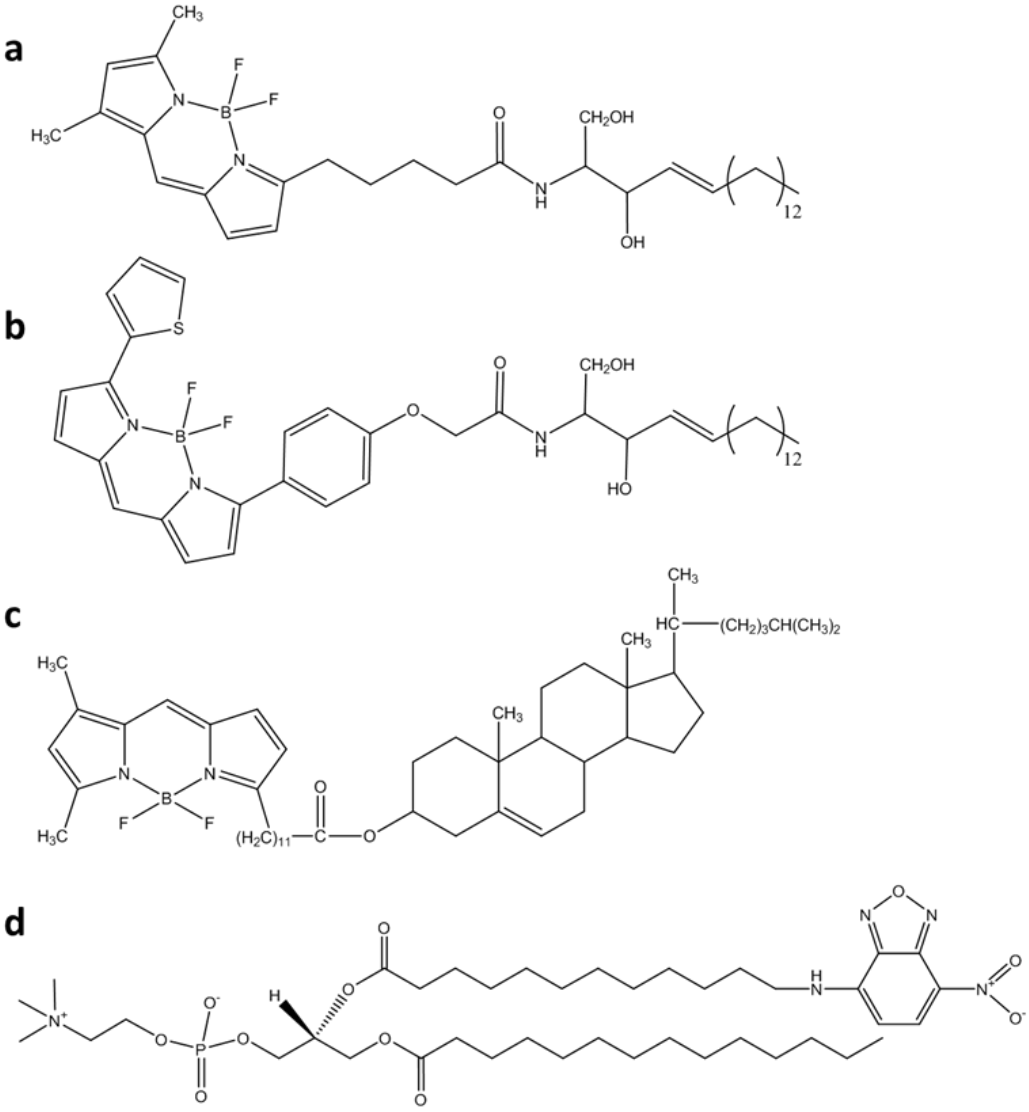

Figure 4.2 *Chemical structures of the bodipy FL C_5 ceramide (a) and bodipy TR ceramide (b), cholesteryl bodipy FL C_{12} (c) and (14:0-12:0) NBD-PC (d).*

4.2.1.3 Characteristics of glycolipid vesicles

A very high yield of spherical vesicles prepared in the presence of 1-5 mol % glycolipid was observed. Liposomes containing the synthetic glycolipid exhibit characteristics not observed in phospholipid-based GUVs. The differences include a strong tendency to form chains and clusters (figure 4.3), which was not observed in the absence of the glycolipid, with the exception of GUVs formed in the presence of 30% cholesterol (see chapter 3, figure 3.1a). The presence of the synthetic glycolipid also leads to formation of higher numbers of multilamellar and elongated vesicles.

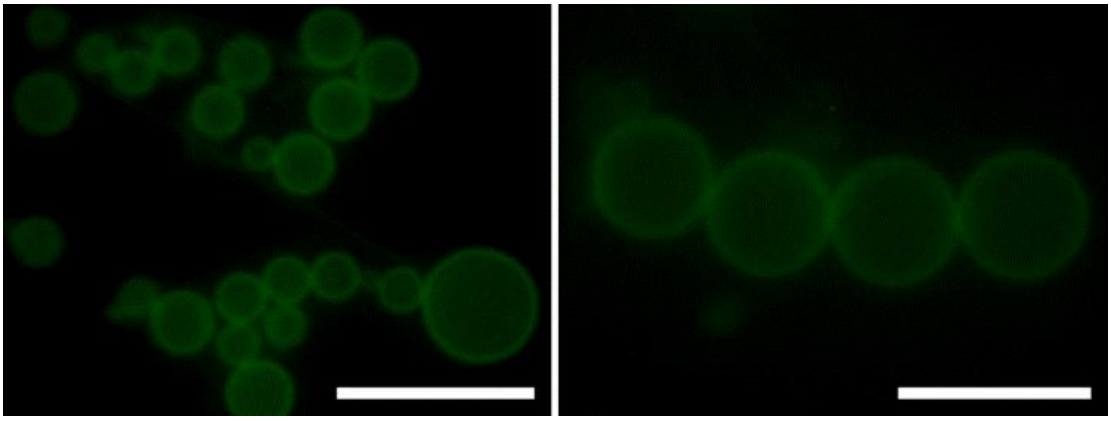

Figure 4.3 *Clusters of GUVs containing the synthetic glycolipid, formed by gentle hydration method, composed of 1:9 glycolipid–phospholipid mixtures and 0.1% of bodipy FL ceramide. Scale bar = 10 µm.*

A size distribution analysis of liposomes prepared by the gentle hydration method composed of 1:9 glycolipid/phospholipid (DOPC) was performed using the method described in section 3.3.2. In comparison with vesicles composed of 1:9 DPPC/DOPC prepared in the same way, the glycolipid-GUVs were significantly smaller and had narrower size distributions (figure 4.4).

The vesicles containing the synthetic glycolipid were rather stable. No changes in the shape or stability of the vesicles stored at room temperature were observed for up to 12 days, which is longer than for phospholipid-based vesicles. Hydrogen bonding interactions altering the polarity of the lipid head group are believed to be the reason of the improved stability.[436]

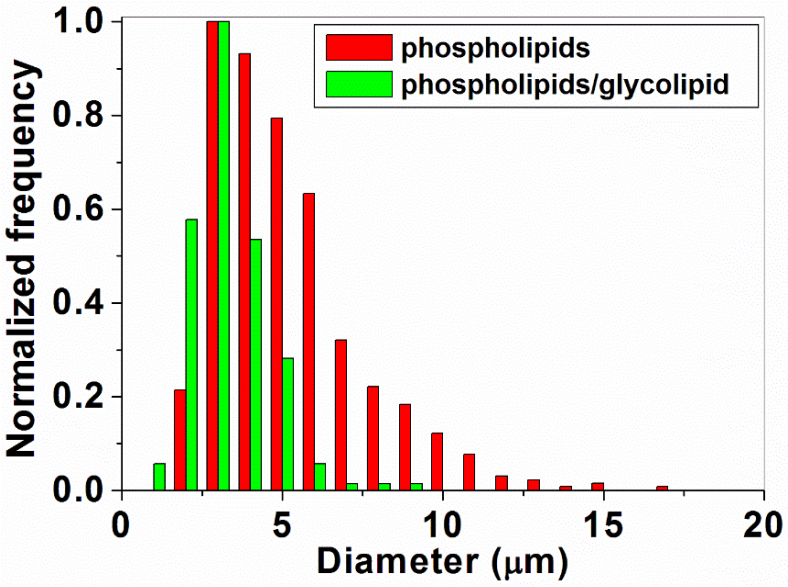

Figure 4.4 *Size distribution of GUVs prepared by gentle hydration method from lipid film containing only phospholipids (red) or 1:9 glycolipid/phospholipid mixtures (green).*

4.2.2 Glycolipid phase behavior – lamellar phase formation

Model membranes composed of variety of lipid mixtures are commonly used to study lipid phase behavior.[60,437] The coexistence of various lamellar phases (mainly the liquid ordered L_o and liquid-disordered L_d) was previously shown for variety of lipid mixtures, such as ternary mixtures containing DOPC, cholesterol and DPPC or sphingomyelin (SM) and in fact substitution of DPPC for SM results in only small differences in the phase diagrams.[145,149,399] The 1:1:1 DPPC/DOPC/cholesterol, 1:1:1 BSM/DOPC/ cholesterol and 23:47:30 BSM/DOPC/cholesterol lipid mixtures were previously used to form vesicles exhibiting phase separation (chapter 3 figure 3.8). The synthetic glycolipid used here and the sphingomyelin share some structural similarities. GUVs containing the synthetic glycolipid were therefore formed in the presence of fluorescent dyes and analyzed using fluorescent microscopy to investigate whether the synthetic glycolipid causes phase behavior similar to that observed for membranes in the presence of sphingomyelin.

4.2.2.1 The effect of glycolipid concentration on lipids phase behavior

Giant unilamellar vesicles were prepared using the gentle hydration method from DOPC in mixtures with increasing concentrations of the synthetic glycolipid (figure 4.5). Fluorescent dyes, bodipy FL C_5 ceramide and bodipy TR ceramide were added to the lipid mixture in order to facilitate observation of phase separation by widefield fluorescence microscopy. The glycolipid appears to be uniformly and fully incorporated within the bilayer as no lipid phase separation or residual material remaining after hydration was observed. The presence of the synthetic glycolipid leads to formation of higher numbers of multilamellar and elongated vesicles. Also the size and yield of vesicles decreased with an increase of glycolipid content within the bilayer, with the most drastic effect observed at 20 mol % of glycolipid. This effect is very similar to behaviour observed for vesicles formed with high cholesterol content within DOPC/DPPC lipid mixtures discussed in section 3.3.3 (see figure 3.5).

Vesicles containing identical lipid compositions as shown in figure 4.5 were also prepared using a rapid hydration method (data not shown). The size and the appearance of GUVs prepared by the gentle and rapid hydration methods were almost identical. The glycolipid was uniformly distributed within the bilayer and no phase separation was detected. This suggests that the observations with regard to the appearance and size

decrease accompanying the increase in glycolipid concentration were due to the presence of glycolipid (and not related to the method of preparation).

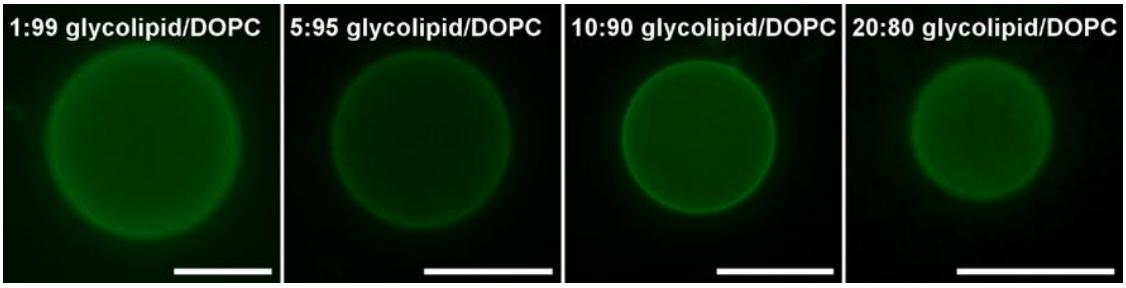

Figure 4.5 *Fluorescence microscopy images of GUVs prepared by gentle hydration from mixtures of synthetic glycolipid, DOPC (lipid composition at the top of the image) and 0.1% of bodipy FL C_5 ceramide. Scale bar = 10 µm.*

4.2.2.2 The effect of cholesterol concentration on lipid phase behavior

The effect of cholesterol on glycolipid containing membranes was evaluated. Cholesterol is known to induce phase separation in membranes of various compositions.[145,150,397,438] Moreover its presence was implicated in the formation of sphingomyelin/cholesterol rich domains within biological membranes.[155,193] The phase behaviour of glycolipid in the ternary lipid mixtures was analysed in vesicles composed of DOPC, 5 mol % glycolipid, 0.05 mol % cholesteryl bodipy FL C_{12} and various concentrations of cholesterol and DOPC, prepared using gentle hydration method (figure 4.6). The cholesteryl bodipy dye was previously used to study lipid phase behaviour.[439] It was shown to preferentially partition into the cholesterol-rich liquid-ordered phase due to its structural similarity to cholesterol (figure 4.2c).

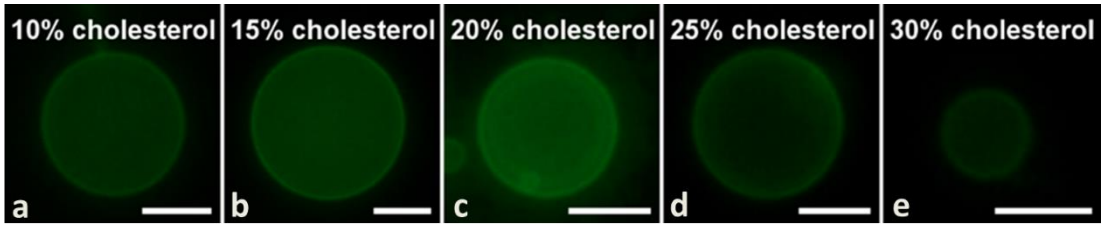

Figure 4.6 *Fluorescence microscopy images of GUVs prepared by gentle hydration method from lipid mixtures containing 0.05% cholesteryl bodipy FL C_{12} and a) 85:10:5 DOPC/ cholesterol/glycolipid; b) 80:15:5 DOPC/cholesterol/glycolipid; c) 75:20:5 DOPC/cholesterol/ glycolipid; d) 70:25:5 DOPC/cholesterol/glycolipid; e) 65:30:5 DOPC/cholesterol/glycolipid. Scale bar = 5 µm.*

Within lipid bilayers containing both the glycolipid and various concentrations of cholesterol, the fluorescent cholesteryl bodipy dye was uniformly distributed and no

evidence of lipid-ordered and lipid-disordered phase coexistence was observed. However, increasing concentrations of cholesterol present within the bilayer lead to a decrease in the number of vesicles formed. Also, significantly smaller average diameters of the liposomes were related to high cholesterol content within the membrane.

4.2.2.3 Analysis of lipid phase behavior using fluorescent dye pairs

Vesicles were also prepared using equimolar concentrations of the synthetic glycolipid, DOPC and cholesterol. The coexistence of the lipid phase separation for similar lipid mixtures, but with either DPPC or sphingomyelin instead of the glycolipid was shown in figure 3.8 (see section 3.3.4). The 33% content is above glycolipid's solubility within the lipid bilayer and guarantee its oversaturation in the membrane. Lipid vesicles with equimolar mixtures of the glycolipid, DOPC and cholesterol were formed in the presence of both of the ceramide-based dyes; bodipy FL C_5 (green) and bodipy TR ceramide (red) which, based on their structural features were expected to partition into the glycolipid-rich phase (figure 4.2 a and b). This was done in order to determine whether the small difference in the structure of the fluorescent tag, may alter their behavior within the coexisting lamellar phases. Phase separation was not observed and both dyes seemed to be co-localized and uniformly distributed within the membrane. To test if either of the two fluorescent ceramide dyes was capable of detecting phase separation within the bilayer, they were used in pairs with other well-known dyes, the cholesteryl bodipy FL C_{12} and the NBD-PC (figure 4.7). The cholesteryl bodipy FL C_{12} (figure 4.2c) is a cholesterol analogue, that partitions into cholesterol-rich domains, also known as lipid rafts or lipid-disordered lamellar phases. NBD-PC (figure 4.2d) is known to partition into phospholipid-rich domains.[225,440,441] In fact, the cholesteryl bodipy FL C_{12} dye was previously used to observe phase separation within lipid bilayers formed from DPPC/DOPC/cholesterol and BSM/DOPC/cholesterol mixtures (chapter 3, figure 3.8).

The use of glycolipid/DOPC lipid mixtures with the above pairs of fluorescent dyes was to examine whether the phase separation of the glycolipid from either the phospholipid-rich or cholesterol-rich domains was occurring. Since both pair of dyes were homogenously dispersed within the lipid bilayer of liposomes and separation of the fluorescent dyes was not observed (figure 4.7) it was concluded that the synthetic glycolipid was also uniformly distributed in the lipid bilayer of vesicles with all of the lipid mixtures studied.

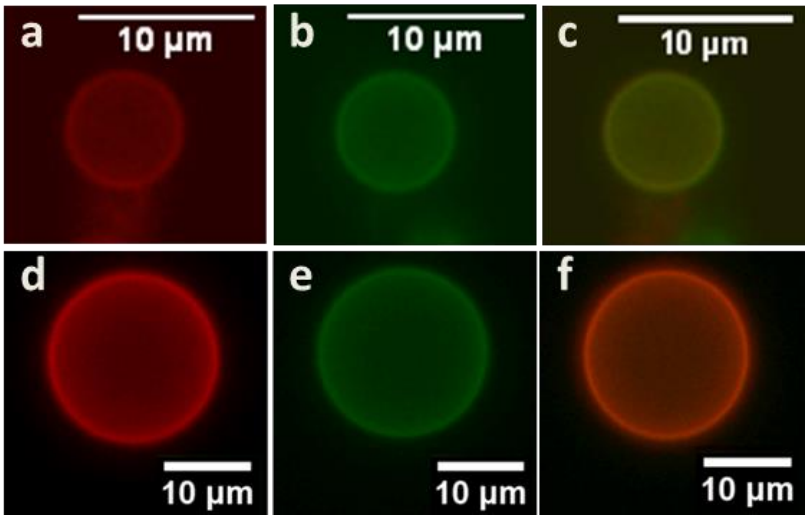

Figure 4.7 *Fluorescent microscopy images of GUVs (33:33:33 DOPC/glycolipid/cholesterol) prepared by gentle hydration. Lipid bilayer was labelled with: (a-c) 0.05% cholesteryl bodipy FL C_{12} and 0.05% bodipy TR ceramide; (d-f) 0.05% bodipy TR ceramide 1% NBD-PC; (c & f) overlay of the two images.*

It is important to note that the preference of a given fluorescent lipid to partition into either the liquid-ordered or liquid-disordered phase is strongly influenced by its structure, mainly the size, chemical character and location of the tag within the lipid molecule. The dye's preference towards one of the lipid phases also strongly depends on the characteristics of the other lipids present in the mixture. For that reason the choice of the dye should be carefully considered and partitioning preferences of a given dye should be tested individually for every lipid mixture.

4.2.2.4 Lipid phase behavior in GUVs formed by inverted emulsion method

Vesicles containing the synthetic glycolipid were also prepared using the inverted emulsion method. GUVs were observed within the bulk of the aqueous solution as well as on the surface of mineral oil droplets. As discussed in section 3.3.1 formation of mineral oil droplets is a common artifact of this method. Fluorescent dye was included in the lipid mixture to analyze the lipid distribution on the surface of the droplets. Similarly to results described above (gentle and rapid hydration methods), glycolipid incorporation lead to its uniform distribution within the lipid bilayer, for liposomes present in the bulk and attached onto the surface of the oil droplet.

In order to analyze the behavior of the synthetic glycolipid on the surface attached vesicles two fluorescent dyes; bodipy TR ceramide and NBD-PC were also incorporated into the bilayer (figure 4.8 a and b). Both of these dyes were uniformly distributed as shown in the overlay of the images (figure 4.8c) and the fluorescent intensity profile

(figure 4.8d) and therefore no phase separation was observed on the surface of mineral oil droplets. However it was presumed that the vesicles present on the surface of the oil droplets are very likely the source of material for the formation of the lipid tubules (described later).

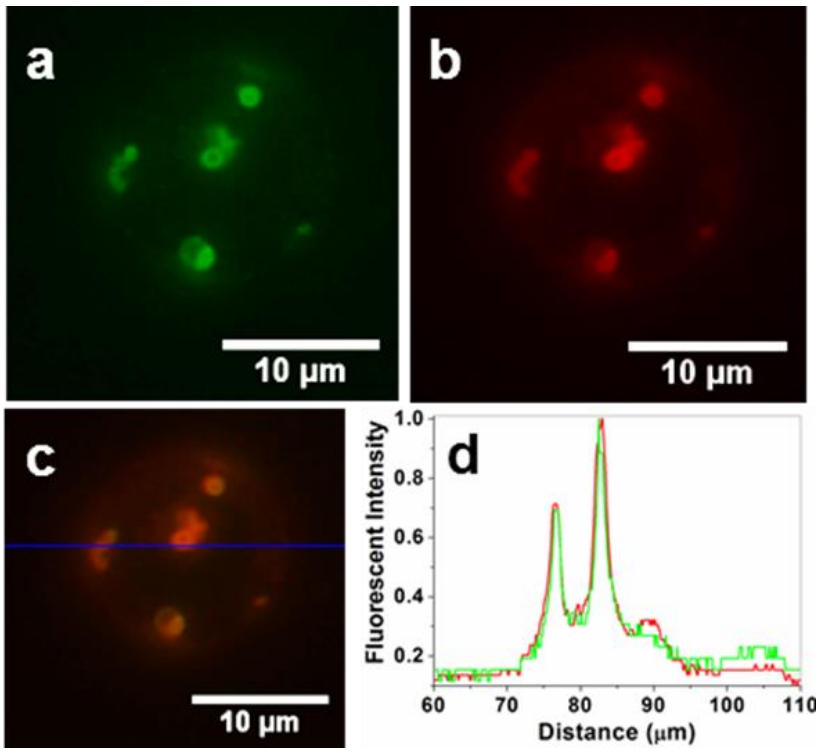

Figure 4.8 *Fluorescent microscopy images of GUVs attached to the surface of the mineral oil droplet; (a-c) composed of 80:20 DOPC/glycolipid with 0.1% bodipy FL C_5 ceramide and1% NBD-PC); (d) fluorescent intensity profile (cross-section intensity).*

4.2.3 Glycolipid phase behavior – non-lamellar phases

Lipid mixtures containing up to 5 mol % of the synthetic glycolipid form GUVs with a uniform distribution of the bilayer components. Incorporation of larger quantities of the glycolipids (10 mol % and above), results in the simultaneous formation of both, lipid vesicles and tubular structures as illustrated in figure 4.9. Imaging of both of these at the same time was challenging, mainly due to the difference in their size and localization within the focal plane.

Lipid tubules were initially observed in the sample from electroformation, where the lipid film was swelled in aqueous solvent with an aid of an AC field (figure 4.10). They were usually observed in form of bundles of tubules resembling overall spherical structures and were present mainly in the vicinity of the glass capillary, onto which the

lipid film was deposited, however the majority seemed to be floating freely in solution as opposed to being attached to the lipid film deposited on the surface of glass capillary. The number of tubular structures increased with higher concentration of the synthetic glycolipid included in the initial lipid mixture.

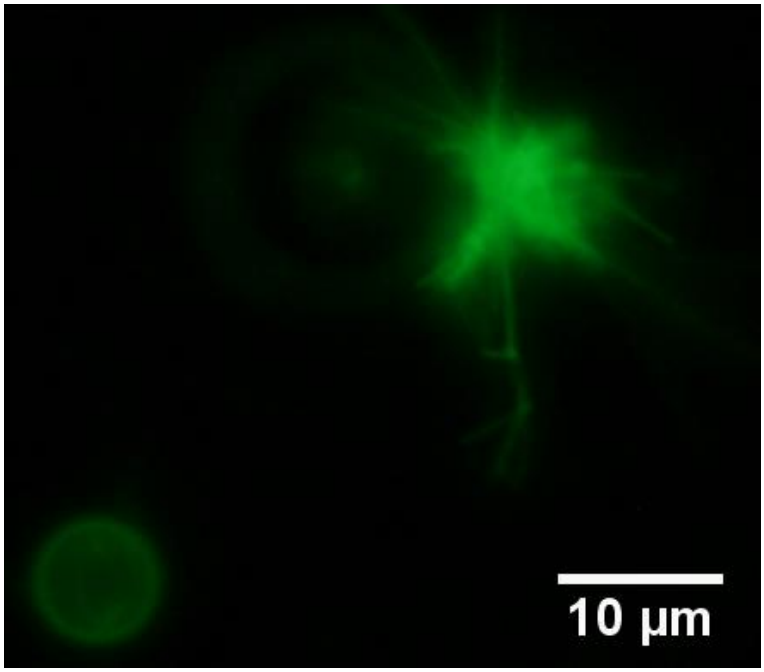

Figure 4.9 *Simultaneous formation of vesicles and tubular structures from lipid mixtures containing above 5% of the synthetic glycolipid (here 10:90 glycolipid/DOPC) by gentle hydration method. Scale bar = 10 µm.*

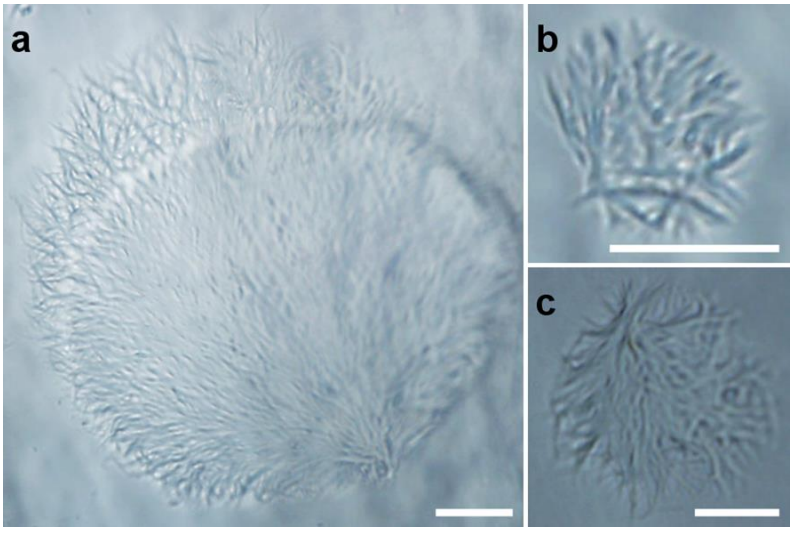

Figure 4.10 *Phase contrast images of tubules formed by the electroformation method in aqueous solvent from a lipid composition 20:80 glycolipid/DOPC. Scale bar = 10 µm.*

Both vesicles and tubules were also observed in lipid preparations containing more than 5% glycolipid prepared by the gentle (figure 4.9) and rapid hydration (figure

4.11) methods (indicating again that the structure are not an artifact of a particular preparation method). In fact the same type of self-assembled structures are formed by all of these methods, as long as the glycolipid content is kept identical. This clearly suggested that presence of the lipid tubules (at glycolipid concentration above 5 mol %) can be fully attributed to the behavior of the protected glycolipid within the phospholipid membrane. Tubules were formed both in the presence (figure 4.11) and absence (figure 4.10) of fluorescent dyes, which eliminates the possibility of dye-induced phase separation. However the presence of the fluorescent ceramide dyes in the tubules is a conformation that these types of dyes can be used to observe glycolipid behavior within the membrane. Since the fluorescence images show the ceramide dyes to be uniformly distributed, it suggest that the lipid composition in the tubules is also homogenous.

Lipid tubules formed from binary mixtures (glycolipid and DOPC) were also analyzed using polarized light microscopy (figure 4.11 middle panel). In this method the polarized light interacts with the birefringent sample and generates a bright image with a black background (see section 2.3.2). As the lipid tubules formed here can be visualized using polarized light microscopy, it is clear that they are not an amorphous material but possess some degree of structural order. Similar properties were observed for ternary lipid mixtures containing the synthetic glycolipid, DOPC and cholesterol, however, in those lipid mixtures the presence of crystalline material was shown to be due to the presence of cholesterol and were most likely cholesterol crystals.

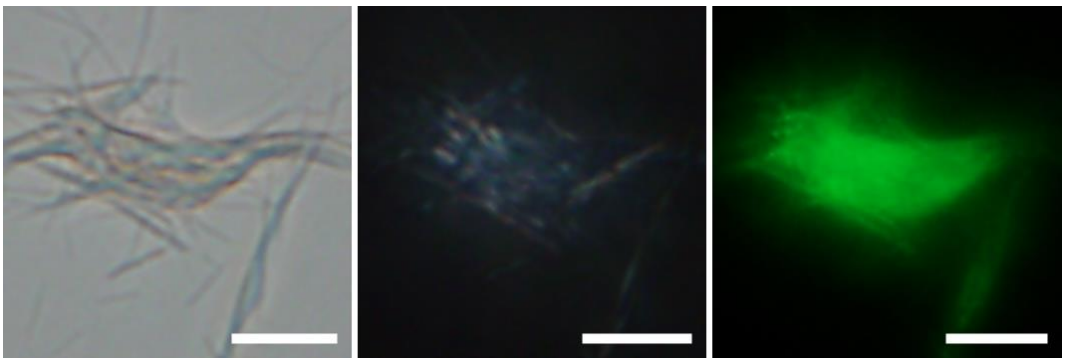

Figure 4.11 *Optical microscopy images of tubular structures observed in binary mixtures of DOPC/glycolipid with 0.1% of bodipy FL C5 ceramide; left panel; phase contrast, middle panel; polarization; right panel, fluorescence due to presence of the dye. Scale bar = 5 µm.*

Different behavior was observed while using the inverted emulsion method. A Relatively small number of vesicles (compared to the hydration methods) were present within the aqueous solvent and on the surface of mineral oil droplets, as shown in the figure 4.8. Rather, the tubular structures which in the case of hydration methods were

found in the aqueous solvent, here were formed within the interior of the mineral oil droplets (figure 4.12 d-e). Moreover, with increasing size of the droplet, which in turn means a higher concentration of the lipid molecules, the size of the tubule bundles increases. The overall size of the bundles of tubular structures was similar in both solvents (water and oil) as shown in figure 4.12. Given that the synthetic glycolipid was fully dispersed in both the chloroform and the mineral oil, the formation of the tubular structures cannot be attributed to its insolubility in either of the solvents but rather is an outcome of oversaturation within the lipid bilayer.

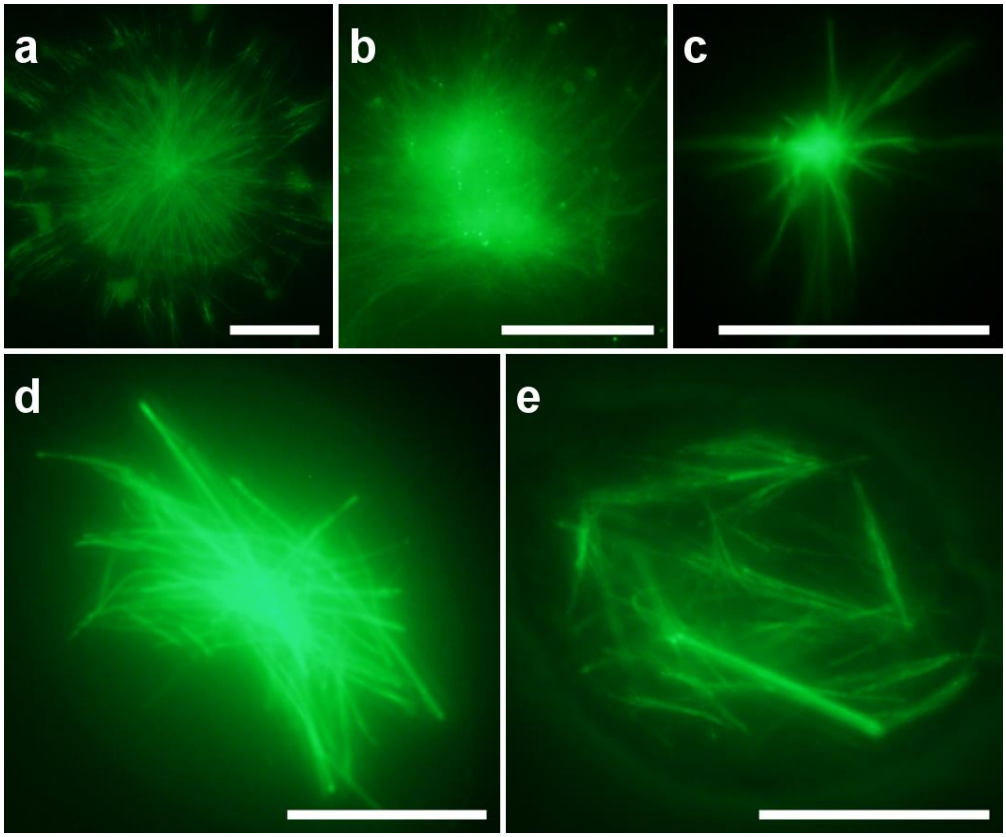

Figure 4.12 *Fluorescence microscopy images of tubules formed in aqueous solvent (a-c) and in mineral oil (d-e). Scale bar = 20 µm.*

The above observations suggest the formation of a columnar lipid phase, where in aqueous solvent the tubules consists of lipid molecules arranged hexagonally and in mineral oil they exhibit inverted hexagonal packing. It was estimated, based on the size of the tubular structures, that they were formed by several layers of lipid with a hexagonal arrangement. Extensive studies of phospholipid phase behavior indicate that pure DOPC or DOPC/cholesterol mixtures do not exhibit a lamellar to hexagonal phase transition. This type of behavior was observed after the inclusion of non-membrane forming lipids, usually PE.[139,408] This strongly suggests that the glycolipid must be present within the

tubular structures in order to drive this behavior as similar structures are not observed in its absence.

Taken together, these observations support the initial assumption that the glycolipid is incorporated in both the lipid vesicles and the tubular structures. However whether the glycolipid is present in these structures at concentrations identical to those used in the lipid film preparation cannot be confirmed unambiguously, although there is no evidence to suggest otherwise.

Formation of the hexagonal and inverted hexagonal phases has been observed for a variety of lipids, including various glycolipids.[204,442,443] The transition between lamellar and hexagonal or inverted hexagonal arrangements have been shown to occur in biological membranes due to the presence of high concentrations of lipids with a tendency to form non-lamellar structures.[137] These types of lipid phases are associated with a variety of biological processes, including the formation of tight junctions or as intermediates in membrane fusion.[444] Factors affecting lipid phase behavior have previously been reviewed[137] and include the properties of the headgroup (mainly its hydrophilicity), type of chain linkage, structure of hydrocarbon chain or the nature of the solute.

At glycolipid concentrations below 5 mol %, only the lamellar phase was observed. Above that concentration, which also is considered to be the solubility of the glycolipid within bilayer, coexistence of lamellar and columnar (arrangement depends on the solvent system) lipid phases was observed. The transition between lamellar and hexagonal lipid phases is driven by the curvature stress exerted,[445] which in the lipid mixtures studied here, occurs via a high concentration of the synthetic glycolipid present within the lipid membrane.

This behavior may be considered in terms of the packing parameter $\rho = v / a\ l$, which depends on the nature and area of the head group, *a* and the length *l* and volume, *v* of the hydrocarbon chains. The packing parameter is commonly used to predict the type of self-assembled structure formed by a given lipid.[134]

Lamellar phase formation is preferred in the case of lipid mixtures with an overall packing parameter of $\rho < 1$, which, based on the experimental results presented above is the case for lipid mixtures with a synthetic glycolipid content below 5 mol %. The structure of the protected glycolipid used here, consists of bulky sugar-based head group and two asymmetrical, fully saturated hydrocarbon tail groups, which results in a larger head group area, *a*, and smaller value for the volume hydrocarbon chain, *v* when

compared with the phospholipid components. Therefore in lipid mixtures containing 10 mol % or more of the glycolipid, the packing parameter will have a value below 1, resulting in the occurrence of the normal hexagonal phase (H_I), where the sugar based head groups are facing the toward the aqueous solvent (figure 4.13). The presence of flexible linker in the structure of the synthetic glycolipid allows the reorientation of head-group, possibly resulting in larger ($\rho > 1$) value of the packing parameter and making the formation of inverted hexagonal phase (H_{II}) possible.

The transition between lipid phases can be triggered by changing the environmental conditions, e.g. temperature or hydration.[139] In the system studied here the hexagonal phase was observed within the aqueous solvent. In the presence of the hydrophobic solvent the formation of an inverted hexagonal phase with the hydrocarbon chains facing the solvent, is expected to be more energetically favorable. The possibility of the formation of the inverted hexagonal phase within the aqueous solvent due to slightly hydrophobic character of the protected groups present on the sugar moiety was also considered. However due to the presence of l4 and 8-carbon long chains the H_I phase was presumed to be entropically more favorable.

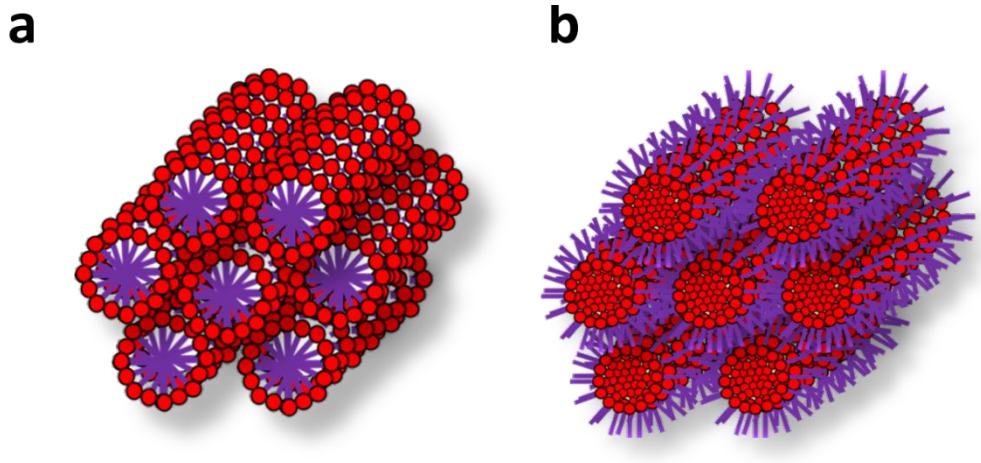

Figure 4.13 *Schematic representation of the arrangement of lipids in columnar phases; (a) normal hexagonal phase (H_{II}) with glycolipid headgroups oriented towards the aqueous solvent and inverted hexagonal phase (H_I), where the glycolipid tail groups are oriented towards the mineral oil solvent.*

4.3 Conclusions

A protected synthetic glycolipid has been incorporated into GUV membranes by a variety of methods at biologically relevant concentrations in binary mixtures with DOPC and in ternary mixtures with DOPC and cholesterol. In both cases, the glycolipid was fully dispersed in the solvent prior to the preparation and homogenously distributed within the lipid bilayer. At glycolipid concentrations below 5 mol % only the lamellar lipid phase was observed, giving rise to large numbers of vesicles. Coexistence of the lipid-disordered and lipid-ordered lamellar phases was not observed in the range of concentrations where the glycolipid was soluble in the vesicle membrane. Liposomes were prepared in the presence of various glycolipid and cholesterol concentrations, and increasing their concentration was shown to decrease the size of vesicles formed. The preparation of liposomes containing the synthetic glycolipids was not affected by the method of preparation or the presence of fluorescent dyes within the membrane.

Synthetic glycolipid concentrations above 10% lead to the formation of lipid tubules, which are composed of columnar lipid phases. The arrangement of lipid molecules in either the hexagonal or inverted hexagonal phases was dependent on the chemical nature of the solvent system used. The glycolipid was shown to be homogenously distributed within the tubular structures. Since the tubules were optically birefringent, it was presumed that they exhibit some degree of structural order as opposed to resembling aggregated material. Their formation was shown both in aqueous solvent and in mineral oil droplets, therefore suggesting the hexagonal and inverted hexagonal lipid arrangement respectively. The formation of the bundles of tubular structures was found to arise from cooperative action of both the glycolipid and DOPC since none of these components form similar structures separately.

There is a growing interest in the use of a variety of glycolipids incorporated into GUVs for variety of applications, including studies of molecular recognition or targeted drug delivery. Phase behaviour of both naturally occurring and synthetic glycolipids, and factors affecting their behaviour and their potential applications have not been fully explored. This work contributes to the understanding of concentration-dependent phase behaviour of synthetic glycolipid.[49]

Chapter 5

Encapsulation and aggregation of BSA in Giant Unilamellar vesicles

5.1 Introduction

An important feature of building a model cell is the requirement to encapsulate biomolecules, such as nucleic acids, peptides or proteins, within the interior of the phospholipid vesicles. There are a large number of methods available to do this and the choice of a suitable method needs to be carefully considered as it may affect the activity of the biomolecules. Upon encapsulation various processes can be observed within the interior of the vesicle, such as nucleic acid amplification or protein synthesis. One of the advantages of using liposomes as reaction vessels is the small volume, therefore small amounts of reagents are required. In order to evaluate the reactions or processes occurring within vesicles, the encapsulation efficiency and the concentration of molecules within a specific vesicles need to be quantified.[188] There are several methods for the estimation of encapsulation efficiency, reporting the efficiency as either the average amount of solute per vesicle in suspension[446] or as a quantity obtained for a single vesicle,[61,447] protein subunit[448] or for a biological cell.[449] The suitability of the method of quantification strongly depends on the application. Drug or gene delivery studies are more concerned in analysing the average encapsulation efficiency, however if chemical or biochemical reactions are studied within a model cell consisting of a single liposome, then the concentration of individual reagents may be crucial.

Assembly processes are at the centre of minimal cell research. Formation of the lipid bilayer, folding of protein or formation of signalling complexes are just a few examples of assembled structures inherent to biological cells and are often recreated in model cells. One of the assembly processes commonly occurring in cells is protein aggregation; which may be defined as a non-native assembly process leading to formation of species with a molecular weight higher than a monomer.[450] Virtually all proteins are susceptible to aggregation depending on the solution conditions, such as pH, ionic strength, temperature, presence of denaturants or the characteristics of the surface (charge distribution and presence of hydrophobic patches) of a protein molecule.[254] These various solution conditions and the protein properties will allow aggregates to form by different aggregation mechanisms[254,451] and result in the formation of various types of protein particles, from fibril-type structures to amorphous aggregates.[452] Aggregation processes may be reversible or can result in the formation of insoluble particulates.[254]

Protein aggregation, its mechanisms and the conditions under which it occurs has been extensively studied.[291,292,295,450,453] These studies provide valuable insights into

protein structure, stability and the folding process. Understanding how and why proteins aggregate is extremely important in various branches of food and in the biopharmaceutical industry.[256] The effects of protein aggregates present in biopharmaceutical formulations include decreased efficacy and stability or in some cases immunogenic response in patients.[257] Formation of protein aggregates has also been linked to several diseases such as Alzheimer's or Parkinson's disease and therefore better understanding of the aggregation process may lead to development of new strategies resulting in its prevention.[258,259]

Protein aggregation studies have traditionally been performed in bulk. This approach offers the possibility of performing analysis across a range of conditions, using a variety of instrumentation, and provides specific details about the mechanisms leading to aggregation. However care must be taken when interpreting results of such studies as the conditions in which they are performed lack the complexity of the cellular environment, such as molecular crowding or protein-membrane interactions. The conditions under which *in viv*o studies may be carried out are however significantly limited due to the sensitivity of cell culture. Additionally the interior of a cell is filled with a variety of biomolecules and therefore identifying the key factors that play a role in the aggregation process is extremely difficult. Furthermore several studies have emphasized the role of lipid bilayers in the aggregation process and this type of interaction cannot be reproduced unless supported lipid bilayers or giant unilamellar vesicles are used.[293,454,455]

Firstly a method to quantify the amount of protein encapsulated in a GUV is presented. Aggregation of BSA was then analysed in solution to select a set of conditions where aggregation occurs. Formation of aggregates in solution was monitored by Thioflavin T (ThT) fluorescence and solution turbidity. ThT becomes fluorescent upon binding to either protein aggregates or amyloid fibrils. Finally, BSA was encapsulated into GUVs and its aggregation *in-situ* was monitored using phase contrast and fluorescence microscopy. Fractal analysis of the aggregates formed in solution and in liposomes is used to compare the aggregates formed in each case.

5.2 Results and discussion

5.2.1 Production and characterisation of emerald variant green fluorescent protein (EmGFP)

Emerald variant of green fluorescent protein (EmGFP) was expressed in *E.coli* as described in the experimental section 2.7. Transformed *E.coli* cells were inspected using fluorescence microscopy (figure 5.1). Bacterial cells expressing EmGFP emit green fluorescence (emission maximum at 509 nm), which can was observed under fluorescence microscope upon excitation with blue light (excitation maximum at 487 nm).

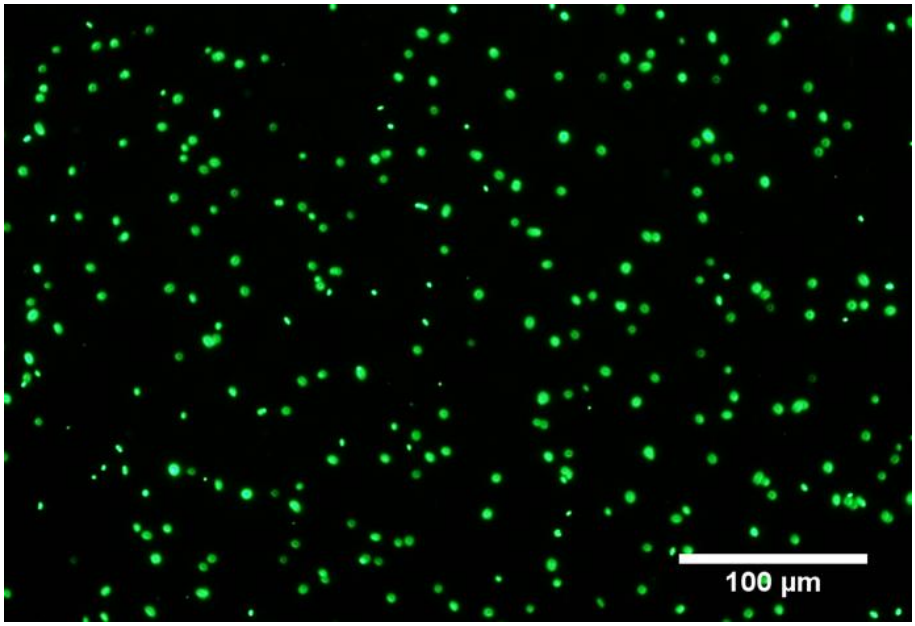

Figure 5.1 *Fluorescence microscopy image of bacterial cells (E.coli) expressing EmGFP; image was acquired using the FITC filter set.*

Following cell lysis, the lysate, containing GFP was purified on a Ni-NTA column (figure 5.2). The protein fractions corresponding to the second peak were selected based on visual inspection of the solution (green colour is indicative of the presence of EmGFP). Selected fractions were analysed by reducing SDS-PAGE (figure 5.3). The presence of a single band corresponding to EmGFP monomer confirms the purity of the solution.

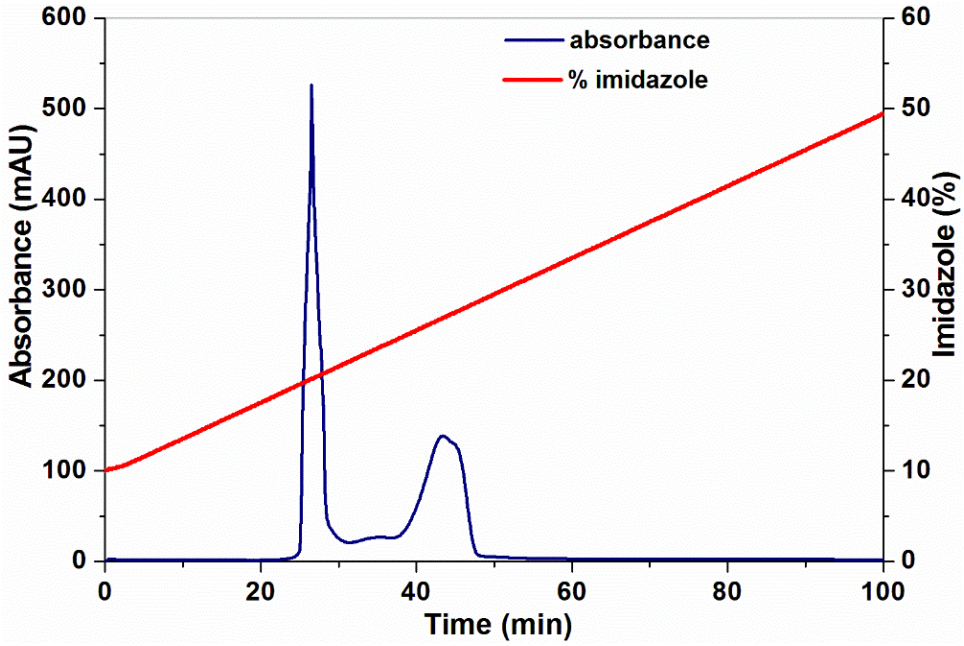

Figure 5.2 *Affinity chromatography purification of EmGFP protein. The fractions corresponding to the second peak contain the purified EmGFP.*

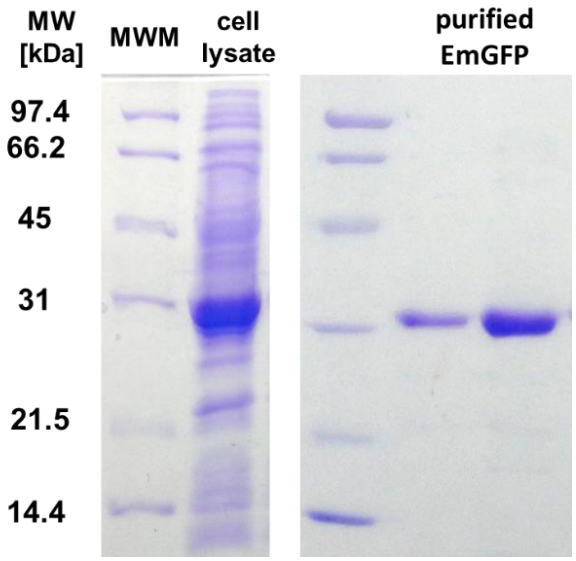

Figure 5.3 *SDS-PAGE gel of the cell lysate and purified EmGFP. MWM, is the molecular weight marker. Two concentrations of the purified EmGFP were run to determine if any low concentration contaminants were present.*

Purified EmGFP was also analyzed with size exclusion HPLC (SE-HPLC). The presence of a single peak at 19.11 min confirmed the purity of the EmGFP (figure 5.4). From the calibration of the Superdex 75 10/300 GL SE-HPLC column (for details see section 2.9), a peak at 19.11 min indicates a molecular weight in the region of 30.5 kDa, which is consistent with the molecular weight of a EmGFP monomer.

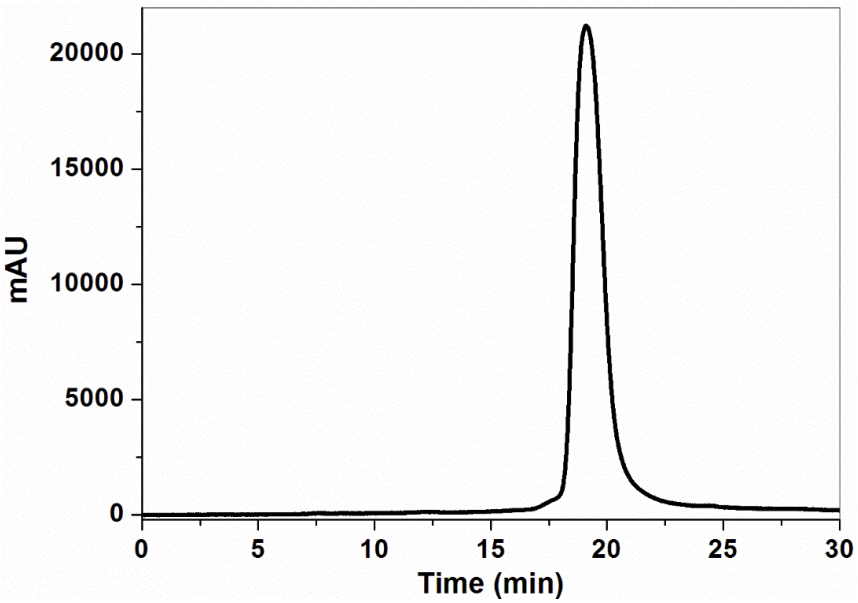

Figure 5.4 *SE-HPLC profile of purified EmGFP in 100 mM sodium phosphate buffer pH 7.4.*

Purified EmGFP solution was stored in the dark at 4°C and was stable for several weeks.

5.2.2 Quantification of protein concentration in GUVs

As discussed in the chapter 2 (section 2.3), the amount of light absorbed by a fluorescent molecule and emitted in the form of fluorescence can be related to its concentration by the following equation;

$$F = kcQI \qquad 5.1$$

where k is a constant, c is the concentration of the fluorophore, Q is the quantum yield and I_0 is the intensity of light illuminating the solution.[351] The above equation relates values of F and c at low concentrations of the fluorophore. Since $kc \propto A$ the fluorescence intensity is also directly proportional to the absorbance but only at low concentrations of fluorescent molecules. Therefore the relationship between the fluorescence and the concentration of a fluorophore must also be analysed. Here a concentration range between 0.2 and 1.2 mg/ml was analysed. As will be shown in this chapter, the relationship between fluorescence intensity and protein concentration is linear for the selected range of EmGFP concentrations.

The concentration of protein was estimated based on the measurement of fluorescence emitted by the emerald variant of GFP. Fluorescent protein was chosen over other light emitting molecules, such as luciferase or small organic molecules, due to its compatibility and inert nature in respect to other biological molecules and the possibility that it can be synthesized *in situ* inside a model or biological cell.[456]

5.2.2.1 Calibration curve

In order to obtain a calibration plot allowing for the quantification of protein concentration within GUVs, glass capillaries filled with a solution of EmGFP were used. A similar approach was previously used by Leonhardt *et al.*,[449] where rectangular PDMS microchannels were used for the quantification of expression levels of GFP in mammalian cells. The choice was dictated by the similarity of the cross-sectional geometry and the focal depth of both the capillaries and the vesicles. In both cases the objective was focused at the center of the capillary (in the z-direction), (for experimental details see section 2.10). Empty glass capillaries were also observed under identical conditions to ensure no background fluorescence was contributing to calibration measurement.

5.2.2.2 Image analysis

Images used for fluorescence intensity measurements were recorded with the FITC excitation-emission filter engaged and using CellF software with a manually set exposure time. The intensity of the illuminating beam of light, monitored using the MultiSpeck multispectral fluorescence microscopy standard, showed no significant fluctuations for up to 280 hours of usage of the mercury burner. After that time the burner was replaced. Imaging of EmGFP was performed in a manner that ensured the preservation of the EmGFP fluorescence; the focusing and centering (placing an object of interest in the center of the field of view) steps were performed promptly, usually with the use of neutral density filters reducing the intensity of illuminating light, up to 50%. Background subtraction and flat-field correction were performed when necessary.[457–459] Image processing and fluorescence intensity measurements were performed using CellF and ImageJ software.

The first method used to prepare the calibration curve involved the measurement of fluorescence intensity at a point in the middle of the glass capillary filled with GFP solution (figure 5.5). The glass capillary was first filled with the protein solution using a syringe and a silicon connector. Capillaries were placed onto a glass slide and imaged using a 10X objective. All of the above steps were performed in the dark to prevent bleaching of the EmGFP solution. Measurements for the calibration plot were performed with five different EmGFP concentrations and capillaries of various diameters.

Another calibration curve was obtained by measuring fluorescence intensity across the width of the capillary and plotting the area under the intensity curve for each

EmGFP concentration and various capillary diameters (figure 5.6). This approach offers more consistent results, especially in cases where the solutions exhibits uneven mixing of the fluorophore or is adsorbing onto the glass surface.[460] In the case of EmGFP none of these characteristics were observed.

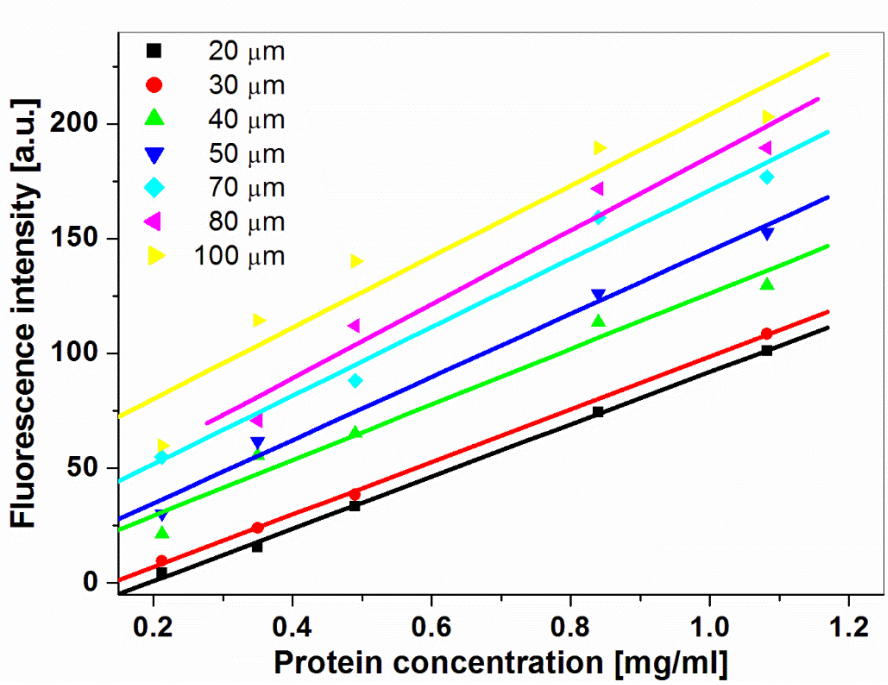

Figure 5.5 *Calibration plot for protein quantification based on point measurement of fluorescence intensity within a range of different size capillaries.*

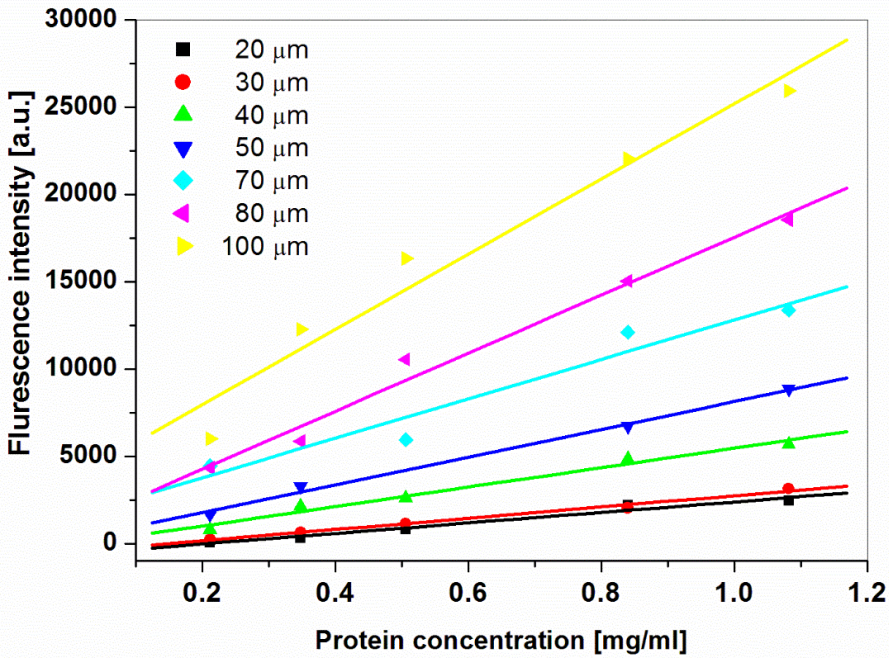

Figure 5.6 *Calibration plot for protein quantification based on the cross-sectional measurement of fluorescence intensity within a range of different size capillaries.*

The calibration plot of EmGFP concentration as a function of the fluorescence intensity and capillary diameter was recorded using a 10x objective. Since images of vesicles encapsulating EmGFP were recorded using either 60 or 100x objectives, a scaling factor was determined for each objective pair (table 5.1). A scaling factor allows one to convert the fluorescence intensity recorded by the higher magnification objectives to a value for a 10x lens, which then can be used to obtain the concentration of EmGFP from the calibration plot.

Table 5.1 *Conversion table listing fluorescence intensity measurements obtained using a fluorescent standard and a range of objectives. The scaling factor allows conversion of intensity between higher magnification lenses used for imaging of GUVs and the 10x lens used to obtain measurements for the calibration curve.*

Lens	**10x**	**20x**	**40x**	**60x***	**60x****	**60x****	**60x****	**100x**
Exposure time	10 ms	10 ms	10 ms	10 ms	10 ms	5 ms	2 ms	10 ms
Scaling factor (for 10x calibration)	-	0.353	0.264	0.147	0.1276	0.184	0.349	0.137

* UPlanFLN objective ** UPlanSapo objective

The calibration plots shown in figure 5.5 and 5.6 allow one to obtain the concentration of protein encapsulated within vesicles of sizes similar to the sizes of capillaries. These results are also represented in the form of a surface plot (figure 5.7).

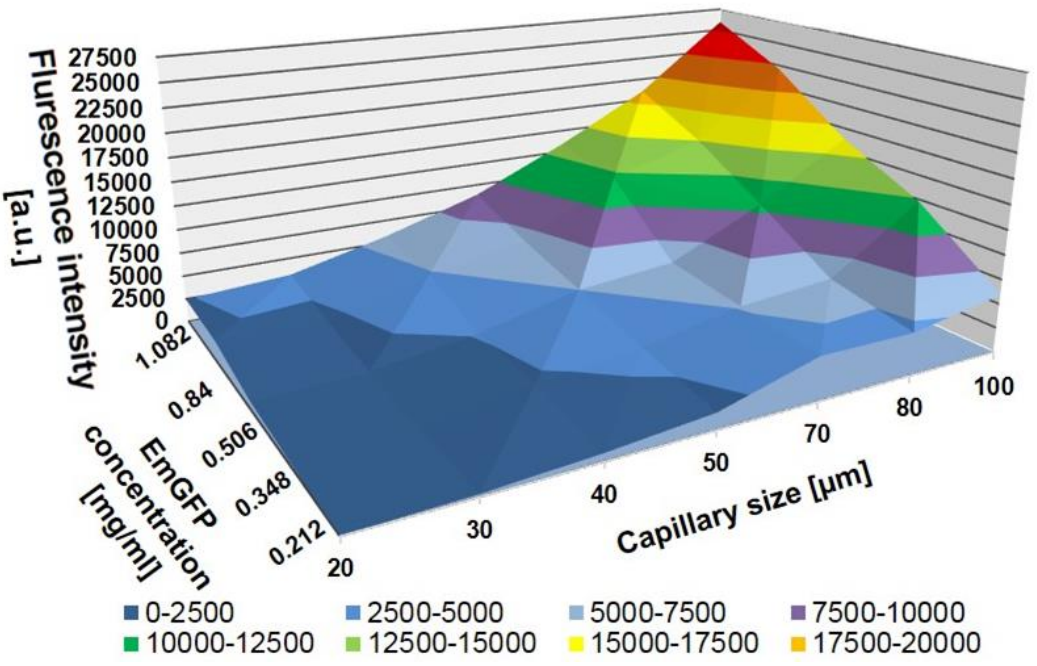

Figure 5.7 *Surface plot of calibration for protein concentration determination based on the cross-sectional measurement of fluorescence intensity.*

This method can be used to quantify concentrations of fluorescent proteins upon encapsulation inside giant unilamellar vesicles. Fluorescence measurements are sensitive to solution conditions; therefore the calibration and the encapsulation should be performed using identical buffer conditions. If changes are introduced, the impact on the fluorescence intensity should be examined.

Due to the sensitivity of fluorescence measurements to buffer conditions, the multiple steps involved in the vesicle preparation process, and variation in the performance of the equipment (such as short time changes in the intensity of illuminating light), the concentration of protein encapsulated may only be estimated to the nearest 0.1 mg/ml.[304]

5.2.3 Encapsulation of molecules inside GUVs

5.2.3.1 EmGFP encapsulation inside giant unilamellar vesicles (GUVs)

Encapsulation of EmGFP inside GUVs was performed using either the inverted emulsion or cDICE method as described in section 2.4. The osmotic pressure was balanced by the addition of sucrose to the external solution. The concentration of sucrose required was assessed experimentally for every protein concentration used. Once the vesicles were formed, images were recorded. Next, the background fluorescence and the fluorescence intensity across the diameter of the vesicle was measured. Background subtraction was performed either using rolling ball toll in ImageJ or by manual subtraction of the fluorescence intensity measured in the area of the image surrounding the vesicle. The second method was used more often as it allows for more control of the intensity subtraction and it represents a more accurate approach in the case of an uneven background due to the presence of out of focus vesicles. The value for the intensity obtained (usually as an area under the fluorescence intensity curve) was then multiplied by the scaling factor appropriate for a given set of objectives. The concentration of EmGFP was obtained using the calibration plots shown in figures 5.6 and 5.7. EmGFP in the concentration range of 0.1 to 1 mg/ml was successfully encapsulated within lipid vesicles. Encapsulation efficiencies were calculated as ratios of EmGFP concentration in individual vesicles to its concentration in the solution used for encapsulation. Examples of vesicles encapsulating EmGFP and corresponding encapsulation efficiencies are shown in figure 5.8. The observed difference in intensity between the two images corresponds to the difference in the EmGFP concentration.

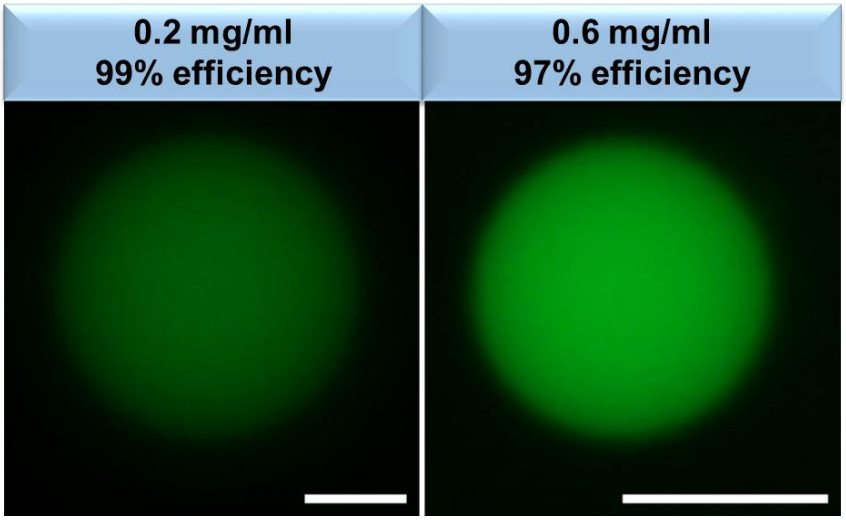

Figure 5.8 *EmGFP encapsulated into GUVs; the concentration of protein and the efficiency of the encapsulation are indicated above. Scale bar = 20 µm.*

Encapsulation of EmGFP was also be performed in vesicles composed of mixtures of phospholipids and the galactose-based synthetic glycolipid described in chapter 4 and can be seen in figure 5.9. No difference in the vesicle yield or the encapsulation efficiency was found when compared to the phospholipid-based GUVs.

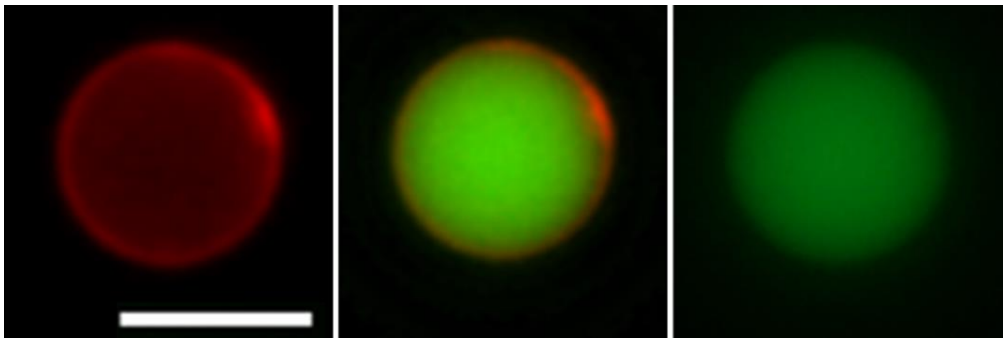

Figure 5.9 *EmGFP at a concentration of 0.34 mg/ml encapsulated in GUVs containing a 95:5 phospholipid (DOPC)-glycolipid mixture and 0.05% bodipy TR ceramide. Vesicles were imaged with the CY5 (left) and FITC (right) fluorescence filters. Scale bar = 10 µm.*

5.2.3.2 EmGFP/BSA mixtures encapsulation inside GUVs

Bovine serum albumin (BSA) was also encapsulated in GUVs at concentrations ranging from 10 to 100 mg/ml. Just as for EmGFP encapsulation, rupture of vesicles due to the osmotic pressure differences between the interior and exterior of the vesicle was prevented by the addition of sucrose to the external solution. BSA is not fluorescent in the visible region of the spectrum and therefore direct measurement of its concentration

inside vesicles using the method described in section 5.2.2 is not possible. In order to provide the means for quantification based on fluorescence measurements, up to 0.5% of EmGFP was added to BSA solutions before encapsulation. Examples of vesicles encapsulating mixtures of BSA with EmGFP are shown in figure 5.10.

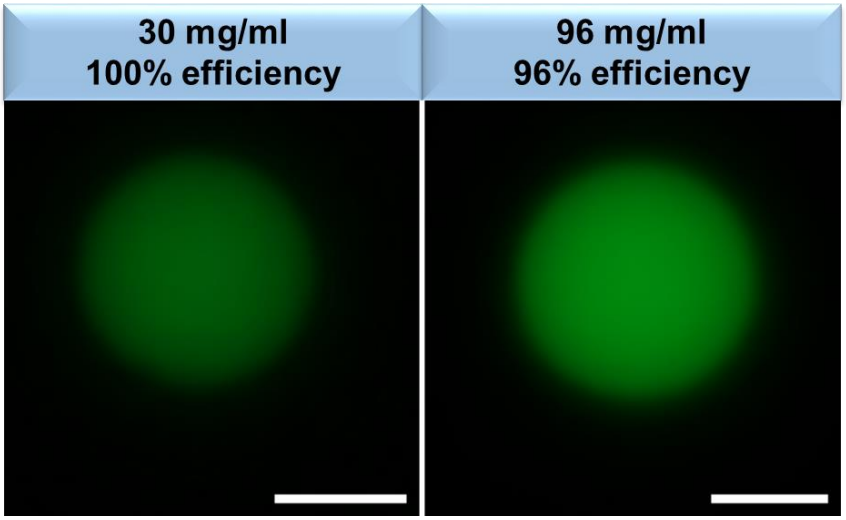

Figure 5.10 *EmGFP and BSA mixtures encapsulated in GUVs. The total protein concentration and the efficiency of encapsulation are shown above. Scale bar = 10 µm.*

The concentration of EmGFP inside the GUVs was obtained using the method described in section 5.2.2. It was previously shown that fluorescence intensity measurements are sensitive to solution conditions such as buffer type, pH and ionic strength.[304] The effect of BSA on the fluorescence intensity of EmGFP was analyzed by comparing emission spectra of EmGFP at a known concentration with and without BSA in the solution (figure 5.11). It was found that the addition of BSA results in an increase in the fluorescence intensity of the EmGFP solution by 5.4%. Due to this, the fluorescence intensity used to obtain the concentration of EmGFP was corrected for this effect. One thing to note is that this method to determine the BSA concentration assumes that there is complete mixing of the two proteins and that the solution encapsulated is representative of the stock solution. No phase separation of the BSA and GFP solutions were observed.

Once the concentration of EmGFP (corrected for the effect of BSA present in the solution) was obtained from the calibration plot and its content in the mixture with BSA was known (up to 0.5% of total protein concentration), the concentration of BSA in the individual vesicles could be calculated. Examples of protein concentrations in vesicles and encapsulation efficiencies are shown in figure 5.10.

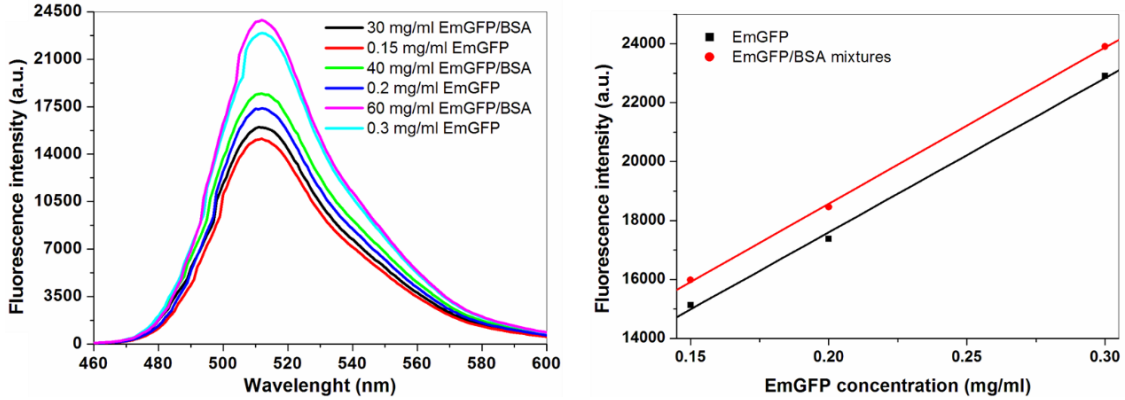

Figure 5.11 *Comparison of the emission spectra (left) and the fluorescence intensity at 512 nm of an EmGFP solution and EmGFP/BSA mixtures with identical EmGFP content.*

Vesicles containing protein solutions were stable for several days at room temperature. They were also stable after incubation at 65°C for up to 2 hours. The number of vesicles gradually decreased over time but no significant decrease in protein concentration within the remaining vesicles was observed, suggesting that no leakage of content took place.

The values representing encapsulation efficiencies shown in figures 5.8 to 5.10 are only examples of the efficiencies obtained under specified conditions. In fact various encapsulation efficiencies ranging from approximately 25-110% of the stock protein solution were observed within any given experiment. The distributions of various efficiencies were not analyzed. This variation in encapsulation efficiency, however not its extent, was previously published.[188,461,462] The solute occupancy distribution inside vesicles was shown to be determined by a power law, resulting in a range of solute concentrations observed for a given vesicle size. The presence of "super-filled" vesicles, containing concentrations of protein significantly exceeding (up to 50 times) the concentration within the bulk solution has previously been reported[462] for small vesicles (up to 1μm in size) , and it is not clear if the enhancement of entrapment occur in giant vesicles to the same extent as this issue is still being investigated.[462]

The observation of vesicles showing either very low or very high encapsulation efficiency have been attributed to the mechanism of droplet formation and the redistribution of solutes from larger droplets between two smaller ones during the fragmentation step.[462] The heterogeneity of solute concentration within w/o droplets was suggested to be the source in the variability of encapsulation efficiencies observed. Additionally, the range of protein concentrations observed here may be in fact be limited,

since the vesicles would become unstable due to the osmotic pressure differences between the interior and the exterior of the vesicle.

5.2.4 Screening conditions promoting BSA aggregation in solution

The process of protein aggregation and the conditions leading to it have been studied extensively.[291,292,295,450,453] Bovine serum albumin (BSA) is often selected for such studies as a model globular protein. The range of solution conditions under which BSA forms aggregates were measured first. Relatively short incubation times were used since identical experimental conditions were later replicated in phospholipid vesicles. Previously published results suggests that the aggregation of BSA can be induced in acidic buffer conditions.[321,463,464] Additionally these studies showed that the presence of high salt concentrations enhances the aggregation process. The effect of a range of acidic pHs on the aggregation of BSA was measured.

Solutions of BSA at 10 mg/ml in buffers of various pH (2.2, 3, and 4) and with various concentrations of NaCl (0 to 100 mM) were prepared in a 96 well plate. For comparison, BSA at physiological pH was also prepared. Thioflavin T (200 μM) was added to the solution and fluorescence intensity of the dye was monitored at 485 nm (following excitation at 435 nm). Increases in the fluorescence intensity of ThT is most often used to confirm the formation of amyloid-like fibrils, particularly the cross-β-sheet structure commonly found in amyloid proteins,[465,466] although an increase in fluorescence intensity is also observed for amorphous protein aggregates.[277,278] The absorbance at 600 nm was also recorded in order to monitor the formation of amorphous protein aggregates and the corresponding decrease in % transmission due to the formation of large particles.

5.2.4.1 Monitoring BSA behaviour upon incubation at room temperature

Upon incubation at room temperature the highest ThT fluorescence intensity was observed for BSA at 10 mg/ml in a glycine-HCl buffer at pH 3 with 100 mM NaCl (figure 5.12 left), indicating the formation of some type of BSA aggregate. No significant increase in absorbance at 600 nm was observed (figure 5.12 right panel), which suggests that aggregates formed are too small to be detected using this technique.

For glycine-HCl at pH 2.2 and sodium acetate at pH 4 (data not shown), no significant increase in fluorescence intensity over the three day observation period was seen. Additionally no change in % transmission and no visible aggregates were observed

using phase contrast microscopy for BSA solutions at 10 mg/ml incubated in any of the buffers analysed.

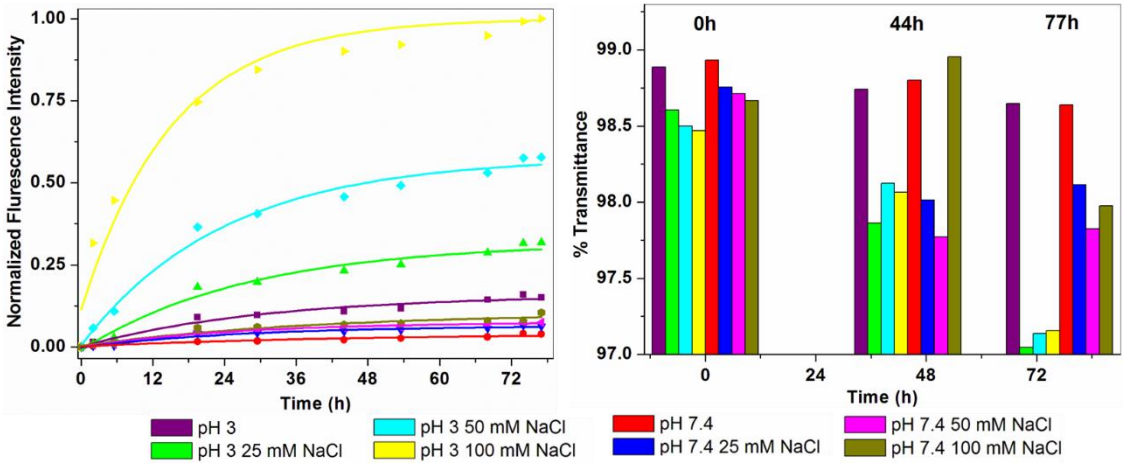

Figure 5.12 *Observation of BSA behavior in solutions at 10 mg/ml under various buffer conditions during incubation at room temperature.*

5.2.4.2 Monitoring BSA behavior after heating

Protein aggregation is often induced by an exposure to increased temperature which aids protein unfolding.[467] BSA buffer solutions at various pH and NaCl concentrations were incubated at 65°C. This temperature has been shown to cause partial unfolding of BSA at pH 3.[468] It has also been shown that amyloid-like fibrils are formed in BSA in glycine-HCl at pH 3 upon incubation at 65°C.[464]

As shown in figure 5.13 an increase in ThT fluorescence was observed at pH 3 and pH 7.4 indicating the formation of aggregates. However due to the lack of a lag phase, characteristic of the growth profiles for fibrils,[453] it is most likely that these aggregates are amorphous. Detection of amyloid-like fibril formation needs to be confirmed using other methods (such as TEM), since ThT is capable of non-specific binding under various conditions.[466] A reduction in % transmission was also observed, most prominent in the case of BSA solutions at pH 3 in the presence of 50 mM NaCl. No significant increase in the ThT fluorescence was observed for BSA in buffer at pH 2.2 (data not shown). Aggregates formed under conditions tested above were imaged using various modes of light microscopy (figure 5.14).

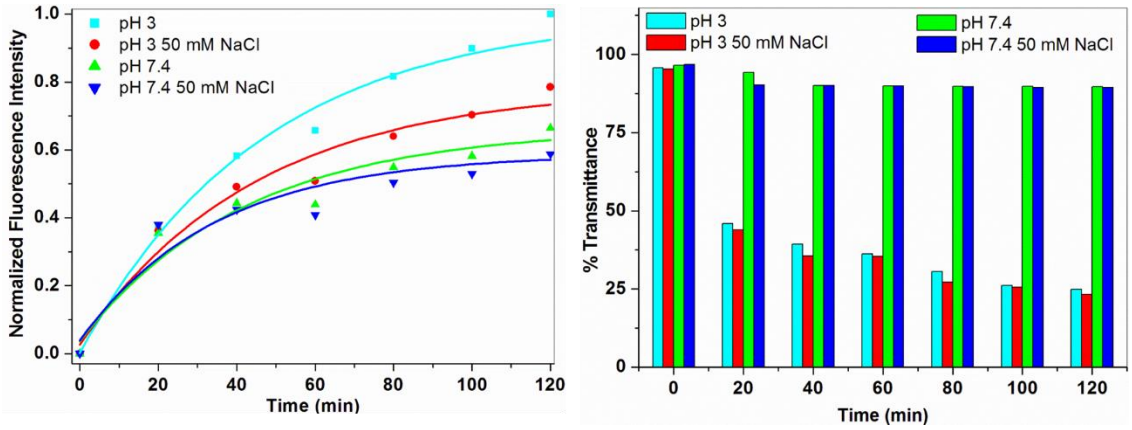

Figure 5.13 *Aggregation of BSA in different solution conditions during incubation at 65°C.*

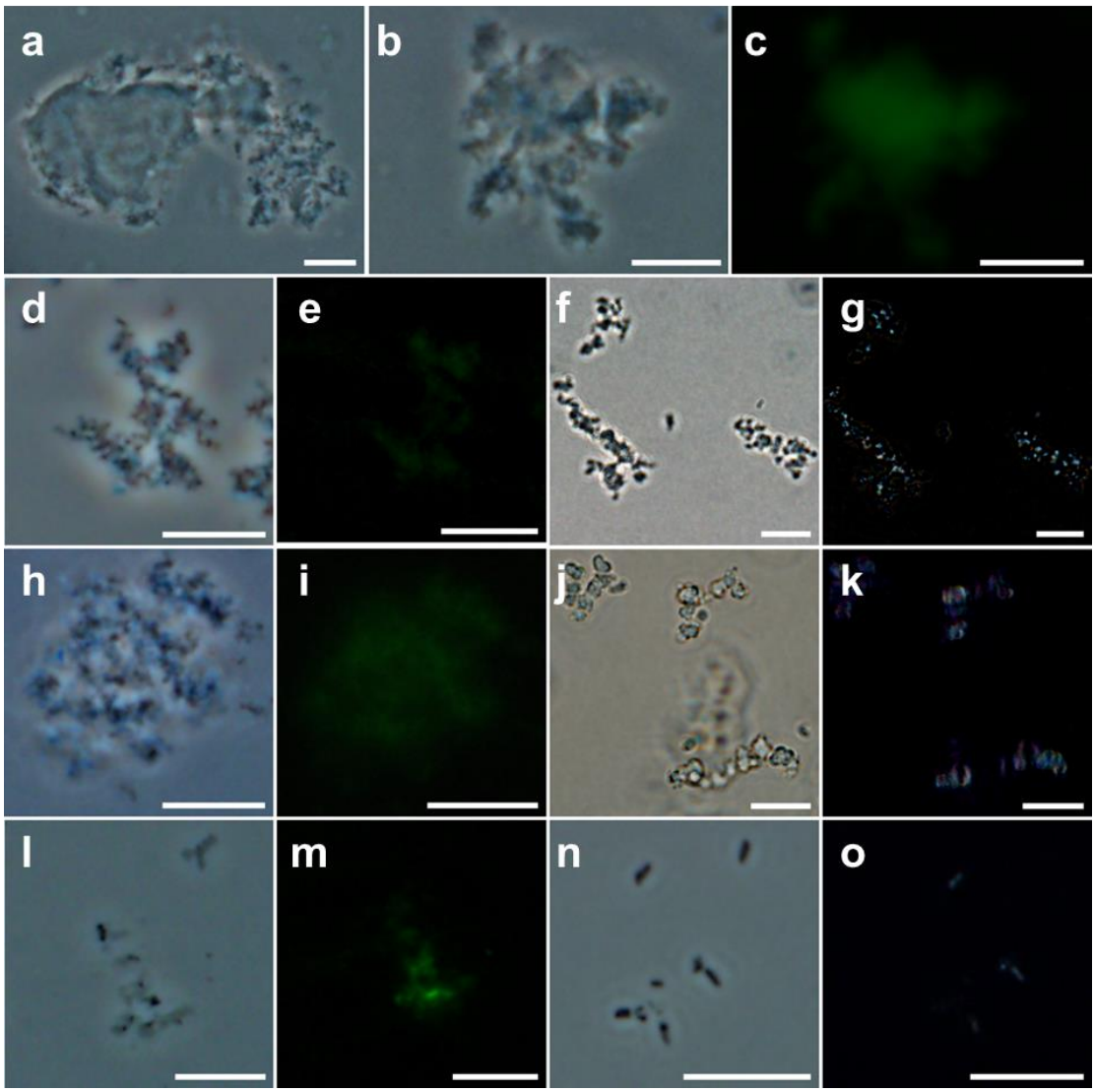

Figure 5.14 *BSA aggregates formed after incubation at 65°C at pH 2.2 (a-c), pH 3 (d-g), pH 3 with 50 mM NaCl (h-k) and at pH 7.4 (l-o). Images were recorded using polarized light microscopy (f, j, l), fluorescence microscopy with a FITC emission/excitation filter (c, h, n) and with a phase contrast. Brightness and contrast adjusted to aid visualization. Scale bar = 10 µm.*

Upon visual inspection of BSA solutions at pH 2.2 in the presence of 50 mM NaCl, the formation of a weak, clear protein gel was observed. This is in agreement with previous studies.[321] Large portions of the gel were observed with smaller particulates present at the edge of the gel, which were imaged (figure 5.14a). The presence of a green fluorescent signal co-localized with the gel material suggests binding of ThT in these regions. However the polarized microscopy did not confirm the presence of any ordered structures, suggesting that no amyloids are present and it is therefore more likely that the gel is formed from a network of amorphous aggregates.

Aggregates formed at pH 3 appear to be amorphous by phase contrast microscopy (figure 5.15d, f, h and j). However observation under polarized light revealed that the structures formed are optically birefringent which indicates that these structures are ordered (figure 5.15 g and k) and may suggest the presence of amyloid material in these aggregates. Very small aggregates were formed at pH 7.4 in the presence of NaCl. No aggregates were observed in BSA solutions at pH 2.2 and pH 7.4 in the absence of salt.

5.2.5 Encapsulation and aggregation of BSA in GUVs

BSA at 10, 20 and 40 mg/ml in glycine-HCl (pH 2.2 and 3), sodium acetate (pH 4) and sodium phosphate (pH 7.4) buffers with increasing concentrations of NaCl (0-100 mM) was encapsulated in phospholipid-based liposomes using the inverted emulsion method (see section 2.4.6 and 2.11.2). Initially, when encapsulation was performed in the presence of 100 mM NaCl, a very low yield of vesicles was achieved. Therefore, NaCl concentrations of 50mM were used thereafter. Thioflavin T was added to the solutions at 200 µM. Solutions of BSA containing 0.5% of protein labelled with a FITC dye were also encapsulated in GUVs (but never simultaneously with ThT as both emit green fluorescence). Images of vesicles were recorded both immediately after formation and after the specified incubation period. In the case of incubation at 65°C, the vesicle suspension was cooled to room temperature for at least 60 minutes before imaging.

Concentrations of BSA in excess of 10mg/ml were required to observe aggregation inside GUVs, since aggregates larger than 1µm in size are necessary to observe the aggregates by optical microscopy. The absence of aggregates at 10 mg/ml can be linked to the encapsulation efficiency discussed in section 5.2.3. Quantification of protein concentration in individual vesicles was not possible as the acidic pH leads to quenching of GFP fluorescence.[304]

5.2.5.1 Observation of vesicles encapsulated with BSA

Vesicles encapsulating various concentrations of BSA at pH 2.2, 3 and 7.4 at 0 mM and 50 mM NaCl were incubated at room temperature. Fluorescence and phase contrast images were recorded after vesicle formation and every 24 hours thereafter. Previous observations of protein-filled vesicles suggest that vesicles formed at neutral pH are stable for several days (see section 5.2.3). However phospholipid-based liposomes formed at acidic pH were found to remain stable for roughly four days of incubation at room temperature. After that time the number of vesicles observed started to decrease. Additionally, the average size of GUVs observed appears to decrease overtime, suggesting that larger vesicles are significantly less stable under these conditions.

Incubation at room temperature did lead to a minor increase in the ThT fluorescence of the protein encapsulated in the vesicles (compared to the background) for liposomes formed at pH 3 in the presence of 50 mM NaCl. No other solution condition produced any aggregation that could be imaged by light microscopy at room temperature.

5.2.5.2 Observation of BSA aggregates formation in vesicles at pH 2.2 after incubation at 65°C

At pH 2.2 and after incubation at 65°C there were indications of BSA aggregates either on the membrane (figure 5.15a) or within the interior of the vesicle (figure 5.15c).

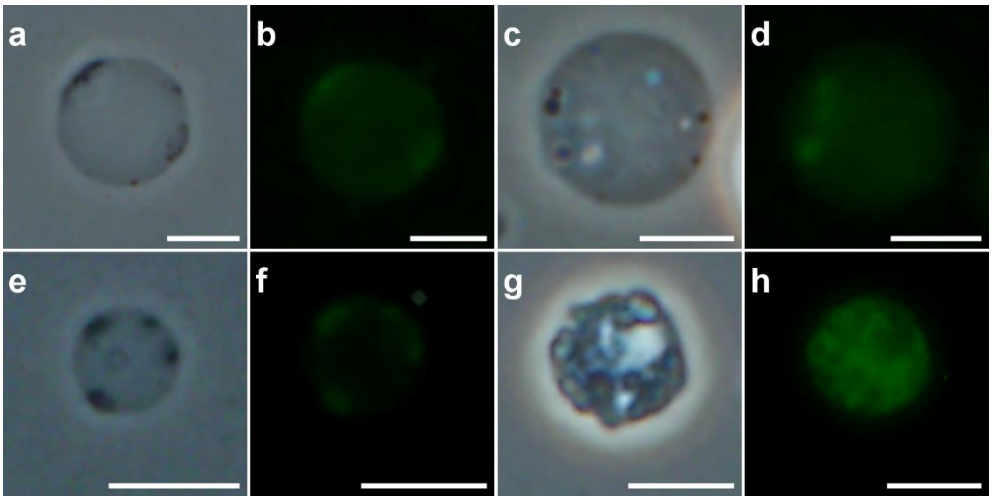

Figure 5.15 *Phase contrast and fluorescence microscopy images of GUVs containing BSA solutions at pH 2.2 without NaCl (a-d) and in the presence of 50 mM NaCl (e-h) after incubation at 65°C for 90 minutes (and returned to room temperature for imaging). Brightness and contrast adjusted to aid visualization. Scale bar = 5 µm.*

Regions in which increased ThT fluorescence was observed are co-localized with the aggregates observed by phase contrast. In bulk, BSA solutions in glycine-HCl buffer at pH 2.2 with 50 mM NaCl after incubation at 65°C form a weak protein gel. BSA solutions after encapsulation in vesicles and incubation under the same conditions formed aggregates similar to those formed in the absence of salt. However they appear to be somewhat larger and present in slightly greater number (figure 5.15e). Additionally, structures which appear to be formed on the surface of the lipid bilayer were observed by phase contrast (figure 5.15g). The increase in the fluorescence intensity of ThT appears to be highly inhomogeneous and restricted to the interior of vesicles (figure 5.15h).

5.2.5.3 Observation of BSA aggregates in vesicles at pH 3 after incubation at 65°C

The interior of vesicles encapsulating BSA at pH 3 both in the presence of 50 mM NaCl and in its absence, appear darker under phase contrast observation compared to those formed at neutral pH. Phase contrast microscopy produces images that can be roughly interpreted as density maps.[469] The amplitude and intensity observed in phase contrast images are related to refractive index and optical path length, therefore image density can be utilized as a scale for approximating relationships between various structures. Essentially, a structure having increasing density are visualized as darker objects relative to the background. In case of BSA containing vesicles at neutral pH the density inside vesicles is comparable to that of the bulk solution. However at pH 3 the density inside vesicles is significantly higher.

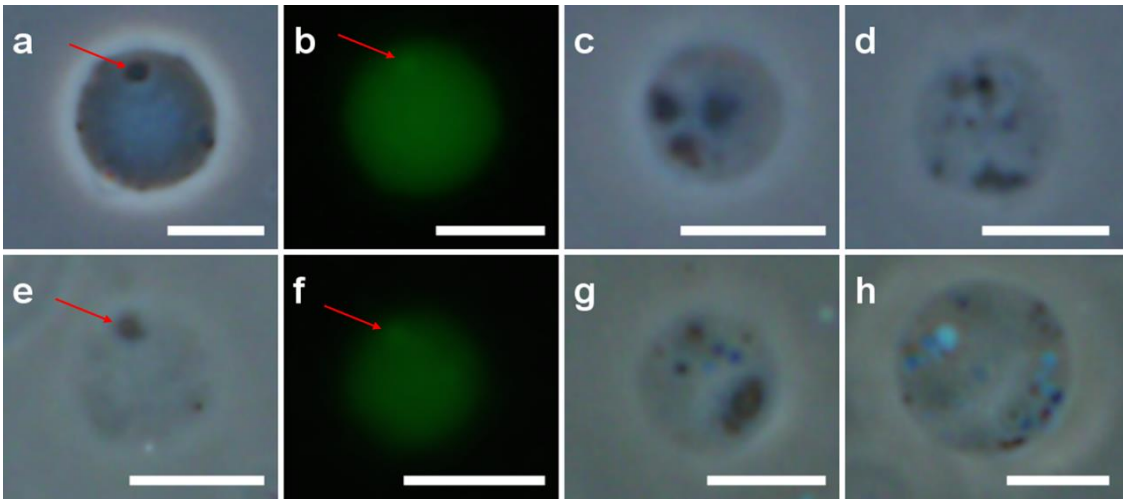

Figure 5.16 *Phase contrast and fluorescence microscopy images of GUVs containing BSA solutions at pH 3 without NaCl (a-d) and in the presence of 50 mM NaCl (e-h) after incubation at 65°C for 90 minutes (and returned to room temperature for imaging). Brightness and contrast were adjusted to aid visualization. Scale bar = 5 µm.*

As shown in figure 5.16, the presence of micrometer-sized aggregates were observed in several GUVs. The aggregates occurred throughout the vesicle and were polydisperse in size. Significant increases in ThT fluorescence were observed in the majority of vesicles, even in vesicles were phase contrast microscopy did not indicate the presence of aggregates (most probably due to the formation of aggregates smaller than 1μm. Smaller areas of more intense green fluorescence were co-localized with the aggregates observed with light microscopy as shown in figure 5.16 a, b, e and f.

5.2.5.4 Observation of BSA aggregates in vesicles at pH 7.4 after incubation at 65°C

BSA aggregates were also observed, albeit significantly less frequently in vesicles formed at pH 7.4, but only after the concentration of encapsulated protein was increased to 40 mg/ml. The increase in fluorescence intensity of ThT was significantly lower than at pH 3. Any ThT fluorescence observed was quite uniform, with increases in the intensity co-localized with aggregates large enough to be observed by phase contrast microscopy.

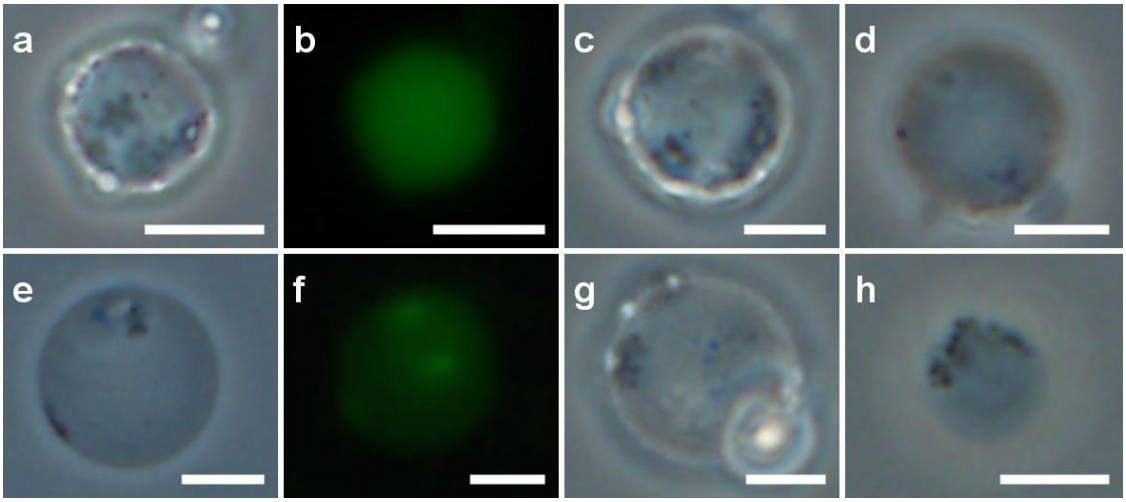

Figure 5.17 *Phase contrast and fluorescence microscopy images of GUVs containing a BSA solution at pH 7.4 without NaCl (a-d) and in the presence of 50 mM NaCl (e-h) after incubation at 65°C for 90 minutes (imaged at room temperature). Brightness and contrast were adjusted to aid visualization. Scale bar = 5 μm.*

5.2.5.5 Observation of BSA aggregates formed in the presence of FITC-labelled BSA

Vesicles encapsulating a mixture of BSA and 0.5% of FITC-labelled BSA at a total protein concentration of 40 mg/ml, in buffer at pH 3 and pH 7.4 with 50 mM NaCl were found to contain aggregates similar to those observed in the unlabelled BSA (figure 5.18).

FITC is commonly used to label proteins for fluorescent microscopy applications.[470] A previous study showed that the labeled protein preferentially partitions into the more concentrated phase after liquid-liquid phase separation and that labelling the protein is the equivalent of adding an attractive component to the protein-protein interaction potential, making the labeled protein more prone to aggregation than the unlabelled protein.[289] The FITC-labelled BSA was added in order to investigate whether similar behavior will be observed in case of BSA, and if so, can it be used to obtain images with better quality than those in the presence of ThT dye. This was not possible as the fluorescence images show uniform distribution of the labelled protein (figure 5.18). The preferential partitioning of the FITC-labelled BSA was however not observed (but can't be ruled out due to the limitations of wide field fluorescence microscopy) for the solid-liquid phase separation of BSA encapsulated inside GUVs.

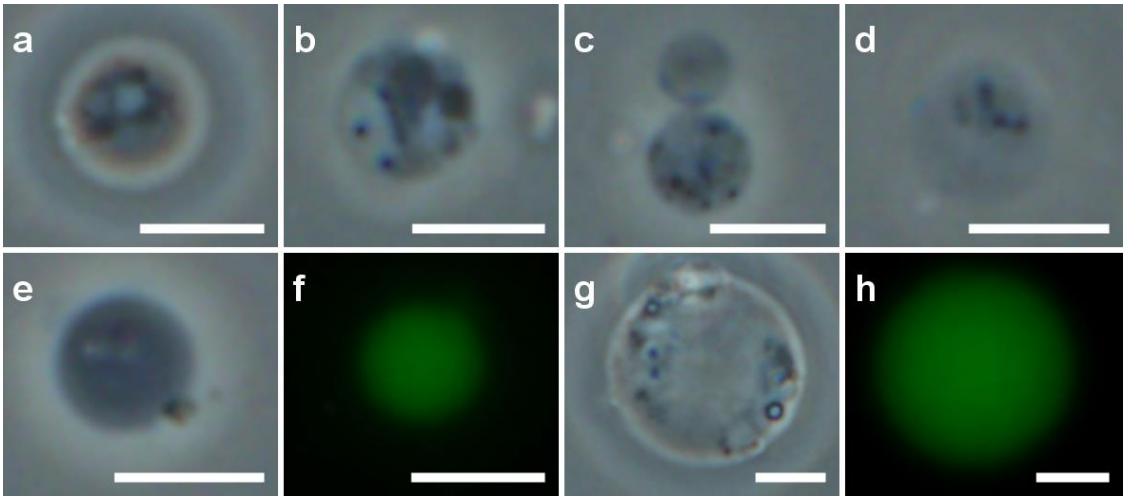

Figure 5.18 *Phase contrast and fluorescence microscopy images of GUVs containing BSA and 0.5% FITC-labelled BSA at total protein concentration of 40 mg/ml, in buffer at pH 3 (a-d) and pH 7.4 (e-h) with 50 mM NaCl after incubation at 65°C for 90 minutes (imaged at room temperature). Brightness and contrast were adjusted to aid visualization. Scale bar = 5 µm.*

5.2.6 Fractal analysis

Describing the appearance of amorphous aggregates is generally quite difficult due to their irregular shape. However their morphological features can be described using a fractal dimension (see section 2.14), a single value representing a structural complexity of a given type of aggregate.

Prior to the analysis the images of aggregates, typically recorded in RGB format, images were converted to a binary format (figure 5.19). The analysis of the images was performed using a box counting method as described in section 2.14.2 using the FracLacv.2.5 plugin for ImageJ.[395] Values for the fractal dimension were obtained for each of the twelve grid positions selected for each image and the final value of D_B was then reported as an average.

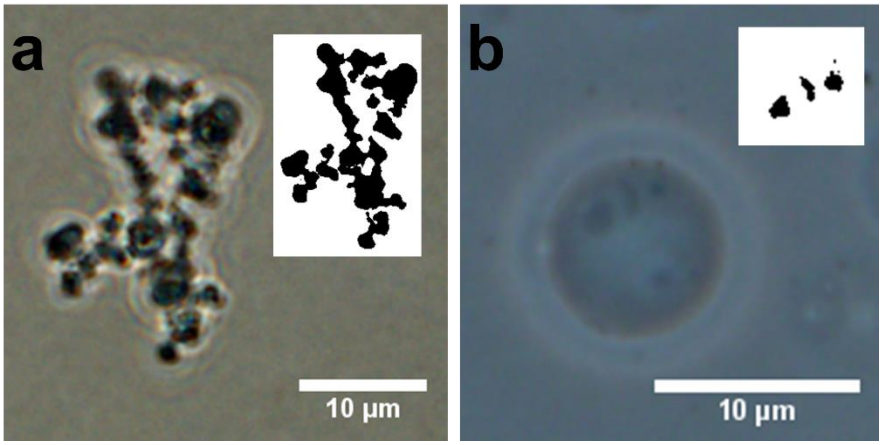

Figure 5.19 *Phase contrast images of BSA aggregates prepared in buffer solution (a) and inside GUVs (b) at pH 3, after incubation at 65°C. Insets: the corresponding binary images used for fractal dimension calculations.*

The fractal dimension analysis of aggregates formed at pH 3 after incubation at 65°C are shown in table 5.1. The D_B values reported in the table represent an average of 20 high contrast images of aggregates formed under specified conditions.

Table 5.1 *Comparison of fractal dimension values for BSA aggregates formed at pH 3 in solution and inside GUVs.*

	Aggregates formed in solution		**Aggregates formed in vesicles**	
	No NaCl	50 mM NaCl	No NaCl	50 mM NaCl
Fractal dimension (D_B) (average)	1.56	1.58	1.50	1.51
Standard deviation	0.069	0.086	0.119	0.128
Coefficient of variation	4.4%	5.4%	7.9%	8.5%

Fractal dimension values of 1.56 and 1.58 were calculated for BSA aggregates formed in buffer solution at pH 3 without NaCl and in the presence of 50 mM NaCl

respectively). Values of the fractal dimension calculated for aggregates grown inside vesicles are 1.5 and 1.51 for the formation in the absence of NaCl and in 50mM NaCl containing solution respectively. High contrast images of BSA aggregates inside GUVs were much more difficult to obtain. The interior appeared darker than in case of empty liposomes and therefore any structures formed inside were generally harder to focus on. Additionally any aggregates present inside vesicles were generally located at different focal depths and image quality was worse due to the presence of large halos surrounding the out of focus membrane. Due to these difficulties, the values of fractal dimensions were calculated based on the analysis of only ten images (where good data was obtained) for each of the buffer conditions analyzed.

Fractal analysis of protein aggregation, mainly protein gel formation have been extensively studied for various types of proteins.[471–476] Values of the fractal dimension between 1.5 and 2.8 for amorphous aggregates[477–479] and protein gels[480] have been reported. They vary greatly depending on the nature of the protein used, its concentration and solution conditions. Fractal dimension values also differ depending on the method used in calculations, however the D_B values obtained using rheological determination and the box-counting method remain in good agreement.[476]

Fractal analysis of BSA aggregates has previously been studied. The values of D_B published were generally higher than the ones calculated here, most probably due to the differences in experimental conditions used to form the aggregates between that study and this. One such study reported fractal dimension value of 1.68 for heat-induced aggregates of BSA formed at pH 7 in the presence of $CaCl_2$ calculated using box-counting method.[481] The general trend illustrating the increase in the value of D_B observed for solutions at higher NaCl concentration have previously reported by Kumagai et al. was also observed here.[482] Nonetheless it is important to note that the previous studies used significantly different solution and heating conditions.[474,483] Other approaches to calculating the fractal dimension have been employed, such as evaluation of D_B based on the light scattering experiments.[473,484]

5.3 Conclusions

The preparation of model cells requires encapsulation of biomolecules inside lipid vesicles. The choice of the encapsulation method depends on the nature and stability of the biomolecules, but also on the composition of the lipid bilayer. Here two methods, the

continuous droplet interface crossing encapsulation (cDICE) and the inverted emulsion method were used to successfully encapsulate BSA and EmGFP under various solution conditions. The methods of protein quantification presented here allow for the fast determination of protein concentration inside individual vesicles.

Calibration plots for encapsulated protein at various capillary diameters were combined to create a surface plot, allowing the determination of protein content inside vesicles across a range of diameters. This method was used to measure the concentration of EmGFP and EmGFP/BSA protein mixture after its encapsulation in GUVs. Both methods used here showed encapsulation efficiencies ranging from around 25 - 110% of the protein content in the bulk solution. This observation remains in agreement with published results.[188] The variation in the encapsulation efficiency is linked to the nature of the vesicle preparation process.

Aggregation of BSA was analyzed both in solution and after encapsulation into GUVs. The formation of BSA aggregates was induced at acidic pH and incubation at elevated temperature. The formation of aggregates in solution was monitored by ThT fluorescence and by the analysis of the solution turbidity. In vesicles, a similar analysis was performed using phase contrast and fluorescence microscopy. Formation of BSA aggregates was observed at various pHs after protein unfolding at 65°C but it was most prominent at pH 3 in both the bulk solution and inside GUVs. Fractal dimension analysis was performed in order to describe the morphological feature of aggregates formed under various conditions. Relatively similar values for the fractal dimensions were obtained, slightly lower for the aggregates formed inside vesicles compare to those formed in bulk solution at given solution condition. Generally higher D_B values were observed for solutions at higher NaCl concentration.

The results presented here illustrate how model membranes can be used as vessels for analysis of protein aggregation processes. Among the main advantages of this approach is the cell-like size of vesicles (and hence very small volumes) or the presence of a lipid bilayer which may be implicated in some aggregation processes.

Chapter 6

Protein self-assembly following *in-situ* expression inside an artificial cell

6.1 Introduction

Advances in synthetic biology now allow artificial cells to be formed from a minimum number of components to perform specific functions. Several examples have been discussed in the introduction.[14,47,485,486] Protein synthesis inside vesicles is vital for minimal cell development. The requirement for increased complexity within the minimal cell will require the production and assembly of protein (or protein and nucleic acid) components *in-situ*. This approach can be difficult due to rapid energy depletion within the system once protein translation occurs and subsequent protein degradation by enzymes present in *E.coli* or wheat germ extracts.[66–68] However, development of purified cell-free expression systems has provided a better tools for synthetic biology and minimal cell research in particular.[68]

The assembly of proteins inside cells is a feature of normal biological function[487] and can sometimes be associated with of the pathology of diseases such as cataract disease[325,488] and sickle cell anemia.[489] Protein phase diagrams have been instrumental in explaining many of these biological condensation events.[490] However, the connection between *in-vitro* bulk measurements and those performed under physiologically relevant conditions is not always clear. At the same time, observing protein assembly in live cells is now possible due to advances in imaging technologies and labeling techniques. However linking these in-cell experiments and those performed *in-vitro* is complex due to the inherent complexity of the cellular environment and the potential for fluorescent labels to alter the conditions under which condensation events occur.[289] Therefore, there is a need to observe the condensation of proteins in more physiologically relevant conditions, and without the use of fluorescent labels.

Self-organization (steady-state) and self-assembly (equilibrium) driven by non-covalent interactions are essential processes in biological systems.[491] Virtually all biomolecules undergo self-assembly which defines the structure and function for that molecule.[492] Assembly processes have been explored by synthetic biology, especially in the development of minimal cells.[133] The organization of proteins, mainly components of the cell's cytoskeleton and spindle apparatus have been previously studied by encapsulating the components required for assembly within a vesicle,[97,98] for example embryos or egg extracts of variety of microorganisms have been used for this purpose.[100–102,493] Noireaux and Libchaber showed the cell-free *in-situ* expression of α-hemolysin inside lipid vesicles, followed by formation of a membrane pore via assembly of the α-

hemolysin heptamer.[51] Hence, while a number of assembly processes have been observed inside vesicles, either by encapsulation or after *in-situ* expression, there is still a requirement to link these observations to studies performed under more explicit control to explain fully the process of assembly and how it is altered by the other components required for normal cell function.

Here an approach to observe the condensation of proteins in model cells in physiologically relevant conditions is proposed. The P23T mutant of human gamma D crystallin was expressed *in-situ* following the encapsulation of a cell-free expression system inside a cell sized GUV. P23T is a mutant of HGD which aggregates at physiological temperatures (due to an inverted temperature dependence of the solubility line[282]). By analysing the fractal dimension of the aggregates formed, it was possible to distinguish these aggregates from those formed by non-specific interactions without the need for labelling.

6.2 Results and discussion

6.2.1 Protein expression in cell-free expression system

The P23T single mutant of human γD-crystallin was obtained by site-directed mutagenesis (section 2.7.3). The incorporation of the single amino acid substitution, proline (CCC) to tyrosine (ACC), at position 23 was confirmed by sequencing (figure 6.1).

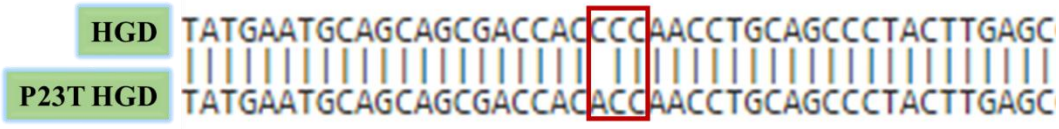

Figure 6.1 *Sequence of the P23THGD plasmid DNA aligned against the WT HGD using BLAST (NCBI).*

The HGDP23T mutant (referred to as P23T throughout) and EmGFP plasmid DNAs were expressed in a purified *E. coli* based cell-free transcription and translation system, PURExpress using a protocol described in section 2.8. Degradation of RNA by traces of RNAse from the DNA purification step was prevented by adding RNAse Inhibitor to the reaction mixture.P23T and EmGFP plasmids were used at a concentration of 350 ng per 25 μl reaction volume.

6.2.1.1 Monitoring the time required for completion of the expression process

The cell-free expression mix was used to express EmGFP in a 386-well plate. The point at which the protein expression reaction was completed was determined by monitoring the change in the fluorescence intensity over time (figure 6.2). It was found that the expression of EmGFP proceeded for roughly 6 hours and no significant increase in fluorescence intensity was observed beyond that point (figure 6.3). The only exception was the measurement after 24 hours, where a slight increase in fluorescence intensity was observed. This is mostly likely due to a small increase in concentration as a result of reduced volume due to evaporation (condensation was observed on the cover of the plate).

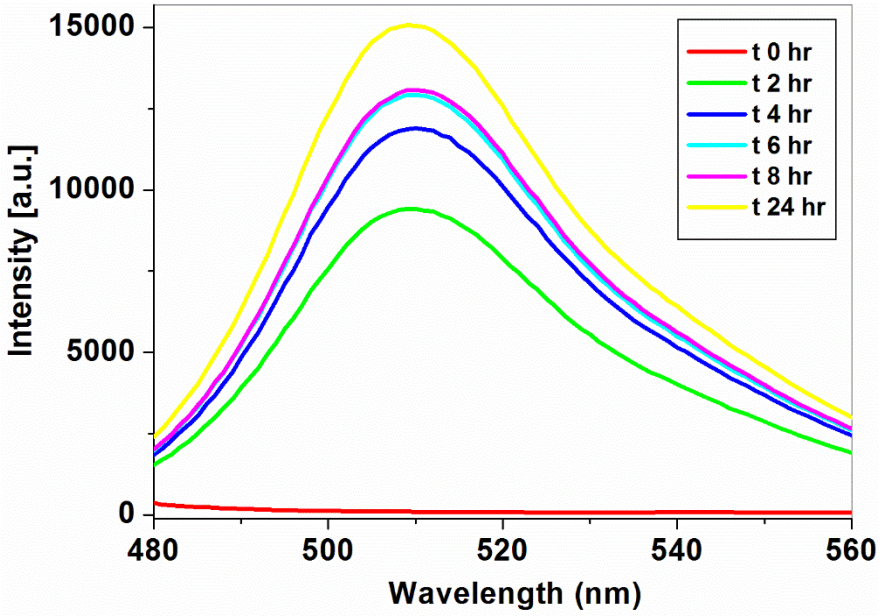

Figure 6.2 *Fluorescence intensity spectra recorded over 24 hours for EmGFP expressed in a cell-free expression medium.*

Previous work suggests that termination of the expression reaction occurs within 3 hours due to degradation of the ribosomes.[74] Therefore we are confident that all of the transcription/translation factors of the cell-free expression kit had been consumed and the protein concentration did not increase further after 6 hours.

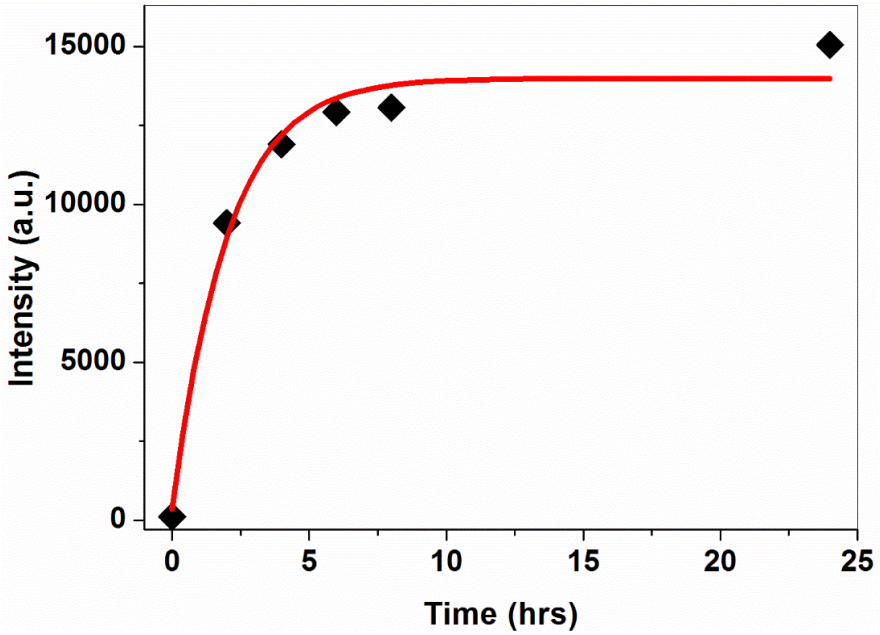

Figure 6.3 *EmGFP concentration changes during expression in a cell-free expression medium monitored by the increase in the fluorescent intensity over 24 hours. The expression reaction is finished within ~ 6 hours.*

6.2.1.2 Determination of the concentration of protein expressed in the cell-free system

Successful expression of P23T in the cell-free expression system was confirmed by SDS-PAGE analysis (figure 6.4 line 8). P23T was expressed in a manner identical to one described in section 2.8, in a small volume vial. BSA was used as a standard for quantification (figure 6.4 lines 2-6). By running the BSA at different concentrations, it was possible to relate the intensity of the protein band to its concentration in an unknown (i.e. P23T expressed in the cell-free expression system). The measurement of the band intensity was performed using ImageJ software.[339] The intensity of BSA bands was used to construct a calibration plot (figure 6.5), from which the concentration of P23T was obtained. The location of the P23T band was determined by comparison to the location of the band for HGD obtained from a purified protein solution (figure 6.4 line 9), the molecular weight markers (figure 6.4 lines 1 and 10) and the cell-free expression mix without DNA (figure 6.4 line 7). The final concentration of P23T following 24 hours incubation at 37°C was found to be 0.13 (+/-0.02) mg/ml. The accuracy of determining protein concentration by this method depends on the quality of the gel (background and the signal-to-noise ratio) and the quality of the image (scanner specifications).[494]

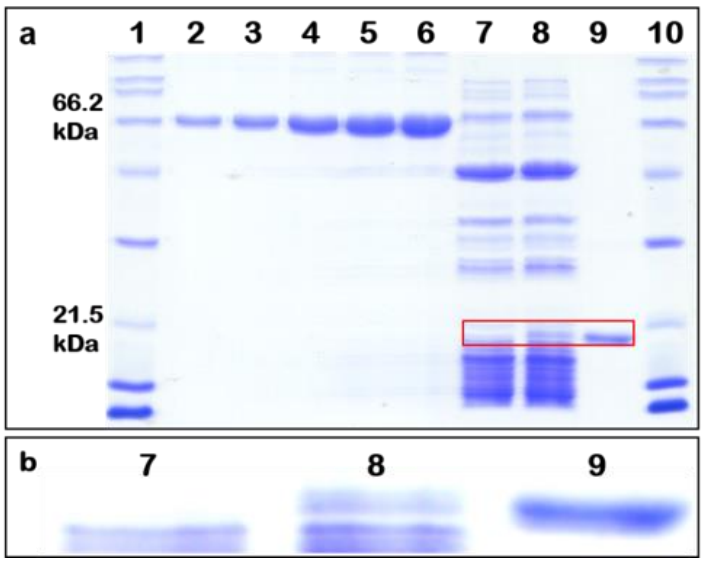

Figure 6.4 *Expression of P23T in a cell-free expression system; (a) lines 1 and 10 show molecular weight marker; 2-6 BSA standards for quantification, line 7 cell free expression system without DNA plasmid; 8, cell free expression system with P23T DNA plasmid; 9, purified HGD solution for comparison; (b) excised lines (7-9).*

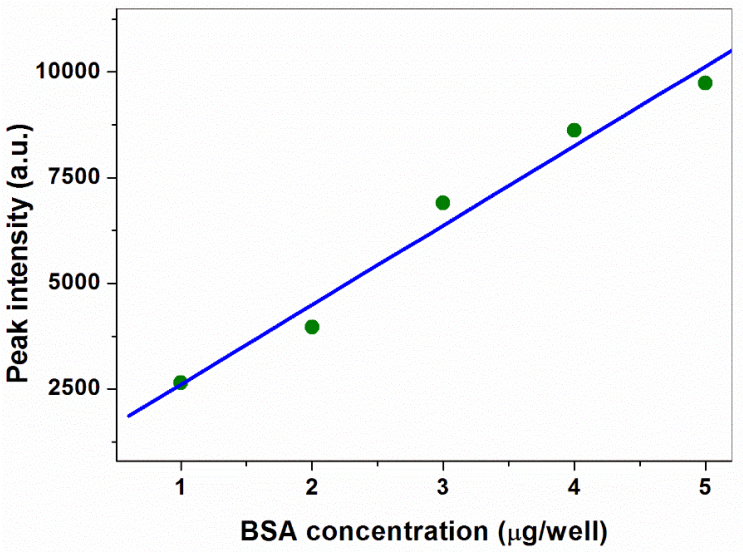

Figure 6.5 *Calibration plot for determination of protein concentration from a SDS-PAGE analysis obtained from five BSA concentrations*

Protein quantification using the SDS-PAGE gel is commonly performed using BSA as a standard. However due to the significant difference in the size between P23T HGD and BSA, a second quantification using HGD as a standard was performed (figure 6.6). The final concentration of P23T expressed under identical conditions (in a different experiment) and determined by comparison with HGD was also 0.13 (+/-0.02) mg/ml.

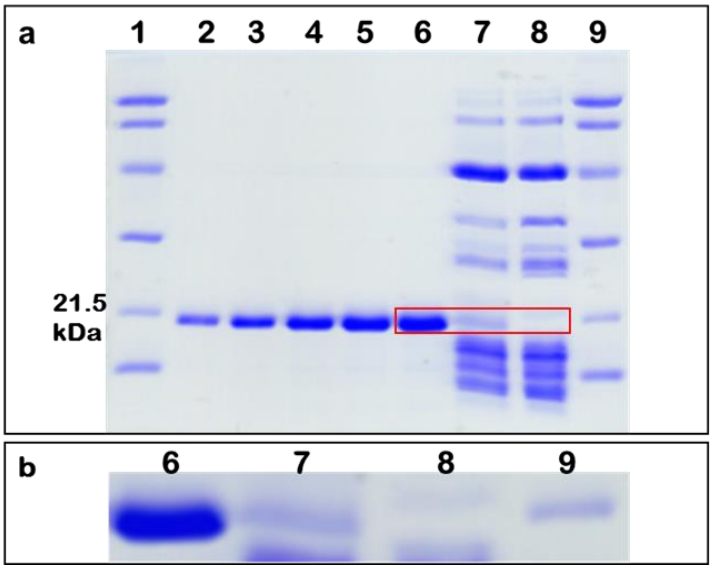

Figure 6.6 *Expression of P23T in cell-free expression system. Lines 1 and 9 show molecular weight marker, 2-6, HGD standards for quantification, line 7, cell free expression system with HGD (P23T) DNA plasmid, line 8, cell free expression system without DNA plasmid; (b) excised lines 6-9).*

6.2.2 P23T aggregate formation in solution after expression in a cell-free expression system

The cell-free reaction expressing P23T protein was incubated at 37°C for several days. Small and difficult to resolve aggregates were observed after 8 hours. After 20 hours, the formation of defined amorphous protein aggregates was observed by phase contrast microscopy (figure 6.7 a). The P23T aggregates were also imaged using transmission electron microscopy (figure 6.7 b). The size of the aggregates increased over a number of days and eventually they grow to several microns in size. Since protein expression ceases after ~24 hours, the slow growth of the aggregates reflects the kinetics of the aggregation process, and not an increase in protein concentration over time.

To ensure that the aggregates observed are those formed by the assembly of P23T, and not due to non-specific aggregation of other components within the PURExpress system, a cell-free expression mix without P23T plasmid DNA was incubated under the same conditions and imaged over a number of days. In this solution (in the absence of P23T) several clusters with sizes up to few micrometers were observed (figure 6.8). However, even a cursory analysis suggests that the morphology of the aggregates in the absence of P23T is significantly different. Furthermore, the number of aggregates formed was far lower.

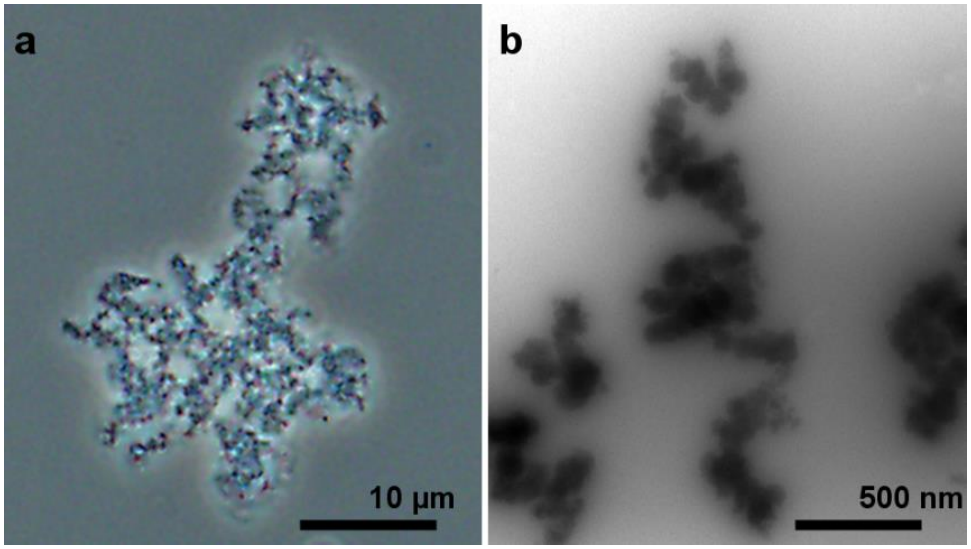

Figure 6.7 *HGDP23T expressed in solution in a cell-free expression system. Images recorded with (a) phase contrast light microscopy and (b) TEM.*

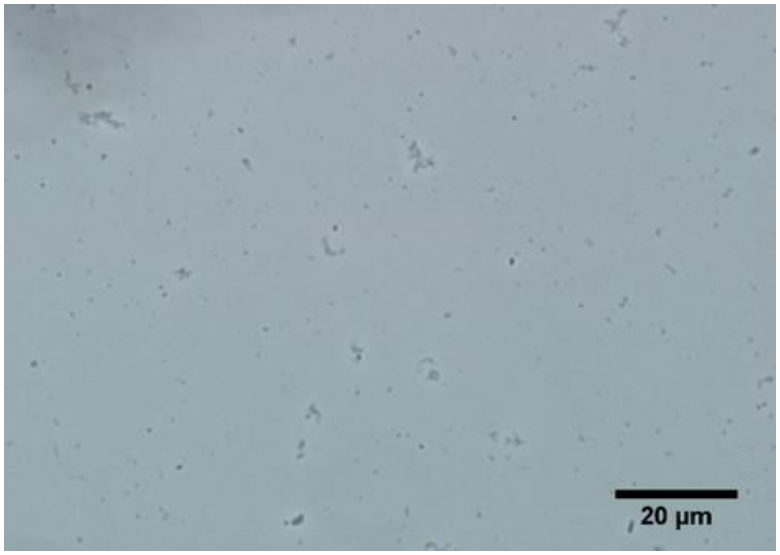

Figure 6.8 *Phase contrast image of particles formed within the cell-free transcription-translation system (without the P23T HGD plasmid DNA) after 3 days of incubation at 37°C.*

The most interesting property of the P23T mutant of HGD is the inverse temperature dependence of the solubility line (figure 6.9), i.e. the protein is more soluble at lower temperatures and aggregates "melt" upon cooling.[282] For the aggregates formed in the cell-free expression mixture expressing P23T, the aggregation process was reversible with temperature. Upon cooling to 4°C, the size and number of aggregates formed in the cell-free solution significantly decreased and this was not observed for the aggregates observed in the control sample. This strongly suggests that the aggregation observed in the cell-free expression system is primarily caused by the self-association of expressed P23T. However, the formation of P23T aggregates occurs at protein

concentrations that are significantly lower than in purified protein solutions (at 37°C, ~0.7 mg/ml).

There is a difference between the appearance of aggregates of P23T formed in the cell-free system and those formed from purified P23T solutions.[282] The aggregates formed in the purified single-component solutions used to determine the solubility line appear very dense, and are almost exclusively spherical aggregates of several microns in size. Those produced in the cell-free expression system are less dense, with an appearance typical of amorphous protein aggregates formed by self-association (figure 6.7). Hence, while it appears that there is a sufficiently high concentration of P23T within the cell free expression system to allow protein assembly to occur, the kinetics for the formation of the aggregates are quite different when compared to a purified protein solution.

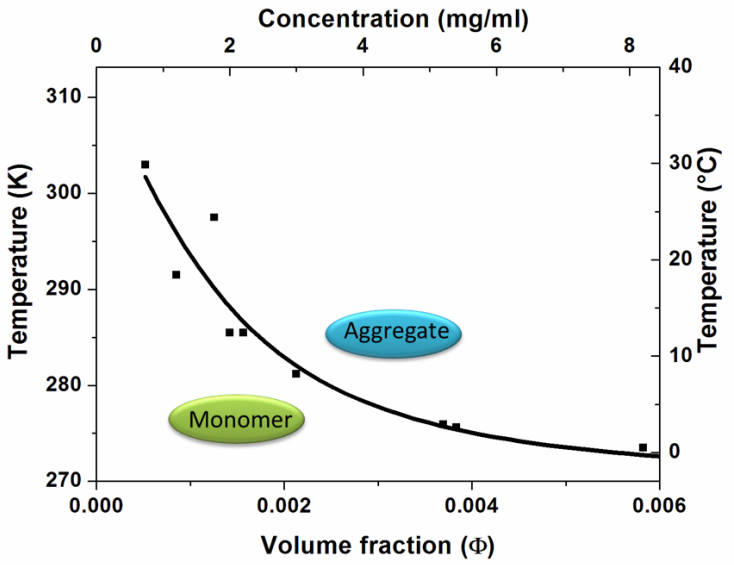

Figure 6.9 *The solubility line for the P23T mutant of HGD, taken from Pande et al., 2005.*

6.2.3 Protein aggregate formation in GUVs after expression in cell-free system

6.2.3.1 P23T mutant of human γD-crystallin

To further explore this self-assembly, the cell-free transcription-translation system, together with plasmid DNA for P23T was encapsulated in phospholipid-based giant unilamellar vesicles. The encapsulation process was performed at 4°C to prevent expression taking place outside of the GUVs. The solution on the exterior of the GUVs contained a solution of the PURExpress mix but containing only the low molecular weight

components (i.e. without ribosomes or enzymes). This is necessary since previous studies have shown that a significant decrease in protein expression levels occurs when buffer is used as the external solvent.[365] This ensures that the osmotic pressure inside and outside of the vesicle are similar (reducing rupture) and eliminates any dilution of the components required for protein expression inside the vesicle due to diffusion across the membrane. After encapsulation, the suspension containing vesicles was incubated at 37°C to allow protein expression to proceed. Due to the inverted solubility of P23T, once the protein is expressed, self-assembly can occur within the vesicle without changing the temperature (figure 6.10). Phase contrast images of the vesicles were recorded every 24 hours for up to 10 days. After that time most of vesicles had ruptured or degraded.

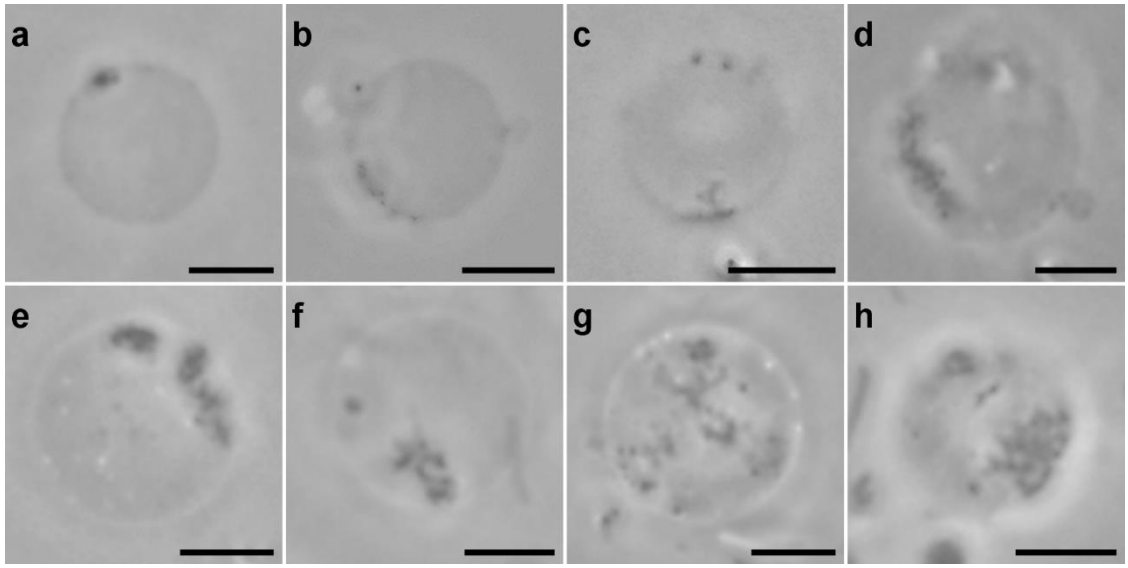

Figure 6.10 *Phase contrast images of GUVs containing P23T aggregates formed after expression in a cell-free system, imaged immediately after formation (a) and then every 24 hours (b-h) (i.e. 8 days are shown here). Scale bar = 5 µm. Each vesicle is indicative of those in the suspension (i.e. the same vesicle was not monitored over 8 days).*

Following encapsulation and during the first 24 hours of incubation at 37°C (during which time all of the expression occurs), no evidence of protein aggregation was observed. The first appearance of small aggregates (~1 µm in size) was observed 24 - 48 hours after encapsulation (i.e. 18 - 42 hours after expression has ceased). By day 4, larger aggregates with a more branched structure were observed. The aggregate size continued to increase for a further 2-3 days. After day seven the size of aggregates remained unchanged and the number of vesicles in general began to decrease.

The aggregation process within the GUVs occurs more slowly than in the un-encapsulated cell-free expression mix. The most likely explanation for this is

heterogeneity in the concentration of the encapsulated solute.[188,461,462] This means that the concentration of the components of the cell-free expression system vary greatly among the vesicles, and in general is lower than in the un-encapsulated solution. These variations of the concentration of the individual components of the cell-free expression system result in the expression of various quantities of protein which we can assume is generally lower than measured for the un-encapsulated solution. Therefore it was expected that at any given time point, the sizes of aggregates varied between vesicles with similar diameters. Moreover some vesicles did not show any signs of aggregation, due to encapsulation of insufficient amounts of the components of the PURExpress system for protein expression to actually occur inside. Therefore, we expect that in the majority of vesicles, the concentration of expressed protein is lower than 0.13mg/ml, which was the concentration determined from the expression of P23T in un-encapsulated cell free expression medium.

In general, larger aggregates formed in GUVs with larger diameters. This was expected, since encapsulation of larger volumes of the cell-free expression system results in expression of higher numbers of P23T molecules and therefore within the vesicle, more material is available to form aggregates.

For both encapsulated and un-encapsulated cell-free expression mixture, the rate of aggregation is significantly slower than for purified solutions of P23T. At 1 mg/ml large aggregates (sizes exceeding the detection range of QLS) were observed after 10-20 min[282] for purified P23T. The main reason for this observation is simply the lower concentration of the protein inside the vesicles.

6.2.3.2 Wild type HGD

As a control, wild type HGD was also expressed inside GUVs (figure 6.11). Purified WT HGD is soluble at 37°C and doesn't form amorphous aggregates at the concentrations of protein expressed in the vesicle.[282] Within the interior of the GUVs no aggregation was observed. After three days small clusters were observed in several vesicles in close proximity to the lipid bilayer. For these experiments, a fluorescent dye (0.05 % of bodipy TR ceramide) was integrated into the phospholipid mixture during GUV formation (figure 6.12).

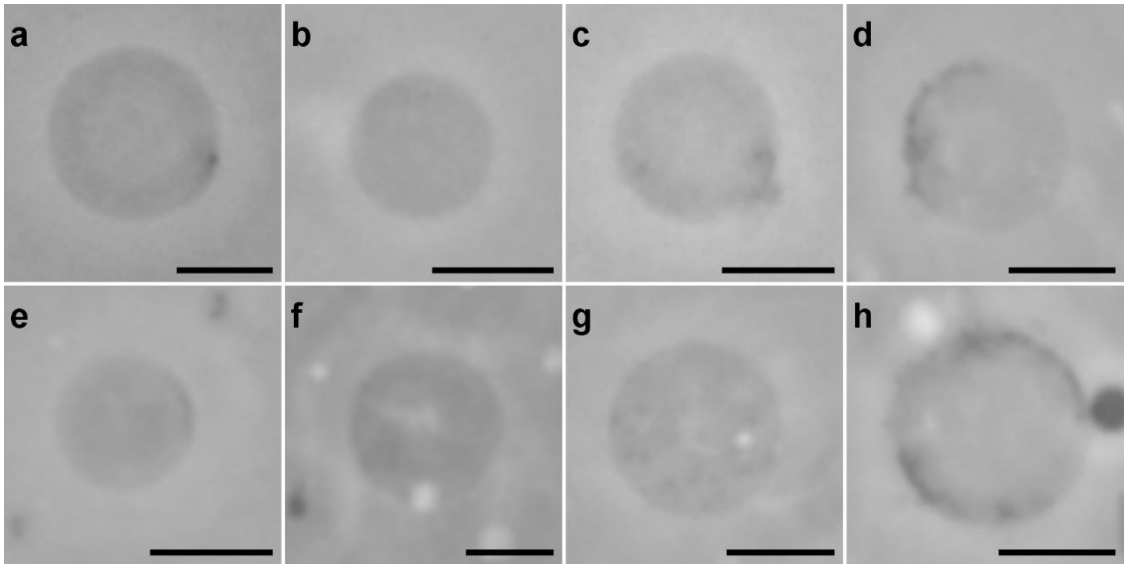

Figure 6.11 *Phase contrast images of GUVs upon expression of WT HGD in cell-free expression system, imaged immediately after formation (a) and then every 24 hours (b-h) (i.e. 8 days are shown here). Scale bar = 5 µm. Each vesicle is indicative of those in the suspension (i.e. the same vesicle was not monitored over 8 days). Scale bar = 5 µm.*

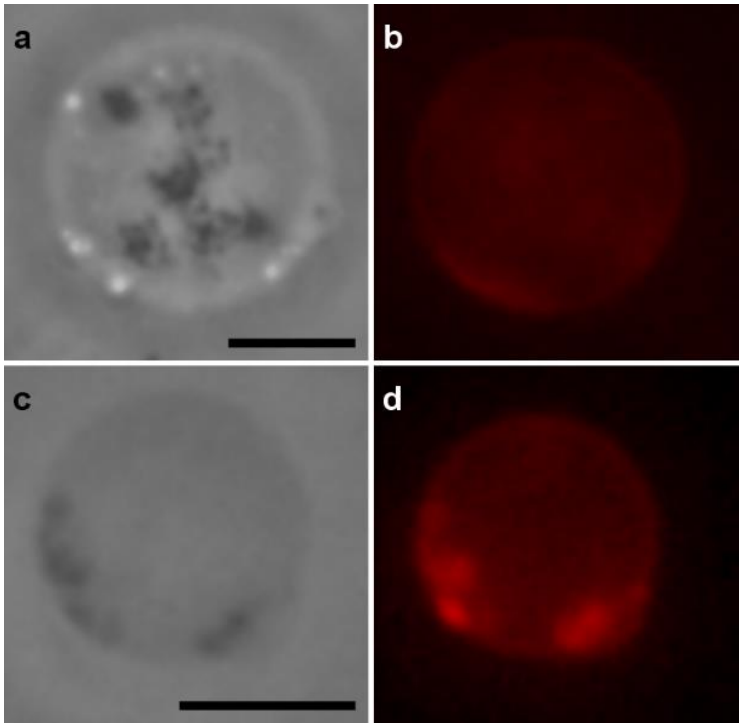

Figure 6.12 *Self-assembled structures formed inside GUVs labelled with 0.05 % of the fluorescent dye, bodipy TR ceramide, upon expression of P23T (a and b) and WT HGD (c and d). Scale bar 5 = µm.*

The regions where aggregation is visible by phase contrast microscopy corresponds to areas where there is an increase of the fluorescent dye concentration within the lipid membrane (Figure 6.12 c and d). This was not found in similar experiments

performed in vesicles containing P23T aggregates (Figure 6.12 a and b), where the fluorescent dye is more evenly distributed in vesicles containing P23T mutant. It remains unclear whether the formation of these clumps in the HGD containing solutions is due aggregation of cell-free expression components or HGD, but in either case, it appears to occur only at the membrane, and not in the interior of the vesicles, which distinguishes it from the P23T aggregation observed previously.

6.2.4 Fractal analysis

Due to the significant experimental differences in the morphology and kinetics of aggregate formation in the P23T containing vesicles, compared with purified P23T solutions, further analysis of the aggregates was performed. Comparisons of the aggregate sizes in different vesicles is not appropriate, since each vesicle contained a slightly different concentration of expressed P23T, which influences the overall size of the aggregates formed. However comparing the overall shape of aggregates (i.e. the fractal dimension), will provide some useful insights. We performed this comparison based on the fractal dimension analysis in an identical manner as described in sections 2.14 and 5.2.6, using the box counting method available through FracLac plugin for ImageJ software.

The fractal dimension of P23T aggregates formed after expression in a cell-free system firstly in solution (Figure 6 a) and then inside GUVs (Figure 6 b) was calculated. Images of aggregates obtained by phase contrast microscopy were converted to binary images prior to analysis (Figure 6, inserts).

The average of the mean values for D_B obtained for P23T aggregates formed in solution and inside GUVs are presented in table 6.1. The differences in these values, are very small and may be caused by the differences in the volume and the environment in which the aggregation took place.

There was more variation in the fractal dimension values calculated for each aggregate formed inside vesicles than for aggregates formed in solution. This can be caused by the variation of encapsulation efficiency, and therefore various protein concentrations within individual vesicles and the component of the cell-free expression mix.[495] The imaging of aggregates entrapped inside GUVs is also slightly more challenging compared to imaging aggregates free in solution.

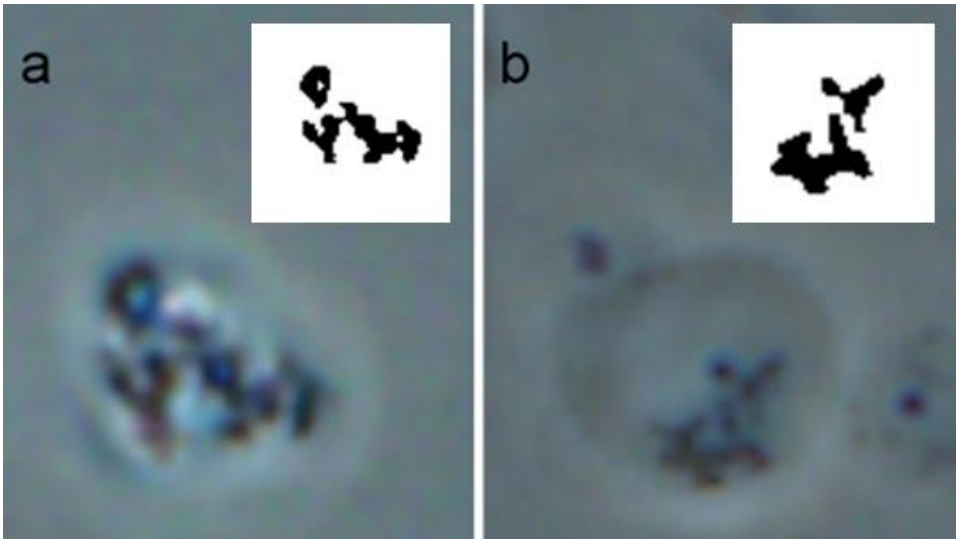

Figure 6.13 *Phase contrast and binary images of aggregates prepared in solution (a) and inside GUVs (b) for fractal dimension calculations.*

Table 6.1 *Comparison of fractal dimension values for P23T HGD aggregates formed in solution and inside GUVs.*

	Aggregates in solution	Aggregates inside GUVs
Fractal dimension (D_B) (average)	1.38	1.34
Standard deviation	0.095	0.159
Coefficient of variation	6.9 %	11.9 %

The values for the fractal dimension of P23T aggregates are significantly different from those obtained for BSA aggregates formed at pH 3 after thermal denaturation (1.51 and 1.5 for aggregates formed in the presence of 50 mM NaCl and in its absence, respectively).

Fractal analysis of protein aggregates has been extensively studied for various types of proteins.[471–476] Values of the fractal dimension between 1.5 and 2.8 have been observed for various types of aggregates (including amorphous aggregates and protein gels.[477–480] These values vary greatly depending on the nature of the protein used, its concentration and the solution conditions. The fractal dimension values also differ depending on the method used in calculations, however the D_B values obtained using rheological determination and the box-counting method remain in good agreement.[476]

Previously published fractal dimension values, ranging from 1.5 to 2.8 have been measured for aggregates formed in purified protein solutions. These aggregates formed via processes driven by non-specific interactions between unfolded or partially unfolded species (induced by heat denaturation or extreme pHs) and are compact structures. The P23T aggregates with fractal dimensions of ~1.3 were formed in the cell-free expression system, suggesting the formation of loose amorphous material, quite different to those observed in purified solutions. The formation of aggregates at such low P23T concentration is already somewhat surprising, since it is below the solubility boundary for the purified protein. Hence, the formation of aggregates with a significantly different fractal dimension is not unexpected. If it was possible to produce higher concentration of P23T from the cell-free expression system, we would expect the fractal dimension to increase. At the very least, this very specific fractal dimension for the P23T aggregates distinguishes them from other non-specific aggregates and provides further confirmation of P23T specific aggregates after expression of the protein. Interestingly these measurements are consistent with the values for of fractal dimension reported for sparse, less compact protein self-assemblies found in nature.[496]

6.2.5 Protein expression in mammalian cells

Here an EmGFP fusion protein of both human γD-crystallin and the P23T mutant were expressed in HEK 293T/17 mammalian cells to monitor expression and aggregation of these proteins inside cells.

6.2.5.1 Mammalian expression vectors

Plasmid DNA with the HGD gene fused to EmGFP was designed for propagation in *E.coli* and optimal expression in mammalian cells. It was synthesized by GeneArt (ThermoFisher, Germany). The HGD gene was inserted into the pcDNA6.2_C-EmGFPDEST mammalian vector at the attL2/attL1 site (figure 6.14). The EmGFP-HGD vector contained a blasticidin resistance gene for selection of stable transfected cell lines.

The EmGFP-P23T vector was obtained by site directed mutagenesis of the EmGFP-HGD mammalian expression vector using protocol described in section 2.9.3. The Vivid Colors™ pcDNA™ 6.2/EmGFP GW/TOPO mammalian expression vector was used to express free-EmGFP (not fused to any other protein).

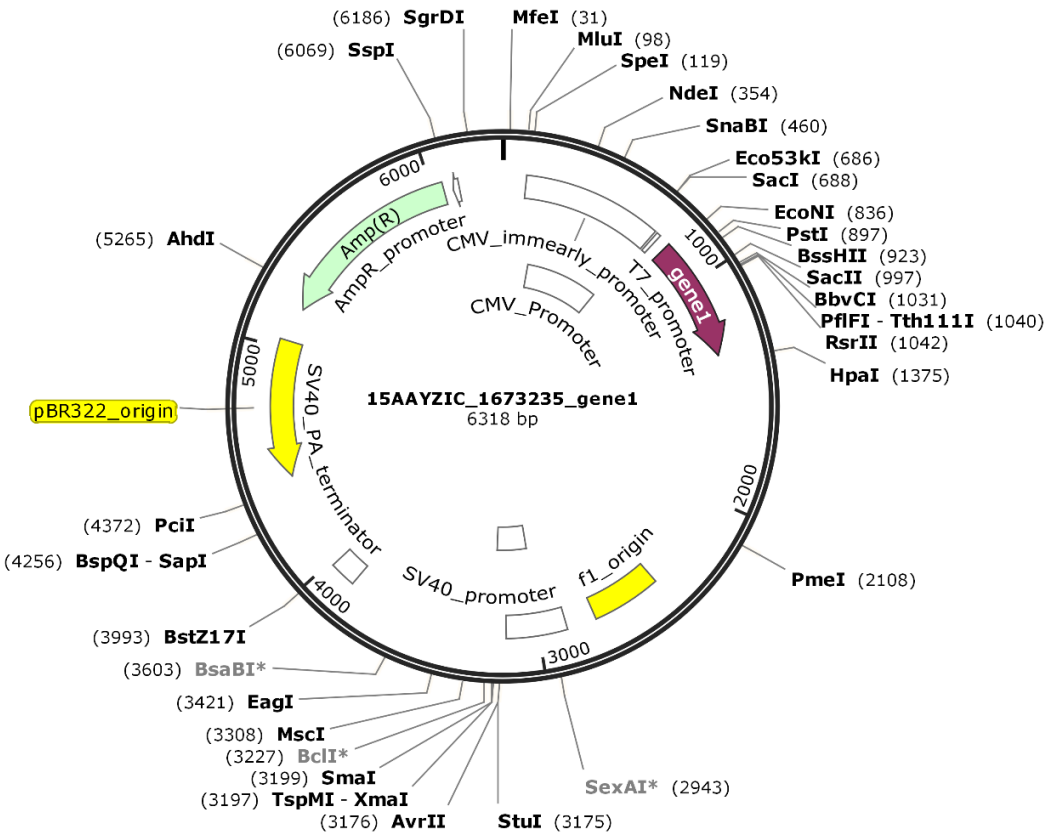

Figure 6.14 *Map of the mammalian vector pcDNA6.2_C-EmGFP-DEST_A321 with a HGD gene obtained using SnapGene software.*

Transfection of HEK 293T/17 mammalian cells with the three vectors was performed using lipofectamine 2000 (section 2.13). After transfection, cells were imaged using fluorescence microscopy to confirm the presence of EmGFP expressing cells. Relatively high transfection efficiencies (ca. 70-90%) were obtained depending on the type of the vector or the type of culture flask used (figure 6.15).

Images of both transient and stable transfected HEK cell lines were obtained using an upright microscope at either 60x or 100x. In order to do that, cells were grown on glass surface chambers or coverslips. These surfaces were coated with poly-D-lysine since HEK cells do not easily grow on glass directly. Transfected cells attached more efficiently to the pretreated surface in the presence of fetal bovine serum as opposed to bovine calf serum, which was routinely used to maintain the cell growth.

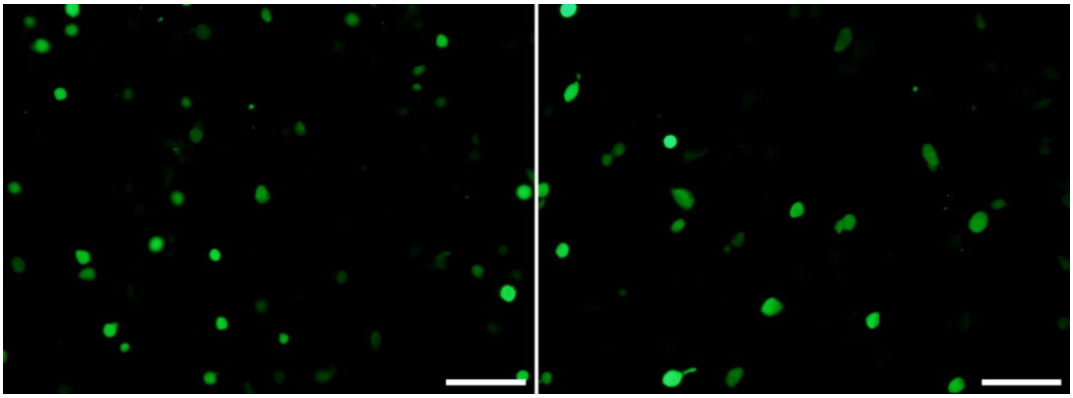

Figure 6.15 *HEK 293T/17cells after transfection with the EmGFP-HGD (left) and the EmGFP-P23T (right) plasmid DNA, grown in a 6-well plate. Scale bar = 100 µm.*

6.2.5.2 EmGFP expression in HEK 293T/17 mammalian cells

HEK cells expressing EmGFP are shown in figure 6.16. The transfection efficiency was higher for this plasmid than for either of the fusion protein plasmids. These cells easily attached to the pretreated glass surfaces (poly-D-lysine). The EmGFP was evenly distributed within the cells and no signs of aggregation were observed. The areas where the fluorescence intensity is lower corresponds to the location of cellular organelles, such as the nucleus.

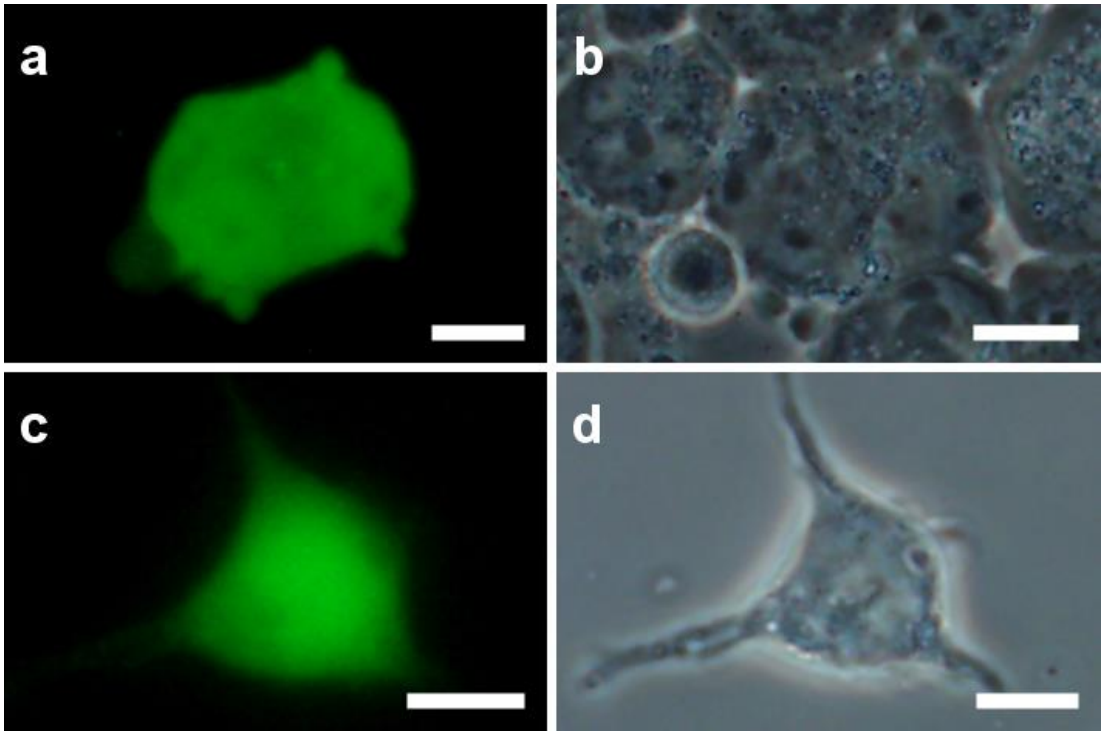

Figure 6.16 *Phase contrast and fluorescence microscopy images of HEK 293T/17cells expressing the EmGFP. Scale bar = 10 µm.*

It was important to ensure that the EmGFP didn't aggregate by itself inside cells, since as part of a fusion protein, it will be used to detect regions of protein aggregation in cells expressing HGD and P23T. For in-cell measurements (unlike in the GUVs described earlier), fluorescent tags are essential to distinguish the protein of interest from the rest of the cellular milieu.

6.2.5.3 HGD expression in HEK 293T/17 mammalian cells

HEK cells expressing the EmGFP-HGD fusion protein are shown in figure 6.17. These cells required a much longer time period to attach to the pretreated glass surfaces. The attachment was however significantly improved in the presence of 10% fetal calf serum. The growth rate of the EmGFP-HGD expressing cells was slightly slower compared to those expressing EmGFP or the P23T fusion protein.

The expressed EmGFP-HGD was evenly distributed within the cells suggesting that the presence of the EmGFP tag does not affect the HGD solubility (at the relatively low concentrations that are likely to be achieved in the cell in any case). Again areas with lower fluorescence intensity corresponds to cellular organelles (figure 6.17a).

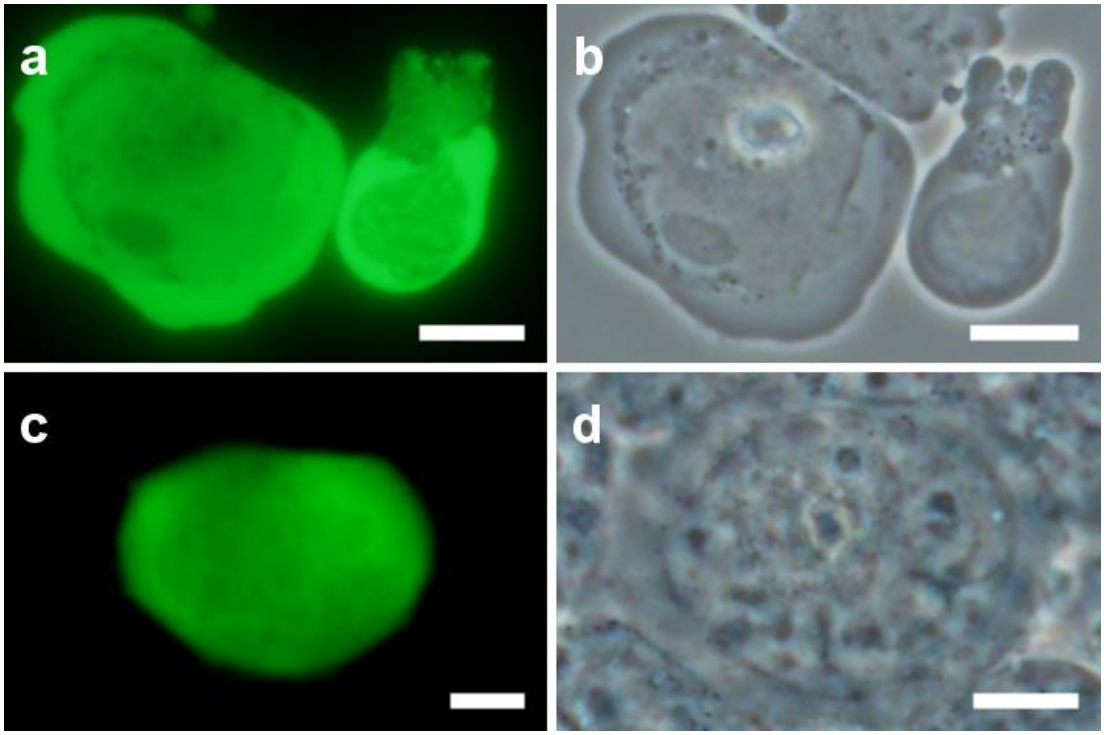

Figure 6.17 *Phase contrast and fluorescence microscopy images of HEK 293T/17cells expressing the EmGFP-HGD fusion protein. Scale bar = 10 µm.*

6.2.5.4 HGDP23T expression in HEK 293T/17 mammalian cells

HEK cells expressing the EmGFP-P23T fusion protein are shown in figure 6.18. These cells exhibited a similar growth rate and the ability to adhere to the poly-D-lysine pretreated glass surface as the EmGFP expressing cells.

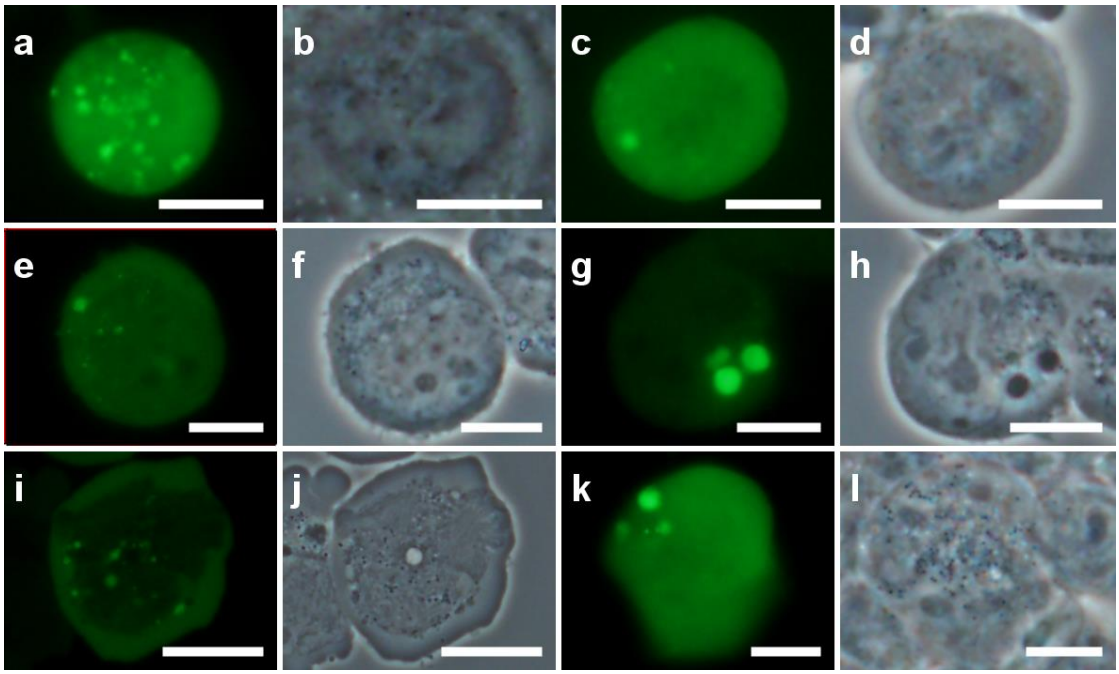

Figure 6.18 *Phase contrast and fluorescence microscopy images of HEK 293T/17cells expressing the EmGFP-P23THGD fusion protein. Scale bar = 10 µm.*

Within the interior of the cells (of both transient and stable cell lines) areas of increased fluorescence intensity were observed. These regions of increased intensity are located throughout the cells in which they are observed (figure 6.18 a, e and i) and correspond to sizes up to 1 µm. These areas are expected to represent the self-assembly structures composed of the EmGFP-P23T fusion proteins. Additionally, formation of 2 to 3 larger areas, with sizes up to 5 µm, within a single cell was also observed (figure 6.18 c, g and k). No difference in the average size of the aggregates was observed between transient and stable transfectants. The larger structures observed possibly consist of intracellular vesicles entrapping the overexpressed and self-assembled proteins as these structures appear in close vicinity to the cell membrane. Fluorescent labeling of other cellular structures would be required to more precisely asses the location of the aggregates within the cell interior.

The increase of the intensity observed by fluorescence microscopy does not always corresponds to the increased in density in the phase contrast image, which was

expected since there is little difference in refractive index between the cell organelles and protein aggregates.

The P23T aggregate formation was observed in HEK cells within three days after transfection (two days from the seeding on the glass slide), which is consistent with our observation in cell-free expression system. However, more investigation is required to assess what effect cell division has on the aggregate formation and growth. The aggregates formed in HEK cells had sizes ranging from 1 µm to 5 µm. These sizes are slightly larger than the average aggregate sizes observed in vesicles (up to ~3.5 µm, which is not at all surprising considering the larger size of the cells (~15 µm).

Various mammalian cell lines have been used to study cellular processes such as protein-protein interactions, protein behavior, localization within cellular environment[497–499] or protein aggregation.[500,501] Those studies usually involve expression of fusion proteins or other methods of fluorescent labelling in order to avail of various supperresolution microscopy techniques.[502] Careful interpretation of such studies is necessary not only due to the complexity of the cellular environment but also due to the possible effect which various strategies of protein labelling may have on its behavior.[289,503–505] Comparison to the experiments in model cells mimicking studied process may make the interpretation less problematic.

6.3 Conclusions

An approach to investigate protein condensation in physiologically relevant conditions has been discussed. This can be achieved with *in-situ* expression of a protein (the P23T mutant of human gamma D crystallin) from a cell-free expression medium encapsulated in a giant unilamellar vesicle of cell-size. The formation of self-assembled P23T structures was observed following *in-situ* expression using a cell-free expression system encapsulated in a GUV. Due to the low protein concentration, these structures were formed after incubation for several hours at 37°C. Measuring the fractal dimension of the aggregates formed allowed P23T specific aggregates to be distinguished from those formed via non-specific interactions without the need for labeling.

The formation of self-assembled protein structures in a GUV encapsulating the cell-free expression system, occurs at much lower concentrations than for purified protein in an *in-vitro* system. We have chosen to express the P23T mutant of human gamma-D crystallin, since it forms amorphous protein assemblies with an inverse temperature

dependence of the solubility line (i.e. it forms reversible aggregates at higher temperatures that return to a monomeric state when the temperature is lowered). This inversion of the temperature dependence of the solubility line in the mutant occurs without a change in protein structure, which makes it possible to both express protein and monitor assembly at 37°C over a number of days.

The HGD and the P23T mutant was also expressed in mammalian cells. The crowded cellular environment and the presence of the tag protein was shown not to affect the solubility of the wt HGD protein. In case of the P23T single mutant fusion protein, the formation of the protein aggregates observed by fluorescence microscopy suggest a formation of self-assembled protein structures, similar to those observed in label-free conditions in giant unilamellar vesicles.

Summary and Concluding Remarks

Building even a simple artificial or minimal cell can be a complex process, requiring suitable preparation techniques and functionalisation of both the membrane surface and the interior of the cell. In this thesis a critical comparison of the methods to prepare giant unilamellar vesicles as basic building block for an artificial cell has been discussed. The relative merits of these preparation methods when applied to the encapsulation of biomolecules was also presented. This comparison of experimental techniques provides reliable information for tailoring the selection of experimental approach when building an artificial cell.

Bottom-up approaches to synthetic biology allow formation of minimal cells composed of the basic components required to perform specific functions. To-date many processes and chemical reactions have been studied in minimal cells; many more remain to be explored. In order to broaden the range of the applications, both the surface and the interior of the model cell needs to be functionalized with versatile molecules.

The growing interest in incorporating glycolipids into lipid bilayers is driven by the increasing number of their biomedical applications, primarily targeted drug delivery. Glycolipids are ideal candidates since the complementarity of sugar residues is vital to the molecular recognition in biological cells. The specificity and mode of interaction can be modified by altering the functionality of the sugar-based head group. Furthermore, the structure, glycolipid concentration and the nature of solvent, can significantly alter the phase behaviour of the glycolipid within a membrane. We have shown how a change in the concentration of an acetylated, galactose-based glycolipid can change the lipid phase behaviour, leading to the formation of either lamellar or columnar lipid phases. This behaviour needs to be carefully considered when designing a minimal cell, since phase separation and consecutive formation of non-lamellar phases may alter the distribution within the bilayer or diminish the number of glycolipid molecules remaining available for interactions with other particles or cells.

The self-assembly of proteins is required to maintain the structure and biological function of a cell. Proteins may also self-assemble in response to a change in environmental conditions, in some cases leading to disease. Studies of the aggregation process, have traditionally been performed *in-vitro*, mainly in solutions of purified proteins. This approach provides vital information regarding the mechanism or the nature

of the forming structures, however it also has a significant drawbacks as it lack the complexity of the cellular environment. On the other hand studies in cells are limited due to the sensitivity of cell culture and the identification of the key factors that play a role in the aggregation process may be difficult to elucidate. A minimal l cell provides an idea platform to carry out such analysis, as it provides a controlled, cell-like conditions.

Aggregation of BSA in GUVs was induced under harsh environmental conditions (beyond the sensitivity of cell) and analysed using a fluorescent dye (Thioflavin T) and various modes of microscopy. To examine protein assembly under more physiologically relevant conditions, the P23T mutant of human gamma D crystallin was examined after *in-situ* expression from a cell free expression system inside a GUV. We have shown that the aggregation observed is specifically related to P23T and not non-specific aggregation of other components and occurs at a rate that is determined by the concentration of protein in the vesicles. Furthermore, the self-assembly of P23T was also be induced following transfection in mammalian cells. The analysis of the P23T self-assembly in minimal and biological cells furthers our understanding of the mechanism by which this mutation which causes genetic cataract leads to condensation in lens fiber cells.

References

[1] W. W. Gibbs, *Sci. Am.* **2004**, *290*, 74–81.

[2] E. D. Cameron, C. J. Bashor, J. J. Collins, *Nat. Rev. Microbiol.* **2014**, *12*, 381–90.

[3] J. Monod, F. Jacob, *Cold Spring Harb. Symp. Quant. Biol.* **1961**, *26*, 389–401.

[4] V. Noireaux, *Médecine Sci. M/S* **2015**, *31*, 1126–32.

[5] M. M. Hanczyc, S. M. Fujikawa, J. W. Szostak, *Science* **2003**, *302*, 618–22.

[6] S. S. Mansy, J. W. Szostak, *Cold Spring Harb. Symp. Quant. Biol.* **2009**, *74*, 47–54.

[7] R. V Solé, *Int. J. Biochem. Cell Biol.* **2009**, *41*, 274–84.

[8] A. C. Forster, G. M. Church, *Mol. Syst. Biol.* **2006**, *2*, 45.

[9] M. C. Jewett, A. C. Forster, *Curr. Opin. Biotechnol.* **2010**, *21*, 697–703.

[10] S. Rasmussen, L. Chen, M. Nilsson, S. Abe, *Artif. Life* **2003**, *9*, 269–316.

[11] D. A. Hammer, N. P. Kamat, *FEBS Lett.* **2012**, *586*, 2882–90.

[12] M. Marguet, C. Bonduelle, S. Lecommandoux, *Chem. Soc. Rev.* **2013**, *42*, 512–29.

[13] R. J. R. W. Peters, M. Marguet, S. Marais, M. W. Fraaije, J. C. M. van Hest, S. Lecommandoux, *Angew. Chem. Int. Ed. Engl.* **2014**, *53*, 146–50.

[14] D. G. Gibson, J. I. Glass, C. Lartigue, V. N. Noskov, R.-Y. Chuang, M. a Algire, G. a Benders, M. G. Montague, L. Ma, M. M. Moodie, et al., *Science* **2010**, *329*, 52–56.

[15] A. P. Liu, D. a Fletcher, *Nat. Rev. Mol. Cell Biol.* **2009**, *10*, 644–650.

[16] P. Schwille, *Science* **2011**, *333*, 1252–1254.

[17] F. Caschera, V. Noireaux, *Curr. Opin. Chem. Biol.* **2014**, *22*, 85–91.

[18] H. McAdams, L. Shapiro, *Science (80-.).* **1995**, *269*, 650–656.

[19] H. H. McAdams, A. Arkin, *Curr. Biol.* **2000**, *10*, R318–R320.

[20] T. S. Gardner, C. R. Cantor, J. J. Collins, *Nature* **2000**, *403*, 339–42.

[21] M. B. Elowitz, S. Leibler, *Nature* **2000**, *403*, 335–8.

[22] A. Becskei, B. Séraphin, L. Serrano, *EMBO J.* **2001**, *20*, 2528–35.

[23] L. You, R. S. Cox, R. Weiss, F. H. Arnold, *Nature* **2004**, *428*, 868–71.

[24] J. Bonnet, P. Yin, M. E. Ortiz, P. Subsoontorn, D. Endy, *Science* **2013**, *340*, 599–603.

[25] P. Siuti, J. Yazbek, T. K. Lu, *Nat. Biotechnol.* **2013**, *31*, 448–52.

[26] D.-K. Ro, E. M. Paradise, M. Ouellet, K. J. Fisher, K. L. Newman, J. M. Ndungu, K. A. Ho, R. A. Eachus, T. S. Ham, J. Kirby, et al., *Nature* **2006**, *440*, 940–3.

[27] C. J. Paddon, P. J. Westfall, D. J. Pitera, K. Benjamin, K. Fisher, D. McPhee, M. D.

Leavell, A. Tai, A. Main, D. Eng, et al., *Nature* **2013**, *496*, 528–32.

[28] M. H. Larson, L. A. Gilbert, X. Wang, W. A. Lim, J. S. Weissman, L. S. Qi, *Nat. Protoc.* **2013**, *8*, 2180–96.

[29] L. S. Qi, M. H. Larson, L. A. Gilbert, J. A. Doudna, J. S. Weissman, A. P. Arkin, W. A. Lim, *Cell* **2013**, *152*, 1173–83.

[30] J. D. Sander, J. K. Joung, *Nat. Biotechnol.* **2014**, *32*, 347–55.

[31] D. Rath, L. Amlinger, A. Rath, M. Lundgren, *Biochimie* **2015**, *117*, 119–28.

[32] E. M. Kennedy, B. R. Cullen, *Virology* **2015**, *479-480*, 213–20.

[33] G. M. Church, Y. Gao, S. Kosuri, *Science* **2012**, *337*, 1628.

[34] E. Callaway, *Nature* **2014**, DOI 10.1038/nature.2014.15179.

[35] D. A. Malyshev, K. Dhami, T. Lavergne, T. Chen, N. Dai, J. M. Foster, I. R. Corrêa, F. E. Romesberg, *Nature* **2014**, *509*, 385–8.

[36] D. Summerer, S. Chen, N. Wu, A. Deiters, J. W. Chin, P. G. Schultz, *Proc. Natl. Acad. Sci. U. S. A.* **2006**, *103*, 9785–9.

[37] Q. Wang, A. R. Parrish, L. Wang, *Chem. Biol.* **2009**, *16*, 323–36.

[38] T. S. Young, P. G. Schultz, *J. Biol. Chem.* **2010**, *285*, 11039–44.

[39] K. U. Walter, K. Vamvaca, D. Hilvert, *J. Biol. Chem.* **2005**, *280*, 37742–6.

[40] B. N. Armbruster, X. Li, M. H. Pausch, S. Herlitze, B. L. Roth, *Proc. Natl. Acad. Sci. U. S. A.* **2007**, *104*, 5163–8.

[41] R. L. Koder, J. L. R. Anderson, L. A. Solomon, K. S. Reddy, C. C. Moser, P. L. Dutton, *Nature* **2009**, *458*, 305–9.

[42] T. A. Farid, G. Kodali, L. A. Solomon, B. R. Lichtenstein, M. M. Sheehan, B. A. Fry, C. Bialas, N. M. Ennist, J. A. Siedlecki, Z. Zhao, et al., *Nat. Chem. Biol.* **2013**, *9*, 826–33.

[43] P. Q. Nguyen, Z. Botyanszki, P. K. R. Tay, N. S. Joshi, *Nat. Commun.* **2014**, *5*, 4945.

[44] Y. Liu, H. Shin, J. Li, L. Liu, *Appl. Microbiol. Biotechnol.* **2015**, *99*, 1109–18.

[45] K. Hagen, M. Engelhard, G. Toepfer, *Ambivalences of Creating Life*, Springer International Publishing, Cham, **2016**.

[46] S. F. Fenz, K. Sengupta, *Integr. Biol.* **2012**, *4*, 982.

[47] F. Wu, C. Tan, *Wiley Interdiscip. Rev. Nanomedicine Nanobiotechnology* **2014**, *6*, 369–383.

[48] C. Martino, S. H. Kim, L. Horsfall, A. Abbaspourrad, S. J. Rosser, J. Cooper, D. a. Weitz, *Angew. Chemie - Int. Ed.* **2012**, *51*, 6416–6420.

[49] U. M. Migas, L. Abbey, T. Velasco-Torrijos, J. J. McManus, *Soft Matter* **2014**, *10*, 3978–83.

[50] R. Sachse, S. K. Dondapati, S. F. Fenz, T. Schmidt, S. Kubick, *FEBS Lett.* **2014**, *588*, 2774–81.

[51] V. Noireaux, A. Libchaber, *Proc. Natl. Acad. Sci. U. S. A.* **2004**, *101*, 17669–17674.

[52] L. Li, X. Liang, M. Lin, F. Qiu, Y. Yang, *J. Am. Chem. Soc.* **2005**, *127*, 17996–17997.

[53] H. G. Döbereiner, J. Käs, D. Noppl, I. Sprenger, E. Sackmann, *Biophys. J.* **1993**, *65*, 1396–403.

[54] G. Lei, R. C. MacDonald, *Biophys. J.* **2003**, *85*, 1585–1599.

[55] Y. Inaoka, M. Yamazaki, *Langmuir* **2007**, *23*, 720–728.

[56] M. R. Horton, S. Manley, S. R. Arevalo, A. E. Lobkovsky, A. P. Gast, *J. Phys. Chem. B* **2007**, *111*, 880–885.

[57] S. Manley, M. R. Horton, S. Lecszynski, A. P. Gast, *Biophys. J.* **2008**, *95*, 2301–2307.

[58] P. J. Quinn, *Prog. Lipid Res.* **2010**, *49*, 390–406.

[59] S. L. Veatch, I. V Polozov, K. Gawrisch, S. L. Keller, *Biophys. J.* **2004**, *86*, 2910–2922.

[60] E. Sezgin, I. Levental, M. Grzybek, G. Schwarzmann, V. Mueller, A. Honigmann, V. N. Belov, C. Eggeling, Ü. Coskun, K. Simons, et al., *Biochim. Biophys. Acta - Biomembr.* **2012**, *1818*, 1777–1784.

[61] L. M. Dominak, C. D. Keating, *Langmuir* **2007**, *23*, 7148–7154.

[62] C.-S. Chen, J. Yao, R. A. Durst, *J. Nanoparticle Res.* **2006**, *8*, 1033–1038.

[63] N. Berclaz, M. Müller, P. Walde, P. L. Luisi, *J. Phys. Chem. B* **2001**, *105*, 1056–1064.

[64] M. Abkarian, E. Loiseau, G. Massiera, *Soft Matter* **2011**, *7*, 4610.

[65] F. C. Tsai, B. Stuhrmann, G. H. Koenderink, *Langmuir* **2011**, *27*, 10061–10071.

[66] T. Kigawa, T. Yabuki, N. Matsuda, T. Matsuda, R. Nakajima, A. Tanaka, S. Yokoyama, *J. Struct. Funct. Genomics* **2004**, *5*, 63–8.

[67] M. Harbers, *FEBS Lett.* **2014**, *588*, 2762–73.

[68] Y. Shimizu, A. Inoue, Y. Tomari, T. Suzuki, T. Yokogawa, K. Nishikawa, T. Ueda, *Nat. Biotechnol.* **2001**, *19*, 751–755.

[69] Y. Shimizu, T. Kanamori, T. Ueda, *Methods* **2005**, *36*, 299–304.

[70] Y. Shimizu, T. Ueda, *Methods Mol. Biol.* **2010**, *607*, 11–21.

[71] J. W. Whittaker, *Biotechnol. Lett.* **2013**, *35*, 143–52.

[72] X. Ge, D. Luo, J. Xu, *PLoS One* **2011**, *6*, e28707.

[73] Y. Katayama, K. Shimokata, M. Suematsu, T. Ogura, T. Tsukihara, S. Yoshikawa, H. Shimada, *J. Bioenerg. Biomembr.* **2010**, *42*, 235–40.

[74] T. Stögbauer, L. Windhager, R. Zimmer, J. O. Rädler, *Integr. Biol.* **2012**, *4*, 494.

[75] S. Yokoyama, *Curr. Opin. Chem. Biol.* **2003**, *7*, 39–43.

[76] S. Mikami, M. Masutani, N. Sonenberg, S. Yokoyama, H. Imataka, *Protein Expr. Purif.* **2006**, *46*, 348–57.

[77] V. V Zeenko, C. Wang, M. Majumder, A. A. Komar, M. D. Snider, W. C. Merrick, R. J. Kaufman, M. Hatzoglou, *RNA* **2008**, *14*, 593–602.

[78] M. C. Jewett, K. A. Calhoun, A. Voloshin, J. J. Wuu, J. R. Swartz, *Mol. Syst. Biol.* **2008**, *4*, 220.

[79] A. K. Brödel, A. Sonnabend, S. Kubick, *Biotechnol. Bioeng.* **2014**, *111*, 25–36.

[80] A. van Dalen, M. van der Laan, A. J. M. Driessen, J. A. Killian, B. de Kruijff, *FEBS Lett.* **2002**, *511*, 51–58.

[81] R. Kalmbach, I. Chizhov, M. C. Schumacher, T. Friedrich, E. Bamberg, M. Engelhard, *J. Mol. Biol.* **2007**, *371*, 639–48.

[82] N. T. Hovijitra, J. J. Wuu, B. Peaker, J. R. Swartz, *Biotechnol. Bioeng.* **2009**, *104*, 40–9.

[83] Y. Moritani, S. M. Nomura, I. Morita, K. Akiyoshi, *FEBS J.* **2010**, *277*, 3343–52.

[84] A. R. Long, C. C. O'Brien, N. N. Alder, *PLoS One* **2012**, *7*, e46332.

[85] G. Murtas, Y. Kuruma, P. Bianchini, A. Diaspro, P. L. Luisi, *Biochem. Biophys. Res. Commun.* **2007**, *363*, 12–17.

[86] Y. Kuruma, P. Stano, T. Ueda, P. L. Luisi, *Biochim. Biophys. Acta - Biomembr.* **2009**, *1788*, 567–574.

[87] Z. Nourian, W. Roelofsen, C. Danelon, *Angew. Chemie - Int. Ed.* **2012**, *51*, 3114–3118.

[88] P. Walde, S. Ichikawa, *Biomol. Eng.* **2001**, *18*, 143–177.

[89] K. Hosoda, T. Sunami, Y. Kazuta, T. Matsuura, H. Suzuki, T. Yomo, *Langmuir* **2008**, *24*, 13540–8.

[90] A. Fischer, A. Franco, T. Oberholzer, *ChemBioChem* **2002**, *3*, 409.

[91] K. Shohda, T. Sugawara, *Soft Matter* **2006**, *2*, 402.

[92] G. Murtas, *Syst. Synth. Biol.* **2010**, *4*, 85–93.

[93] A. P. Liu, D. A. Fletcher, *Biophys. J.* **2006**, *91*, 4064–70.

[94] K. Kurihara, M. Tamura, K.-I. Shohda, T. Toyota, K. Suzuki, T. Sugawara, *Nat. Chem.* **2011**, *3*, 775–81.

[95] K. Kurihara, Y. Okura, M. Matsuo, T. Toyota, K. Suzuki, T. Sugawara, *Nat. Commun.* **2015**, *6*, 8352.

[96] G. Tsuji, S. Fujii, T. Sunami, T. Yomo, *Proc. Natl. Acad. Sci. U. S. A.* **2016**, *113*, 590–5.

[97] L. L. Pontani, J. Van Der Gucht, G. Salbreux, J. Heuvingh, J. F. Joanny, C. Sykes, *Biophys. J.* **2009**, *96*, 192–198.

[98] S. K. Vogel, P. Schwille, *Curr. Opin. Biotechnol.* **2012**, *23*, 758–765.

[99] E. Abu Shah, M. Malik-Garbi, K. Keren, *Methods Cell Biol.* **2015**, *128*, 287–301.

[100] A. Walrant, D. S. Saxton, G. P. Correia, J. L. Gallop, *Methods Cell Biol.* **2015**, *128*, 125–47.

[101] R. Farhadifar, C. F. Baer, A.-C. Valfort, E. C. Andersen, T. Müller-Reichert, M. Delattre,

D. J. Needleman, *Curr. Biol.* **2015**, *25*, 732–40.

[102] J. C. Gatlin, A. Matov, A. C. Groen, D. J. Needleman, T. J. Maresca, G. Danuser, T. J. Mitchison, E. D. Salmon, *Curr. Biol.* **2009**, *19*, 287–96.

[103] S. Kulin, R. Kishore, K. Helmerson, L. Locascio, *Reactions* **2003**, 8206–8210.

[104] T. Oberholzer, M. Albrizio, P. L. Luisi, *Chem. Biol.* **1995**, *2*, 677–682.

[105] M. C. M. van Oers, F. P. J. T. Rutjes, J. C. M. Van Hest, *Curr. Opin. Biotechnol.* **2014**, *28*, 10–16.

[106] G. P. Robbins, R. L. Saunders, J. B. Haun, J. Rawson, M. J. Therien, D. A. Hammer, *Langmuir* **2010**, *26*, 14089–96.

[107] G. P. Robbins, D. Lee, J. S. Katz, P. R. Frail, M. J. Therien, J. C. Crocker, D. A. Hammer, *Soft Matter* **2011**, *7*, 769–779.

[108] V. P. Torchilin, *Drug Delivery in Oncology*, Wiley-VCH Verlag GmbH & Co. KGaA, Weinheim, Germany, **2011**.

[109] H. S. S. Qhattal, T. Hye, A. Alali, X. Liu, *ACS Nano* **2014**, *8*, 5423–40.

[110] L. Arabi, A. Badiee, F. Mosaffa, M. R. Jaafari, *J. Control. Release* **2015**, *220*, 275–86.

[111] J. A. Maki, G. M. Culver, *Methods* **2005**, *36*, 313–20.

[112] M. C. Jewett, B. R. Fritz, L. E. Timmerman, G. M. Church, *Mol. Syst. Biol.* **2013**, *9*, 678.

[113] K. Takiguchi, A. Yamada, M. Negishi, Y. Tanaka-Takiguchi, K. Yoshikawa, *Langmuir* **2008**, *24*, 11323–11326.

[114] J. D. Halley, D. A. Winkler, *Complexity* **2008**, *14*, 10–17.

[115] L. F. Lindoy, I. M. Atkinson, *Self-Assembly in Supramolecular Systems*, Royal Society Of Chemistry, **2000**.

[116] I. W. Hamley, V. Castelletto, *Angew. Chem. Int. Ed. Engl.* **2007**, *46*, 4442–55.

[117] J. P. Hill, L. K. Shrestha, S. Ishihara, Q. Ji, K. Ariga, *Molecules* **2014**, *19*, 8589–8609.

[118] J. A. Marsh, S. A. Teichmann, *Annu. Rev. Biochem.* **2015**, *84*, 551–75.

[119] M. Antonietti, S. Förster, *Adv. Mater.* **2003**, *15*, 1323–1333.

[120] H. K. Baca, E. C. Carnes, C. E. Ashley, D. M. Lopez, C. Douthit, S. Karlin, J. C. Brinker, *Biochim. Biophys. Acta - Gen. Subj.* **2011**, *1810*, 259–267.

[121] R. D. Cadena-Nava, M. Comas-Garcia, R. F. Garmann, A. L. N. Rao, C. M. Knobler, W. M. Gelbart, *J. Virol.* **2012**, *86*, 3318–26.

[122] J.-M. Lehn, *Reports Prog. Phys.* **2004**, *67*, 249–265.

[123] J.-M. Lehn, *Angew. Chem. Int. Ed. Engl.* **2013**, *52*, 2836–50.

[124] H. Lodish, A. Berk, S. L. Zipursky, P. Matsudaira, D. Baltimore, J. Darnell, **2000**.

[125] J. Cerný, P. Hobza, *Phys. Chem. Chem. Phys.* **2007**, *9*, 5291–303.

[126] E. V. Anslyn, D. A. Dougherty, *Modern Physical Organic Chemistry*, University Science

Books, **2006**.

[127] S. Miyamoto, P. A. Kollman, *Proc. Natl. Acad. Sci. U. S. A.* **1993**, *90*, 8402–6.

[128] L. Maibaum, A. R. Dinner, D. Chandler, *J. Phys. Chem. B* **2004**, *108*, 6778–6781.

[129] C. M. Bryant, D. J. McClements, *Trends Food Sci. Technol.* **1998**, *9*, 143–151.

[130] P. Atkins, J. de Paula, *Atkins' Physical Chemistry*, OUP Oxford, **2010**.

[131] G. Bozzuto, A. Molinari, *Int. J. Nanomedicine* **2015**, *10*, 975–99.

[132] D. Chandler, *Nature* **2005**, *437*, 640–7.

[133] G. Tresset, *PMC Biophys.* **2009**, *2*, 3.

[134] V. V Kumar, *Proc. Natl. Acad. Sci. U. S. A.* **1991**, *88*, 444–8.

[135] J. Israelachvili, *Intermolecular and Surface Forces*, Academic Press, New York, USA, **1992**.

[136] P. R. Cullis, M. J. Hope, C. P. S. Tilcock, *Chem. Phys. Lipids* **1986**, *40*, 127–144.

[137] J. M. Seddon, *Biochim. Biophys. Acta* **1990**, *1031*, 1–69.

[138] G. Lindblom, L. Rilfors, *Biochim. Biophys. Acta - Rev. Biomembr.* **1989**, *988*, 221–256.

[139] S.-J. Marrink, A. E. Mark, *Biophys. J.* **2004**, *87*, 3894–3900.

[140] B. de Kruijff, *Nature* **1997**, *386*, 129–30.

[141] M. Eeman, M. Deleu, *Base* **2010**, *14*.

[142] A. Tardieu, V. Luzzati, F. C. Reman, *J. Mol. Biol.* **1973**, *75*, 711–733.

[143] M. J. Janiak, D. M. Small, G. G. Shipley, *J. Biol. Chem.* **1979**, *254*, 6068–78.

[144] J. Hjort Ipsen, G. Karlström, O. G. Mourtisen, H. Wennerström, M. J. Zuckermann, *Biochim. Biophys. Acta - Biomembr.* **1987**, *905*, 162–172.

[145] S. L. Veatch, S. L. Keller, *Phys. Rev. Lett.* **2002**, *89*, 268101.

[146] S. L. Veatch, S. L. Keller, *Biophys. J.* **2003**, *85*, 3074–3083.

[147] T. Heimburg, *Thermal Biophysics of Membranes*, John Wiley & Sons, **2008**.

[148] S. L. Veatch, S. L. Keller, *Biochim. Biophys. Acta - Mol. Cell Res.* **2005**, *1746*, 172–185.

[149] J. Juhasz, F. J. Sharom, J. H. Davis, *Biochim. Biophys. Acta - Biomembr.* **2009**, *1788*, 2541–2552.

[150] K. Suga, H. Umakoshi, *Langmuir* **2013**, *29*, 4830–8.

[151] P. Rock, M. Allietta, W. W. Young, T. E. Thompson, T. W. Tillack, *Biochemistry* **1990**, *29*, 8484–8490.

[152] B. Ramstedt, J. P. Slotte, *FEBS Lett.* **2002**, *531*, 33–37.

[153] J. P. Slotte, *Biochim. Biophys. Acta* **2016**, *1858*, 304–10.

[154] K. Simons, E. Ikonen, *Nature* **1997**, *387*, 569–572.

[155] K. Simons, J. L. Sampaio, *Cold Spring Harb. Perspect. Biol.* **2011**, *3*, 1–17.

[156] M. Carquin, L. D'Auria, H. Pollet, E. R. Bongarzone, D. Tyteca, *Prog. Lipid Res.* **2015**, *62*, 1–24.

[157] K. Simons, D. Toomre, *Nat. Rev. Mol. Cell Biol.* **2000**, *1*, 31–39.

[158] L. J. Pike, *J. Lipid Res.* **2003**, *44*, 655–67.

[159] A. Radhakrishnan, T. G. Anderson, H. M. McConnell, *Proc. Natl. Acad. Sci. U. S. A.* **2000**, *97*, 12422–7.

[160] R. G. W. Anderson, K. Jacobson, *Science* **2002**, *296*, 1821–5.

[161] D. A. Brown, E. London, *Annu. Rev. Cell Dev. Biol.* **1998**, *14*, 111–36.

[162] K. Jacobson, O. G. Mouritsen, R. G. W. Anderson, *Nat. Cell Biol.* **2007**, *9*, 7–14.

[163] S. Mañes, G. del Real, C. Martínez-A, *Nat. Rev. Immunol.* **2003**, *3*, 557–68.

[164] J. Fantini, N. Garmy, R. Mahfoud, N. Yahi, *Expert Rev. Mol. Med.* **2004**, *4*, 1–22.

[165] P. Walde, K. Cosentino, H. Engel, P. Stano, *ChemBioChem* **2010**, *11*, 848–865.

[166] A. D. Bangham, *BioEssays* **1995**, *17*, 1081–1088.

[167] J. P. Reeves, R. M. Dowben, *J. Cell. Physiol.* **1969**, *73*, 49–60.

[168] A. Jesorka, O. Orwar, *Annu. Rev. Anal. Chem. (Palo Alto. Calif).* **2008**, *1*, 801–832.

[169] Y. P. Patil, S. Jadhav, *Chem. Phys. Lipids* **2014**, *177*, 8–18.

[170] M. I. Angelova, D. S. Dimitrov, *Faraday Discuss. Chem. SO* **1986**, *81*, 303–311.

[171] M. I. Angelova, S. Soléau, P. Méléard, F. Faucon, P. Bothorel, *Trends Colloid Interface Sci. VI* **1992**, *89*, 127–131.

[172] D. J. Estes, M. Mayer, *Colloids Surfaces B Biointerfaces* **2005**, *42*, 115–123.

[173] S. Manley, V. D. Gordon, *Curr. Protoc. Cell Biol.* **2008**, 1–13.

[174] A. Moscho, O. Orwar, D. T. Chiu, B. P. Modi, R. N. Zare, *Proc. Natl. Acad. Sci. U. S. A.* **1996**, *93*, 11443–7.

[175] K. S. Horger, D. J. Estes, R. Capone, M. Mayer, *J. Am. Chem. Soc.* **2009**, *131*, 1810–9.

[176] S. Pautot, B. J. Frisken, D. a. Weitz, *Langmuir* **2003**, *19*, 2870–2879.

[177] K. Nishimura, H. Suzuki, T. Toyota, T. Yomo, *J. Colloid Interface Sci.* **2012**, *376*, 119–125.

[178] S. Pautot, B. J. Frisken, D. a Weitz, *Proc. Natl. Acad. Sci. U. S. A.* **2003**, *100*, 10718–10721.

[179] C. E. S. Guedes, J. G. B. Lima, E. Helfer, P. S. T. Veras, A. Viallat, *PLoS One* **2015**, *10*, e0134925.

[180] C. K. Haluska, K. A. Riske, V. Marchi-Artzner, J.-M. Lehn, R. Lipowsky, R. Dimova, *Proc. Natl. Acad. Sci. U. S. A.* **2006**, *103*, 15841–6.

[181] S. Ohki, K. Arnold, *Colloids Surfaces B Biointerfaces* **2000**, *18*, 83–97.

[182] E. Lorenceau, A. S. Utada, D. R. Link, G. Cristobal, M. Joanicot, D. A. Weitz, *Langmuir* **2005**, *21*, 9183–6.

[183] S. Sugiura, T. Kuroiwa, T. Kagota, M. Nakajima, S. Sato, S. Mukataka, P. Walde, S. Ichikawa, *Langmuir* **2008**, *24*, 4581–4588.

[184] T. Kuroiwa, H. Kiuchi, K. Noda, I. Kobayashi, M. Nakajima, K. Uemura, S. Sato, S. Mukataka, S. Ichikawa, *Microfluid. Nanofluidics* **2008**, *6*, 811–821.

[185] M. Pons, M. Foradada, J. Estelrich, *Int. J. Pharm.* **1993**, *95*, 51–56.

[186] N. Oku, R. C. Macdonald, *Biochim. Biophys. Acta - Biomembr.* **1983**, *734*, 54–61.

[187] P. Walde, *BioEssays* **2010**, *32*, 296–303.

[188] P. Stano, *Biotechnol. J.* **2011**, *6*, 850–859.

[189] J. M. Berg, J. L. Tymoczko, L. Stryer, **2002**.

[190] J. Li, X. Wang, T. Zhang, C. Wang, Z. Huang, X. Luo, Y. Deng, *Asian J. Pharm. Sci.* **2015**, *10*, 81–98.

[191] G. van Meer, D. R. Voelker, G. W. Feigenson, *Nat. Rev. Mol. Cell Biol.* **2008**, *9*, 112–124.

[192] T. J. McIntosh, S. A. Simon, D. Needham, C. H. Huang, *Biochemistry* **1992**, *31*, 2012–2020.

[193] L. J. Pike, *J. Lipid Res.* **2006**, *47*, 1597–1598.

[194] M. A. Chesters, *Glycoconj. J.* **1999**, *16*, 1–6.

[195] B. K. Gillard, L. T. Thurmon, D. M. Marcus, *Glycobiology* **1993**, *3*, 57–67.

[196] R. Malhotra, *Biochem. Anal. Biochem.* **2012**, *01*, 1–5.

[197] G. John, J. H. Jung, H. Minamikawa, K. Yoshida, T. Shimizu, *Chemistry* **2002**, *8*, 5494–500.

[198] M. Corti, L. Cantù, P. Brocca, E. Del Favero, *Curr. Opin. Colloid Interface Sci.* **2007**, *12*, 148–154.

[199] M. Köberl, A. Schöppe, H.-J. Hinz, G. Rapp, *Chem. Phys. Lipids* **1998**, *95*, 59–82.

[200] H. J. Hinz, H. Kuttenreich, R. Meyer, M. Renner, R. Fründ, R. Koynova, A. I. Boyanov, B. G. Tenchov, *Biochemistry®* **1991**, *30*, 5125–5138.

[201] M. Hato, H. Minamikawa, K. Tamada, T. Baba, Y. Tanabe, **1999**.

[202] D. a. Mannock, R. N. McElhaney, *Curr. Opin. Colloid Interface Sci.* **2004**, *8*, 426–447.

[203] M. Hato, *Curr. Opin. Colloid Interface Sci.* **2001**, *6*, 268–276.

[204] J. M. Seddon, O. Ces, R. H. Templer, D. A. Mannock, R. N. McElhaney, in *Mol. Cryst. Liq. Cryst.*, **2003**.

[205] D. Marsh, *Chem. Phys. Lipids* **2011**, *164*, 177–183.

[206] D. Marsh, *Chem. Phys. Lipids* **2012**, *165*, 23–31.

[207] R. Y. Patel, P. V. Balaji, *Int. J. Carbohydr. Chem.* **2011**, *2011*, 1–9.

[208] S. Degroote, J. Wolthoorn, G. Van Meer, *Semin. Cell Dev. Biol.* **2004**, *15*, 375–387.

[209] S. Hakomori, *Proc. Japan Acad. Ser. B* **2005**, *81*, 189–203.

[210] K. Kasahara, Y. Sanai, *Trends Glycosci. Glycotechnol.* **2001**, *13*, 251–259.

[211] B. Westerlund, J. P. Slotte, *Biochim. Biophys. Acta - Biomembr.* **2009**, *1788*, 194–201.

[212] G. Gupta, A. Surolia, *FEBS Lett.* **2010**, *584*, 1634–1641.

[213] S. V Evans, C. Roger MacKenzie, *J. Mol. Recognit.* **1999**, *12*, 155–68.

[214] A. R. Todeschini, S. I. Hakomori, *Biochim. Biophys. Acta - Gen. Subj.* **2008**, *1780*, 421–433.

[215] S. I. Hakomori, *Glycoconj. J.* **2000**, *17*, 143–51.

[216] K. Iwabuchi, S. Yamamura, A. Prinetti, K. Handa, S. Hakomori, *J. Biol. Chem.* **1998**, *273*, 9130–8.

[217] Y. A. Hannun, *Science* **1996**, *274*, 1855–9.

[218] C. Erridge, E. Bennett-Guerrero, I. R. Poxton, *Microbes Infect.* **2002**, *4*, 837–851.

[219] K. Bock, M. E. Breimer, A. Brignole, G. C. Hansson, K. A. Karlsson, G. Larson, H. Leffler, B. E. Samuelsson, N. Strömberg, C. S. Edén, *J. Biol. Chem.* **1985**, *260*, 8545–51.

[220] C. Rodighiero, Y. Fujinaga, T. R. Hirst, W. I. Lencer, *J. Biol. Chem.* **2001**, *276*, 36939–45.

[221] A. R. Wellburn, *New Phytol.* **1997**, *135*, 115–121.

[222] D. K. Hincha, I. Bakaltcheva, J. M. Schmitt, *Plant Physiol.* **1993**, *103*, 59–65.

[223] G. Hölzl, P. Dörmann, *Prog. Lipid Res.* **2007**, *46*, 225–243.

[224] A. Minoda, N. Sato, H. Nozaki, K. Okada, H. Takahashi, K. Sonoike, M. Tsuzuki, *Eur. J. Biochem.* **2002**, *269*, 2353–2358.

[225] T. Baumgart, G. Hunt, E. R. Farkas, W. W. Webb, G. W. Feigenson, *Biochim. Biophys. Acta - Biomembr.* **2007**, *1768*, 2182–2194.

[226] O. Maier, V. Oberle, D. Hoekstra, *Chem. Phys. Lipids* **2002**, *116*, 3–18.

[227] P. J. Russell, *IGenetics: A Molecular Approach*, Benjamin Cummings, **2010**.

[228] C. Levinthal, *Mossbauer Spectrosc. Biol. Syst. Proc.* **1969**, *67*, 22–26.

[229] J. D. Bryngelson, P. G. Wolynes, *Proc. Natl. Acad. Sci. U. S. A.* **1987**, *84*, 7524–8.

[230] B. Honig, *J. Mol. Biol.* **1999**, *293*, 283–93.

[231] A. J. Parodi, *Annu. Rev. Biochem.* **2000**, *69*, 69–93.

[232] E. Shakhnovich, *Chem. Rev.* **2006**, *106*, 1559–88.

[233] P. G. Wolynes, *Biochimie* **2015**, *119*, 218–230.

[234] A. Perez, J. A. Morrone, C. Simmerling, K. A. Dill, *Curr. Opin. Struct. Biol.* **2016**, *36*, 25–31.

[235] A. M. Stanley, K. G. Fleming, *Arch. Biochem. Biophys.* **2008**, *469*, 46–66.

[236] A. I. Bartlett, S. E. Radford, *Nat. Struct. Mol. Biol.* **2009**, *16*, 582–8.

[237] A. Gershenson, L. M. Gierasch, *Curr. Opin. Struct. Biol.* **2011**, *21*, 32–41.

[238] X. Yu, C. Wang, Y. Li, *BMC Bioinformatics* **2006**, *7*, 187.

[239] J. Janin, R. P. Bahadur, P. Chakrabarti, *Q. Rev. Biophys.* **2008**, *41*, 133–80.

[240] T. Ushiki, *Arch. Histol. Cytol.* **2002**, *65*, 109–126.

[241] L. D. Muiznieks, F. W. Keeley, *Biochim. Biophys. Acta* **2013**, *1832*, 866–75.

[242] B. Byrne, S. Iwata, *Curr. Opin. Struct. Biol.* **2002**, *12*, 239–243.

[243] M. Luckey, *Membrane Structural Biology: With Biochemical and Biophysical Foundations*, Cambridge University Press, **2008**.

[244] W. H. Roos, R. Bruinsma, G. J. L. Wuite, *Nat. Phys.* **2010**, *6*, 733–743.

[245] H. Fraenkel-Conrat, R. C. Williams, *Proc. Natl. Acad. Sci. U. S. A.* **1955**, *41*, 690–8.

[246] J. B. Bancroft, G. J. Hills, R. Markham, *Virology* **1967**, *31*, 354–379.

[247] A. E. Pritchard, C. S. McHenry, *J. Biol. Chem.* **2001**, *276*, 35217–22.

[248] J. T. Gallagher, *Biochem. Soc. Trans.* **2006**, *34*, 438–41.

[249] M. Beck, V. Lucić, F. Förster, W. Baumeister, O. Medalia, *Nature* **2007**, *449*, 611–5.

[250] M. A. D'Angelo, M. W. Hetzer, *Trends Cell Biol.* **2008**, *18*, 456–66.

[251] W. Antonin, J. Ellenberg, E. Dultz, *FEBS Lett.* **2008**, *582*, 2004–16.

[252] R. J. Jackson, C. U. T. Hellen, T. V Pestova, *Nat. Rev. Mol. Cell Biol.* **2010**, *11*, 113–27.

[253] N. J. Gay, M. F. Symmons, M. Gangloff, C. E. Bryant, *Nat. Rev. Immunol.* **2014**, *14*, 546–558.

[254] H.-C. Mahler, W. Friess, U. Grauschopf, S. Kiese, *J. Pharm. Sci.* **2009**, *98*, 2909–34.

[255] L. O. Narhi, J. Schmit, K. Bechtold-Peters, D. Sharma, *J. Pharm. Sci.* **2012**, *101*, 493–8.

[256] M. C. Manning, D. K. Chou, B. M. Murphy, R. W. Payne, D. S. Katayama, *Pharm. Res.* **2010**, *27*, 544–75.

[257] J. S. Bee, T. J. Goletz, J. A. Ragheb, *J. Pharm. Sci.* **2012**, *101*, 3580–5.

[258] C. A. Ross, M. A. Poirier, *Nat. Med.* **2004**, *10 Suppl*, S10–7.

[259] A. Aguzzi, T. O'Connor, *Nat. Rev. Drug Discov.* **2010**, *9*, 237–48.

[260] J. García De La Torre, M. L. Huertas, B. Carrasco, *Biophys. J.* **2000**, *78*, 719–30.

[261] J. M. Finke, M. Roy, B. H. Zimm, P. A. Jennings, *Biochemistry* **2000**, *39*, 575–83.

[262] J. Lyklema, *Fundamentals of Interface and Colloid Science: Soft Colloids*, Academic

Press, **2005**.

[263] W. Wang, C. J. Roberts, *Aggregation of Therapeutic Proteins*, John Wiley & Sons, **2010**.

[264] G. Bhak, Y.-J. Choe, S. R. Paik, *BMB Rep.* **2009**, *42*, 541–51.

[265] A. J. Geddes, K. D. Parker, E. D. T. Atkins, E. Beighton, *J. Mol. Biol.* **1968**, *32*, 343–358.

[266] M. Biancalana, S. Koide, *Biochim. Biophys. Acta* **2010**, *1804*, 1405–12.

[267] G. P. Gorbenko, P. K. J. Kinnunen, *Chem. Phys. Lipids* **2006**, *141*, 72–82.

[268] C. G. Glabe, R. Kayed, *Neurology* **2006**, *66*, S74–8.

[269] F. Chiti, C. M. Dobson, *Annu. Rev. Biochem.* **2006**, *75*, 333–66.

[270] T. Kitada, S. Asakawa, N. Hattori, H. Matsumine, Y. Yamamura, S. Minoshima, M. Yokochi, Y. Mizuno, N. Shimizu, *Nature* **1998**, *392*, 605–8.

[271] D. M. Skovronsky, V. M.-Y. Lee, J. Q. Trojanowski, *Annu. Rev. Pathol.* **2006**, *1*, 151–70.

[272] A. V Maltsev, S. Bystryak, O. V Galzitskaya, *Ageing Res. Rev.* **2011**, *10*, 440–52.

[273] K. Iqbal, F. Liu, C.-X. Gong, *Nat. Rev. Neurol.* **2015**, *12*, 15–27.

[274] A. Diack, J. Alibhai, R. Barron, B. Bradford, P. Piccardo, J. Manson, *Int. J. Mol. Sci.* **2016**, *17*, 82.

[275] Y. Furukawa, N. Nukina, *Biochim. Biophys. Acta* **2013**, *1832*, 1271–8.

[276] M. Owczarz, P. Arosio, *Biophys. J.* **2014**, *107*, 197–207.

[277] P. Sen, S. Fatima, B. Ahmad, R. H. Khan, *Spectrochim. Acta. A. Mol. Biomol. Spectrosc.* **2009**, *74*, 94–9.

[278] M. Harel, L. K. Sonoda, I. Silman, J. L. Sussman, T. L. Rosenberry, *J. Am. Chem. Soc.* **2008**, *130*, 7856–61.

[279] S. E. Bondos, A. Bicknell, *Anal. Biochem.* **2003**, *316*, 223–31.

[280] E. J. Waters, G. Alexander, R. Muhlack, K. F. Pocock, C. Colby, B. K. O'Neill, P. B. Hoj, P. Jones, *Aust. J. Grape Wine Res.* **2005**, *11*, 215–225.

[281] A. Pande, J. Pande, N. Asherie, A. Lomakin, O. Ogun, J. King, G. B. Benedek, *Proc. Natl. Acad. Sci. U. S. A.* **2001**, *98*, 6116–20.

[282] A. Pande, O. Annunziata, N. Asherie, O. Ogun, G. B. Benedek, J. Pande, *Biochemistry* **2005**, *44*, 2491–2500.

[283] J. F. Hejtmancik, M. Kantorow, *Exp. Eye Res.* **2004**, *79*, 3–9.

[284] H. Bloemendal, W. de Jong, R. Jaenicke, N. H. Lubsen, C. Slingsby, A. Tardieu, *Prog. Biophys. Mol. Biol.* **2004**, *86*, 407–485.

[285] A. Pande, K. S. Ghosh, P. R. Banerjee, J. Pande, *Biochemistry* **2010**, *49*, 6122–9.

[286] P. R. Banerjee, S. S. Puttamadappa, A. Pande, A. Shekhtman, J. Pande, *J. Mol. Biol.* **2011**, *412*, 647–59.

[287] J. J. McManus, A. Lomakin, O. Ogun, A. Pande, M. Basan, J. Pande, G. B. Benedek, *Proc.*

Natl. Acad. Sci. U. S. A. **2007**, *104*, 16856–16861.

[288] S. James, M. K. Quinn, J. J. McManus, *Phys. Chem. Chem. Phys.* **2015**, *17*, 5413–20.

[289] M. K. Quinn, N. Gnan, S. James, A. Ninarello, F. Sciortino, E. Zaccarelli, J. J. McManus, *Phys. Chem. Chem. Phys.* **2015**, *17*, 31177–87.

[290] A. C. McUmber, T. W. Randolph, D. K. Schwartz, *J. Phys. Chem. Lett.* **2015**, *6*, 2583–7.

[291] S. James, J. J. McManus, *J. Phys. Chem. B* **2012**, *116*, 10182–8.

[292] A. Blumlein, J. J. McManus, *Biochim. Biophys. Acta* **2013**, *1834*, 2064–70.

[293] D. Radovan, N. Opitz, R. Winter, *FEBS Lett.* **2009**, *583*, 1439–45.

[294] K. Sasahara, K. Morigaki, K. Shinya, *FEBS J.* **2014**, *281*, 2597–612.

[295] J. S. Philo, T. Arakawa, *Curr. Pharm. Biotechnol.* **2009**, *10*, 348–51.

[296] I. Moreno-Gonzalez, C. Soto, *Semin. Cell Dev. Biol.* **2011**, *22*, 482–7.

[297] O. Shimomura, F. H. Johnson, Y. Saiga, *J. Cell. Comp. Physiol.* **1962**, *59*, 223–39.

[298] F. H. Johnson, O. Shimomura, Y. Saiga, L. C. Gershman, G. T. Reynolds, J. R. Waters, *J. Cell. Comp. Physiol.* **1962**, *60*, 85–103.

[299] H. Morise, O. Shimomura, F. H. Johnson, J. Winant, *Biochemistry* **1974**, *13*, 2656–62.

[300] O. Shimomura, *FEBS Lett.* **1979**, *104*, 220–222.

[301] D. C. Prasher, V. K. Eckenrode, W. W. Ward, F. G. Prendergast, M. J. Cormier, *Gene* **1992**, *111*, 229–33.

[302] M. Chalfie, Y. Tu, G. Euskirchen, W. W. Ward, D. C. Prasher, *Science* **1994**, *263*, 802–5.

[303] S. Inouye, F. I. Tsuji, *FEBS Lett.* **1994**, *341*, 277–280.

[304] R. Y. Tsien, *Annu. Rev. Biochem.* **1998**, *67*, 509 – 544.

[305] F. Yang, L. G. Moss, G. N. Phillips, *Nat. Biotechnol.* **1996**, *14*, 1246–51.

[306] O. Shimomura, *J. Microsc.* **2005**, *217*, 1–15.

[307] R. N. Day, M. W. Davidson, "Introduction to Aequorea victoria Fluorescent Proteins; Zeiss campus," can be found under http://zeiss-campus.magnet.fsu.edu/articles/probes/jellyfishfps.html, **2016**.

[308] R. Heim, D. C. Prasher, R. Y. Tsien, *Proc. Natl. Acad. Sci. U. S. A.* **1994**, *91*, 12501–4.

[309] R. Heim, A. B. Cubitt, R. Y. Tsien, *Nature* **1995**, *373*, 663–4.

[310] S. Delagrave, R. E. Hawtin, C. M. Silva, M. M. Yang, D. C. Youvan, *Biotechnology. (N. Y).* **1995**, *13*, 151–4.

[311] A. B. Cubitt, L. A. Woollenweber, R. Heim, *Methods Cell Biol.* **1999**, *58*, 19–30.

[312] N. C. Shaner, G. G. Lambert, A. Chammas, Y. Ni, P. J. Cranfill, M. A. Baird, B. R. Sell, J. R. Allen, R. N. Day, M. Israelsson, et al., *Nat. Methods* **2013**, *10*, 407–9.

[313] G. Rosenblum, C. Chen, J. Kaur, X. Cui, Y. E. Goldman, B. S. Cooperman, *Nucleic Acids*

Res. **2012**, *40*, e88.

[314] P. Xi, *Optical Nanoscopy and Novel Microscopy Techniques*, CRC Press, **2014**.

[315] E. J. Cohn, in *Adv. Mil. Med. Sci. World War II* (Ed.: E.C. Andrus), Boston: Little, Brown And Company, **1948**, pp. 364–443.

[316] K. A. Majorek, P. J. Porebski, A. Dayal, M. D. Zimmerman, K. Jablonska, A. J. Stewart, M. Chruszcz, W. Minor, *Mol. Immunol.* **2012**, *52*, 174–82.

[317] D. C. Carter, J. X. Ho, *Adv. Protein Chem.* **1994**, *45*, 153–203.

[318] T. Peters, *Adv. Protein Chem.* **1985**, *37*, 161–245.

[319] A. Bujacz, *Acta Crystallogr. D. Biol. Crystallogr.* **2012**, *68*, 1278–89.

[320] C. Wischke, H. H. Borchert, *Pharmazie* **2006**, *61*, 770–4.

[321] T. Estey, J. Kang, S. P. Schwendeman, J. F. Carpenter, *J. Pharm. Sci.* **2006**, *95*, 1626–39.

[322] S. Bassnett, Y. Shi, G. F. J. M. Vrensen, *Philos. Trans. R. Soc. Lond. B. Biol. Sci.* **2011**, *366*, 1250–64.

[323] J. F. Hejtmancik, *Semin. Cell Dev. Biol.* **2008**, *19*, 134–49.

[324] C. E. Jones, D. A. Atchison, R. Meder, J. M. Pope, *Vision Res.* **2005**, *45*, 2352–66.

[325] U. P. Andley, *Prog. Retin. Eye Res.* **2007**, *26*, 78–98.

[326] A. Tardieu, F. Vérétout, B. Krop, C. Slingsby, *Eur. Biophys. J.* **1992**, *21*, 1–12.

[327] M. Delaye, A. Tardieu, *Nature* **1983**, *302*, 415–417.

[328] E. Héon, M. Priston, D. F. Schorderet, G. D. Billingsley, P. O. Girard, N. Lubsen, F. L. Munier, *Am. J. Hum. Genet.* **1999**, *65*, 1261–1267.

[329] C. Slingsby, N. J. Clout, *Eye (Lond).* **1999**, *13 (Pt 3b*, 395–402.

[330] J. F. Hejtmancik, M. I. Kaiser-Kupfer, J. Piatigorsky, in *Metab. Mol. Basis Inherit. Dis.*, New York: McGraw Hill, **2001**, pp. 6033–6062.

[331] F. Ji, L. M. I. Koharudin, J. Jung, A. M. Gronenborn, *Proteins* **2013**, *81*, 1493–8.

[332] A. Pande, J. Zhang, P. R. Banerjee, S. S. Puttamadappa, A. Shekhtman, J. Pande, *Biochem. Biophys. Res. Commun.* **2009**, *382*, 196–9.

[333] M. Abramowitz, M. W. Davidson, "The Microscopy," **2015**.

[334] G. Binnig, C. F. Quate, *Phys. Rev. Lett.* **1986**, *56*, 930–933.

[335] M. Abramowitz, *Microscope Basics and Beyond*, Lake Success, N.Y., **2003**.

[336] D. B. Murphy, M. W. Davidson, *Fundamentals of Light Microscopy and Electronic Imaging*, John Wiley & Sons, Inc., Hoboken, NJ, USA, **2012**.

[337] M. D. Abràmofff, P. J. Magalhães, S. J. Ram, *Biophotonics Int.* **2005**, *11*, 36–43.

[338] T. Collins, *Microsc. Microanal.* **2007**, *13*, 1674–1676.

[339] C. a Schneider, W. S. Rasband, K. W. Eliceiri, *Nat. Methods* **2012**, *9*, 671–675.

[340] J. Mutterer, E. Zinck, *J. Microsc.* **2013**, *252*, 89–91.

[341] T. G. Rochow, E. G. Rochow, *An Introduction to Microscopy by Means of Light, Electrons, X-Rays, or Ultrasound*, Plenum Press, **1978**.

[342] A. Dopico, *Methods in Membrane Lipids*, Springer Science & Business Media, **2007**.

[343] A. T. Ngo, Z. J. Jakubek, Z. Lu, B. Joós, C. E. Morris, L. J. Johnston, *Biochim. Biophys. Acta* **2014**, *1838*, 2861–9.

[344] G. B. Alsop, D. Zhang, *J. Cell Sci.* **2004**, *117*, 1591–602.

[345] L. Finzi, C. Bustamante, G. Garab, C. B. Juang, *Proc. Natl. Acad. Sci. U. S. A.* **1989**, *86*, 8748–52.

[346] M. Wolman, F. H. Kasten, *Histochemistry* **1986**, *85*, 41–9.

[347] Y. Abraham, R. Elbaum, *New Phytol.* **2013**, *197*, 1012–9.

[348] R. Weaver, *Am. Lab.* **2003**, *35*, 55–61.

[349] K. R. Spring, M. W. Davidson, "Introduction to Fluorescence Microscopy," can be found under http://www.microscopyu.com/articles/fluorescence/fluorescenceintro.html, **2015**.

[350] B. Herman, V. E. Centonze Frohlich, J. R. Lakowicz, D. B. Murphy, K. R. Spring, M. W. Davidson, "Fluorescence Microscopy," can be found under http://micro.magnet.fsu.edu/primer/techniques/fluorescence/fluorhome.html, **2015**.

[351] B. Herman, *Fluorescence Microscopy*, Bios Scientific Publishers, **1998**.

[352] J. W. Lichtman, J.-A. Conchello, *Nat. Methods* **2005**, *2*, 910–919.

[353] A. Sharma, S. G. Schulman, *Introduction to Fluorescence Spectroscopy*, Wiley, **1999**.

[354] J. R. Lakowicz, *Principles of Fluorescence Spectroscopy*, Kluwer Academic/Plenum, **1999**.

[355] T. Ueno, T. Nagano, *Nat. Methods* **2011**, *8*, 642–645.

[356] S. W. Hell, *Nat. Methods* **2009**, *6*, 24–32.

[357] J.-A. Conchello, J. W. Lichtman, *Nat. Methods* **2005**, *2*, 920–931.

[358] T. J. Fellers, M. W. Davidson, "Introduction to Confocal Microscopy," can be found under http://olympus.magnet.fsu.edu/primer/techniques/confocal/confocalintro.html, **2012**.

[359] H. H. Rose, *Sci. Technol. Adv. Mater.* **2008**, *9*, 014107.

[360] R. Egerton, *Physical Principles of Electron Microscopy: An Introduction to TEM, SEM, and AEM*, Springer Science & Business Media, **2006**.

[361] D. B. Williams, C. B. Carter, *Transmission Electron Microscopy: A Textbook for Materials Science, Volume 2*, Springer Science & Business Media, **2009**.

[362] L. Reimer, H. Kohl, *Transmission Electron Microscopy: Physics of Image Formation*, Springer Science & Business Media, **2008**.

[363] J. J. Bozzola, L. D. Russell, *Electron Microscopy: Principles and Techniques for Biologists*, Jones & Bartlett Learning, **1999**.

[364] Y. Okumura, H. Zhang, T. Sugiyama, Y. Iwata, *J. Am. Chem. Soc.* **2007**, *129*, 1490–1491.

[365] K. Nishimura, T. Matsuura, K. Nishimura, T. Sunami, H. Suzuki, T. Yomo, *Langmuir* **2012**, *28*, 8426–32.

[366] T. Velasco-Torrijos, L. Abbey, R. O'Flaherty, *Molecules* **2012**, *17*, 11346–11362.

[367] M. Uhlén, *Biotechniques* **2008**, *44*, 649–654.

[368] J. Porath, *Protein Expr. Purif.* **1992**, *3*, 263–281.

[369] R. J. Hamilton, P. A. Sewell, *Introduction to High Performance Liquid Chromatography*, Chapman And Hall, **1982**.

[370] R. Westermeier, *Electrophoresis in Practice*, Wiley And Son, **2001**.

[371] N. Louis, C. Evelegh, F. L. Graham, *Virology* **1997**, *233*, 423–429.

[372] F. L. Graham, J. Smiley, W. C. Russell, R. Nairn, *J. Gen. Virol.* **1977**, *36*, 59–74.

[373] B. Dalby, S. Cates, A. Harris, E. C. Ohki, M. L. Tilkins, P. J. Price, V. C. Ciccarone, *Methods* **2004**, *33*, 95–103.

[374] B. B. Mandelbrot, *The Fractal Geometry of Nature*, Henry Holt And Company, **1983**.

[375] G. Liew, J. J. Wang, P. Mitchell, T. Y. Wong, *Circ. Cardiovasc. Imaging* **2008**, *1*, 156–61.

[376] L. S. Liebovitch, *Fractals and Chaos Simplified for the Life Sciences*, OUP USA, **1998**.

[377] S. S. Cross, *Micron* **1994**, *25*, 101–13.

[378] Y. Meyer, *Progress in Wavelet Analysis and Applications: Proceedings of the International Conference "Wavelets and Applications," Toulouse, France - June 1992*, Atlantica Séguier Frontières, **1993**.

[379] D. Sornette, *Critical Phenomena in Natural Sciences: Chaos, Fractals, Selforganization and Disorder: Concepts and Tools*, Springer Science & Business Media, **2004**.

[380] S. Ţălu, S. Giovanzana, *HVM Bioflux* **2012**, *4*, 14–18.

[381] K. M. Iftekharuddin, W. Jia, R. Marsh, *Mach. Vis. Appl.* **2003**, *13*, 352–362.

[382] Y. Kam, A. Karperien, B. Weidow, L. Estrada, A. R. Anderson, V. Quaranta, *BMC Res. Notes* **2009**, *2*, 130.

[383] H. F. Jelinek, E. Fernandez, *J. Neurosci. Methods* **1998**, *81*, 9–18.

[384] A. Karperien, H. Ahammer, H. F. Jelinek, *Front. Cell. Neurosci.* **2013**, *7*, 3.

[385] T. Matsuyama, R. M. Harshey, M. Matsushita, *Fractals* **1993**, *01*, 302–311.

[386] M. Tokuyama, K. Kawasaki, *Phys. Lett. A* **1984**, *100*, 337–340.

[387] N. E. Kurland, J. Kundu, S. Pal, S. C. Kundu, V. K. Yadavalli, *Soft Matter* **2012**, *8*, 4952.

[388] T. G. Smith, G. D. Lange, W. B. Marks, *J. Neurosci. Methods* **1996**, *69*, 123–136.

[389] C. A. Long, J. E. Long, *Acta Anat. (Basel).* **1992**, *145*, 201–6.

[390] R. J. Wingate, T. Fitzgibbon, I. D. Thompson, *J. Comp. Neurol.* **1992**, *323*, 449–74.

[391] B. Mandelbrot, *Science (80-.).* **1967**, *156*, 636–638.

[392] W. Seffens, *Science (80-.).* **1999**, *285*, 1228.

[393] T. Verbovšek, *Geol. Q.* **2010**, *53*, 241–248.

[394] I. V. Grossu, D. Felea, C. Besliu, A. Jipa, C. C. Bordeianu, E. Stan, T. Esanu, *Comput. Phys. Commun.* **2010**, *181*, 831–832.

[395] A. Karperien, "FracLac for ImageJ," can be found under http://rsb.info.nih.gov/ij/plugins/fraclac/FLHelp/Introduction.htm, **n.d.**

[396] L. A. Bagatolli, *Biochim. Biophys. Acta - Biomembr.* **2006**, *1758*, 1541–1556.

[397] G. W. Feigenson, *Biochim. Biophys. Acta - Biomembr.* **2009**, *1788*, 47–52.

[398] P. J. Quinn, *Langmuir* **2013**, *29*, 9447–9456.

[399] S. L. Veatch, S. L. Keller, *Phys. Rev. Lett.* **2005**, *94*, 3–6.

[400] L.-R. Montes, A. Alonso, F. M. Goñi, L. a Bagatolli, *Biophys. J.* **2007**, *93*, 3548–3554.

[401] M. Fröhlich, V. Brecht, R. Peschka-Süss, *Chem. Phys. Lipids* **2001**, *109*, 103–12.

[402] P. Méléard, C. Gerbeaud, T. Pott, M. D. Mitov, *Electromechanical Properties of Model Membranes and Giant Vesicle Deformations in Perspectives in Supramolecular Chemistry*, John Wiley & Sons, Ltd., Chichester, UK, **2000**.

[403] P. Girard, J. Pécréaux, G. Lenoir, P. Falson, J.-L. Rigaud, P. Bassereau, *Biophys. J.* **2004**, *87*, 419–29.

[404] N. Rodriguez, F. Pincet, S. Cribier, *Colloids Surfaces B Biointerfaces* **2005**, *42*, 125–130.

[405] D. J. Estes, M. Mayer, *Biochim. Biophys. Acta - Biomembr.* **2005**, *1712*, 152–160.

[406] L. A. Bagatolli, T. Parasassi, E. Gratton, *Chem. Phys. Lipids* **2000**, *105*, 135–147.

[407] T. Hamada, Y. Kishimoto, T. Nagasaki, M. Takagi, *Soft Matter* **2011**, *7*, 9061.

[408] L. Yang, L. Ding, H. W. Huang, *Biochemistry* **2003**, *42*, 6631–6635.

[409] M. Iwamori, A. Sakai, N. Minamimoto, Y. Iwamori, K. Tanaka, D. Aoki, S. Adachi, T. Nomura, *J. Biochem.* **2011**, *150*, 515–523.

[410] E. Doncel-Pérez, I. García-Álvarez, A. Fernández-Mayoralas, M. Nieto-Sampedro, *Bioorg. Med. Chem. Lett.* **2013**, *23*, 435–9.

[411] K. Syal, K. Maiti, K. Naresh, D. Chatterji, N. Jayaraman, *Adv. Exp. Med. Biol.* **2015**, *842*, 309–27.

[412] D. Kitamoto, H. Isoda, T. Nakahara, *J. Biosci. Bioeng.* **2002**, *94*, 187–201.

[413] N. Taniguchi, A. Suzuki, Y. Ito, H. Narimatsu, T. Kawasaki, S. Hase, *Experimental Glycoscience*, Springer Japan, Tokyo, **2008**.

[414] V. Faivre, V. Rosilio, *Expert Opin. Drug Deliv.* **2010**, *7*, 1031–48.

[415] E. Plouguerné, B. A. P. da Gama, R. C. Pereira, E. Barreto-Bergter, *Front. Cell. Infect.*

Microbiol. **2014**, *4*, 174.

[416] A. D. J. Cortés-Sánchez, H. Hernández-Sánchez, M. E. Jaramillo-Flores, *Microbiol. Res.* **2013**, *168*, 22–32.

[417] B. L. Stocker, M. S. M. Timmer, *ChemBioChem* **2013**, *14*, 1164–1184.

[418] D. M. Singh, X. Shan, J. H. Davis, D. H. Jones, C. W. Grant, *Biochemistry* **1995**, *34*, 451–63.

[419] V. Castro, S. V. Dvinskikh, G. Widmalm, D. Sandström, A. Maliniak, *Biochim. Biophys. Acta - Biomembr.* **2007**, *1768*, 2432–2437.

[420] J. Kapla, B. Stevensson, M. Dahlberg, A. Maliniak, *J. Phys. Chem. B* **2012**, *116*, 244–252.

[421] J. M. Alam, M. Yamazaki, *Chem. Phys. Lipids* **2011**, *164*, 166–74.

[422] J. Kubiak, J. Brewer, S. Hansen, L. A. Bagatolli, *Biophys. J.* **2011**, *100*, 978–86.

[423] G. J. L. Bernardes, R. Kikkeri, M. Maglinao, P. Laurino, M. Collot, S. Y. Hong, B. Lepenies, P. H. Seeberger, *Org. Biomol. Chem.* **2010**, *8*, 4987–4996.

[424] N. Brodersen, A. Arbuzova, A. Herrmann, H. Egger, J. Liebscher, *Tetrahedron* **2011**, *67*, 7763–7774.

[425] R. E. Bruehl, F. Dasgupta, T. R. Katsumoto, J. H. Tan, C. R. Bertozzi, W. Spevak, D. J. Ahn, S. D. Rosen, J. O. Nagy, *Biochemistry* **2001**, *40*, 5964–5974.

[426] C. S. Shi, G. Y. Shi, S. M. Hsiao, Y. C. Kao, K. L. Kuo, M. Chih-Yuan, C. H. Kuo, B. I. Chang, C. F. Chang, C. H. Lin, et al., *Blood* **2008**, *112*, 3661–3670.

[427] W.-L. Lin, C.-F. Chang, C.-S. Shi, G.-Y. Shi, H.-L. Wu, *Arterioscler. Thromb. Vasc. Biol.* **2013**, *33*, 2366–73.

[428] N. Kawasaki, C. D. Rillahan, T.-Y. Cheng, I. Van Rhijn, M. S. Macauley, D. B. Moody, J. C. Paulson, *J. Immunol.* **2014**, *193*, 1560–6.

[429] W. C. Chen, N. Kawasaki, C. M. Nycholat, S. Han, J. Pilotte, P. R. Crocker, J. C. Paulson, *PLoS One* **2012**, *7*, 1–9.

[430] N. Hashida, N. Ohguro, N. Yamazaki, Y. Arakawa, E. Oiki, H. Mashimo, N. Kurokawa, Y. Tano, *Exp. Eye Res.* **2008**, *86*, 138–149.

[431] W. C. Chen, G. C. Completo, D. S. Sigal, P. R. Crocker, A. Saven, J. C. Paulson, *Blood* **2010**, *115*, 4778–4786.

[432] M. Magalhães, D. Farinha, M. C. Pedroso de Lima, H. Faneca, *Int. J. Nanomedicine* **2014**, *9*, 4979–89.

[433] U. Kauscher, M. C. A. Stuart, P. Drücker, H. J. Galla, B. J. Ravoo, *Langmuir* **2013**, *29*, 7377–7383.

[434] K. Venken, T. Decruy, S. Aspeslagh, S. Van Calenbergh, B. N. Lambrecht, D. Elewaut, *J. Immunol.* **2013**, *191*, 2174–83.

[435] H. Bouvrais, T. Pott, L. A. Bagatolli, J. H. Ipsen, P. Méléard, *Biochim. Biophys. Acta* **2010**, *1798*, 1333–1337.

[436] N. Ahmad, R. Muhammad, H. A. Tajuddin, M. Misran, *Colloids Surfaces A Physicochem.*

Eng. Asp. **2014**, *443*, 96–101.

[437] M. Fidorra, A. Garcia, J. H. Ipsen, S. Härtel, L. A. Bagatolli, *Biochim. Biophys. Acta - Biomembr.* **2009**, *1788*, 2142–2149.

[438] H. Martinez-Seara, T. Róg, M. Karttunen, I. Vattulainen, R. Reigada, *PLoS One* **2010**, *5*, e11162.

[439] K. Trajkovic, C. Hsu, S. Chiantia, L. Rajendran, D. Wenzel, F. Wieland, P. Schwille, B. Brügger, M. Simons, *Science* **2008**, *319*, 1244–1247.

[440] D. L. Marks, R. Bittman, R. E. Pagano, *Histochem. Cell Biol.* **2008**, *130*, 819–832.

[441] J. E. Shaw, R. F. Epand, R. M. Epand, Z. Li, R. Bittman, C. M. Yip, *Biophys. J.* **2006**, *90*, 2170–2178.

[442] I. N. Zahid, O. K. Abou-Zied, R. Hashim, T. Heidelberg, *J. Phys. Chem. C* **2011**, *115*, 19805–19810.

[443] I. N. Zahid, O. K. Abou-Zied, R. Hashim, T. Heidelberg, *Langmuir* **2012**, *28*, 4989–4995.

[444] A. Schöppe, H.-J. Hinz, R. Gerdes, H. Redlich, G. Rapp, *Chem. Phys. Lipids* **1999**, *103*, 95–115.

[445] N. Janes, *Chem. Phys. Lipids* **1996**, *81*, 133–150.

[446] J.-P. Colletier, B. Chaize, M. Winterhalter, D. Fournier, *BMC Biotechnol.* **2002**, *2*, 9.

[447] B. Lohse, P.-Y. Bolinger, D. Stamou, *J. Am. Chem. Soc.* **2008**, *130*, 14372–3.

[448] S. K. Das, M. Darshi, S. Cheley, M. I. Wallace, H. Bayley, *Chembiochem* **2007**, *8*, 994–9.

[449] C. Leonhardt, G. Schwake, T. R. Stögbauer, S. Rappl, J.-T. Kuhr, T. S. Ligon, J. O. Rädler, *Nanomedicine* **2014**, *10*, 679–88.

[450] A. L. Fink, *Fold. Des.* **1998**, *3*, R9–23.

[451] W. Wang, S. Nema, D. Teagarden, *Int. J. Pharm.* **2010**, *390*, 89–99.

[452] M. R. H. Krebs, K. R. Domike, A. M. Donald, *Biochem. Soc. Trans.* **2009**, *37*, 682–6.

[453] J. E. Gillam, C. E. MacPhee, *J. Phys. Condens. Matter* **2013**, *25*, 373101.

[454] K. Sasahara, K. Morigaki, T. Okazaki, D. Hamada, *Biochemistry* **2012**, *51*, 6908–19.

[455] M. Gao, R. Winter, *J. Diabetes Res.* **2015**, *2015*, 1–21.

[456] S. S. Gambhir, S. S. Yaghoubi, *Molecular Imaging with Reporter Genes*, Cambridge University Press, **2010**.

[457] J. C. Waters, J. R. Swedlow, *Eval. Tech. Biochem. Res.* **2007**, 36–42.

[458] J. C. Waters, *J. Cell Biol.* **2009**, *185*, 1135–1148.

[459] V. C. Coffman, J.-Q. Wu, *Trends Biochem. Sci.* **2012**, *37*, 499–506.

[460] R. A. Messing, *J. Non. Cryst. Solids* **1975**, *19*, 277–283.

[461] T. Pereira de Souza, P. Stano, P. L. Luisi, *Chembiochem* **2009**, *10*, 1056–63.

[462] P. Stano, T. P. de Souza, P. Carrara, E. Altamura, E. D'Aguanno, M. Caputo, P. L. Luisi, F. Mavelli, *Mech. Adv. Mater. Struct.* **2014**, *22*, 748–759.

[463] C. Veerman, L. M. C. Sagis, J. Heck, E. Van Der Linden, *Int. J. Biol. Macromol.* **2003**, *31*, 139–146.

[464] M. Bhattacharya, N. Jain, S. Mukhopadhyay, *J. Phys. Chem. B* **2011**, *115*, 4195–4205.

[465] L. C. Serpell, M. Sunde, C. C. Blake, *Cell. Mol. Life Sci.* **1997**, *53*, 871–87.

[466] R. Eisert, L. Felau, L. R. Brown, *Anal. Biochem.* **2006**, *353*, 144–146.

[467] A. Hawe, M. Wiggenhorn, M. van de Weert, J. H. O. Garbe, H.-C. Mahler, W. Jiskoot, *J. Pharm. Sci.* **2012**, *101*, 895–913.

[468] N. R. Maddux, I. T. Rosen, L. Hu, C. M. Olsen, D. B. Volkin, C. R. Middaugh, *J. Pharm. Sci.* **2012**, *101*, 2017–24.

[469] D. B. Murphy, R. Oldfield, S. Schwartz, M. W. Davidson, "Introduction to Phase Contrast Microscopy," can be found under file:///D:/Papers/8.Techniques, Methods Microscopy/2. Phase contrast/Nikon MicroscopyU _ Phase Contrast Microscopy _ Introduction.html, **2013**.

[470] C. Obermaier, A. Griebel, R. Westermeier, *Methods Mol. Biol.* **2015**, *1295*, 153–65.

[471] L. G. B. Bremer, T. van Vliet, P. Walstra, *J. Chem. Soc. Faraday Trans. 1 Phys. Chem. Condens. Phases* **1989**, *85*, 3359–3372.

[472] L. G. B. Bremer, B. H. Bijsterbosch, R. Schrijvers, T. van Vliet, P. Walstra, *Colloids and Surfaces* **1990**, *51*, 159–170.

[473] T. Hagiwara, H. Kumagai, K. Nakamura, *Biosci. Biotechnol. Biochem.* **1996**, *60*, 1757–63.

[474] T. Hagiwara, H. Kumagai, T. Matsunaga, *J. Agric. Food Chem.* **1997**, *45*, 3807–3812.

[475] S. Ikeda, E. A. Foegeding, T. Hagiwara, *Langmuir* **1999**, *15*, 8584–8589.

[476] A. Marangoni, *Food Hydrocoll.* **2000**, *14*, 61–74.

[477] L. R. De Young, A. L. Fink, K. A. Dill, *Acc. Chem. Res.* **1993**, *26*, 614–620.

[478] Y. Panyukov, I. Yudin, V. Drachev, E. Dobrov, B. Kurganov, *Biophys. Chem.* **2007**, *127*, 9–18.

[479] K. A. Markossian, I. K. Yudin, B. I. Kurganov, *Int. J. Mol. Sci.* **2009**, *10*, 1314–45.

[480] M. M. Ould Eleya, S. Ko, S. Gunasekaran, *Food Hydrocoll.* **2004**, *18*, 315–323.

[481] T. Hagiwara, H. Kumagai, K. Nakamura, *Food Hydrocoll.* **1998**, *12*, 29–36.

[482] H. Kumagai, T. Matsunaga, T. Hagiwara, *Biosci. Biotechnol. Biochem.* **1999**, *63*, 223–5.

[483] R. R. G. Maciel, A. A. de Almeida, O. G. C. Godinho, F. D. S. Gorza, G. C. Pedro, T. F. Trescher, J. R. Silva, N. C. de Souza, *Biomed Res. Int.* **2013**, *2013*, 461365.

[484] C. Honda, H. Kamizono, T. Samejima, K. Endo, *Chem. Pharm. Bull. (Tokyo).* **2000**, *48*, 464–6.

[485] J. C. Blain, J. W. Szostak, *Annu. Rev. Biochem.* **2014**, *83*, 615–40.

[486] M. C. Huber, A. Schreiber, P. von Olshausen, B. R. Varga, O. Kretz, B. Joch, S. Barnert, R. Schubert, S. Eimer, P. Kele, et al., *Nat. Mater.* **2015**, *14*, 125–32.

[487] C. P. Brangwynne, *Soft Matter* **2011**, *7*, 3052.

[488] N. Asherie, *Proc. Natl. Acad. Sci. U. S. A.* **2011**, *108*, 437–438.

[489] M. H. Steinberg, *ScientificWorldJournal.* **2008**, *8*, 1295–324.

[490] A. Lomakin, N. Asherie, G. B. Benedek, *Proc. Natl. Acad. Sci.* **1999**, *96*, 9465–9468.

[491] E. Karsenti, *Nat. Rev. Mol. Cell Biol.* **2008**, *9*, 255–62.

[492] T. Misteli, *J. Cell Biol.* **2001**, *155*, 181–5.

[493] R. Heald, *J. Cell Biol.* **1997**, *138*, 615–628.

[494] T. Ferreira, W. Rasband, **2012**, DOI 10254/nanohub-r6612.8.

[495] P. Stano, P. Carrara, Y. Kuruma, T. Pereira de Souza, P. L. Luisi, *J. Mater. Chem.* **2011**, *21*, 18887.

[496] M. Guthold, W. Liu, B. Stephens, S. T. Lord, R. R. Hantgan, D. A. Erie, R. M. Taylor, R. Superfine, *Biophys. J.* **2004**, *87*, 4226–36.

[497] J. Lippincott-Schwartz, E. Snapp, A. Kenworthy, *Nat. Rev. Mol. Cell Biol.* **2001**, *2*, 444–56.

[498] A. Miyawaki, A. Sawano, T. Kogure, *Nat. Cell Biol.* **2003**, *Suppl*, S1–7.

[499] E. Snapp, *Curr. Protoc. Cell Biol.* **2005**, *Chapter 21*, Unit 21.4.

[500] J. Tyedmers, A. Mogk, B. Bukau, *Nat. Rev. Mol. Cell Biol.* **2010**, *11*, 777–788.

[501] Y. M. Ramdzan, S. Polling, C. P. Z. Chia, I. H. W. Ng, A. R. Ormsby, N. P. Croft, A. W. Purcell, M. A. Bogoyevitch, D. C. H. Ng, P. A. Gleeson, et al., *Nat. Methods* **2012**, *9*, 467–70.

[502] M. Fernández-Suárez, A. Y. Ting, *Nat. Rev. Mol. Cell Biol.* **2008**, *9*, 929–43.

[503] Y. S. Sun, J. P. Landry, Y. Y. Fei, X. D. Zhu, J. T. Luo, X. B. Wang, K. S. Lam, *Langmuir* **2008**, *24*, 13399–405.

[504] C. A. Teske, M. Schroeder, R. Simon, J. Hubbuch, *J. Phys. Chem. B* **2005**, *109*, 13811–7.

[505] L. Yin, W. Wang, S. Wang, F. Zhang, S. Zhang, N. Tao, *Biosens. Bioelectron.* **2015**, *66*, 412–6.